Understanding the impact of marine iodine chemistry on climate and air quality

Tomás M. Sherwen

PhD

University of York

Chemistry

July 2016

Abstract

Halogens have an established impact on atmospheric composition, but further quantification of their global air-quality and climatic impacts is needed. This thesis documents the development of a simulation to represent the atmospheric chemistry of iodine within a wider halogen framework. Following the development of the iodine simulation (Chapter II-III), a coupled model is presented (Chapter IV) that brings together and builds upon previous halogen (Cl,Br) studies in GEOS-Chem. Finally this model is used to investigate impacts of halogens on climate (Chapter V), and iodine sourced aerosol (Chapter VI).

Significant implications of halogens on oxidants are shown. Iodine alone reduces the tropospheric O_3 burden by ∼9 %, with "coupled" halogens (Cl,Br,I) reducing it by ∼15 %. Global mean OH concentrations decrease by 4.5 % on inclusion of halogens. However, this is due to competing factors. The O_3 loss decreases primary production, whereas conversion of HO_2 to OH via photolysis of hydrohalic acids tends to increase it. Chlorine provides a potent new oxidant in the model. For some VOCs (C_2H_6, $(CH_3)_2CO$) Cl oxidation provides up to ∼20 % of their sink.

The effect of halogens on the tropospheric O_3 radiative forcing (RF_{TO3}) is investigated. Halogens cause a feedback effect, dampening the increase of tropospheric O_3 between the pre-industrial and the present day by ∼20 %, therefore reducing RF_{TO3}. Aerosol-phase iodine is also investigated and shown to regionally contribute up to 101 % of DMS sourced sulfate aerosol mass. In the pre-industrial, iodine aerosol can regionally contribute up to 21 % of the sulfate mass.

Iodine and halogen chemistry in general are required to understand tropospheric composition and processes. Uncertainty in the emissions, chemistry and loss processes for halogens is high. Further in-situ observations and elucidation of key parameters in laboratories are urgently needed to refine our understanding of this important aspect of atmospheric chemistry.

Contents

List of Tables

List of Figures

Acknowledgements

I thank you Mat and Lucy for giving me the opportunity to undertake a PhD. You gave tireless feedback, encouragement, and direction.

The research group at WACL is brilliant, friendly, and highly collaborative. I am grateful for all the discussion, collaboration, general fun, and most of all the willingness to bounce ideas off each other. I especially thank Sina, Rosie, Pete, Rachel, Kelly, Steve, Eric, Ben, Dan... and everyone else in the WACL/Evans group!

To my many co-authors and collaborators: I thank you all for your time, for everything you have helped me learn and do, and for the jokes that have kept the PhD fun. I look forward to working with you all in the future and appreciate all your contributions so far.

The short time I spent visiting the Jacob group really helped crystallise the ideas in this thesis. Thanks Tom, Johan, and Roísín for being a great laugh and making the whole experience great fun (even that Rod Stewart tribute concert!) as well as very productive. I am also grateful to everyone else I met on the several visits to Harvard/U.S.A.

To Sarah, James, Antara, and Jamie: Thanks for all the puns and silly animal videos, they have filled so many long days in the office with laugher.

To my wonderful fiancée Eleanor: I will remain forever grateful for your unwavering support and love, even in the numerous less positive days of my PhD when everything seemed to be broken or lost. I am very lucky to have such a lovely, intelligent, and wise person in my life.

To my open-minded and engaged family. You gave me the freedom to explore and the confidence to jump into the unknown. Thanks mum and dad for everything from giving me rides to chess club to encouraging me in my ridiculously long list of hobbies. Without your support I would never have applied for, let alone submitted this PhD.

Declaration

The research described in this thesis is original work, which was undertaken at the University of York during 2012–2016 and which has not been presented for a research degree at this or any other univeristy. Except where stated, all of the work contained within this thesis represents the original contribution of the author. Some parts of this thesis have been published in journals; where items were published jointly with collaborators, the author of this thesis is responsible for the material presented here or if not it is explicitly stated. For each published item the primary author is the first listed author. Publications are listed at the beginning of the chapter to which they relate.

Chapter 1

Introduction

1.1 Introduction

This chapter provides some background on the composition (Sect. 1.3), structure, and key chemical cycles of oxidants in the atmosphere closest to the surface on Earth (Sect. 1.3.2). In particular, focus is given to ozone (O_3) due to its importance for air-quality (Sect. 1.2.2) and climate change (Sect. 1.2.1). The models that are used to represent the physics and chemistry of the atmosphere are described (Sect. 1.4), with more detail describing chemical transport models (CTMs, Sect. 1.4.1). The chemistry and effects of halogens in the troposphere are then considered (Sect. 1.5), with particular focus on iodine (Sect. 1.6.2).

After discussing the background science for this thesis, this chapter presents the goals of this work (Sect. 1.9), and concludes with a brief description the content of the following chapters within this thesis (Sect. 1.10).

1.2 Motivations

1.2.1 Climate change

A large body of scientific evidence has established that humans are having a warming effect the planet (Myhre et al., 2013). This comes from atmospheric composition changes, from pre-industrial to present-day, altering the amount of energy absorbed at different levels of Earth's atmosphere. This change is quantified in terms of the difference between present-day and pre-industrial in energy per unit area (in units of W m^{-2}) at the tropopause, and referred to as the "radiative forcing" (Myhre et al., 2013). The radiative forcing caused by the changing concentration of different species is shown by species in Figure 1.1a.

In the case of O_3, the emissions of precursors that form O_3 have increased from pre-industrial times to present, leading to an increase in the tropospheric O_3 burden (Marenco et al., 1994) as shown in Figure 1.1b (Young et al., 2013). Increase in O_3 from has been shown to cause a warming effect with a radiative forcing amounting to $\sim$0.4 W m^{-2} (Myhre et al., 2013). This compares with the total anthropogenic effective radiative forcing over the industrial era (1750-2000) of 2.3 (1.1 to 3.3) W m^{-2} (Myhre et al., 2013) as shown diagrammatically in Figure 1.1a.

1.2.2 Air-quality

The detrimental impact of air-quality pollutants (e.g. O_3, benzene, NO_2, aerosols, etc) is also well established (Ainsworth et al., 2012; Fowler et al., 2008). Many species that are climate gases (see Fig 1.1a) are also air-quality gases or lead to the formation of air-quality gases.

A good example of this is O_3, which is not only a strong long-wave light-absorber, but is also toxic to plants, animals, and humans (Ainsworth et al. 2012, and citations within) and associated with aerosol formation (Finlayson-Pitts and Pitts, 1997). One metric for the scale of air-quality as an issue is annual excess attributable deaths, which have been estimated at 7 million in 2010 (World Health Organistion, 2014). Although estimates of health impacts exist, improving understanding of impacts and the spatial distribution in present and future remains a significant scientific question.

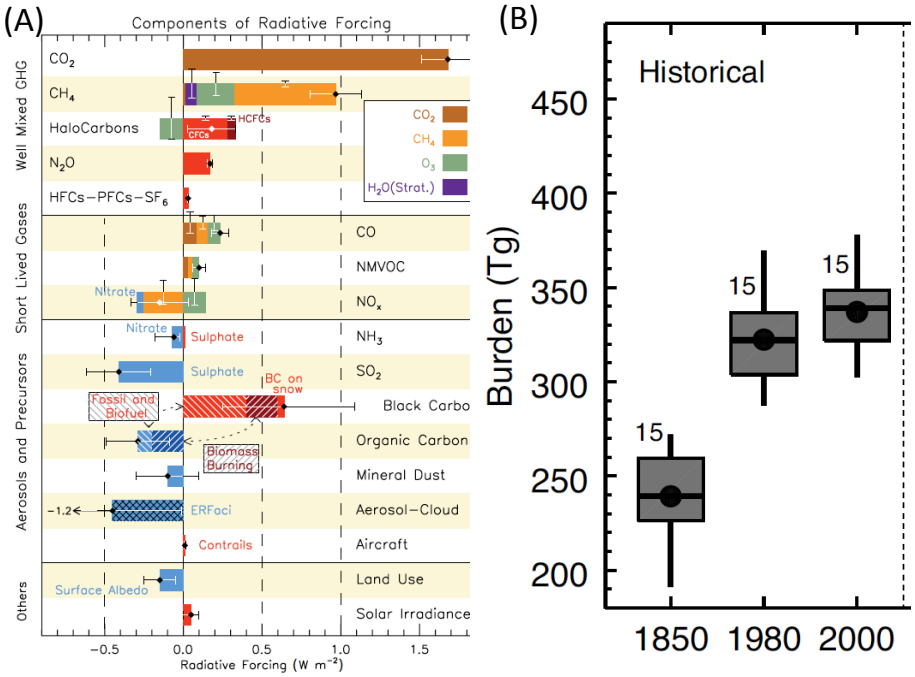

Figure 1.1 – (A)"Radiative Forcing bar chart for the period 1750-2011 based on emitted compounds (gases, aerosols or aerosol precursors) or other changes." Reproduced from Myhre et al. (2013). (B) Tropospheric O_3 burden in pre-industrial (1850) and present (1980, 2000). Reproduced from Young et al. (2013).

1.3 Chemistry in the troposphere: the air we breathe

As humans, we live and breathe in the bottom ∼15 km of the atmosphere, which is referred to as the troposphere. This is where majority (∼90 %) of the earth's atmospheric mass resides. From life's perspective the chemistry, composition, and climate in this part of the atmosphere is vital. The composition is largely inert, in the form of nitrogen (N_2, 78%), oxygen (O_2, 21%), water (H_2O, ∼1%) and noble gases (e.g. Ar, ∼1%). However reactive minor constituents have a significant role in defining the rate of processes that determine the concentration of both climate and air-quality gases. The chemistry of the troposphere is driven by the sun's energy, which drives photolysis of molecules to give highly reactive intermediates.

A range of species are emitted into the troposphere by humans (anthropogenic), biological (biotic), or by physical (abiotic) processes. The fate of an emitted species is generally increasing chemical oxidation until they are removed from the atmosphere by wet and dry deposition, or biological uptake. The cycles of the chemical families of oxides of nitrogen

(NO_x=NO+NO_2) and oxides of hydrogen (HO_x=HO+HO_2) drive the chemical pathways of most emitted species.

1.3.1 Composition and structure

The atmosphere can be split into regions based on changes temperature, as shown in Figure 1.2. The two regions closest to the surface, are separated by a region (tropopause) where air with decreasing temperature with altitude (troposphere) meets air with increasing temperature with altitude (stratosphere). Mixing between these regions is limited by the stability of the stratosphere, leading to a timescale of mixing from the troposphere to the stratosphere of 5-10 years (Brasseur and Jacob, 2016).

The air closest to the surface experiences the direct effects of the surface (e.g. heating, cooling and friction) causing it to be more turbulent than the air above. This air is referred to as the planetary boundary layer (PBL) and its extent is highly variable from a few hundred meters to a few kilometers (Brasseur and Jacob, 2016). This region is where essentially all life resides and where almost all chemical compounds are emitted from biogenic and anthropogenic sources.

The chemistry in the troposphere is driven by photons from the sun. The photons that reach the surface have been attenuated by the atmosphere above. Notably the O_3 in the stratosphere significantly reduces the number of ultra-violet (UV) photons which make it to the troposphere. Thus some compounds are essentially inert in the troposphere (e.g. N_2O, Halons, Chlorofluorocarbons etc.).

1.3.2 Tropospheric oxidants and chemistry

The chemistry of the troposphere controls the concentration of a range of climate gases including ozone (O_3), methane (CH_4) (Kim et al., 2011; Voulgarakis et al., 2013; Young et al., 2013) and aerosols (Koch et al., 2011). The chemistry also determines human and agriculture's exposure to air-quality pollutants such as O_3 and aerosols (Ainsworth et al., 2012; Fiore et al., 2012; Fowler et al., 2008). The chemical cycles maintaining concentrations of these atmospheric constituents are complex, and depend strongly upon the concentrations of O_3 and of the hydroxyl radical (OH) as key oxidants. Understanding

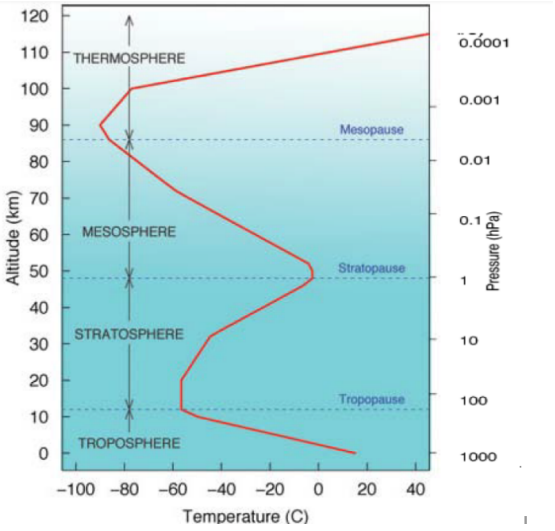

Figure 1.2 – Temperature profile of the atmosphere up to ∼100km, with named regions and boundaries annotated. Figure reproduced from Brasseur and Jacob (2016).

the budgets and controls on these gases is therefore central to assessments of tropospheric chemistry (Voulgarakis et al., 2013).

1.3.2.1 HO_x chemistry

The chemistry of O_3 and OH in the troposphere is coupled and the main factors have been understood for about 30 years (Logan, 1983). The photolysis of O_3 produces an electronically excited oxygen atom (O^1D), which can react with a water molecule to produce two OH radicals (Eqns. 1.1 and 1.2). OH dictates the lifetimes of many pollutants, including CO and CH_4, which it ultimately oxidises to H_2O and CO_2. This leads to OH often being described as "nature's cleanser" (Wayne, 2000) as it oxidises emitted species (e.g. volatile organic compounds (VOCs)) leading to their increased solubility and therefore removal from the atmosphere.

$$O_3 \xrightarrow{h\nu} O^1D + O_2 \tag{1.1}$$

$$O^1D + H_2O \rightarrow OH + OH \tag{1.2}$$

OH can then react with O_3 to produce HO_2, which leads to a catalytic destruction of O_3 (Eqns. 1.3-1.4).

$$OH + O_3 \rightarrow HO_2 + O_2 \tag{1.3}$$

$$HO_2 + O_3 \rightarrow OH + 2\,O_2 \tag{1.4}$$

$$Net : 2\,O_3 \rightarrow 3\,O_2$$

Subsequent reactions of OH with organic compounds (hydrocarbons, oxygenates, CH_4, CO, etc.), produces peroxy radicals (RO_2=HO_2+organic peroxy radicals). The two major OH loss pathways in clean air (low NO_x conditions) for CO (Reactions 1.5-1.7) and CH_4 (Reactions 1.8-1.10) are shown below. Under higher NO_x conditions the major pathways are different, as we now discuss (Sect. 1.3.2.2).

$$CO + OH \rightarrow H + CO_2 \tag{1.5}$$

$$H + O_2 + M \rightarrow HO_2 + M \tag{1.6}$$

$$HO_2 + HO_2 + M \rightarrow H_2O_2 + M \tag{1.7}$$

$$Net : CO + OH + HO_2 \rightarrow CO_2 + H_2O_2$$

$$CH_4 + OH \rightarrow CH_3 + H_2O \tag{1.8}$$

$$CH_3 + O_2 \xrightarrow{M} CH_3O_2 \tag{1.9}$$

$$CH_3O_2 + HO_2 \xrightarrow{M} CH_3OOH + O_2 \tag{1.10}$$

$$Net : CH_4 + OH + HO_2 \rightarrow CH_3OOH + H_2O$$

1.3.2.2 NO_x chemistry

The fate of the RO_2 depends critically on the concentration of oxides of nitrogen (NO_x). NO reacts with O_3 and produces NO_2 (eqn 1.11), which is photolysed to back to NO (eqn. 1.12). This does not lead to O_3 production or loss and is referred to as a "null cycle" (Eqns. 1.11-1.13).

$$NO + O_3 \rightarrow NO_2 + O_2 \tag{1.11}$$

$$NO_2 \xrightarrow{h\nu} NO + O \tag{1.12}$$

$$O_2 + O + M \rightarrow O_3 + M \tag{1.13}$$

$$Net : \textit{null cycle}$$

The effect on O_3 of HO_x and NO_x chemistry depends on NO and VOC concentrations in a complex way and is extensively discussed in the literature (e.g. Atkinson 2000). Essentially, if sufficient nitrogen oxide (NO) is available, the dominant fate of peroxy radicals (HO_2, RO_2) is to oxidise NO to nitrogen dioxide (NO_2) (Eqn. 1.14), allowing the formation of O_3 via photolysis of NO_2 (Eqn. 1.16)). However if NO_x concentrations are lower (e.g. in the remote atmosphere) O_3 destruction through HO_x cycling dominates (Eqns. 1.3-1.4) .

$$HO_2 + NO \rightarrow NO_2 + OH \tag{1.14}$$

$$NO_2 \xrightarrow{h\nu} NO + O \tag{1.15}$$

$$O_2 + O \xrightarrow{M} O_3 \tag{1.16}$$

$$Net : \textit{null cycle}$$

At very high NO_x concentrations the reaction between NO_2 and OH becomes significant. This leads to lower RO_2 concentrations and therefore lower O_3 concentrations.

1.3.3 Tropospheric ozone (O_3)

Tropospheric O_3 is not directly emitted in the troposphere, but is produced by the oxidation of CO, CH_4, and VOCs in the presence of oxides of nitrogen (NO_x) as already described above. As O_3 concentrations are highly spatially and temporally variable, and cannot be measured everywhere for reasons of practicality, numerical models are often

required to give the answers required for scientific questions (e.g. on air-quality). Furthermore, as O_3 is too reactive to have an ice core record, models are required to simulate pre-industrial O_3 concentrations, which are required to calculate radiative forcings.

Models are used to describe the production and loss of O_3 globally, and constraints for global O_3 concentrations are possible from surface, ozone-sonde, and satellite measurements. Tropospheric O_3 has a source via transport from the stratosphere (∼500 Tg, Young et al. 2013), and is lost to the Earth's surface via dry deposition (∼1000 Tg, Hardacre et al. 2015). The production of O_3 in the troposphere is ∼5000 Tg O_3 yr^{-1}, which after subtracting its chemical loss leads to a net chemical production of the order of ∼500 Tg O_3 yr^{-1} (Young et al., 2013). Average values for these terms and standard deviation between atmospheric chemistry models are given in Table 1.1, these values are taken from the Atmospheric Chemistry and Climate Model Inter-comparison Project (ACCMIP, Young et al. 2013).

Table 1.1 – Average modelled values for key O_3 processes in the troposphere. The standard deviation is given in brackets. Table/values are reproduced from Young et al. (2013). PO_x=chemical production(Z), LO_x=chemical loss (X), Deposition=deposition to the surface(Y), Stratosphere=flux from the stratosphere, and lifetime = burden/(X + Y)

Chemical Production (PO_x) / Tg Yr^{-1}	Chemical Loss (LO_x) / Tg Yr^{-1}	Deposition Tg Yr^{-1}	Stratosphere Tg Yr^{-1}	Lifetime Days
5110 (±606)	4668 (±727)	1003 (±200)	552 (±168)	22.3 (±2.0)

1.4 Atmospheric modelling

Models of the atmosphere are used to represent our current understanding of chemical and physical processing, thus enabling prediction of composition for the past, present and future. These models can be more or less spatially complex, e.g. from zero dimensional (box-) models, which represent processes occurring in a single air parcel, to models with three dimensional (3D) representation of transport, emission, chemical and physical processes in the atmosphere. Models can also be more or less encompassing, from considering one aspect of the Earth system (e.g. atmospheric) to models that consider coupling between different aspects (e.g. cryosphere and ocean) like General Circulation Models (GCMs) or Earth System Models (ESMs).

To study effects of chemical or physical processes on the atmosphere over large spatial scales, 3D models need to be used. These models need to calculate the role of transport on concentration of atmospheric composition. They can either calculate meteorological parameters online for each time-step or use offline variables from other models to reduce computational cost. These models have been extensively described previously, for instance by Brasseur and Jacob (2016). This thesis' focus is the chemistry of the troposphere so, instead of considering the chemistry of the whole atmosphere (i.e. troposphere and stratosphere) and interactive linking of other parts of the Earth system (e.g. hydrosphere, geosphere, and cyrosphere), a model that only considers tropospheric processes is used. Chemical Transport Models (CTMs) are ideally suited for this. They have more detailed chemistry than ESMs or GCMs. These models are typically run for annual time scales and use "offline" meteorology. This makes them useful tools for comparing with observations and evaluating processes.

1.4.1 Chemical Transport Models (CTMs)

Chemical transport models tend to be Eulerian (with a fixed spatial reference frame) and either regional (e.g. CMAQ, WRF-Chem), or global (e.g. TOMCAT, GEOS-Chem) in perspective. Some Lagrangian/semi-Lagrangian (moving reference frame) models exist like CLaMs (McKenna, 2002a,b), STOCHEM (Collins et al., 2000) or MPI-ECHAM5 (Roeckner et al., 2003). Due to the need to solve continuity equations that represent chemistry and physical processing for all boxes, these models can fast become computationally expensive. Some processes are therefore calculated offline or parameterised to allow computation cost to be spent on answers to a particular scientific question, such as the global distribution of O_3.

These model have consider a range processes to calculate the concentrations of compounds in the atmosphere. These processes are explained below.

1.4.1.1 Emissions

Chemical Transport Models need to consider the emissions from biogenic and anthropogenic sources. These emissions are built in a variety of different ways. For anthropogenic emissions theses are essentially built up from country/industry sectorial emissions

that have been reported by industry and government, and these can be constrained to observations. For biogenic and abiotic emissions, inventories are based on observations and typically scaled to parameters available to models (e.g. land type) or from satellites (e.g. chlorophyll) to form climatologies or just spatial datasets. These emissions then can be scaled with activity factors, such as season, day of week, on-line variables such as temperature and wind speed, and diurnal variations (e.g. Keller et al. 2014).

Biogenic emissions include carbon monoxide (CO, e.g. from combustion), methane (CH_4, e.g. from wetlands), a range of VOCs (e.g. Isoprene, Monoterpenes, Methyl Butenol), NO_x (e.g. soils, lightning), sulfur dioxide (SO_2, e.g. from degassing and eruptive volcanos), biomass burning, and aerosols (e.g. Black and organic carbon, mineral dust, and sea-salt).

Anthropogenic emissions include CO, CH_4 (e.g. from fossil-fuels), alkenes (e.g. C_2H_2, propene), alkanes (e.g. C_3H_8), a range of higher weight VOCs (e.g. benzene, toluene, and xylene), ammonia (NH_3), SO_2 (e.g. from power plants), NO_x (e.g. industrial, automative, aircraft and shipping), biofuel emissions, and aerosols (e.g. Black and organic carbon, PM_{10}, $PM_{2.5}$).

Some emissions such as biomass burning can arguably be a mixture of anthropogenic and natural, due to displaced agriculture causing land-use change or anthropogenically driven climate change effects on wildfire regions.

1.4.1.2 Chemistry

Chemical transformations within a grid-box for a given time-step are solved by considering concentrations of species at the end of the previous time-step, then integrating the chemical rate equations (Jacobson and Turco, 1994) forwards. The chemical equations are represented as a series of ordinary differential equations, one per reaction in the model's chemistry scheme. Integrating these simultaneous differential equations is the most numerically intense part of the CTM calculation. Once a solution is converged upon within the set tolerances, the CTM outputs the data or continues to the next time-step. CTMs typically include HO_x, NO_x, VOC chemistry and a representation of aerosol processes. Processes such as calculating phase equilibrium reactions or detailed, explicit VOCs oxidation chemistry are not included due to expense. Instead, a play off between explicit chemistry and representation of key observable components is made.

A central part of calculating the rate of reaction is calculation of a photolysis rate. Simplified representations of photolysis are used by CTMs which consider a limited binning of a spectrum by wavelength (e.g. FAST-J, Wild et al. 2000), instead of an entire high resolution absorption spectrum. This is then combined with fields of key absorbing species (e.g. aerosols, clouds, and O_3) to allow for photolysis rates to be calculated.

1.4.1.3 Transport

Transport in a CTM framework is driven by the stored output from other models. The models that are used for this purpose tend to be GCMs, ESMs, or weather forecasting models. These are run with observational assimilation in them and "nudged" to match observations. The input to CTMs typically includes meteorology variables such as wind vectors, temperature, pressures, and water content fields. The downside of using these offline fields in CTMs is that chemistry-climate interactions cannot be quantified as feedbacks between the chemical composition and transport are not possible.

1.4.1.4 Deposition

Atmospheric removal via wet deposition occurs in both frontal and convective clouds. This can be calculated from the inputted meteorology, which typically includes liquid water/ice content of each grid box and is combined with Henry's law values for a given species (Liu et al., 2001) to evaluate loss of a particular compound to rain.

Dry deposition is typically calculated using a resistance in series scheme (Wesely, 1989). This is dependent on surface type, which is defined in models by land type maps (e.g. Olson et al. 2001). Where deposition occurs on to water, the deposition will be highly dependent on ions and DOM present in the aqueous phase (Sarwar et al., 2016). When deposition occurs to land with vegetation present, then resultant uptake will be heavily dependent on the uptake into the plant's stomata and the meteorology (Wesely and Hicks, 2000). For some species like O_3, dry deposition is very uncertain and highly dependent on land type (Hardacre et al., 2015).

1.5 Halogens in the troposphere

The aims of thesis are to better understand the role of halogens in defining the composition of the troposphere. Historically the scientific focus on atmospheric halogens (Cl, Br, I) has been on the stratosphere. A lot of this work was driven by discovery of polar O_3 column depletion in the 1980s and 1990s, and led to a detailed understanding of halogen's ability to catalytically destroy O_3. A large body of work exists to explain O_3 loss in the stratosphere (e.g. Montzka et al. 2011; Reimann et al. 2014; Solomon et al. 1994). Over the decades that followed, the understanding of the impacts of reactive halogens in the troposphere has been increasing. Techniques to measure species at lower concentrations have been developed along with the accompanying theory on their reactions and sources (Simpson et al., 2015). The main sources and processes are shown schematically in Figure 1.5a, alongside a simplified halogen reaction scheme in Figure 1.5b.

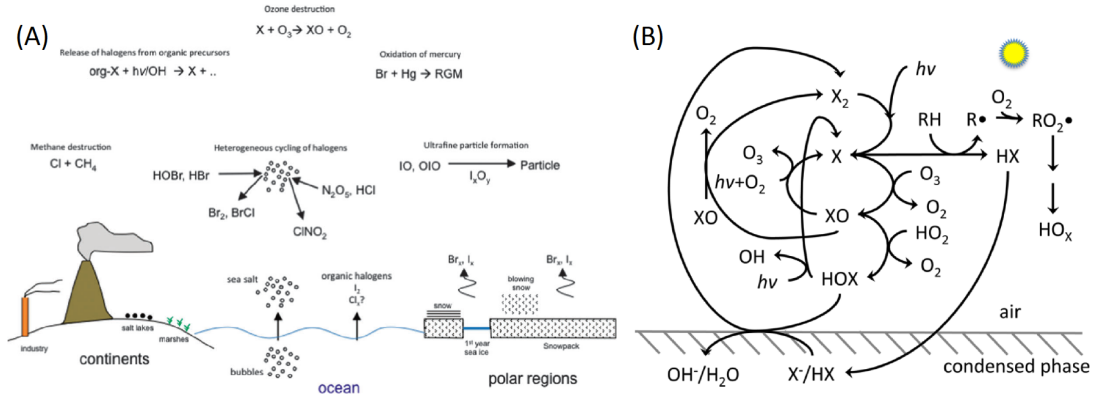

Figure 1.3 – (A) Schematic representation of the main halogen processes in the troposphere. Reproduced from Saiz-Lopez and von Glasow (2012). (B) Simplified schematic reaction scheme for tropospheric halogens ("X", X=Cl, Br,I). Reproduced from Simpson et al (2015).

Bromine and iodine have been identified as additional sinks for tropospheric O_3 and as sources of perturbations to OH cycling (Chameides and Davis, 1980; von Glasow et al., 2004). However, other than at the surface at polar spring time, halogen chemistry had not been considered significant on a global scale in the troposphere. This started to change in the late 2000s with observations reported by Read et al. (2008). These measurements showed the potential for a global impact of bromine and iodine as significant concentrations of IO and BrO ($\sim$1-4 pmol mol^{-1}) were seen at Cape Verde in the North Atlantic. These observations were thought to be representative of the open ocean, rather

then previous measurements which all had been coastal, and thus suggested a widespread role for halogens. The observed diurnal O_3 loss at this location was greater than that shown by models that only included conventional NO_x and HO_x chemistry, but could be accounted for by including halogen chemistry. This is shown by Figure 1.4 from Read et al. (2008) which shows modelled concentrations with and without halogen chemistry alongside observations.

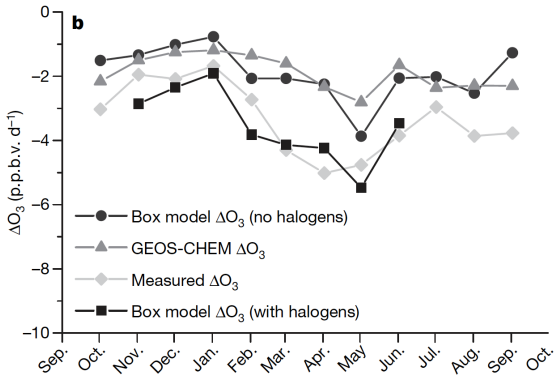

Figure 1.4 – Observed (diamonds) and modelled average monthly diurnal cycle (ΔO_3, over 8 h (09:00-17:00 UT) at Cape Verde. Modelled values are from GEOS-Chem (triangles), from a box-model with (squares) and without halogen chemistry (circles). Reproduced from Read et al. (2008).

Halogens are known to destroy O_3 through catalytic cycles (Chameides and Davis, 1980), such as those shown in reactions 1.17-1.19 and 1.21-1.24. Tropospheric halogens have also been shown to change OH concentrations (Bloss et al., 2005a) and perturb OH to HO_2 ratios towards OH (Chameides and Davis, 1980) by photolysis of HOX (Reactions 1.17-1.19). Halogens perturb the NO to NO_2 ratio towards NO_2 (Reactions 1.21-1.24) and reduce NO_x concentrations by hydrolysis of XNO_3 (Reaction 1.20). These perturbations also indirectly decrease O_3 formation (von Glasow et al., 2004; Schmidt et al., 2016).

$$O_3 + X \rightarrow XO + O_2 \tag{1.17}$$

$$HO_2 + XO \rightarrow HOX + O_2 \tag{1.18}$$

$$HOX \xrightarrow{h\nu} OH + X \tag{1.19}$$

$$Net : HO_2 + O_3 \rightarrow 2O_2 + OH$$

$$XNO_3 + H_2O \xrightarrow{aq.} HOX + HNO_3 \tag{1.20}$$

$$X + O_3 \rightarrow XO + O_2 \tag{1.21}$$
$$XO + NO_2 \xrightarrow{M} XNO_3 \tag{1.22}$$
$$XNO_3 \xrightarrow{h\nu} X + NO_3 \tag{1.23}$$
$$NO_3 \xrightarrow{h\nu} NO + O_2 \tag{1.24}$$

$$net : O_3 + NO_2 \rightarrow NO + 2\,O_2$$

Halogens directly oxidise organics species via hydrogen abstraction to RO_2 species, with Cl radical reactions proceeding the fastest (Atkinson et al., 2006; Sander et al., 2011). This can lead to significant O_3 formation (Knipping and Dabdub, 2003), for instance on regional scale when Cl concentrations are high where $ClNO_2$ concentrations are elevated (Sarwar et al., 2014).

They also play an important role in determining the chemistry of mercury (Holmes et al., 2009; Parrella et al., 2012; Wang et al., 2015; Coburn et al., 2016) by converting elemental mercury to methyl mercury (Reactions 1.25-1.27).

$$Hg + Br \xrightarrow{M} HgBr \tag{1.25}$$
$$HgBr \xrightarrow{M} Hg + Br \tag{1.26}$$
$$HgBr + X \xrightarrow{M} HgBrX \tag{1.27}$$

The literature on tropospheric halogens has been the topic of several recent reviews, which cover the background in more detail (Simpson et al., 2015; Saiz-Lopez et al., 2012b; Saiz-Lopez and von Glasow, 2012). However, many uncertainties still exist, notably with heterogeneous halogen chemistry (Abbatt et al., 2012; Crowley et al., 2010; Saiz-Lopez and von Glasow, 2012), and gas-phase iodine chemistry (Saiz-Lopez et al., 2014; Sommariva et al., 2012).

1.6 Atmospheric iodine

Much of the focus for the stratospheric work has been on the chemistry of bromine and chlorine. However, in the troposphere iodine is thought to play the dominant role (Simpson et al., 2015). Historically, the dominant source of iodine in the atmosphere was thought to be iodinated organic compounds from the ocean (Carpenter, 2003). Initially methyl iodide (CH_3I) was considered the largest source, but it was realised that, despite their low concentrations, other organo-halogens (CH_2I_2, CH_2IBr, CH_2ICl) with faster photolysis rates would lead to these compounds having a greater flux (Chuck et al., 2005; Jones et al., 2010; Law and Sturges, 2006). More recently, the emission of inorganic halogen compounds (I_2 and HOI) has been identified as a significant flux of iodine into the atmosphere (Carpenter et al., 2013).

Due to the short lifetimes and their low atmospheric concentrations, measuring iodine species poses significant challenges and so the observational dataset is sparse. For decades, measurements have focused on organic compounds and mainly on CH_3I (Saiz-Lopez and von Glasow, 2012). Technique development for in-situ measurements has led to an increase in data availability over the last decade, for both organic (e.g. CH_3I and CH_2IX, with X=Cl, Br, I) and inorganic (e.g. IO, OIO, I_2) species (Saiz-Lopez et al., 2012b). In addition, satellites have attempted to obtain global coverage, but retrieval at tropospheric concentrations is problematic (Schönhardt et al., 2008).

The tropospheric chemistry of iodine has been described in detail in recent publications (Saiz-Lopez and von Glasow, 2012; Sommariva et al., 2012) and is shown schematically in Figure 1.5. The following sections describe the chemistry of iodine from its sources (Sect. 1.6.1), to its effects on key oxidant cycles (Sect. 1.6.2), its loss processing in the atmosphere (Sect. 1.6.3), and previous modelling (Sect. 1.7).

1.6.1 Sources

1.6.1.1 Organic iodine

Organo-iodine emissions are overwhelmingly oceanic and these are highly spatially variable. Sources are from biotic (e.g. micro- and macro- algae) and abiotic (e.g. reactions

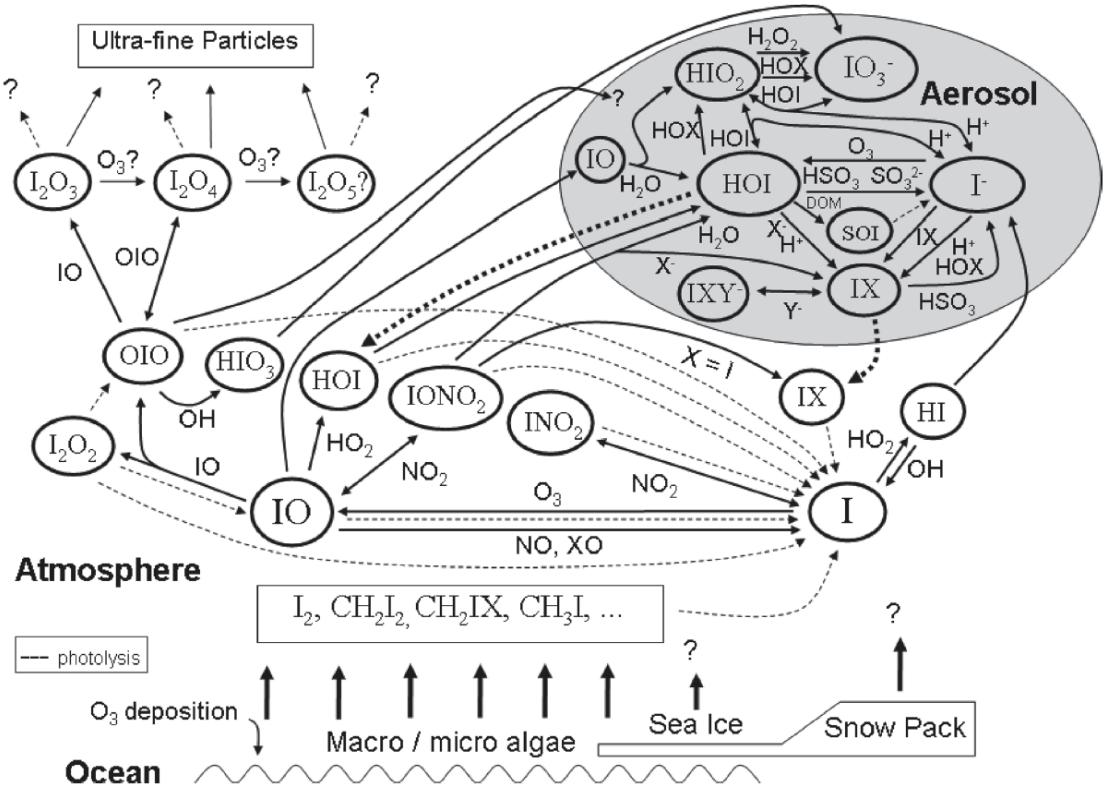

Figure 1.5 – "Simplified schematic of atmospheric iodine photochemistry, based upon current knowledge of gas- and condensed-phase processes". "Dashed lines represent photolysis, whereas dotted lines illustrate phase equilibration from aerosols. X and Y are halogen atoms, DOM is dissolved organic matter, and SOI is soluble organic iodine". Figure and caption reproduced from Saiz-Lopez et al. (2012b).

in surface waters) processes in the oceans, as well as some small terrestrial processes (e.g. biomass burning, rice paddy emissions; Bell et al. 2002). Higher fluxes associated with macroalgae have been noted in coastal regions relative to open oceans (Saiz-Lopez et al., 2012b). However, when the area of oceans are considered, this coastal flux is considered a small fraction of the total global (Saiz-Lopez et al., 2012b). The majority of CH_3I is biotic and abiotically sourced from the oceans (Bell et al., 2002), from oxidation of dissolved organic matter (DOM) and iodide. In addition to oceanic sources, terrestrial sources (e.g. from rice paddies) have also been suggested to contribute significantly (Bell et al., 2002). Di-halogen species (CH_2I_2, CH_2IBr, CH_2ICl) can be formed through biotic or abiotic process, for instance CH_2ICl from CH_2I_2. This is occurs through photolysis of CH_2I_2, then reaction with Cl^- in oceanic surface waters. Following production in the ocean, the transfer of these species into atmosphere is dictated by surface conditions (e.g. wind speed and temperature), species concentrations on both the water and gas side, and the individual species' Henry's law value.

Limited gas and water observations are available for organo-halogens and only a couple flux studies are in the literature for organo-iodine species (Jones et al., 2010; Carpenter et al., 2015). However, as shown in Table 1.3, recent work has brought together available data to estimate global emissions for multiple halogen species (CH_3I, CH_2I_2, CH_2ICl, CH_2IBr; Ordóñez et al. 2012) and solely CH_3I (Ziska et al., 2013).

Table 1.2 – Reported estimates of global iodine species emission budgets in Tg (I) yr^{-1}. Header abbreviations equate to the following publications: J10=Jones et al. (2010); B02=Bell et al. (2002), Z13= Ziska et al. (2013); O12=Ordóñez et al. (2012); B10=Breider (2010). (*) Ziska et al. (2013) CH_3I emissions only include oceanic sources.

Species	J10	B02	Z13	O12	B10
CH_3I	0.3	0.275	0.16-0.18(*)	0.271	0.223
CH_2I_2	0.11	-	-	0.11	0.105
CH_2ICl	0.17	-	-	0.168	0.012
CH_2IBr	0.05	-	-	0.05	0.053
CH_2H_5I	0.02	-	-	-	0.023
CH_3H_7I	<0.01	-	-	-	0.008
Total	0.65	-	-	0.588	0.528

1.6.1.2 Inorganic iodine

Similarly to organo-iodine, significant coastal concentrations of I_2 have been measured (McFiggans et al., 2000), but until I_2 was measured by Lawler et al. (2013), no remote open ocean mixing ratio observations were available of inorganic iodine. Furthermore, no measurements of in-situ emission fluxes of inorganic iodine species have been made in the open-ocean. However, multiple studies have found that observed open-ocean IO concentration and diurnal profiles cannot be explained with the known organic sources (Großmann et al., 2013; Jones et al., 2010; Mahajan et al., 2010). These studies have invoked an additional iodine flux from a short-lived compound, assumed to be I_2, to reproduce surface IO observations.

Proposed mechanisms for this missing ocean source have been: UV stimulated emission (Miyake and Tsunogai, 1963); reaction between DOM, O_3, and iodide (stimulating release of organo-iodide species, Martino et al. 2009); laminar layer reactions of iodide and O_3 (Carpenter et al., 2013; Garland and Curtis, 1981); and underestimated I_2 release from sea-salt aerosol (Großmann et al., 2013). Further laboratory and field based observations have enabled testing of these proposed mechanisms. For instance, the UV stimulated release has been shown to operate too slowly to contribute significantly within environmental conditions (Truesdale, 2007). Anti-correlation of gaseous IO to ocean DOM and chlorophyll-a concentrations has been measured (Gómez Martín et al., 2013b; Mahajan et al., 2012), which implies a biotic release mechanism or one requiring DOM is not responsible for observed IO concentrations. Furthermore, the suppression of iodine flux with increased DOM concentrations has also been observed under laboratory conditions (Shaw and Carpenter, 2013).

Work has shown aqueous surface oxidation reactions lead to release of inorganic iodine (HOI and I_2) under laboratory conditions (Carpenter et al., 2013; MacDonald et al., 2014; Reeser and Donaldson, 2011). This mechanism was originally proposed by Garland and Curtis (1981) whereby O_3 uptake to the ocean and its subsequent reaction with iodide (I^-) leads to volatilisation of inorganic iodine from the ocean. Prior to Carpenter and co-workers, a direct oxidation source for I_2 had been shown (Hayase et al., 2010; Sakamoto et al., 2009). Significantly, however Carpenter and co-workers found that the magnitude of the inorganic source was "similar" to that from previously reported organic fluxes

and majority in the form of HOI (opposed to I_2). The modelled fluxes for HOI (~7 x10^7 molecules cm^{-2} s^{-1}) and I_2 (~7 x10^6 molecules (I_2) cm^{-2} s^{-1}) from this source were shown to replicate gaseous iodine (IO) measured at Cape Verde (Read et al., 2008; Mahajan et al., 2012). This laboratory work gave a parameterisation for HOI and I_2 fluxes as a function of surface iodide concentration, O_3 concentration, wind speed at 10 meteres, and surface temperature (Carpenter et al., 2013; MacDonald et al., 2014). Considering these inorganic iodine fluxes in global models has lead to an estimation of the inorganic iodine flux of 1.9 Tg (I) yr^{-1} (Saiz-Lopez et al., 2014; Prados-Roman et al., 2015b), larger than the previously assumed I_2 flux of ~1.2 Tg (I) yr^{-1} (Saiz-Lopez et al., 2012a)

Prior to the laboratory work of Carpenter and co-workers (2013), box modelling found that the best fit between modelled and measured IO was by achieved by with a daytime peak in I_2 emissions following actinic flux (Mahajan et al., 2010). The first open-ocean observation of I_2, made at Cape Verde (Lawler et al., 2013), showed a diurnal profile with a night-time peak. The accompanying 1D modelling work, showed that using the laboratory parameterised scheme from Carpenter et al. (2013) or an emission of I_2 fitted to actinic flux gave best comparison with observations.

The global oceanic depositional flux of O_3 is estimated to be 200-350 Tg O_3 yr^{-1} (Ganzeveld et al., 2009), however this number is highly uncertain with recent estimates above this range (361 Tg O_3 yr^{-1}, Hardacre et al. 2015). Considering this O_3 loss is thought to be in large part due to O_3 reaction with ocean iodide (Ganzeveld et al., 2009; Sarwar et al., 2015, 2016) and the range in modelled O_3 dry deposition values (Hardacre et al., 2015), it is clear that further work is needed resolve this possibly large contribution to the biogeochemical O_3 budget.

1.6.2 Chemistry of iodine and its destruction of ozone (O_3)

Although uncertainties exist, the main iodine cycles that lead to the destruction of O_3 were originally highlighted by Chameides and Davis (1980) and are mostly well defined (Atkinson et al., 2000, 2007; Sander et al., 2011), these are discussed below.

Reactions of iodine are now considered in the following sections. Firstly, in terms of interactions with HO_x (Sect. 1.6.2.1) and NO_x cycles (Sect. 1.6.2.2). Then iodine self reactions (IO_x) are then considered (Sect. 1.6.2.3). Finally, the heterogeneous reactions

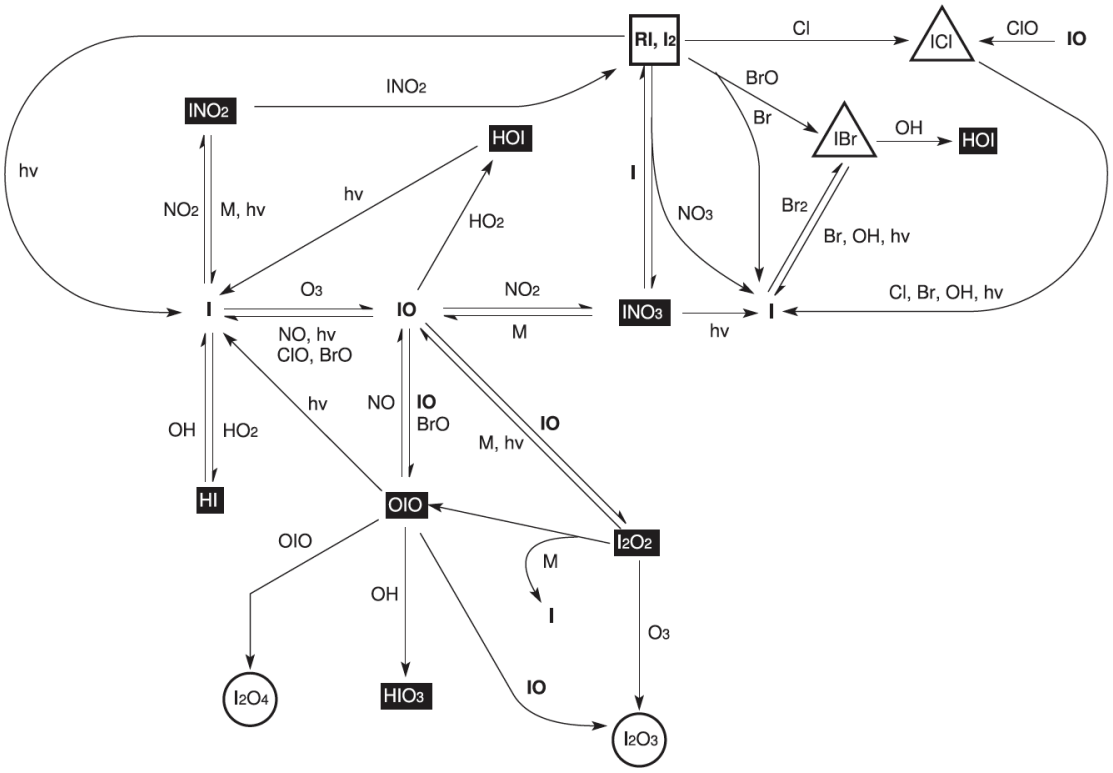

Figure 1.6 – Simplified inorganic iodine gas-phase chemistry schematic. Reproduced from Sommariva et al. (2012). "The unfilled square indicates the iodine source I_2 or iodinated hydrocarbons (RI) the circles indicate the species thought to be involved in new particle formation and the triangles indicate inter-halogen species. Species for which aerosol uptake represents a significant sink are shown in white on black background. Only the most important reactions and species are shown."

of iodine are considered (Sections 1.6.2.5 - 1.6.2.6).

1.6.2.1 HO_x interactions

Atomic iodine reacts directly with O_3 forming IO (Reaction 1.28), but this reaction does not directly deplete O_3 as the atomic oxygen is regenerated (Reaction 1.30) after IO is photolysed (Reaction 1.29), completing a "null cycle".

$$I + O_3 \rightarrow IO + O_2 \tag{1.28}$$

$$IO \xrightarrow{h\nu} I + O \tag{1.29}$$

$$O_2 + O + M \rightarrow O_3 + M \tag{1.30}$$

$$Net : null\ cycle$$

Although the majority of IO is photolysed to regenerate atomic iodine and oxygen (Reaction 1.29), secondary reactions between IO and other trace gases allow for transfer of this odd oxygen (O_x). If reactions can then regenerate atomic iodine without releasing O_x then a catalytic cycle is formed causing loss of O_x and therefore a net decrease in O_3. An effective example of this is the IO reaction with the hydroperoxy radical (Reaction 1.32) forming HOI, which is photolysed (Reaction 1.33) to regenerate atomic iodine without producing an O_x molecule. This also perturbs the HO_2:OH ratio and therefore also decreases O_3 production, and perturbs lifetimes of species which are dependent on OH (e.g. CH_4) (Saiz-Lopez et al., 2012b). This IO reaction route through HO_2 is the major loss route at lower (< 1 pmol mol^{-1}) IO concentrations (Saiz-Lopez et al., 2012a).

$$I + O_3 \rightarrow IO + O_2 \tag{1.31}$$

$$IO + HO_2 \rightarrow HOI + O_2 \tag{1.32}$$

$$HOI \xrightarrow{h\nu} I + OH \tag{1.33}$$

$$net : O_3 + HO_2 \rightarrow OH + 2\,O_2$$

1.6.2.2 NO_x interactions

In semi polluted or polluted atmospheres where NO_x is present in relatively high concentrations (e.g. 1 nmol mol^{-1}), IO interacts significantly with both NO_2 (Reactions 1.35-1.38) and NO (Reactions 1.40-1.42). The efficiency of the reaction of IO with NO_2 reaction (Reaction 1.35) as an ozone-depleting route is limited by the channel for NO_3 photolysis (Reaction 1.38) that releases $2\,O_x$ thus forming a null cycle for O_x.

In addition, the reaction of NO with IO converts NO to NO_2, which increases the NO_2:NO ratio (Saiz-Lopez et al., 2012a) which again shifts the chemical system to reduce O_3 production, but forms a null cycle (Reactions 1.40-1.42).

$$I + O_3 \rightarrow IO + O_2 \tag{1.34}$$
$$IO + NO_2 \xrightarrow{M} INO_3 \tag{1.35}$$
$$INO_3 \xrightarrow{h\nu} I + NO_3 \tag{1.36}$$
$$NO_3 \xrightarrow{h\nu} NO + O_2 \tag{1.37}$$
$$\xrightarrow{h\nu} NO_2 + O \tag{1.38}$$

$$net : O_3 + NO_2 \rightarrow NO + 2\,O_2 \text{ (assuming 1.37)}$$

$$I + O_3 \rightarrow IO + O_2 \tag{1.39}$$
$$IO + NO \xrightarrow{M} I + NO_2 \tag{1.40}$$
$$NO_2 \xrightarrow{h\nu} NO + O \tag{1.41}$$
$$O_2 + O + M \rightarrow O_3 + M \tag{1.42}$$

$$Net : null\ cycle$$

In addition to catalytic destruction through gas-phase chemistry, halogens can interact with NO_x chemistry by removing NO_x heterogeneously through halogen nitrate/nitrite hydrolysis as discussed further in Section 1.6.2.5, which again leads to lower O_3 concentrations.

1.6.2.3 Iodine self reactions and higher oxide chemistry

At higher IO concentrations (>2 pmol mol^{-1}, Saiz-Lopez et al. 2012b) IO can also react with itself (Reactions 1.44-1.59), creating another effective catalytic O_x loss cycle through the $I + O_2$ product channel (Reaction 1.46). The alternate channel (Reaction 1.59) forming I_2O_2 can either form a "null cycle" by photolysing back to OIO+I or thermally decomposing to IO+IO (Reaction 1.47), or be physically lost (e.g. deposition or aerosol uptake) resulting in a termination step.

$$I + O_3 \rightarrow IO + O_2 \tag{1.43}$$

$$IO + IO \xrightarrow{M} OIO + I \tag{1.44}$$

$$\xrightarrow{M} I_2O_2 \tag{1.45}$$

$$OIO \xrightarrow{h\nu} I + O_2 \tag{1.46}$$

$$I_2O_2 \xrightarrow{M} I + O_2 \tag{1.47}$$

$$I_2O_2 \xrightarrow{M} IO + IO \tag{1.48}$$

$$net : 2\,O_3 \rightarrow 3\,O_2 \text{ (assuming 1.46 or 1.47)}$$

Iodine has been shown to form iodine oxide particles (Burkholder et al., 2004; Gómez Martín et al., 2007; McFiggans et al., 2004) primarily through condensation of higher iodine oxides (I_xO_y). However measurements for specific reactions rate constants between higher iodine oxides remain poorly defined and debate continues about possible formation routes as described by recent reviews (Saiz-Lopez et al., 2012b; Sommariva et al., 2012). Essentially the proposed routes are sequential growth through addition of OIO, e.g. continuation of Reactions 1.53, or through sequential addition of O by reaction of I_2O_X with O_3 to form I_2O_{X+1} (Sommariva et al., 2012). However, the latest work has cast doubt on the latar of these routes, suggesting the formation of I_2O_4 is the key step in iodine particle formation (Gómez Martín et al., 2013a).

The reason that higher iodine oxides routes have received so much attention within the literature is because of their potential to form particles within the marine boundary layer. The marine atmosphere represents the most pristine environment on the planet, and is very sensitive to changes and feedbacks in the nature and abundance of these aerosol

precursors (Quinn and Bates, 2011). A new route to forming particles, e.g. a source of cloud condensation nuclei (CCN), within the marine boundary layer could have significant climatic effects.

$$I + O_3 \rightarrow IO + O_2 \tag{1.49}$$

$$IO + IO \rightarrow OIO + I \tag{1.50}$$

$$\rightarrow I_2O_2 \tag{1.51}$$

$$IO + OIO \rightarrow I_2O_3 \tag{1.52}$$

$$OIO + OIO \rightarrow I_2O_4 \tag{1.53}$$

$$I_xO_y \rightarrow aerosol \tag{1.54}$$

The "cut-off" point for oxidation of iodine to higher oxides varies between studies. Some studies include O_3 loss via $I_2O_2 + O_3$ oxidation (Breider, 2010) or do not include reactions past I_2O_2 (Ordóñez et al., 2012). This decision of which reactions to include is highly uncertain, due to unknowns on the reversibility of the higher oxide loss route. One study particularly highlights this, where the majority of iodine driven O_3 loss is observed through the included $I_2O_2 + O_3$ oxidation route (Breider, 2010), which is effectively treating all higher iodine oxides as completely stable. The stability of these compounds get significant attention within literature (Saiz-Lopez et al., 2012b), and some recent work has even considered global impacts of iodine without higher oxides photolysis (Saiz-Lopez et al., 2014).

1.6.2.4 IO + BrO cross-over reactions

The gas-phase chemistry of iodine and other halogens (Br, Cl) chemistry can couple (Sander et al., 2011). With bromine, this can directly lead to O_x loss through reaction of IO + BrO to reform atomic I and Br (Reaction 1.58), or indirectly through production of OIO (Reaction 1.57) which results in the same end products.

$$\mathrm{I} + \mathrm{O_3} \rightarrow \mathrm{IO} + \mathrm{O_2} \tag{1.55}$$

$$\mathrm{BrO} + \mathrm{O_3} \rightarrow \mathrm{BrO} + \mathrm{O_2} \tag{1.56}$$

$$\mathrm{IO} + \mathrm{BrO} \rightarrow \mathrm{OIO} + \mathrm{Br} \tag{1.57}$$

$$\mathrm{IO} + \mathrm{BrO} \rightarrow \mathrm{Br} + \mathrm{I} + \mathrm{O_2} \tag{1.58}$$

$$\mathrm{OIO} \xrightarrow{h\nu} \mathrm{I} + \mathrm{O_2} \tag{1.59}$$

$$net : 2\,\mathrm{O_3} \rightarrow 3\,\mathrm{O_2}$$

This coupling of iodine and bromine chemistry has been shown to increase O_3 depletion four fold (Saiz-Lopez et al., 2012b), and that the total halogen loss of O_3 (inc. Reaction 1.58) is greater than the sum of individual halogen O_3 loss routes (Read et al., 2008).

Equivalent reactions to the reactions 1.55 and 1.58 are known for chlorine species. However, for chlorine these reaction are slower (Sander et al., 2011), due to the relatively less labile nature of chlorine vs. bromine.

1.6.2.5 Iodine interactions with aerosols

The aerosol phase is known to be an iodine sink with I:Na ratios showing enrichment of iodine in marine aerosol relative to the ocean (Duce and Hoffman, 1976). Although iodine uptake take to the aerosol phase has been measured for certain inorganic species (Crowley et al., 2010) the aqueous processing and interactions with the gas phase are complex and considerable uncertainties remain. Of particular note is the speciation of iodine within aerosol, where iodine, iodate and organic iodine are all present (Baker, 2005).

The loss rate of a molecule (X) due to multiphase processing on aerosol can be calculated using Equation 1.60 (as described in detail by Jacob 2000). Where r is the aerosol effective radius, D_g is the gas phase diffusion coefficient of X, c is the average thermal velocity of X, γ is the reactive uptake coefficient, A is the aerosol surface area concentration, and n_X is the gas phase concentration of X.

$$\frac{dn_X}{dt} = -\left(\frac{r}{D_g} + \frac{4}{c\gamma}\right)^{-1} A n_X \tag{1.60}$$

Varying assumptions are made in different modelling studies as to which species to consider uptake for. This varies from a majority of soluble reservoir species (HI, HOI, IO, OIO, HIO_3, INO_2, INO_3; Saiz-Lopez et al. 2007b) to solely HOI, INO_2 and INO_3 (Ordóñez et al., 2012). Uptake values for HOI, INO_2, INO_3, HI, and I_2O_X are described below.

The JPL compilation notes a single experimental study of HOI uptake on H_2SO_4, yielding mass accommodation coefficients (α) in the range 0.02 to 0.07 (Sander et al., 2011). Another two studies on ice and salt are reported in JPL 10-6 with lower limits of >0.0022 and >0.01 respectively (Sander et al., 2011). IUPAC evaluates two experimental studies which "concur [the] uptake coefficient is large", but no recommendation is given due to possible uncertainties in reversibility (Crowley et al., 2010). The γ values used in literature range between 0.01 (Mahajan et al., 2009; Breider, 2010) and 0.5 (Saiz-Lopez et al., 2007b). The higher end of this range originates from an investigation of the sensitivity to this parameter within THAMO by Saiz-Lopez et al. (2007b), for which the base-case was set as 0.02.

For INO_2 and INO_3 no experimental work is available on the uptake parameters and values have previously been estimated by analogy with measured equivalent bromine species. For INO_3 a γ value of 0.01 has been frequently used (Mahajan et al., 2009; Ordóñez et al., 2012), but values have been used up to 0.2 (Bloss et al., 2010). For INO_2 γ values of 0.01 (Mahajan et al., 2009) or 0.02 (Ordóñez et al., 2012; Saiz-Lopez et al., 2007b) have often been used, but γ values up to 0.1 have also been used (Bloss et al., 2010).

The IUPAC compilation includes a recommendation for HI uptake γ on ice of 0.2 (Crowley et al., 2010), based on three experimental studies. A γ value of 0.1 has most often been used in modelling studies (Breider, 2010; Mahajan et al., 2009; Saiz-Lopez et al., 2008). For I_2O_X (X = 2,3,4) no experimental data is available for reactive uptake coefficients. The uptake has been discussed in the literature, including a box model study which tested sensitivity around a base value of 0.02 (Saiz-Lopez et al., 2008). This value is highly uncertain and values up to 1 have been used for gamma in modelling studies (Bloss et al., 2010).

As well as a role as possible source, sink, or cycling for a given halogen, the uptake of soluble halogen species (e.g. XNO_2, XNO_3) provides a sink for NO_y/NO_x from the atmosphere leading to "de-noxifcation". This indirectly will reduce O_3 concentrations,

due to suppression of O_3 production routes via NO_x (Sect. 1.3.2.2).

1.6.2.6 Heterogeneous cycling

Following uptake of iodine onto sea-salt aerosols, acid catalysed cycling of I^+ can lead to the release of IX (X=Cl, Br, I) (McFiggans et al., 2000; Braban et al., 2007). This proceeds via hydrolysis of I^+ (from HOI, INO_2, INO_3) to HOI then oxidation to IX (Reaction 1.61). IX easily volatilises into the gas phase due to its Henry's law solubility.

$$HOI_{(aq)} + X^-_{(aq)} + H^+ \rightarrow IX_{(aq)} + H_2O_{(aq)} \tag{1.61}$$

The ability of this process to occur is acid dependent (Eqns. 1.61), and the resulting split between ICl and IBr will be highly dependent on halide concentrations, which in turn depends on age of aerosol as marine aerosol is known become significantly depleted in bromine and chlorine over time. McFiggans et al. (2002) noted IBr release may dominate ICl production from fresh sea-salt aerosols. More recent laboratory work by Braban et al. (2007) further shown that unless bromide is significantly depleted, that IBr will be the major emission.

This cycling between the gas and aerosol phase has been studied explicitly (Vogt et al., 1999; Pechtl et al., 2007), however it remains a large source of uncertainty. In addition when recent observations of I_2 were made at a remote marine site (Cape Verde, Lawler et al. 2013), the inability to measure di-halogen species (BrCl, ICl, IBr) "strongly suggest[ed]" that models may over predict aerosol recycling.

1.6.2.7 Uncertainties in iodine chemistry

There are significant uncertainties in iodine's chemical kinetics. The reaction mechanisms of iodine have been covered in depth by a range of reviews (Carpenter, 2003; Saiz-Lopez et al., 2012b,a; Simpson et al., 2015), with further recent work assessing uncertainties within known reactions through box-modeling (Sommariva et al., 2012). A schematic representation of the main pathways is shown in Figure 1.6, reproduced from Sommariva et al. (2012).

Through JPL (Sander et al., 2011) and IUPAC (Atkinson et al., 2000, 2006, 2007, 2008) compilations, a large body of experimental and theoretical work on iodine has been evaluated. However the experimental rate data are limited or non-existent for certain processes. For example the ultimate chemical fate of all higher iodine oxides (I_2O_X, where X $\geq$2) is poorly quantified, yet these reactions can significantly affect the IO_x lifetime (Sommariva et al., 2012). I_2O_X forms through combination reactions (see Sect. 1.6.2.3), however questions remain about their polymerisation, photolytic properties and eventual fate as discussed further by Saiz-Lopez et al. (2012b). Recent work has shown some of the key iodine species to be well buffered to mechanism uncertainties, but highlights the sensitivity of iodine concentrations and hence atmospheric impacts of this higher oxide chemistry (Sommariva et al., 2012).

1.6.3 Atmospheric processing

1.6.3.1 Dry and wet deposition

Methods for calculating dry and wet deposition require knowledge of Henry's law values and enthalpies of formation for given species. For iodine these values are known for most species (Sander, 1999, 2015) or have been estimated by analogy with similar most studied bromine species previously (Saiz-Lopez et al., 2007b). For less well defined species, such as I_2O_X, theoretical calculation calculations exist for enthalpies of formation (Kaltsoyannis and Plane, 2008).

1.6.3.2 Photolysis

Iodine has a low ionisation energy and forms labile species. This leads to species with short lifetimes with seconds (I_2/HOI), minutes (CH_2I_2), hours (CH_2ICl), and days (CH_3I).

Absorption cross-sections are recommended for all key iodine species (I_2, HOI, IO, OIO, INO, INO_2, INO_3, CH_3I, CH_2I_2, CH_2IBr and CH_2ICl) within the latest JPL compilation (Sander et al., 2011). Temperature dependencies are not given (except for CH_3I) and uncertainties remain for quantum yields. Higher iodine oxide (for I_xO_y where x and y are greater than 1) cross-sections are not reported in current JPL/IUPAC compilations (Sander et al., 2011). A single study has reported values "likely" values for I_2O_2 and

I_2O_3 from data extracted from a study of the IO spectrum (Spietz et al., 2005). Other modelling studies have assumed I_xO_y to have cross sections equivalent to INO_3 by analogy (Bloss et al., 2010) based on "estimates of Bloss et al. (2001) and Gómez Martín et al. (2005), and ab initio results (Kaltsoyannis and Plane, 2008)".

A previous controversy existed with the magnitude of cross-section of OIO (Carpenter, 2003) as the species was observed in daytime (Stutz et al., 2007). However this is now resolved following work by Gómez Martín et al. (2009). Photolysis has been shown to occur at 500-650 nm and the recommended cross-section is given by JPL (Sander et al., 2011). A second historical controversy revolved around the photolysis channels of INO_3 and this limited the understanding of effectiveness of iodine initiated O_3 destruction (Carpenter, 2003), and this has now also been resolved (Saiz-Lopez et al., 2012b).

1.6.4 Observational constraints

1.6.4.1 Organic iodine species

Making observations of iodine species is challenging as they are very short-lived, due to rapid destruction routes by photolysis or oxidation. The longest lifetime iodine species CH_3I (6 days, Bell et al. 2002) is unsurprisingly the most measured. With that said, the increased availability of observations has enabled increased comparisons with models and the development of global organic halogen emission schemes (Ordóñez et al., 2012). Ordóñez and co-workers (2012) used the correlation between observations of species and their sources (e.g. biotic, abiotic), using satellite chlorophyll-a as a proxy for concentration, and accounted for increased emission in coastal regions versus open oceans using scaling factors. This work included iodo-carbon species (CH_3I, CH_2IBr, CH_2ICl, CH_2I_2) as well as bromo-carbon ($CHBr_3$, CH_2Br_2, CH_2BrCl,$CHBrCl_2$, $CHBr_2Cl$) species. Recently Ziska et al. (2013) have used the growing dataset of ocean surface concentrations to calculate fluxes of halogen species, however CH_3I was the only iodine species calculated.

1.6.4.2 Inorganic iodine species

Differential Optical Absorption Spectroscopy (DOAS) methods led to the first measurements of IO (Alicke et al., 1999). Since then a few studies have explored coastal regions,

where iodine fluxes are higher and observed concentrations from a few to tens of pmol mol^{-1} (see Saiz-Lopez et al. 2012b and citations within). Observations have also shown IO in the Antarctic, over salt lakes, and in volcanic plumes. However for many years the observations were more indicative of localised iodine processes, than of a globally significant phenomena.

Improved approaches allowed detection of lower concentrations of IO from ground stations in open-ocean/remote environments, which are arguably more representative of the global atmosphere over oceans (Mahajan et al., 2010; Read et al., 2008). This suggested that reactive iodine chemistry was more widespread than previously thought. Then with the onset of DOAS techniques that do not require a stationary point (e.g. MAXI-DOAS), detection of IO from ships in the open ocean in the Atlantic, Western Pacific (Großmann et al., 2013), Eastern Pacific (Gómez Martín et al., 2013b; Mahajan et al., 2012) and more recently a circumnavigation (Prados-Roman et al., 2015b) was possible. This increase in observations has enabled datasets of IO observations with extensive geographical coverage (Prados-Roman et al., 2015b), to be produced (Fig 1.7). This has established the global ubiquity of iodine oxide over the open oceans.

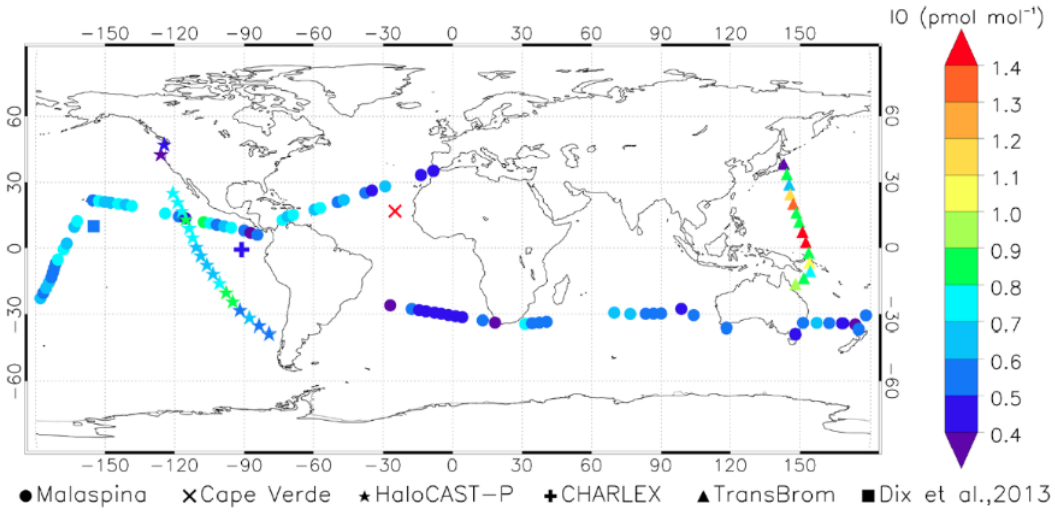

Figure 1.7 – Marine boundary layer iodine monoxide (IO) observations from ship cruise and coastal stations in pmol mol^{-1}. Reproduced from Prados-Roman et al. (2014).

Spatial variability in reported iodine (IO) observations is apparent, with reported values in the eastern Pacific (Gómez Martín et al., 2013b) lower compared to those in the Atlantic (Read et al., 2008) and western Pacific (Großmann et al., 2013). This further poses

questions about precursor sources and source mechanisms. Concurrent measurements of other related parameters (e.g. chlorophyll concentrations, salinity, DOM levels, and O_3; Gómez Martín et al. 2013b) show correlations (e.g. positive to salinity, negative to chlorophyll and DOM) suggesting that an inorganic source mechanism (e.g. Carpenter et al. 2013) is more probable than proposed mechanisms dependent on DOM (Martino et al., 2009). It also raises questions about the role of DOM affecting the flux of iodine, which has also been noted in laboratory work (Shaw and Carpenter, 2013).

In addition to surface measurements, measurements of inorganic iodine within the free troposphere from aircraft (Dix et al., 2013; Volkamer et al., 2015; Wang et al., 2015), balloons (Butz et al., 2009), and mountain tops (Puentedura et al., 2012) have been made. The high (2370 m a.s.l.) ground-based measurements in Tenerife estimate IO concentrations of 0.2-0.4 pmol mol^{-1} (Puentedura et al., 2012). Vertical profiles by aircraft in the East Pacific show values of 0.1-0.2 pmol mol^{-1} in the free troposphere (Dix et al., 2013), and more recent aircraft measurements with larger coverage (Volkamer et al., 2015; Wang et al., 2015) again found sub pmol mol^{-1} concentrations of IO throughout the troposphere and again suggesting iodine's ubiquitous vertical presence.

Detection of IO from space using satellites has also been reported (Schönhardt et al., 2008; Saiz-Lopez et al., 2007a). This suggested localised iodine at high concentrations over the Antarctic continent. It also offered the possibility of a substantially new capacity for increase the spatial coverage of iodine observations. However, when IO was also observed from ships based in the same region, it was at lower concentrations. This either contradicted the satellite values or suggested the presence of iodine much higher in the troposphere (Mahajan et al., 2012) than would be expected.

1.6.4.3 Iodine deposition and terrestrial interactions

Other active areas of iodine research, other that for atmospheric chemistry, are on iodine deficiency for public health and iodine radionuclides. There is little overlap of this research and that on the atmospheric cycles of iodine. Datasets exist for iodine within top-soils, sub-soils and rivers (Johnson, 2003a; Selminen, 2013; Shacklette and Boerngen, 1984), and if this could be combined with knowledge of the uptake to the geosphere and biosphere it would be possible to model cycles between the geosphere, hydrosphere, and atmosphere.

The understanding of the processing of iodine from deposition to the ground to uptake into the biosphere has been the subject of some study (Bowley, 2013; Landis et al., 2012; Shetaya, 2011; Shetaya et al., 2012), however due to large differences between soil and plant types, the ability to generally conceptualise global cycles remains out of reach.

Measurements of deposition of iodine could provide a useful constraint when considering atmospheric cycles of iodine, as emitted iodine must balance that deposited. Miyake and Tsunogai (1963) attempted to quantify an iodine budget from the iodine content of rainfall, however the approach taken has been criticised due to uncertainties (Garland and Curtis, 1981). Motivated by quantifying radionuclides from the nuclear industry, larger datasets have since been reported in the literature for Northern Europe (Aldahan et al., 2009) and Germany (Krupp and Aumann, 1999). A 15 month dataset of dry and wet deposition in the marine environment off the East coast of England has also been reported (Baker et al., 2001). If comparable deposition fluxes could be modelled, then this could provide a useful test of a model's representation of iodine cycling.

1.6.4.4 Iodine aerosol

Iodine enrichment within marine aerosols is well known (Duce and Hoffman, 1976). However speciation within aerosols is poorly defined (Baker, 2005; Pechtl et al., 2007), as is our understanding of the magnitudes of sources: e.g. uptake of gas-phase species vs. enrichment processes at point of aerosol formation. Observations of iodine concentrations in aerosol have been reported (Baker et al., 2001; Baker, 2004, 2005; Gilfedder et al., 2010; Lai et al., 2008; Rancher and Kritz, 1980). Values of coastal, island and continental iodine aerosol observations have been compiled within a recent review (Table 5 of Saiz-Lopez et al. 2012b). Few of these are free from coastal influence and therefore fail to give a picture relevant to the majority of the marine environment. A summary of observations in the literature representative of remote marine boundary layer are given in Table 1.3.

1.7 Previous global modelling

Global and regional tropospheric climate and air-quality models have historically not considered halogen chemistry. The majority of previous halogen chemistry work has used

Table 1.3 – Measured iodine aerosol mass concentrations for open ocean observations.

Reference	Location	Observed aerosol iodine min-**mean**-max ng (I) m^{-3}
Baker (2004)	North Atlantic	1.1-**3.9**-11.6
Baker (2005)	Atlantic	1.9-**3.2**-8.0
Gilfedder et al. (2010)	Eastern Tropical Atlantic	4.6-**8.9**-13
Lai et al. (2008)	Western Pacific	1.3-**3.0**-5.1
Rancher and Kritz (1980)	Equatorial Atlantic	2.0-**5.9**-17

box models (e.g. Sander et al. 1997; Mahajan et al. 2009; McFiggans et al. 2000, 2010; Read et al. 2008; Saiz-Lopez et al. 2007b). More recent work using chemistry transport models has focused on bromine (von Glasow et al., 2004; Parrella et al., 2012) and only more recently considered iodine (Ordóñez et al., 2012; Saiz-Lopez et al., 2012b, 2014; Prados-Roman et al., 2015a).

Iodine chemistry has been shown to effectively destroy O_3 by catalytic chemical cycles (Sect. 1.6.2). When considered alongside bromine chemistry, box model studies have shown the magnitude of these halogen driven O_3 loss processes to be up to 45 % of the total loss (Mahajan et al., 2009; Read et al., 2008).

Within global modelling studies, up to ∼30 % of the O_3 loss in the marine boundary layer (900 hPa <p) has been found to be driven by halogens (Prados-Roman et al., 2015b; Saiz-Lopez et al., 2012b, 2014). Similarly, high levels of halogen-driven O_3 loss are also found in the upper troposphere (350 hPa > p > tropopause), with lower (10-15 %) impacts in the free troposphere (350 hPa < p < 900 hPa) (Saiz-Lopez et al., 2012b, 2014). Combined decreases in tropospheric O_3 burden from halogens of 10-15 % have been reported from simulations considering chlorine, bromine and iodine (Saiz-Lopez et al., 2012b, 2014). This contrasts to values from studies that just consider bromine of 6.5 % (Parrella et al., 2012), and 14 % from work considering bromine and chlorine (Schmidt et al., 2016).

Possibly large impacts on O_3 from iodine in the lower stratosphere have been theorised (Solomon et al., 1994). However, due to reported low concentrations and lack of observations, it was thought that iodine could only have a minor role (Saiz-Lopez et al., 2012b). More recently though observations and modelling have suggested that this may not be the case (Saiz-Lopez et al., 2015).

Iodine can change the local HO_2:OH ratio due to the production of HOI from HO_2 + IO and its subsequent photolysis (as discussed in Sect. 1.6.2.1), or through reducing O_3 and reducing OH's primary source (Sect. 1.6.2). The effect of increasing OH concentrations has been noted by multiple box modelling studies accompanying observations (e.g. Bloss et al. 2005b; McFiggans et al. 2000; Saiz-Lopez et al. 2008). In global studies not considering iodine, the effects of OH have been reported to increase OH:HO_2 (Long et al., 2014; Parrella et al., 2012; Schmidt et al., 2016). In a global simulation including bromine and chlorine chemistry, a 11 % decrease in tropospheric OH was seen (Schmidt et al., 2016). However, in a previous study within the same model, but just considering bromine, a decrease of 4 % was found (Parrella et al., 2012).

Perturbation to the NO:NO_2 ratio has been shown to be significant at higher IO concentrations in polluted coastal locations (McFiggans et al., 2010), due to the ability of IO to oxidize NO into NO_2 (Section 1.4.2.2). The ability of halogens to reduce O_3 production through removal of NO_x by halogen photolysis has been reported from global modelling studies (von Glasow et al., 2004; Parrella et al., 2012; Long et al., 2014; Schmidt et al., 2016). In a recent global model study, which included bromine and chlorine chemistry, the impacts of halogens on NO_x were shown to decrease O_3 production by 10 % (Schmidt et al., 2016).

1.8 Pre-industrial (PI) concentrations

For bromine and chlorine species which have a natural and anthropogenic source (e.g. CH_3Br, CH_3Cl, $CHCl_3$, and CH_2Cl_2), the concentrations were lower in the pre-industrial troposphere. For bromine the Br_y is lower within the stratosphere as well (Montzka et al., 2011; Reimann et al., 2014).

As well as direct emission changes in halogen emissions, indirect oxidant changes such as the increase in pollutants (SO_2) leading to more acidic marine aerosols has been suggested to lead to a greater sea-salt bromine source (Sander et al., 2003). Reductions in tropospheric O_3 concentrations relative to the present-day (See Sect. 1.2.1), would also cause a reduction in iodine flux due to its recently established dependence on O_3 (Carpenter et al., 2013; Garland and Curtis, 1981). This negative feedback loop has also recently been explored within a global model (Prados-Roman et al., 2015a).

The lack of inclusion of halogen chemistry within chemistry and climate models has been suggested as a possible contributing factor of why chemistry-climate models find capturing pre-industrial tropospheric O_3 observations problematic (Parrella et al., 2012; Saiz-Lopez et al., 2012a; Young et al., 2013). This has been apparent and known in the literature for over a decade (Mickley et al., 2001a).

1.9 Goals of this work

This work aims to build a simulation of iodine chemistry to allow for our understanding to be tested on global tropospheric scale. The established global chemistry transport model GEOS-Chem (Bey et al., 2001) will be used as a starting point, with additional chemical and physical processes added to the existing scheme. This will enable quantification of iodine's budget and impacts on O_3, HO_x and NO_x. This will also allow for the testing of recently suggested inorganic fluxes (Carpenter et al., 2013) and their implications.

1.10 Thesis outline

Chapter II ("Development of an iodine simulation") describes the additional processes considered in the iodine simulation (e.g. emissions, chemistry, photolysis, and deposition).

Chapter III ("Iodine's gas phase impacts in the present-day") first evaluates the simulation developed in chapter II against observations. Then it considers the impacts of iodine chemistry globally on oxidants (O_3 and OH). The sensitivity of the simulation to key variables is then considered and compared against observations.

Chapter IV ("Global impacts of tropospheric halogens (Cl, Br, I) on present-day oxidants and composition") describes further developments to the simulation to incorporate bromine (Parrella et al., 2012; Schmidt et al., 2016) and chlorine chemistry (Eastham et al., 2014; Schmidt et al., 2016), with associated cross-over chemistry (JPL/IUPAC) and additional tropospheric sources and chemistry. Changes in the modelled distributions are presented and then the resultant impacts of this "coupled" halogen (Cl, Br, I) simulation are considered on the present-day atmosphere.

Chapter V ("Impact of halogen chemistry on tropospheric O_3 radiative forcing") evaluates the impacts of halogen chemistry on O_3 radiative forcing between pre-industrial and present-day.

Chapter VI ("Global modelling of tropospheric iodine aerosol") considers modelled aerosol-phase iodine. The impacts of iodine on aerosol formation in the marine environment are considered. The modelled concentrations are compared against available observations.

Chapter VII summarises the conclusions of preceding chapters and the key overview messages.

Chapter 2

Development of an iodine simulation

The majority of the content of this chapter has been published in "Iodine's impact on tropospheric oxidants: A global model study in GEOS-Chem.": T. Sherwen, M. J. Evans, L. J. Carpenter, S. J. Andrews, R. T. Lidster, B. Dix, T. K. Koenig, R. Sinreich, I. Ortega, R. Volkamer, A. Saiz-Lopez, C. Prados-Roman, A. S. Mahajan and C. Ordóñez, *Atmos. Chem. Phys.*, 2016, **16**, 11611186.

2.1 Introduction

Iodine plays an important role in the atmosphere. It is crucial for human health in diet (WHO, 2009), perturbs the ozone (O_3) budget and therefore can impact air-quality, crop yields and climate change (Saiz-Lopez et al., 2012b).

The chemistry of reactive halogens and especially iodine is discussed in Chapter I. This Chapter describes the development of a simulation of tropospheric iodine chemistry based within the framework of the GEOS-Chem chemical transport model. It will be used in subsequent chapters to explore the impact of iodine (Chapter III) and the wider halogen chemistry (Chapter IV) on the composition of the present day atmosphere. It is then used to explore the potential role of halogen chemistry on the changing concentration of ozone between the pre-industrial and the present day (Chapter V) and on aerosol production in the atmosphere (Chapter VI).

In this chapter the GEOS-Chem model will be described (Sect. 2.1.1). The chemistry and physics of iodine used in the model is described from emissions (Sect. 2.2), gas-phase chemistry (Sect. 2.3), heterogeneous chemistry (Sect. 2.4), photolysis (Sect. 2.5), iodine and bromine cross-over chemistry (Sect. 2.6), and finally deposition (Sect. 2.7).

For readability the "of-the-shelf" version (v9.2) of the model is referred to as "BROMINE", as it includes a description of bromine chemistry (Parrella et al., 2012). The iodine simulation developed in this chapter is referred to as "Br+I".

2.1.1 GEOS-Chem

GEOS-Chem (http://www.geos-chem.org) is 3D Eulerian chemical transport model (CTM) developed and owned by a global community (Bey et al., 2001). Transport within the model is driven by assimilated meteorological and surface data fields (GEOS-5/GEOS-FP) from NASA's Global Modelling and Assimilation Office (GMAO). The model includes a chemistry scheme which describes O_x, HO_x, NO_x, and VOC chemistry (Mao et al., 2013), bromine chemistry (Parrella et al., 2012), and a mass-based aerosol scheme (Alexander et al., 2012; Jaeglé et al., 2011; Fairlie et al., 2007; Pye and Seinfeld, 2010; Wang et al., 2011). Stratospheric chemistry is climatologically represented based on LINOZ (McLinden

et al., 2000) for O_3 and a linearised chemistry is applied for other species from the Global Modelling Initiative (GMI) as described previously (Murray et al., 2012a). The deposition scheme in GEOS-Chem has recently been updated (Amos et al., 2012).

2.2 Emissions

In addition to the NO_x, SO_2, VOCs, organic and black carbon, dust, and sea-salt emissions incorporated in GEOS-Chem (Sect. 2.2.1), iodine is emitted into the atmosphere in both organic and inorganic forms (See Sections 1.6.1 and 1.6.1.2 in chapter I) which we discuss now in Sections 2.2.2 and 2.2.3.

2.2.1 NO_x, SO_x, VOC, and aerosol emissions

The GEOS-Chem CTM used here includes set of natural and anthropogenic emissions that are processed and inputted into the model by the Havard-NASA EMission COmponent (HEMCO, Keller et al. 2014), which also applies any diel or seasonal scaling. Inventories included are biogenic emissions (MEGAN, Guenther et al. 2012), anthropogenic emissions (EDGAR, Janssens-Maenhout et al. 2011; Olivier et al. 1999; RETRO, Schultz et al. 2008; GEIA, Benkovitz et al. 1996; C_2H_6, Xiao et al. 2008), biomass burning (GFED-3, van der Werf et al. 2010), biofuel emissions (Yevich and Logan, 2003), NO_x (soils, Hudman et al. 2012; lightning, Murray et al. 2012a; ships, Vinken et al. 2011; and aircraft, Stettler et al. 2011), and aerosol emissions (e.g. sea-salt, Jaeglé et al. 2011; dust, Fairlie et al. 2010; Black and organic carbon, Bond et al. 2007). In addition to global inventories, higher resolution inventories are used to overwrite regions such as Europe (e.g. EMEP, Vestreng et al. 2009).

2.2.2 Organic iodine emissions

The monthly emission inventory of Ordóñez et al. (2012) for organic iodine compounds (CH_3I, CH_2I_2, CH_2IBr, and CH_2ICl) has been implemented here. This attempts to synthesise the limited observation dataset for these compounds. For CH_3I the work of Bell et al. (2002) is used by Ordóñez et al. (2012). For the other compounds the treatment is

split between the tropics and the extra tropics. For the tropics, fluxes are scaled based on chlorophyll-a determined from satellite. In the extra-tropics two constant uniform fluxes are used in oceanic regions and in coastal regions to provide a 2.5:1 ratio between the two regions. Figure 2.1 shows the distribution and magnitudes of the emissions of organic compounds.

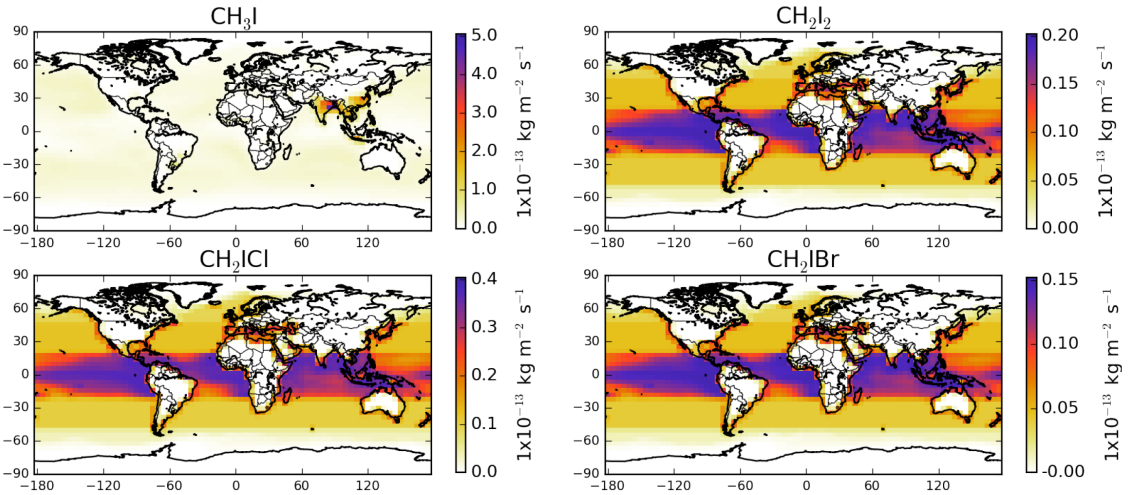

Figure 2.1 – Calculated annual mean organic iodine emissions 1x10^{-13} kg m^{-2} s^{-1}. Monthly emissions are given in the Appendix (Sect. C.1).

2.2.3 Inorganic iodine emissions

Inorganic emissions in this simulation are parameterised following laboratory studies and modelling published by Carpenter et al. (2013). This work parameterised the release of inorganic iodine compounds (HOI, I_2) formed from the uptake of O_3 to the ocean and the subsequent ocean-surface reaction of O_3 with iodide (I^-). The parameterisations for HOI and I_2 are given by Equations 2.2 and 2.1 respectively. Where $[I^-_{(aq)}]$ is in units of mol dm^{-3}, wind speed is in m s^{-1}, O_3 is in nmol mol^{-1}, and the resultant flux is in nmol m^{-2} d^{-1}.

$$Flux_{(I_2)} = [O_{3(g)}] \times [I^-_{(aq)}]^{1.3} \left(1.74 \times 10^9 \times 6.54 \times 10^8 \times \ln(ws)\right) \quad (2.1)$$

$$Flux_{(\mathrm{HOI})} = [\mathrm{O}_{3(g)}] \times \left(4.15 \times 10^5 \times \frac{\sqrt{[\mathrm{I}^-_{(\mathrm{aq})}]}}{ws} - \frac{20.6}{ws} - 2.36 \times 10^4 \times \sqrt{[\mathrm{I}^-_{(\mathrm{aq})}]} \right) \quad (2.2)$$

The parameterisation of Carpenter et al. (2013) requires knowledge of sea surface iodide concentrations. A compilation of surface iodide and iodate concentrations observed from ship cruises and stations was recently published by Chance et al. (2014). Chance and co-workers considered the correlation of iodine species with various physical quantities typically available in global models. They found the greatest correlation of I^- was with the square of sea surface temperature (eqn. 2.3), where sea surface temperature (SST) is in Kelvin, and the resultant iodide concentration $[\mathrm{I}^-_{(aq)}]$ is in units of mol dm^{-3}. This is used in the "Br+I" simulation to parameterise ocean-surface $\mathrm{I}^-_{(aq)}$ concentration.

$$\mathrm{I}^-_{(\mathrm{aq})} = 0.225T^2 + 19 \quad (2.3)$$

Other work used a subset of the same database from Chance et al. (2014), but only considered the Atlantic region to derive another parameterisation (MacDonald et al., 2014). This gave an Arrhenius type parameterisation (Eqn. 2.4). A comparison of the derived ocean I^- concentrations between Chance et al. (2014) and (MacDonald et al., 2014) is shown in Figure 2.3 and 2.2. The parameterisation of Chance et al. (2014) is used here, and in Chapter III, as it considers all available global data and therefore is most appropriate for a global study.

$$\mathrm{I}^-_{(\mathrm{aq})} = 1.46 \times 10^6 + \exp\left(\frac{-9134}{T}\right) \quad (2.4)$$

By combining the parametrisation of Chance et al. (2014) for sea surface iodide with online O_3, wind speed at 10 metres, from model input meteorological fields, and sea surface temperature it is possible to calculate inorganic iodine flux online using Equations 2.2, 2.1 and 2.3. The resultant modelled fluxes are shown in Figure 2.4 and 2.5.

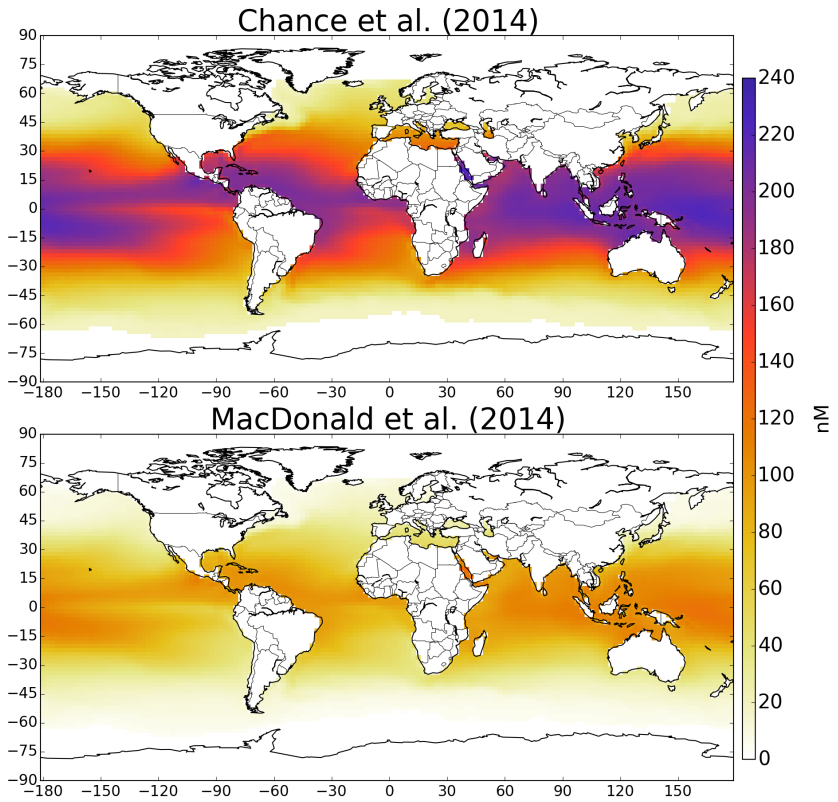

Figure 2.2 – Calculated annual mean ocean-surface iodide concentrations (I^-) in nM. Values are calculated from the highest correlation relationship (square of temperature) presented in Chance et al. (2014) (top) and from Arrhenius relationship from Eq. (1) in MacDonald et al. (2014) (bottom). Annual total emissions are given in Table 2.1.

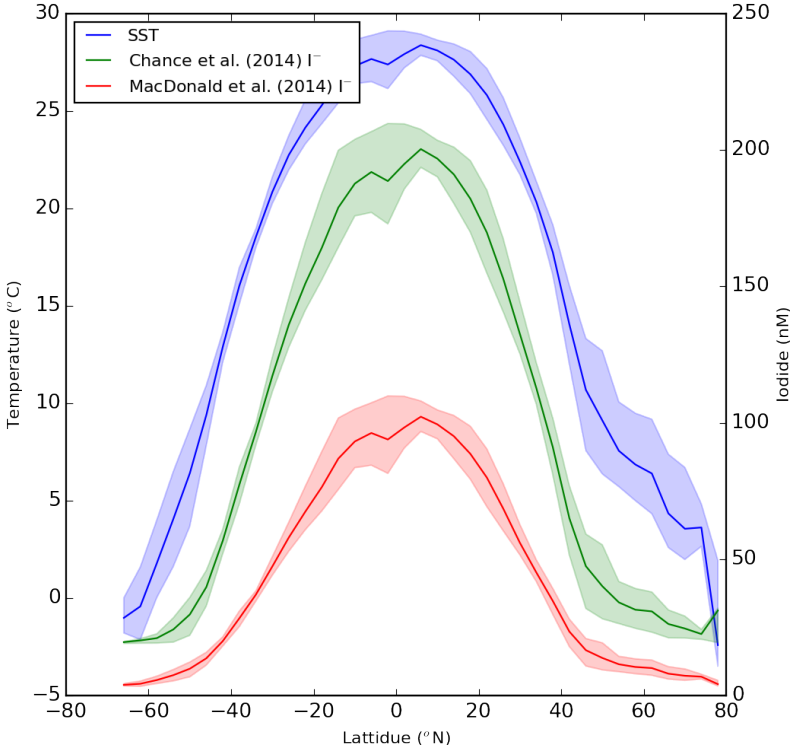

Figure 2.3 – Latitudinal variation in surface iodide concentrations (I^-) in nM. The bold line shows the mean, and shaded areas show 1^{st} and 3^{rd} quartiles. SST = sea surface temperature.

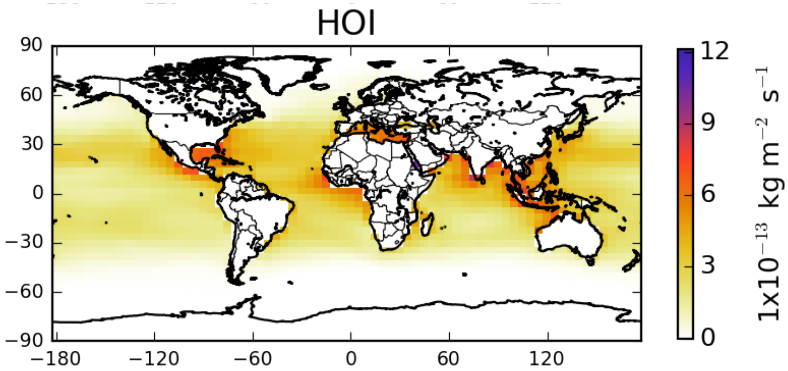

Figure 2.4 – Spatial plot of global annual average HOI emissions implemented in GEOS-Chem. Average monthly emissions by species are given in the Appendix (Section C.1).

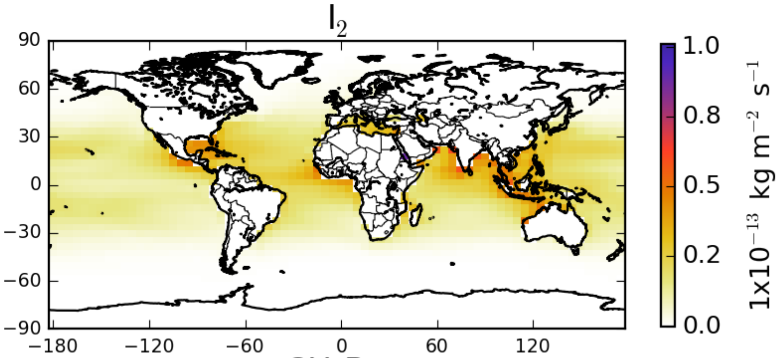

Figure 2.5 – Spatial plot of global annual average I_2 emission implemented in GEOS-Chem. Average monthly emissions by species are given in the Appendix (Section C.1).

2.2.4 Total iodine emissions

Global emission totals from this modelling work are presented in Table 2.1. The organic emissions are consistent with recent work (Saiz-Lopez et al., 2014) as they both use Ordóñez et al. (2012). The inorganic fluxes calculated in this study are however 47 % higher than in previous work (Saiz-Lopez et al., 2014), despite using the same inorganic iodine (HOI, I_2) flux parameterisation (Carpenter et al., 2013). Although model specific differences exist in sea surface temperatures, 10 m wind speeds and O_3 concentration the largest differences lie in the choice of parameterisation for sea surface iodide (See Fig 2.3 and further discussion in chapter III Section 3.7.5). Recent work from Saiz-Lopez et al. (2014) uses MacDonald et al. (2014) and this work uses Chance et al. (2014). Fig. 2.3 shows the significantly higher fluxes found from using the Chance et al. (2014) parameterisation.

HOI represents the single largest source of oceanic iodine (76 %) with averaged oceanic emissions of 1.4 x 10^8 atoms (I) cm^{-2} s^{-1}. This value is towards the lower end of flux values required to reproduce IO observations in recent box modelling studies (Großmann et al., 2013; Jones et al., 2010; Mahajan et al., 2009). Previous studies that did not consider an inorganic iodine source give much lower emissions of iodine (0.58 Tg (I) yr^{-1}, Ordóñez et al. 2012; 0.65 Tg (I) yr^{-1}, Jones et al. 2010). However, these emissions are consistent with organic emissions used here.

Table 2.1 – Total simulated emissions for iodinated species used in this modelling. Values are given as annual totals in $\mathrm{Tg\,(I)\,yr^{-1}}$ of iodine.

Species	Emissions $\mathrm{Tg\,(I)\,yr^{-1}}$
CH_3I	0.26
CH_2I_2	0.11
CH_2ICl	0.18
CH_2IBr	0.05
I_2	0.32
HOI	2.91
Total	3.83

2.3 Gas-phase chemistry

The gas-phase iodine chemistry used in this modelling is shown in Tables 2.2 and 2.3. This is based on the recent IUPAC (Atkinson et al., 2007, 2008) or JPL 10-6 (Sander et al., 2011) evaluations. In addition some reactions are included based on recent work (Sommariva et al., 2012; von Glasow et al., 2002) and these are described in section 2.3.1.

2.3.1 Reactions included, but not present in JPL/IUPAC

The field of iodine chemistry is still young, and some reactions that are used within box model and global studies are not in the IUPAC/JPL compilations due to the uncertainties in the laboratory studies or for other reasons. Different choices have been made regarding reactions included in previous box- (Bloss et al., 2010; Mahajan et al., 2009; Read et al., 2008; Saiz-Lopez et al., 2008; Sommariva et al., 2012) and global- (Breider, 2010; Ordóñez et al., 2012; Saiz-Lopez et al., 2012b, 2014) model studies. The following reactions have been included within this simulation's chemistry scheme (Tables 2.2 and 2.3) although they are not in the IUPAC/JPL compilations.

$$\mathrm{HOI + OH \rightarrow IO + H_2O} \tag{2.5}$$

Uncertainties exist over product channels for reaction 2.5 (Sommariva et al., 2012). Following the work of Sommariva and co-workers, this study assumes the products of IO

Table 2.2 – Bi-molecular and uni-molecular iodine reactions. These are given in the Arrhenius form with the rate equal to $A \cdot \exp\left(\frac{-Ea}{RT}\right)$. Unknown values are represented by a dash and these are set to zero in the model, reducing the exponent to 1. The bi-molecular reactions with an M in them represent termolecular reactions where the pressure dependence is not known or are uni-molecular decomposition reactions. Reactions included, but not in IUPAC/JPL are discussed further in Section 2.3.1.

Rxn ID	Reaction	A	Ea/R	Citation
		$cm^3\,molecules^{-1}\,s^{-1}$	K	
M1	$I + O_3 \rightarrow IO + O_2$	2.10×10^{-11}	-830	Atkinson et al. (2007)
M2	$I + HO_2 \rightarrow HI + O_2$	1.50×10^{-11}	-1090	Sander et al. (2011)
M3	$I_2 + OH \rightarrow HOI + I$	2.10×10^{-10}	–	Atkinson et al. (2007)
M4	$HI + OH \rightarrow I + H_2O$	1.60×10^{-11}	440	Atkinson et al. (2007)
M5	$HOI + OH \rightarrow IO + H_2O$	5.00×10^{-12}	–	Riffault et al. (2005)
M6	$IO + HO_2 \rightarrow HOI + O_2$	1.40×10^{-11}	540	Atkinson et al. (2007)
M7	$IO + NO \rightarrow I + NO_2$	7.15×10^{-12}	300	Atkinson et al. (2007)
M8	$HO + CH_3I \rightarrow H_2O + I\,(CH_2I)$	4.30×10^{-12}	-1120	Atkinson et al. (2008)
M9	$INO + INO \rightarrow I_2 + 2NO$	8.40×10^{-11}	-2620	Atkinson et al. (2007)
M10	$INO_2 + INO_2 \rightarrow I_2 + 2NO_2$	4.70×10^{-12}	-1670	Atkinson et al. (2007)
M11	$I_2 + NO_3 \rightarrow I + INO_3$	1.50×10^{-12}	–	Atkinson et al. (2007)
M12	$INO_3 + I \rightarrow I_2 + NO_3$	9.10×10^{-11}	-146	Kaltsoyannis and Plane (2008)
M13	$I + BrO \rightarrow IO + Br$	1.20×10^{-11}	–	Sander et al. (2011)
M14	$IO + Br \rightarrow I + BrO$	2.70×10^{-11}	–	Bedjanian et al. (1997)
M15	$IO + BrO \rightarrow Br + I + O_2$	3.00×10^{-12}	510	Atkinson et al. (2007)
M16	$IO + BrO \rightarrow Br + OIO$	1.20×10^{-11}	510	Atkinson et al. (2007)
M17	$OIO + OIO \rightarrow I_2O_4$	1.50×10^{-10}	–	Gómez Martín et al. (2007)
M18	$OIO + NO \rightarrow NO_2 + IO$	1.10×10^{-12}	542	Atkinson et al. (2007)
M19	$IO + IO \rightarrow I + OIO$	2.16×10^{-11}	180	Atkinson et al. (2007)
M20	$IO + IO \xrightarrow{M} I_2O_2$	3.24×10^{-11}	180	Atkinson et al. (2007)
M21	$IO + OIO \xrightarrow{M} I_2O_3$	1.50×10^{-10}	–	Gómez Martín et al. (2007)
M22	$I_2O_2 \xrightarrow{M} IO + IO$	1.00×10^{12}	-9770	Ordóñez et al. (2012)
M23	$I_2O_2 \xrightarrow{M} OIO + I$	2.50×10^{14}	-9770	Ordóñez et al. (2012)
M24	$I_2O_4 \xrightarrow{M} 2\,OIO$	3.80×10^{-2}	–	Kaltsoyannis and Plane (2008)
M25	$INO_2 \xrightarrow{M} I + NO_2$	9.94×10^{17}	-11859	McFiggans et al. (2000)
M26	$INO_3 \xrightarrow{M} IO + NO_2$	2.10×10^{15}	-13670	Kaltsoyannis and Plane (2008)

Table 2.3 – Termolecular iodine reactions. The lower pressure limit rate (k_0) is given by: $A_0 \cdot (\frac{300}{T})^x$. The high pressure limit is given by k_∞. Fc characterises the fall off curve of the reaction as described by (Atkinson et al., 2007)

Rxn ID	Reaction	A_0 $cm^6\,molecules^{-2}\,s^{-1}$	x	k_∞ $cm^3\,molecules^{-1}\,s^{-1}$	Fc	Citation
T1	$I + NO + M \rightarrow INO + M$	1.80×10^{-32}	1	1.70×10^{-11}	0.60	Atkinson et al. (2007)
T2	$I + NO_2 + M \rightarrow INO_2 + M$	3.00×10^{-31}	1	6.60×10^{-11}	0.63	Atkinson et al. (2007)
T3	$IO + NO_2 + M \rightarrow INO_3 + M$	7.70×10^{-31}	5	1.60×10^{-11}	0.40	Atkinson et al. (2007)

and H_2O based on laboratory experiments (Riffault et al., 2005) and previous box model analysis (Sommariva et al., 2012).

$$INO_3 + I \rightarrow I_2 + NO_3 \tag{2.6}$$

Reaction 2.6 reaction's rate is based on a single theoretical study (Kaltsoyannis and Plane, 2008). The impact of inclusion within a box model was found to be minimal, except in high iodine and O_3 conditions (Sommariva et al., 2012).

$$OIO + OIO \rightarrow I_2O_4 \tag{2.7}$$

Reaction 2.7 reaction rate is from a single experimental study (Gómez Martín et al., 2007), which yielded a lower limit of $1.2 \pm 0.3 \times 10^{-10}$ cm^3 $molecules^{-1}$ s^{-1}. This reaction is included in this work, along with the reverse reaction (Reaction $I_2O_4 \rightarrow 2\,OIO$).

$$INO_3 \xrightarrow{M} IO + NO_2 \tag{2.8}$$

Reaction 2.8 is included in IUPAC (Atkinson et al., 2007) without direct experimental observation. No recommendation is given in the recent JPL compilation (Sander et al., 2011). The INO_3 thermal stability rate used by previous modelling studies has a significant range (298 K) from 1.08×10^{-2} (Read et al., 2008) to 2.51×10^{-5} cm^3 $molecules^{-1}$ s^{-1} (Sommariva et al., 2012). The latter uses the most recent theoretical study (Kaltsoyannis

and Plane, 2008), which is also used here. The reverse reaction (IO + $NO_2 \xrightarrow{M} INO_3$) has been included ubiquitously in iodine modelling work; and forward reaction ($INO_3 \xrightarrow{M}$ IO + NO_2) is employed in the majority of, but not all studies (Ordóñez et al., 2012). Both reactions are included in this work.

$$IO + OIO \xrightarrow{M} I_2O_3 \tag{2.9}$$

For reaction 2.9, a single experimental study (Gómez Martín et al., 2007) gives an upper limit and lower rate limit of 1.5 x10^{-10} and 1.5 x10^{-11} cm^3 $molecules^{-1}$ s^{-1}, respectively. The higher value is used in this work as in others studies (Saiz-Lopez et al., 2008; Sommariva et al., 2012).

$$I_2O_2 \xrightarrow{M} IO + IO \tag{2.10}$$

$$I_2O_2 \xrightarrow{M} I_2O_3 \tag{2.11}$$

These reactions (2.10 and 2.11) have only been studied theoretically (Kaltsoyannis and Plane, 2008). A temperature dependent rate was calculated theoretically (Ordóñez et al., 2012) which is used in this work.

$$I_2O_4 \xrightarrow{M} 2\,OIO \tag{2.12}$$

The rate for this reaction (Rxn. 2.12) is calculated from the value for binding energy of the dimer (Kaltsoyannis and Plane, 2008). The reverse reaction (OIO+OIO $\rightarrow$ I_2O_4) is also included at the Kaltsoyannis and Plane (2008) rate.

2.4 Heterogeneous chemistry

Reactions occurring within aerosol following uptake (HI, HOI, INO_2, INO_3, I_2O_X) are not treated explicitly but are parameterised using a reactive uptake coefficient (γ).

Heterogeneous uptake rates are computed using the GEOS-Chem standard code (Jacob 2000, as described in Chapter I Sect. 1.6.2.5) from the values of γ given in Table 2.4.

In line with previous studies (McFiggans et al., 2000), this implementation assumes that the uptake of HOI, INO_2 and INO_3 leads to the acid catalysed recycling of iodine back into the gas-phase as IX on sea-salt (as discussed in Section 1.6.2.5). Irreversible loss via uptake of HI on seasalt is assumed to lead to the generation of aerosol-phase iodine. The uptake of I_2O_X (X = 2,3,4) is assumed to lead to the generation of aerosol-phase iodine on any aerosol.

Table 2.4 – Heterogeneous reactions of iodine species. Where measured values have not been reported estimated values are used and no reference is given, further detail on uptake choices is in Sect. 2.4. Stared (*) reactions proceed only on sea-salt aerosols, whereas other reactions proceed on other aerosols.

ID	Reaction	Reactive uptake coefficient (γ)	Reference
K1	HI $\rightarrow$ iodine aerosol	0.10*	Crowley et al. (2010)
K2	$INO_3 \rightarrow 0.5I_2$	0.01*	see Chap. I Sect. 1.6.2.5
K3	HOI $\rightarrow 0.5I_2$	0.01*	Sander et al. (2011)
K4	$INO_2 \rightarrow 0.5I_2$	0.02*	see Chap. I Sect. 1.6.2.5
K5	$I_2O_2 \rightarrow$ iodine aerosol	0.02	see Chap I. Sect. 1.6.2.5
K6	$I_2O_4 \rightarrow$ iodine aerosol	0.02	see Chap. I Sect. 1.6.2.5
K7	$I_2O_3 \rightarrow$ iodine aerosol	0.02	see Chap. I Sect. 1.6.2.5

Stoichiometric emission of I_2 following uptake of species that hydrolyse to I^+ (INO_2, INO_3, HOI) is assumed. This avoids double counting of Br_2 release already included within the model as described by (Parrella et al., 2012). ICl release was not included, due to the lack of inclusion of tropospheric Cl_y chemistry in GEOS-Chem.

Lack of, or limited experimental data reduces certainty on heterogeneous processing of halogens. The reactive uptake coefficients (γ) used in this study are experimentally constrained wherever possible or follow previously estimated values in the literature as described in Chapter I (Sect. 1.6.2.5). The γ values used for each species are shown in table 2.4. The implication of the choice of these value and varying this is considered in Chapter III Section 3.7.2.

2.5 Photolysis

Photolysis rates are calculated online using the standard FAST-J code implementation in GEOS-Chem (Wild et al., 2000). Cross-sections are processed to the 7 wavelength bins

used by FAST-J (Bian and Prather, 2002) as described by (Mao et al., 2010).

For most cross-sections JPL 10-6 (Sander et al., 2011) values were used. For I_2O_X (X = 2,3,4) the same absorption cross section as INO_3 is assumed, an approach used previously (Bloss et al., 2010). For most species (I_2, HOI, IO, OIO, INO, INO_2, I_2O_2, CH_3I, CH_2I_2, CH_2IBr and CH_2ICl) a quantum yield of 1 is assumed, but for INO_3 a quantum yield of 0.21 (Sander et al., 2011) is used. Full literature cross-sections and spectra binned for FAST-J are are shown in Appendix (Sect. C.2)

Table 2.5 – Photolysis reactions of iodine species. For I_2O_X ($_X$=2,3,4) the cross-section of INO_3 is used as described in Sect. 2.5.

ID	Reaction	Cross-section reference
J1	$I_2 \xrightarrow{h\nu} 2I$	Sander et al. (2011)
J2	$HOI \xrightarrow{h\nu} I + OH$	Sander et al. (2011)
J3	$IO \xrightarrow{h\nu} I + [O_3]$	Sander et al. (2011)
J4	$OIO \xrightarrow{h\nu} I + O_2$	Sander et al. (2011)
J5	$INO \xrightarrow{h\nu} I + NO$	Sander et al. (2011)
J6	$INO_2 \xrightarrow{h\nu} I + NO_2$	Sander et al. (2011)
J7	$INO_3 \xrightarrow{h\nu} I + NO_3$	Sander et al. (2011)
J8	$I_2O_2 \xrightarrow{h\nu} I + OIO$	see caption
J9	$CH_3I \xrightarrow{h\nu} I + CH_2O_2$	Sander et al. (2011)
J10	$CH_2I_2 \xrightarrow{h\nu} 2I + (CH_2)$	Sander et al. (2011)
J11	$CH_2ICl \xrightarrow{h\nu} I + (CH_2Cl)$	Sander et al. (2011)
J12	$CH_2IBr \xrightarrow{h\nu} I + (CH_2Br)$	Sander et al. (2011)
J20	$I_2O_4 \xrightarrow{h\nu} 2OIO$	see caption
J21	$I_2O_3 \xrightarrow{h\nu} OIO + IO$	see caption

Notably this work differs from recent global iodine simulations (Saiz-Lopez et al., 2014) in its treatment of I_2O_X (X=2,3,4). In this work, "Br+I" considers the photolysis of these compounds whereas Saiz-Lopez et al. (2014)'s "Base" simulation does not. This means that this "Br+I" simulation would be expected to have more active iodine chemistry than is reported in (Saiz-Lopez et al., 2014).

2.6 Iodine and bromine cross-over chemistry

The bromine simulation in GEOS-Chem is described in (Parrella et al., 2012). Parrella et al. (2012) presented a range of comparisons of the model against satellite BrO obser-

vations. Although in general the model reproduces many of the observed features, there is a systematic underestimation of tropospheric BrO. New aircraft observations show that tropospheric BrO (Volkamer et al., 2015; Wang et al., 2015) may be higher than calculated by the Parrella et al. (2012) scheme. This simulation ("Br+I") also underestimates surface BrO observed in the tropical Atlantic marine boundary layer (900 hPa ¡p) (∼2 pmol mol^{-1}, Read et al. 2008) by a ratio of ∼5 (0.4 pmol mol^{-1}). The uncertainty in BrO concentration is considered as a part of the sensitivity study in Chapter II Section 3.7.4.

In addition to the model low bias at the surface noted already at Cape Verde, it is worth highlighting that BrO concentrations peak in model in the southern oceans with annual average concentrations of ∼5 pmol mol^{-1} (Fig. 2.6) in GEOS-Chem (version v9-2). This peak concentration is attributable to the sea-salt de-bromination flux implemented in Parrella et al. (2012). However, this peak concentration is expected to be lower than that in Parrella et al. (2012) as the bromine scheme implemented in the "off the shelf" GEOS-Chem version v9-2 used here actually uses a different size dependant Br_2 flux (Yang et al., 2008). The fact that the "off the shelf" GEOS-Chem we use here is updated to follow Yang et al. (2008) means that the sea-salt is reduced flux by 64 % (1.4 to 0.51 Tg (Br) yr^{-1}) relative to Parrella et al. (2012). Thus, the source of bromine considered here and the impacts would be expected to be lower that those presented in Parrella et al. (2012).

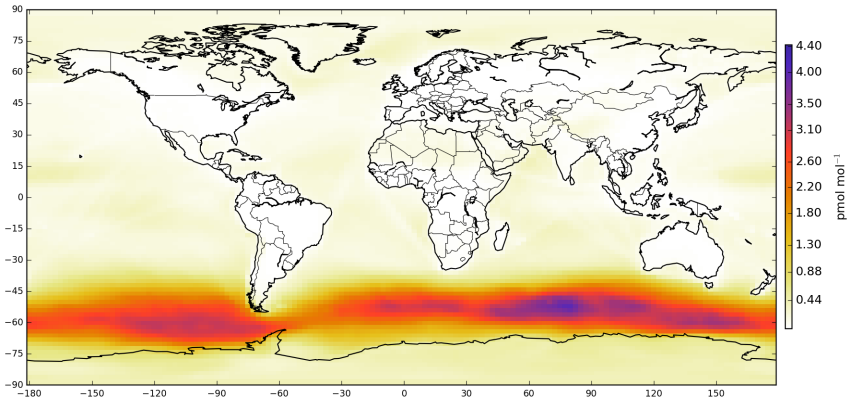

Figure 2.6 – Annual global average surface concentration of BrO in "Br+I" simulation.

2.7 Deposition

Dry deposition of the new iodine compounds is computed via the standard GEOS-Chem implementation of the "resistance-in-series" approach (Wesely, 1989) using literature Henry's law coefficients (Sander, 1999, 2015). This approach is applied to I_2, HI, HOI, INO_2, INO_3, I_2O_2, I_2O_3 and I_2O_4. Aerosol iodine is assumed to have the same dry deposition properties as sulfate aerosol.

Wet deposition is calculated for I_2, HI, HOI, INO_2, INO_3, I_2O_2, I_2O_3 and I_2O_4 for both large scale (frontal) and convective rain by applying scavenging in and below clouds (Liu et al., 2001) using species-specific values for Henry's law coefficients (Sander, 1999, 2015; Vogt et al., 1999) and molar heats of formation (Kaltsoyannis and Plane, 2008; Sander, 1999, 2015) as shown in Table 2.6. Fractionation between gas and liquid on ice is considered (Parrella et al., 2012; Stuart and Jacobson, 2003). Aerosol iodine is assumed to have the same wet deposition properties as sulfate aerosol.

In the simulation iodine deposition is predominantly through HOI (51 %). The remainder is mostly through deposition of INO_3 (20 %) and aerosol iodine formed by heterogeneous loss of gaseous iodine (HI, I_2O_X; 24 %). The majority of the deposition sink is back into the ocean (91 %). The global I_y (I_y is defined in Footnote 1) lifetime is 3.3 days but where depositional scavenging is weakest (upper troposphere, 350 hPa > p > tropopause) this can increase by three orders of magnitude.

2.8 Conclusions

This chapter presents a representation of the tropospheric chemistry of iodine in the GEOS-Chem model. This includes organic and inorganic iodine sources, standard gas-phase iodine chemistry and simplified higher iodine oxide (I_2O_X, X = 2,3,4) chemistry, photolysis, deposition and parametrised heterogeneous reactions.

Table 2.6 – Henry's law coefficients and molar heats of formation of iodine species. Where Henry's law constant equals infinity a very large value is used within the model 1x10^{20} M atm^{-1}. The INO_2 Henry's law constant is assumed equal to that of $BrNO_3$, from Sander (1999, 2015), by analogy. For I_2O_X (X=2,3,4) a Henry's law constant of infinity is assumed by analogy with INO_3. (∗) Effective Henry's law of HI is calculated for acid conditions through $K_H^*(T) = K_H(T) \times (1 + \frac{K_a}{[H^+]})$, where K_a =1×10^9 M is the acid dissociation constant (Bell, 1973).

Num.	Species	Henry's Law Constant M atm^{-1}	Reference	Molar Heat of Formation 298 K/R (K)	Reference
D1	HOI	1.53×10^4	Sander (1999, 2015)	-8.37×10^3	Sander et al. (2006)
D2	HI	2.35×10^0(*)	Sander (1999, 2015)	-3.19×10^3	Sander et al. (2006)
D3	INO_3	∞	Vogt et al. (1999)	-3.98×10^4	Kaltsoyannis and Plane (2008)
D4	I_2O_2	∞	see caption text	-1.89×10^4	Kaltsoyannis and Plane (2008)
D5	I_2	2.63×10^0	Sander (1999, 2015)	-7.51×10^3	Sander et al. (2006)
D6	INO_2	3.00×10^{-1}	see caption text	-7.24×10^3	Sander et al. (2006)
D7	I_2O_3	∞	see caption text	-7.70×10^3	Kaltsoyannis and Plane (2008)
D8	I_2O_4	∞	see caption text	-1.34×10^4	Kaltsoyannis and Plane (2008)

Chapter 3

Iodine's impact on oxidants in the present-day troposphere

The majority of the content of this chapter has been published in the article entitled "Iodine's impact on tropospheric oxidants: A global model study in GEOS-Chem.": T. Sherwen, M. J. Evans, L. J. Carpenter, S. J. Andrews, R. T. Lidster, B. Dix, T. K. Koenig, R. Sinreich, I. Ortega, R. Volkamer, A. Saiz-Lopez, C. Prados-Roman, A. S. Mahajan and C. Ordóñez, *Atmos. Chem. Phys.*, 2016, **16**, 11611186.

3.1 Introduction

Over the last few decades significant research has gone into understanding the production of O_3, due to its adverse impact on health and food security and climate change (Ainsworth et al., 2012; Fowler et al., 2008). Less emphasis has been placed on its loss processes. As discussed in Chapter I, O_3 is chemically lost in the troposphere through its photolysis, in the presence of water vapour, to produce OH and through its reactions with HO_2 and OH. Previous studies (Bloss et al., 2005b; Saiz-Lopez et al., 2008, 2012b) have identified the potential for iodine in the troposphere to provide an additional loss route. This chapter aims to quantify the magnitude of this loss route using the model described in the previous chapters.

First this chapter assesses the new simulation against a range of key observational datasets (Sect. 3.2). The possibly to constrain the model against Iodine deposition is considered in Section 3.3. The modelled composition of simulation "Br+I" is then presented in Section 3.4. The impacts of iodine chemistry are then considered on oxidants in Section 3.5 and 3.6.

For budgets and general analysis the model is run at 2^ox2.5^o resolution for two years (2004 and 2005) discarding the 1^{st} "spin up" year and using the final year (2005) for analysis and budgets. For the sensitivity study (Section 3.7) the model is run with the same period for analysis, but at 4^ox5^o resolution. The model output is discussed with focus on the marine boundary layer (900 hPa < p); the free troposphere (350 hPa < p <900 hPa); and upper troposphere (350 hPa > p > tropopause). Comparisons with observations involve separate spin-up simulations, run with the date appropriate meteorology, sampled at the spatially and temporally nearest grid box to the observations.

3.2 Evaluation of the new simulation ("Br+I")

In this section the iodine simulation ("Br+I", described in chapter II Sections 2.2-2.7) is evaluated against a range of observations. Initially the focus is on observational constraints for those iodine compounds that are directly emitted (Sections 3.2.1-3.2.2), and then on the secondary iodine species which has been most extensively observed (IO, Section 3.2.3).

3.2.1 Organic iodine

Figures 3.1 and 3.2 show annually averaged zonal (Fig. 3.1) and surface (Fig. 3.2) concentrations of organic and inorganic iodine precursors and their degradation products. These figures clearly illustrate the oceanic nature of iodine source species (CH_3I, CH_2I_2, CH_2ICl, CH_2IBr, HOI, I_2), with the highest concentrations over the tropical ocean. These plots also highlight the contribution of the terrestrial CH_3I paddy field source (25 %) to global CH_3I concentrations from the Bell et al. (2002) emissions included in Ordóñez et al. (2012).

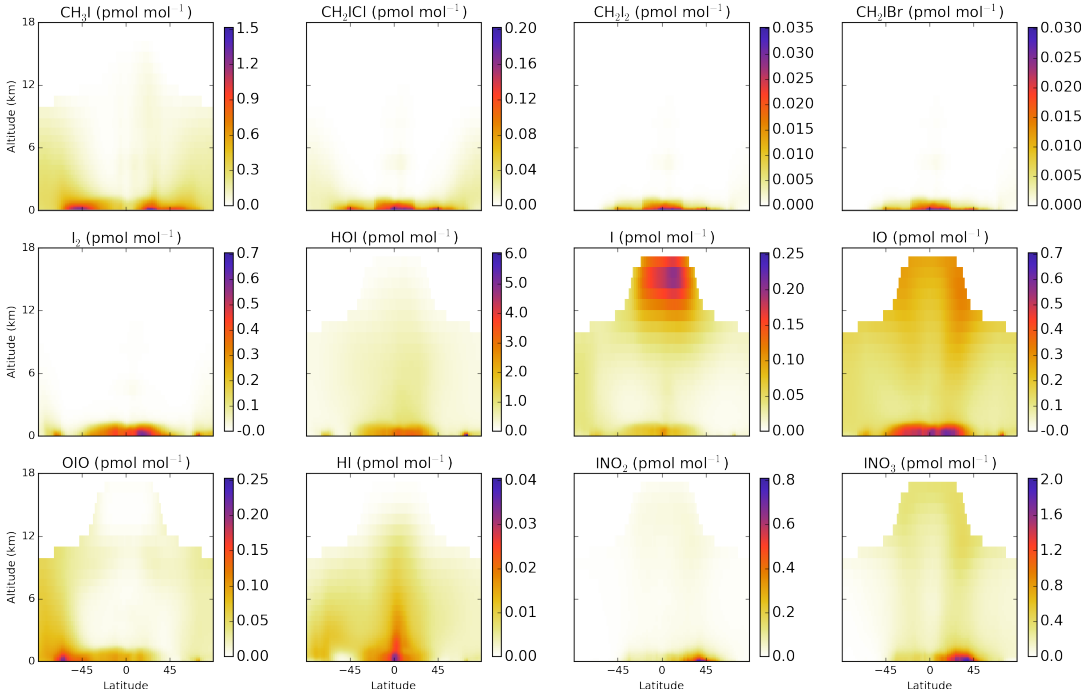

Figure 3.1 – Annual mean zonal tropospheric mixing ratios for precursor and reactive iodine compounds (pmol mol^{-1}). No calculations of concentrations are made within the stratosphere and so this region is left blank.

The emissions used here for organic iodine species have been assessed against observations by Ordóñez et al. (2012) and so a detailed comparison is not made here. A brief comparison is presented here between observations of CH_3I and CH_2ICl (Fig. 3.3) made during the UK Combined Airborne Studies in the Tropics (CAST) campaign over the tropical Pacific (Guam) from January and February of 2014. These observations were made by gas chromatography mass spectrometry (GC-MS) as described in Andrews et al. (2015), using whole air samples from the Facility Airborne Atmospheric Measurement (FAAM) BAe

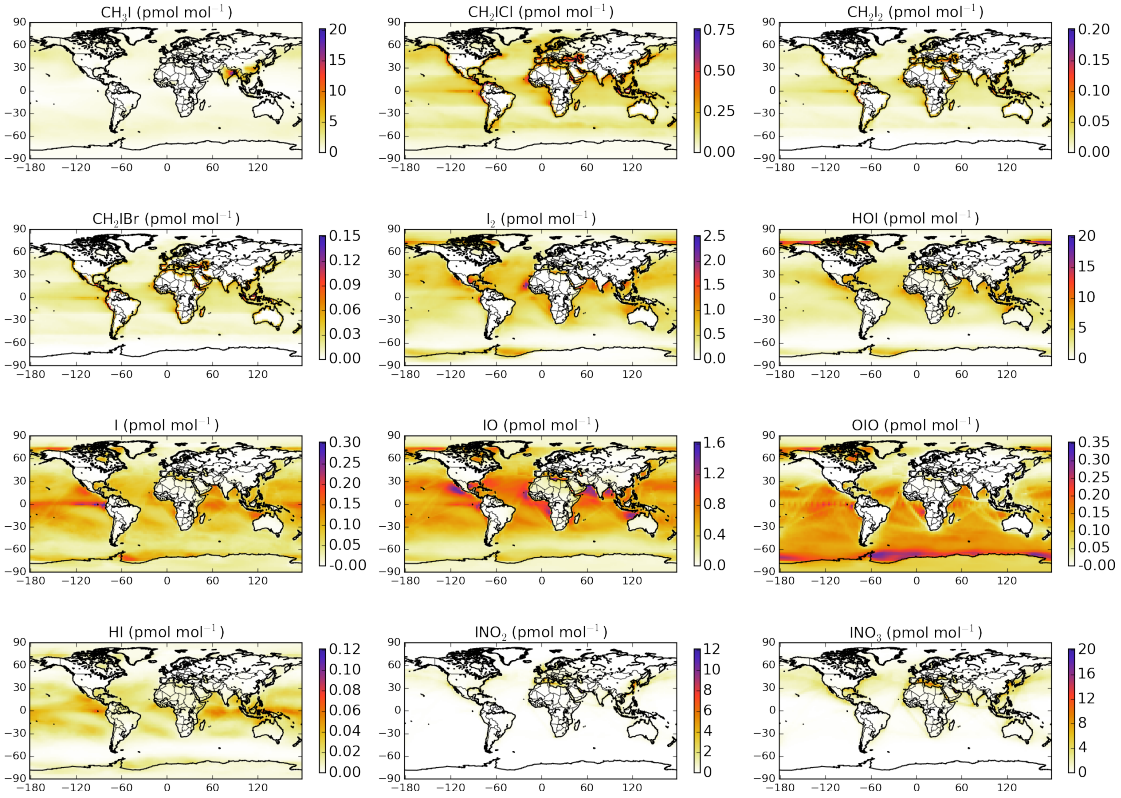

Figure 3.2 – Annual mean surface mixing ratios for precursor and reactive iodine (pmol mol^{-1}).

146-301 atmospheric research aircraft with techniques described in Andrews et al. (2013). The model captures the trend of decreasing concentration with height, but appears to underestimate the CH_3I concentrations (Fig. 3.3). Concentrations of CH_2ICl appear to be better simulated (Fig. 3.3). Although not definitive, this brief comparison suggests the model, if anything, underestimates the concentration of organic iodine.

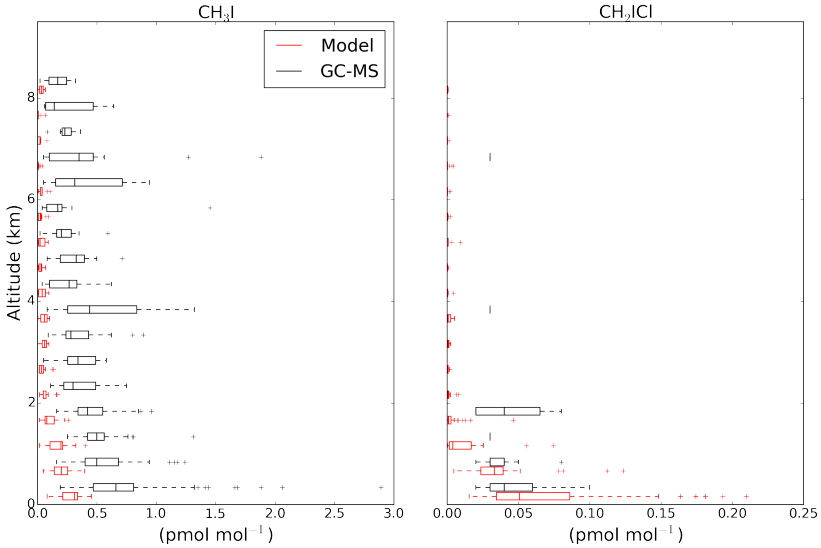

Figure 3.3 – Vertical comparison of observations from the CAST (Combined Airborne Studies in the Tropics) campaign in the mid Pacific (Guam). The observations are shown in black and modelled values in red. The observations are from the FAAM BAE-146 research aircraft Whole Air Samples (WAS) analysed by Gas Chromatography-Mass Spectrometry (GC-MS). The boxplot extents give the inter-quartile range, with the median shown within the box. The whiskers give the most extreme point within 1.5 times the inter-quartile range.

3.2.2 Inorganic iodine

The first in-situ remote open ocean I_2 concentration measurements were made at Cape Verde (Lawler et al., 2014). This dataset reported daytime measurements below the limit of detection and increasing concentrations between dusk and dawn, peaking in the range 0.2 to 1.7 pmol mol^{-1}. The model captures the diurnal variation in I_2 of essentially zero during the day and increasing I_2 concentration during the night peaking just before dawn. However the calculated concentrations peak in the range 2.5 and 7.5 pmol mol^{-1}. Some component of this overestimate probably relates to the assumption made in this model that the heterogeneous recycling of HOI, INO_3 and INO_2 on sea-salt leads to the production of

I_2. In reality this probably leads to the production of ICl and IBr (Braban et al., 2007). In the "Cl+Br+I" version of the model discussed in Chapter IV the chemistry scheme is adapted in this way and the concentrations of I_2 decrease to within the range of 0.07 and 0.13 (for equivalent dates in the 2005 analysis year), which is more consistent with the observations.

3.2.3 Iodine oxide (IO) observations

Effectively, the only secondary iodine compound that has been observed is IO. A comparison of a range of surface observations is shown in Fig. 3.4. Good agreement is seen in the West Pacific (TransBrom, Großmann et al. 2013) and tropical Atlantic at Cape Verde (Mahajan et al., 2010; Read et al., 2008), but the model has a generally high bias compared with other datasets (HALOCast-P, Mahajan et al. 2012; Malasapina, Prados-Roman et al. 2015b).

Biases between the daytime modelled and measured IO at Cape Verde and during the TransBrom cruise biases are 22 and 16 %, respectively. However, the model overestimates the Malasapina cruise IO concentrations (bias +50 to 250 %), and both under- and overestimates values from the HALOCast-P cruise (bias -92 to +280 %). When all observations are latitudinally averaged (onto a 20^o grid) a median bias of +66 % is found.

In Fig. 3.5 a comparison is shown with recent aircraft IO observations from the TORERO campaign (Volkamer et al., 2015; Wang et al., 2015), which took place over the eastern Pacific. The model captures the vertical profile of IO but overestimates the observations (average bias of +82 % within the binned comparison). Biases in the comparison are greatest (bias = +125 %) in the marine boundary layer (900 hPa < p) and lowest (bias = +73 %) in the free troposphere (350 hPa < p <900 hPa). The median bias in the upper troposphere (350 hPa > p > tropopause) is +95 %.

From these comparisons it is evident that the model has some skill in simulating the average global surface distribution of IO (within a factor of 2) and similar skill at reproducing average vertical profiles. However, there is significant variability between locations, datasets and measurement groups. Increased global coverage, especially vertically, and inter-comparison of observational techniques are needed to better constrain the IO distribution.

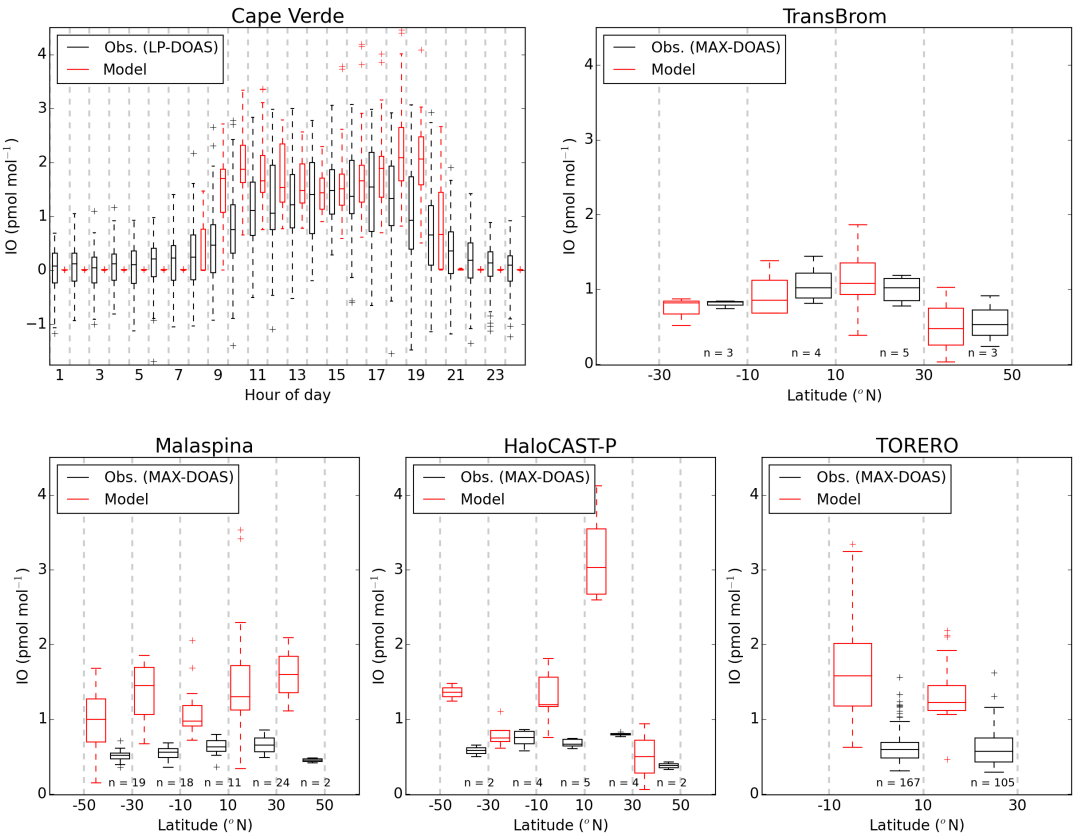

Figure 3.4 – Iodine oxide (IO) surface observations (red) by campaign compared against model (black). Cape Verde measurements are shown against hour of day and others are shown as a function of latitude. Observations are from Cape Verde (Tropical Atlantic, Mahajan et al. 2010; Read et al. 2008), TransBrom (West Pacific, Großmann et al. 2013), the Malaspina circumnavigation (Prados-Roman et al., 2015b), and HaloCAST-P (East Pacific, Mahajan et al. 2012). The number of data points within each latitudinal bin are shown as "n". The boxplot extents give the inter-quartile range, with the median shown within the box. The whiskers give the most extreme point within 1.5 times the interquartile range.

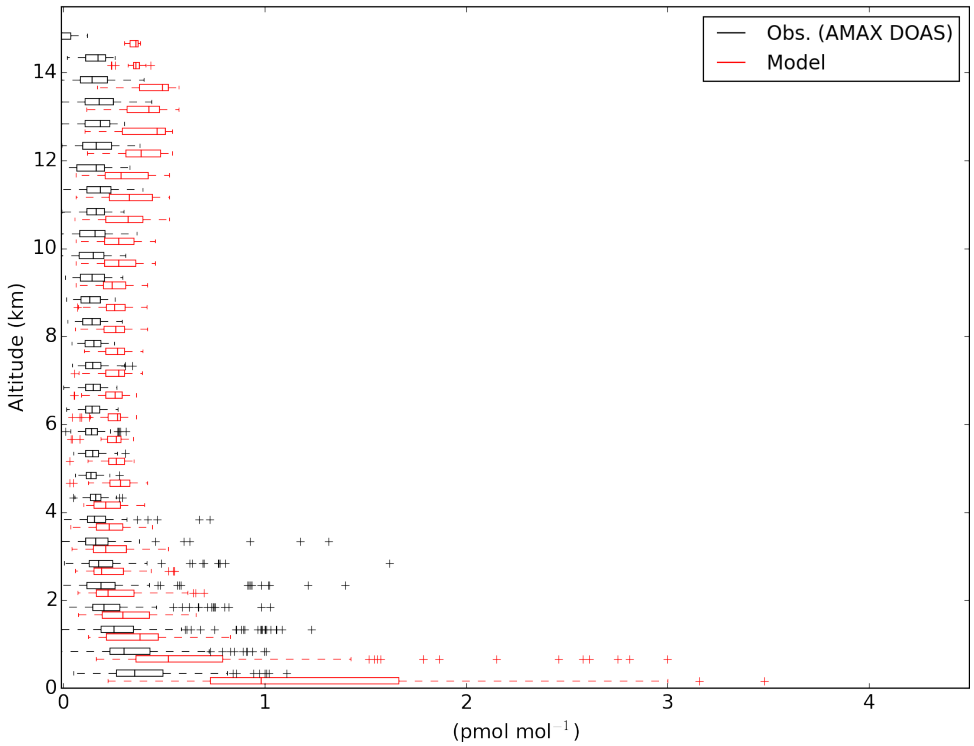

Figure 3.5 – Vertical comparison of modelled and measured iodine oxide (IO) during the TORERO research campaign. Model and observations are in red and black respectively. Measurements were taken aboard the NSF/NCAR GV research aircraft by the University of Colorado airborne Multi-Axis DOAS instrument (CU AMAX-DOAS) as part of the TORERO campaign (Volkamer et al., 2015; Wang et al., 2015) in the eastern Pacific in January and February 2012. The boxplot extents give the inter-quartile range, with the median shown within the box. The whiskers give the most extreme point within 1.5 times the interquartile range.

3.3 Iodine deposition

As discussed in Chapter I (Sect 1.6.4.3) iodine's availability in the biosphere is important due to its role as bio-nutrient (WHO, 2009) and for understanding the distribution of its radionuclides (I^{131} and I^{129}) which may be released from nuclear power stations (Reithmeier et al., 2010). This section describes the deposition of iodine as within the model.

The majority of iodine deposition occurs over the water (see Sect. 3.4.1). However, a proportion of this does occur over the land and it is this deposition that is important for public health as it is this iodine which can be taken up by soils and end up in the food-chain. This deposition is shown as an annual cumulative value per unit area, over all land and oceans (Fig. 3.7), and then just over the land in logarithmic (Fig. 3.8) and linear units (Fig. 3.9).

Measurements of deposition exist from the science community focused on isotopes (Krupp and Aumann, 1999; Aldahan et al., 2009) and some exist from the atmospheric science community (Baker et al., 2001). There are also measurements from the geological community of resultant concentrations in the geosphere (Fuge and Johnson, 1986; Johnson, 2003a,b). To compare against these observations, the processing in the hydrosphere or geosphere following deposition would need to be modelled. However, as the model presented here does not include coupling to a model of hydrosphere or geosphere, it is not possible to include the processing following deposition needed to compare between these values.

The assumption used within the epidemiology community is that the transfer of iodine to the land surface, estimated at $1\text{x}10^{-11}$ g (I) yr^{-1} (J Risher, 2009), decreases from distance from the coast. However, as shown by Figure 3.8, this is more dependent on meteorology (e.g. storm tracks) than distance from coast. This "rule of thumb"' has previously been brought into question (Johnson et al., 2003; Fuge, 2007), and when compared against the country reported iodide deficiency disorder (Fig. 3.6) the correlation is not visually evident. The estimates used by the WHO for fluxes to land are from Whitehead (1984) and give values of deposition of iodine to the soil from rainfall and snowfall 16 g (I) ha^{-1} yr^{-1} and 9.6 g (I) ha^{-1} yr^{-1}, for wet and dry deposition respectively.

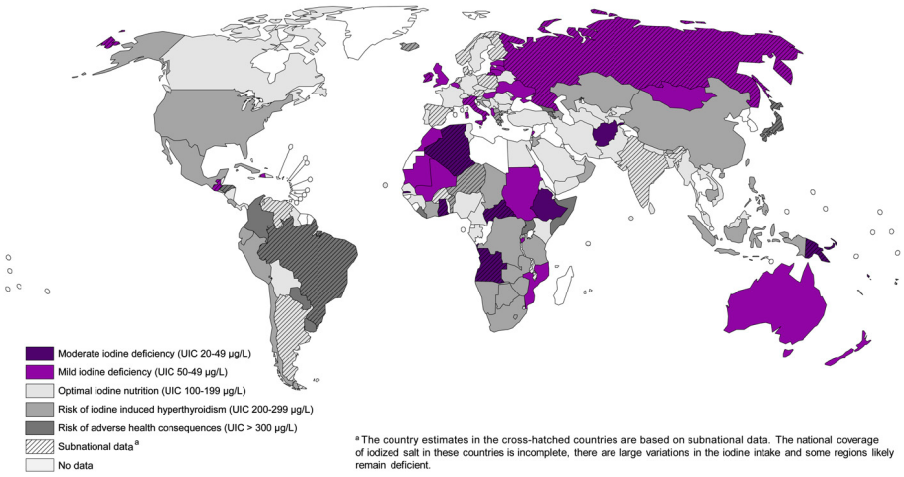

Figure 3.6 – "Degree of public health importance of iodine nutrition in SAC based on median UIC in 2011. SAC, school-age children; UIC, urinary iodine concentration." reproduced from Andersson et al. (2012).

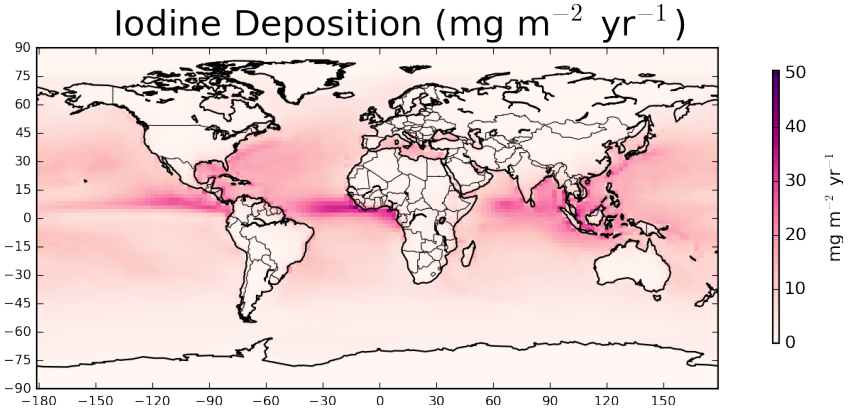

Figure 3.7 – Annual average iodine deposition in mg (I) m^{-2} yr^{-1}.

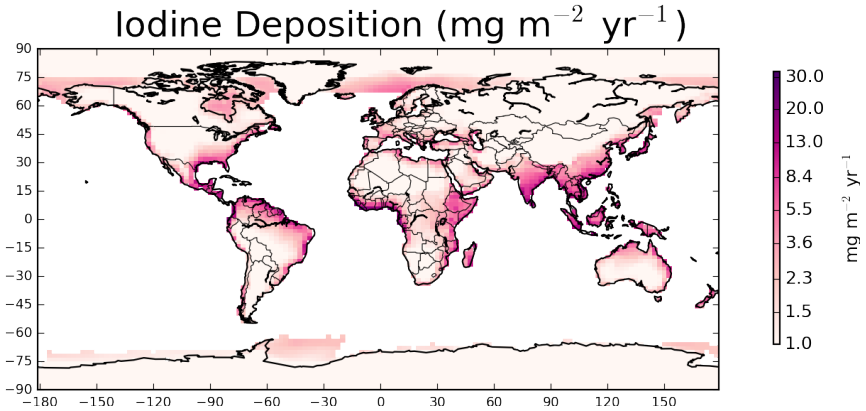

Figure 3.8 – Annual average iodine deposition over land and ice in mg (I) m^{-2} yr^{-1}. Scale is logarithmic.

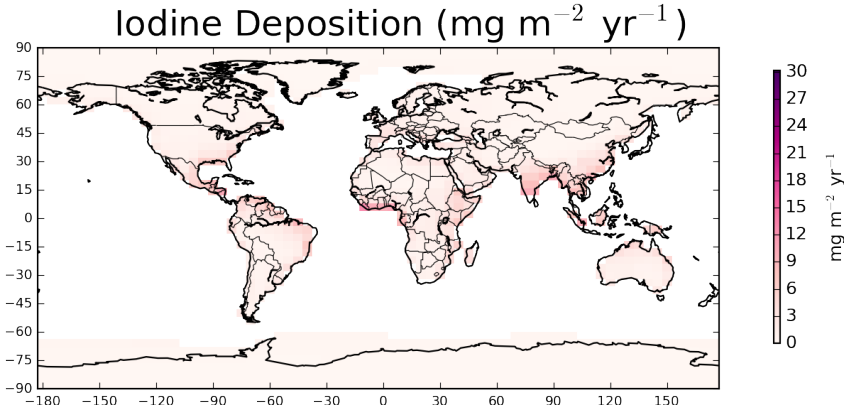

Figure 3.9 – Annual average iodine deposition over land and ice in mg (I) m^{-2} yr^{-1}.

The observations are broadly in the range of 0.3-1.5 mg (I) m^{-2} yr^{-1} (0.3-1.5 mg (I) m^{-2} yr^{-1}, Baker et al. 2001, 0.3-1.5, Aldahan et al. 2009; 1.3-1.7 m^{-2} yr^{-1}) and the model broadly captures the observed range at sites in Weybourne, Denmark, and Germany. However, it significantly (three times) over-estimates the deposition. This may reflect the excess iodine in the model consistent with the IO observation over-estimates or issues with the coarse spatial representation of the model. Interestingly too, the estimated total iodine source from the oceans used by the WHO (J Risher, 2009) is from Kocher (1981) and gives a total flux of 2 Tg (I) yr^{-1}, which compares well with values estimated herein (3.8 Tg (I) yr^{-1} in Chapter II-III and 2.75 Tg (I) yr^{-1} in Chapter IV-VI).

Further work with higher time resolution observations and spatial resolution model output would provide more insight into the model's performance in reproducing iodine deposition.

3.4 Modelled distribution of iodinated compounds

This section considers the averaged distribution of modelled iodine compounds. The global budget of inorganic iodine (I_y, as defined in the Footnote[1]) is considered in Section 3.4.1, with the budget of reactive iodine (IO_x=I+IO) described in Section 3.4.2.

3.4.1 I_y

The modelled iodine system is schematically shown in Figure 3.10. Iodine emissions total 3.8 Tg (I) yr^{-1} with most of this (3.2 Tg (I) yr^{-1}) coming from the inorganic source (84 %). This is comparable to the 83 % calculated by Prados-Roman et al. (2015b) (Ocean only, 60^oS-60^oN). Most (56 %) of the emissions occur in the tropics (22^oS-22^oN). The modelled emissions, which include inorganic emissions, are higher than reported values of 1.8 Tg yr^{-1} (Saiz-Lopez et al., 2012a) and 2.6 Tg (I) yr^{-1} (Saiz-Lopez et al., 2014) which also included an inorganic (fixed) source.

Figures 3.11 and 3.12 show the average vertical and zonal distribution of iodine compounds through the troposphere. As expected given the surface source, the concentration of iodine drops with altitude. This drop is rapid across the top of the boundary layer. The concentrations of the short-lived source gases (CH_2IX (X=Cl,Br,I) and I_2) are negligible outside of the lowest model levels but the concentrations of others (CH_3I and HOI) persist further through the column. For CH_3I this is due to its longer lifetime of ∼4 days. However, the lifetime of HOI is shorter (∼4 min) and its persistence at higher altitudes reflects secondary chemical sources. From the top of the boundary layer to ∼10 km the I_y profile is flat due to the rapid convective mixing within the tropics, however above this mixing zone the concentrations decrease. The inorganic iodine within the tropical (22^oS-22^oN) upper troposphere (>10 km) is approximately equally sourced from an upwards I_y flux (6.6 Gg yr^{-1}) and organic iodine photolysis (7.9 Gg yr^{-1}), overwhelmingly of CH_3I. Overall, atmospheric iodine is dominated by three IO_y species (HOI, IO, and INO_3) with HOI representing the greatest fraction (∼70 %) in the free troposphere (350 hPa < p <900 hPa).

[1] I_y is defined here as I_y= $2I_2$ + HOI + IO + OIO + HI + INO + INO_2 + INO_3 + $2I_2O_2$ + $2I_2O_3$ + $2I_2O_4$.

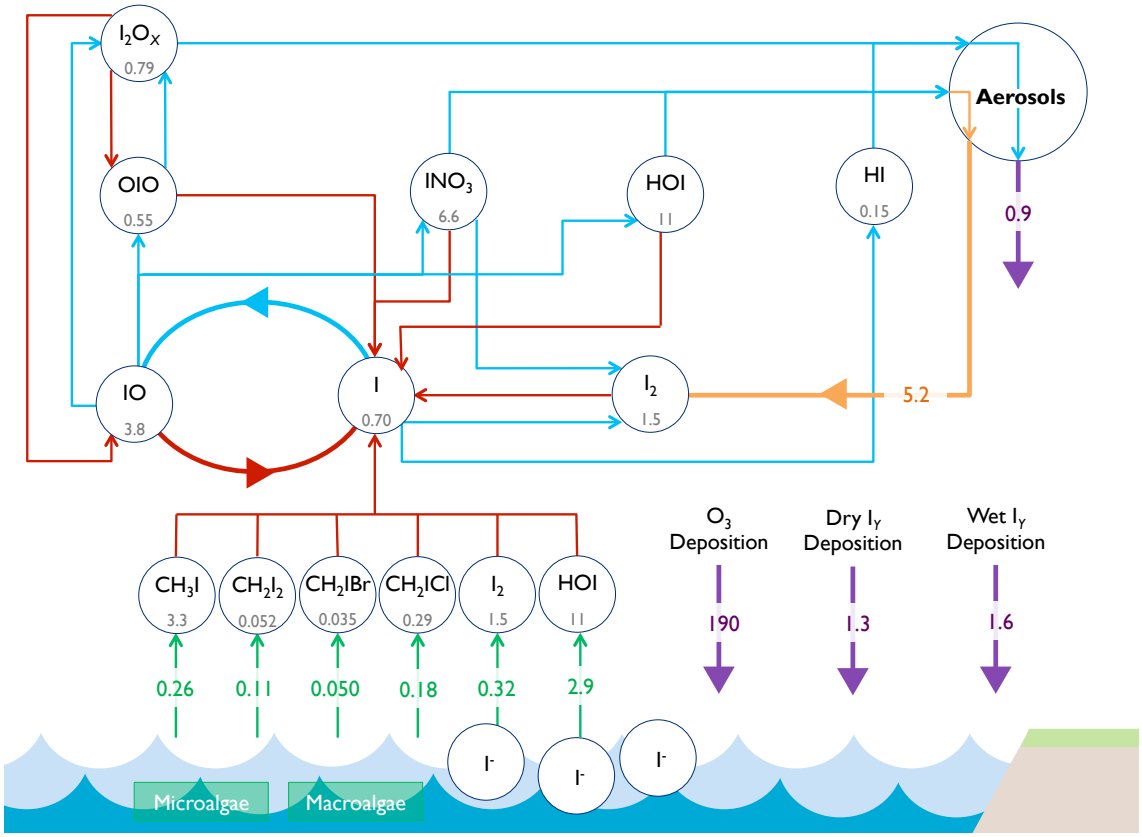

Figure 3.10 – Schematic representation of implemented iodine chemistry in simulation "Br+I". Average global annual mean burdens (Gg I) are shown below key I_y species, with fluxes (Tg (I) yr^{-1}) shown on arrows. Red lines=photolysis, blue=chemical pathways, green lines=emission source, orange lines=heterogeneous pathway, and purple lines=depositional pathway. This equates to a total iodine source and sink of 3.8 Tg (I) yr^{-1}. Oceanic O_3 deposition in Tg is also shown to illustrate the driving force behind the inorganic emissions.

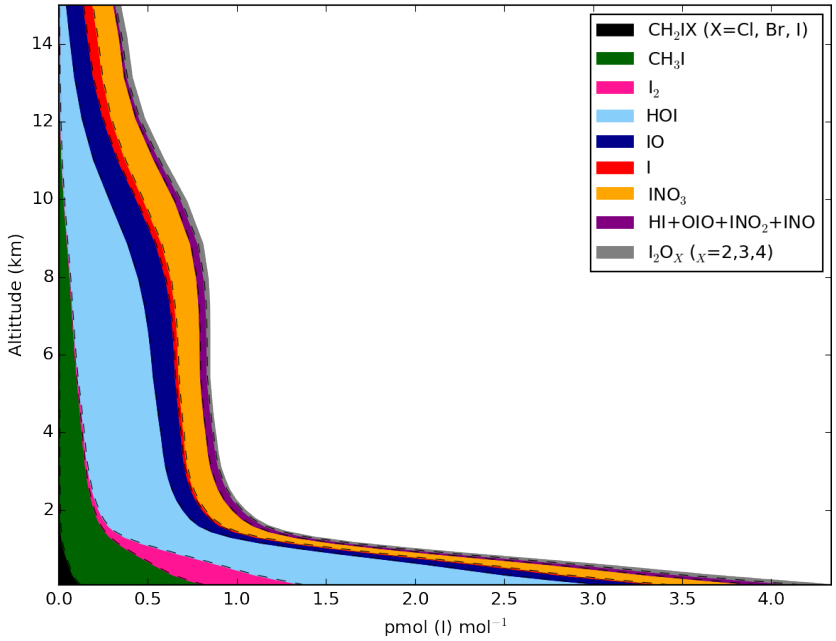

Figure 3.11 – Global annual mean gas-phase iodine speciation with altitude. Mixing ratios are shown in pmol mol^{-1}, with higher iodine oxides (I_2O_X, X = 2, 3, 4) and di-halogenated organics (CH_2IX, X = Cl, Br, I) grouped.

3.4.2 The iodine oxide family: IO_x (I+IO)

Global IO_x production is dominated by inorganic iodine I_y photolysis (HOI, 76 %; OIO, 11 %). The major loss route for IO_x is HOI production through IO's reaction with HO_2 (77 %), with additional loss routes through self-reaction, reaction with NO_x, and BrO contributing 10, 7.7, and 4.6 % respectively.

The global average IO_x lifetime with respect to chemical loss is ∼1 min, but this increases within the tropical upper troposphere (350 hPa > p > tropopause) by up to a factor of nine and beyond latitudes of 80^{o}N and S (up to four times) due to colder temperatures. The major IO formation route (I + O_3) slows in these regions due to colder temperatures, moving the partitioning of IO_x from IO to I. As the IO_x loss routes proceed predominantly through IO, the overall IO_x lifetime thus increases. This causes an increase in the annually averaged I to IO ratio which peaks with a ratio of 0.7-1.4 within the tropical upper troposphere (350 hPa > p > tropopause), where the coldest temperatures are located. This is at the lower end of the daytime range of 1-4 previously calculated (Saiz-Lopez et al., 2014).

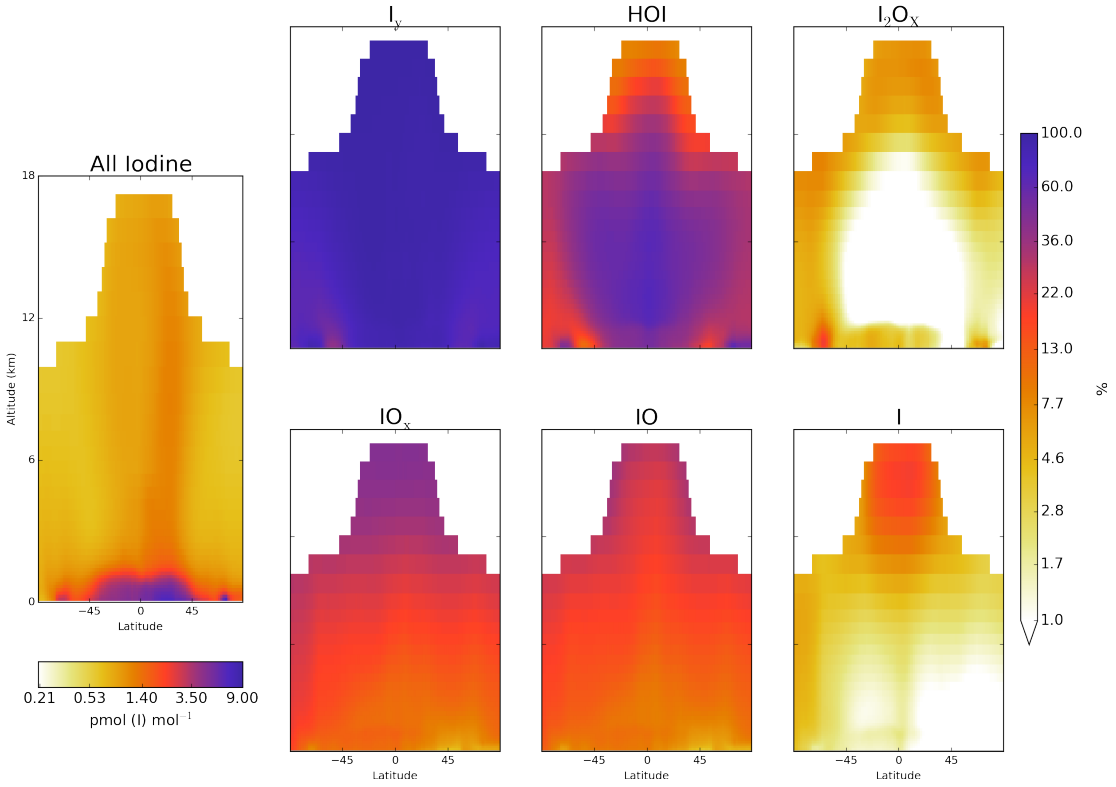

Figure 3.12 – Zonal breakdown of global annual mean iodine speciation by family. First panel shows total gas phase iodine concentration and the following panels show percentage of different compounds to this. Total gas phase iodine ("All iodine") = CH_3I+2CH_2I_2+CH_2IBr+CH_2ICl+2I_2+HOI+IO+OIO+HI+INO_2+INO_3+2I_2O_2 +2I_2O_3+2I_2O_4+I+INO; I_y=2I_2+HOI+IO+OIO+HI+INO+INO_2+INO_3 +2I_2O_2+2I_2O_3+2I_2O_4; IO_x =I+IO.

3.5 Impacts on oxidants

This section considers the iodine simulation ("Br+I") as described in chapter II (Sections 2.2-2.7) on oxidants (OH and O_3). First, the impacts on O_3 are considered in terms of changes in tropospheric O_3 burden (section 3.5.1.1), surface concentrations (section 3.5.1.2), and then the O_x (as defined in the Footnote[2]) budget (section 3.5.1.3). The impacts on OH are then considered in section 3.5.2.

3.5.1 Ozone

3.5.1.1 Tropospheric O_3 burden

On inclusion of iodine ("Br+I"), the calculated global tropospheric O_3 burden drops from 367 to 334 Tg (9.0 %). Figure 3.13 shows the annual average tropospheric column, surface and zonal change in O_3. On average, the O_3 burden in the marine boundary layer (900 hPa < p) decreased by 19.5 %, the free troposphere (350 hPa < p <900 hPa)by 9.8 %, and the upper troposphere (350 hPa > p > tropopause) by 6.2 %. The decrease is greater in the Southern Hemisphere (9.5 %), than the Northern Hemisphere (8.5 %).

Figure 3.14 shows a comparison between a selection of annually averaged O_3 sonde profiles for 2005 (WOUDC, 2014) and the model simulation with ("Br+I") and without iodine ("BROMINE"). A decrease in O_3 concentration is evident throughout the troposphere (average of 3.1 nmol mol^{-1}). No clear decline in model skill at capturing the annual sonde profiles is apparent on inclusion of iodine, with some locations improving and others degrading. An exception to this are O_3 observations in the tropical free troposphere (350 hPa < p <900 hPa) where model O_3 biases are decreased.

[2]Here O_x is defined here as O_3 + NO_2 + $2NO_3$ + PAN + PMN + PPN + HNO4 + $3N_2O_5$ + HNO_3 + BrO + HOBr + $BrNO_2$ + $2BrNO_3$ + MPN + IO + HOI + INO_2 + $2INO_3$ + 2OIO + $2I_2O_2$ + $3I_2O_3$ + $4I_2O_4$ where PAN = peroxyacetyl nitrate, PPN = peroxypropionyl nitrate, MPN = methyl peroxy nitrate, and MPN = peroxymethacryloyl nitrate

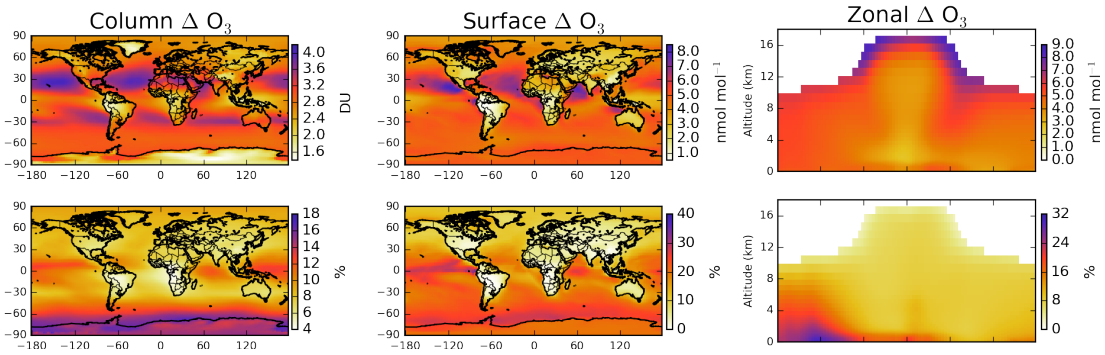

Figure 3.13 – Decreases in annual mean tropospheric column, surface and zonal O_3 with inclusion of iodine ("Br+I"-"BROMINE") chemistry are shown on left, middle and right panels respectively. Upper panels show changes in Dobson units (DU) or nmol mol^{-1} and lower panels show changes in percentage terms.

3.5.1.2 Surface O_3 concentration

Surface (lowermost model level) O_3 shows an average decrease of 3.5 nmol mol^{-1} globally, with large spatial variability (Fig. 3.13). These decreases are greater over the oceans (21 %) than the land (7.3 %). Comparing against the Global Atmospheric Watch (GAW, GAW 2014) surface O_3 observations, there is no obvious decrease in the ability of the model to capture seasonality in surface O_3 although there is systematic decrease in O_3 concentration with the inclusion of iodine (Fig. 3.15).

As with comparison of sonde observations (Fig. 3.14), no clear decline in model skill at capturing annual surface concentrations is apparent on inclusion of iodine. Some locations improve and others degrade. An exception to this is O_3 observations south of $\sim 60^o$S where bias are increased.

3.5.1.3 Tropospheric O_x budget

The impact of iodine on O_3 can be diagnosed by calculating the model's tropospheric odd oxygen (O_x, as defined in Footnote 2) budget as shown in Table 3.1. Iodine provides a global tropospheric O_x loss of 748 Tg yr^{-1} (15 % of the total). This is significantly larger than the 178 Tg yr^{-1} from the bromine chemistry included in the model and is comparable to the sink from the O_3+OH reaction. Overwhelmingly this loss is from the photolysis of HOI after its production from the reaction of IO with HO_2. The O_3 production term

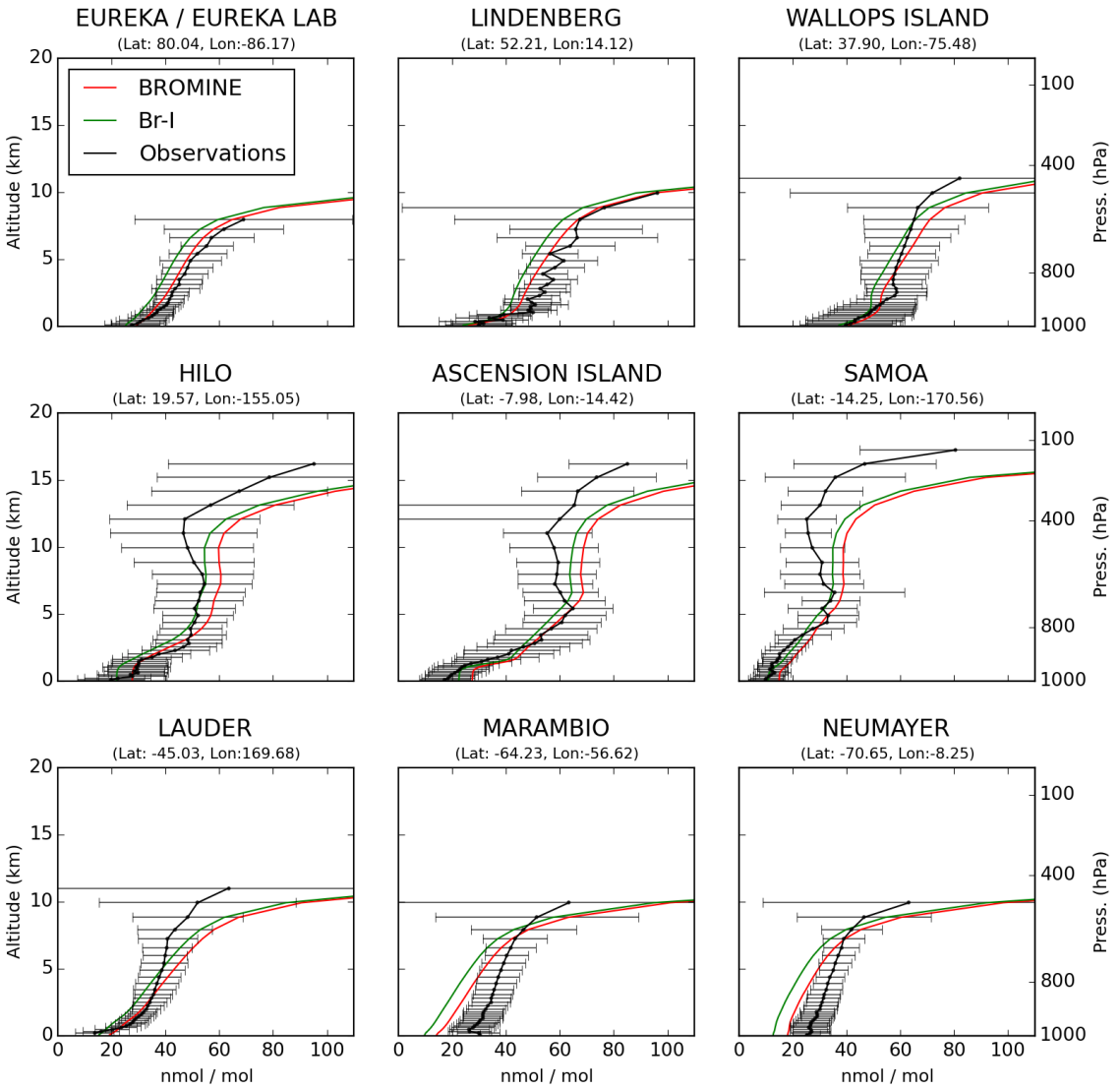

Figure 3.14 – Comparison between annual modelled O_3 profiles and sonde data (2005, WOUDC 2014). Profiles shown are the annual mean of available observations from World Ozone and Ultraviolet Radiation Data Centre (WOUDC, 2014) and model data for 2005 at given locations. Red indicates standard GEOS-Chem (v9-2) including bromine chemistry ("BROMINE") and green with inclusion of iodine chemistry ("Br+I"). Observations (in black) show mean concentrations with upper and lower quartiles given by whiskers.

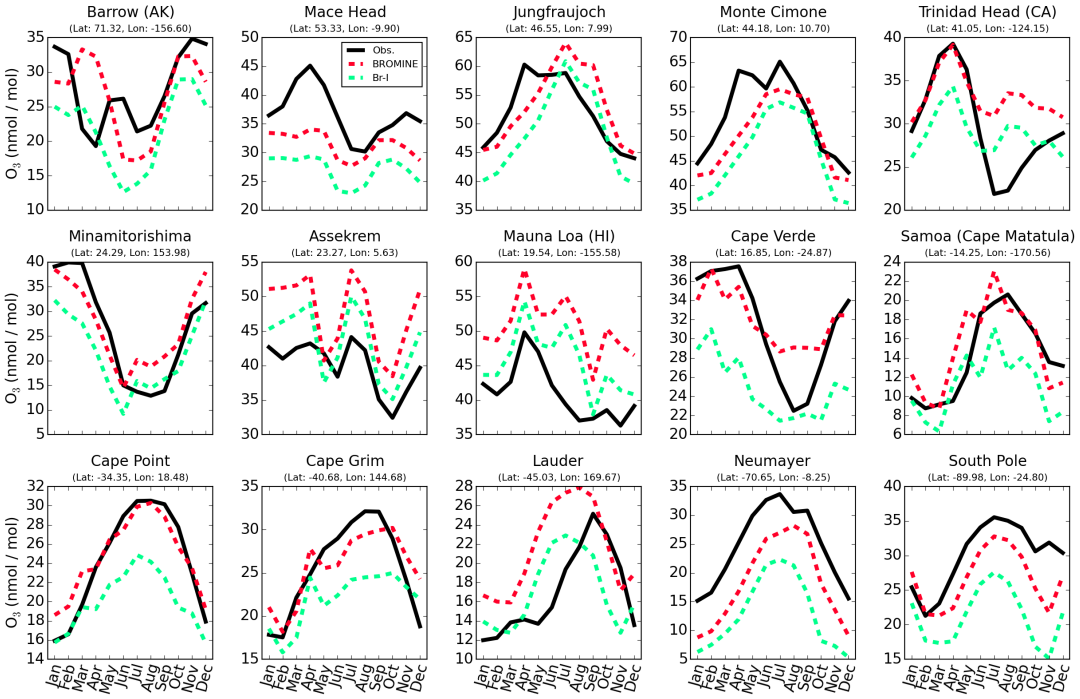

Figure 3.15 – Seasonal cycle of near-surface O_3 at a range of Global Atmospheric Watch (GAW, GAW 2014) sites (Sofen et al., 2016). Observational data shown is a 6 year monthly average (2006-2012). Model data is for 2005. Data is from GAW compiled and processed as described in Sofen et al. (2016). Red indicates standard GEOS-Chem (v9-2) including bromine chemistry ("BROMINE") and green with inclusion of iodine chemistry ("Br+I").

increases slightly (1 %) with the inclusion of iodine reflecting small changes in the total reactive nitrogen partitioning.

Iodine induced O_3 loss within the marine (land masked between 50^{o}S-50^{o}N) troposphere of ∼540 Tg yr^{-1} is comparable to the previous reported value of ∼500 Tg yr^{-1} for the simulation when I_2O_X (X=2,3,4) photolysis is included (Saiz-Lopez et al., 2014).

Figure 3.16 shows the relative importance of different O_x sinks in the vertical. The "classical" O_3 loss routes (hν+H_2O, HO_x) dominate. Globally within the boundary layer iodine represents ∼23 % of the loss. Within the marine boundary layer however, iodine represents ∼33 % of the total O_3 loss routes, which is comparable to the 28 % reported in Prados-Roman et al. (2015a). The mid-troposphere shows a lower significance for iodine chemistry at only 10 % reflecting the lower of IO concentrations (see Figs. 3.8 and 3.9). In the upper troposphere (350 hPa > p > tropopause), 26 % of the total loss is attributable to iodine. The higher IO_x and BrO_x concentrations found in the upper troposphere lead to this increase in the O_3 destruction.

Figure 3.17 shows the zonal variation in the different O_x destruction terms (in terms of the O_3 lifetime). It is evident that, in the model ("Br+I"), iodine destruction is more spatially prevalent than bromine destruction, which is confined predominantly to the Southern Ocean (see Chapter II Fig.2.6 for surface BrO concentrations). The impact of iodine is hemispherically asymmetric reflecting the higher NO_x in the Northern Hemisphere, higher BrO concentrations in the southern oceans and the larger ocean area in the Southern Hemisphere increasing emissions. Convective transport in the tropics rapidly lifts iodine species into the free troposphere (350 hPa < p <900 hPa) where they can destroy O_3.

3.5.2 OH

The inclusion of iodine in the model has little impact on the global mean OH concentrations with it slightly increasing from 12.2 to 12.5x10^5 molecules cm^{-3} (1.8 %). This is in contrast to previous box model studies which investigated the impact of iodine on OH concentration in the Antarctic (Saiz-Lopez et al., 2008), mid-latitude coastal (Bloss et al., 2005b), tropical marine regions (Mahajan et al., 2010), and the free troposphere (Wang et al., 2015) which simulate significant increases in the OH concentration due to IO enhancing conversion of HO_2 to OH.

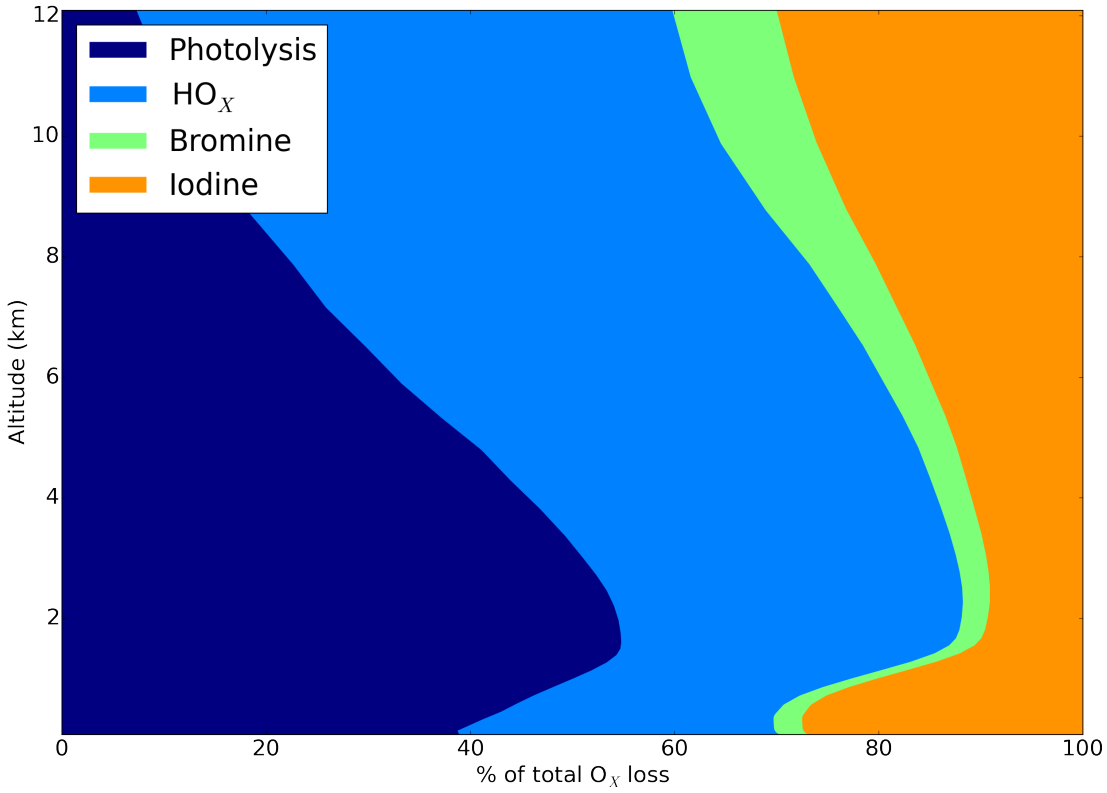

Figure 3.16 – Vertical profile of simulated fractional global annual mean O_x loss by route in the "Br+I" simulation. O_x definition is given in Footnote 2. Photolysis represents loss of O_x due to O_3 photolysis in the presence of water vapour. HO_x loss includes routes via minor NO_x channels. The magnitude of the bromine route is probably underestimated as discussed in Chapter II 2.6

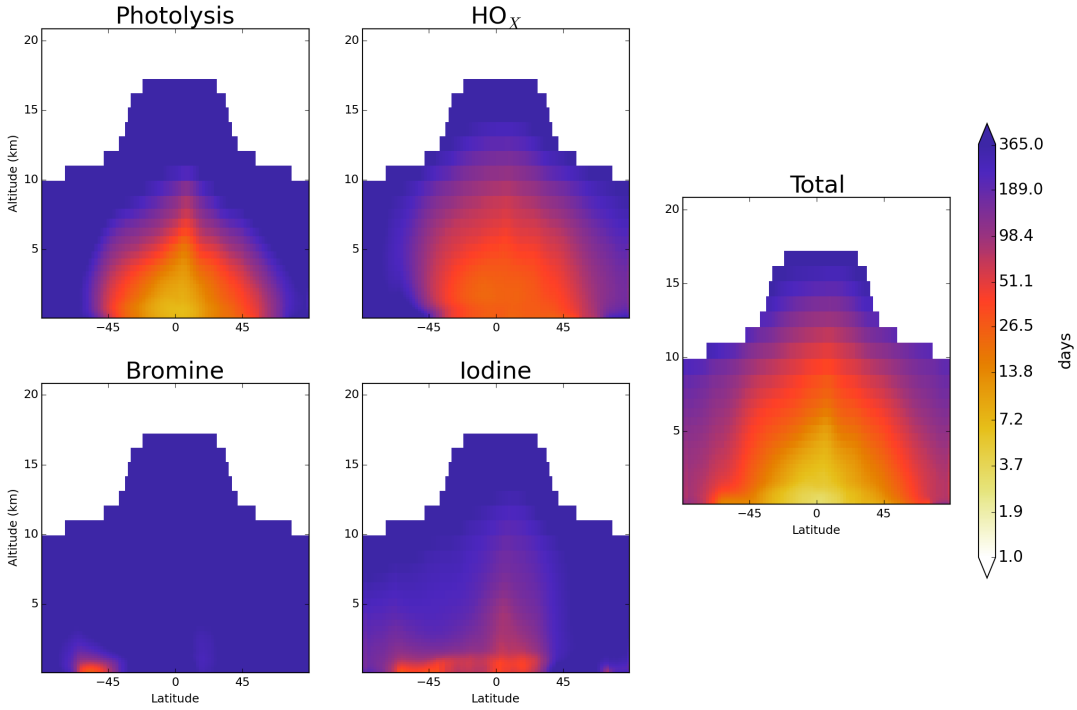

Figure 3.17 – Global annual O_3 mean zonal chemical lifetime for different O_x loss routes (Photolysis, HO_x, Iodine, Bromine, and Total) in the "Br+I" simulation. Values are shown on a log on a scale.

Table 3.1 – Comparison between global tropospheric O_x budgets of simulations "BROMINE", "Br+I" , "IODINE" and "NOHAL" are described here. "BROMINE" includes just bromine chemistry, "Br+I" which includes both iodine and bromine chemistry, "IODINE" only includes iodine chemistry, and "NOHAL" is simulation without iodine or bromine chemistry. Recent average model values from ACCENT (Young et al., 2013) are also shown. For the IO+BrO halogen crossover reaction we allocate half the O_3 loss to bromine and half to iodine. Values are rounded to the nearest integer value.

Scenario	"NOHAL"	"IODINE"	"BROMINE"	"Br+I"	ACCENT
O_3 burden (Tg)	390	357	367	334	340 ± 40
Chemical O_x sources (Tg Yr^{-1})					
$NO + HO_2$	3667	3680	3512	3529	–
$NO + CH_3O_2$	1332	1383	1269	1307	–
Other O_x sources	502	518	505	521	–
Total chemical O_x sources (PO_x)	5501	5581	5286	5357	5110 ± 606
Chemical O_x sinks (Tg Yr^{-1})					
$O_3 + h\nu + H_2O \rightarrow 2OH + O_2$	2579	2271	2425	2119	–
$O_3 + HO_2 \rightarrow OH + O_2$	1391	1186	1274	1080	–
$O_3 + OH \rightarrow HO_2 + O_2$	687	627	621	560	–
$HOBr + h\nu \rightarrow Br + OH$	–	–	166	143	–
$HOBr + HBr \rightarrow Br_2 + H_2O$ (aq. aerosol)	–	–	8	8	–
$BrO + BrO \rightarrow 2Br + O_2$	–	–	12	10	–
$BrO + BrO \rightarrow Br_2 + O_2$	–	–	3	3	–
$BrO + OH \rightarrow Br + HO_2$	–	–	6	5	–
$IO + BrO \rightarrow Br + I + O_2$	–	–	–	7	–
Other bromine O_x sinks	–	–	1	1	–
Total bromine O_x sinks (Tg Yr^{-1})	–	–	195	178	–
$HOI + h\nu \rightarrow I + OH$	–	639	–	583	–
$HOI \rightarrow 0.5I_2$ (sea-salt aerosol)	–	2	–	2	–
$IO + BrO \rightarrow Br + I + O_2$	–	–	–	7	–
$OIO + h\nu \rightarrow I + O_2$	–	114	–	156	–
Other iodine O_x sinks	–	1	–	1	–
Total iodine O_x sinks (Tg Yr^{-1})	–	756	–	748	–
Other O_x sinks	176	181	172	179	–
Total chem. O_x sinks (LO_x)	4833	5021	4687	4864	4668 ± 727
O_3 $P(O_x)$-$L(O_x)$ (Tg Yr^{-1})	668	560	599	493	618 ± 251
O_3 Dry deposition (Tg Yr^{-1})	949	850	886	791	1003 ± 200
O_3 Lifetime (days)	25	22	24	22	22 ± 2
O_3 STE (PO_x-LO_x-Dry dep.) (Tg Yr^{-1})	281	290	287	298	552 ± 168

The small increase that we calculate here is surprising given the 12 % reduction in the primary source (O_3+H_2O+$h\nu$) due to lower O_3 concentrations. However, this is more than compensated for by an increase in the rate of conversion of HO_2 to OH by IO. Previous studies using constrained box models (Bloss et al., 2005b; Saiz-Lopez et al., 2008) could not consider this impact of iodine on the primary production of OH and it appears from the simulations here that the overall impact of iodine on OH essentially cancels out.

3.6 Combined impact of bromine and iodine

The importance of halogen cross-over reactions (BrO+IO) for O_3 loss has been previously highlighted and found to be required to reproduce observed diurnal surface O_3 loss in the marine boundary layer (Read et al., 2008).

To explore these interactions a further, two additional runs were performed. A simulation with iodine but without bromine ("IODINE") and a simulation without any halogens ("NOHAL").

Table 3.1 shows the global tropospheric burdens of O_3 without halogens ("NOHAL"), with just bromine ("BROMINE"), with just iodine ("IODINE") and the combined impact (Br-I). Bromine alone gives a reduction in burden of 5.9 %, iodine alone a reduction of 8.5 % and the combined impact is 14.5 %. The sum of the changes in O_3 burden for the runs considering halogens individually is slightly lower (0.1 %) than when considered simultaneously. Figure 3.18 shows the combined daily surface loss rate of O_3 driven by bromine and iodine (upper panel). This correlates with IO concentrations (Fig. 3.4). Figure 3.18 also shows modelled and observed fractional diurnal fractional O_3 change at Cape Verde in the remote marine boundary layer (lower panel). For this comparison, observations (2006 to 2012, Carpenter et al. 2010) and model data were first processed to average fractional diurnal change by averaging the values by hour of day, then subtracting the maximum average value of the diurnal. This fractional change was then divided by the average maximum value and multiplied by 100, allowing comparison between simulation runs with different O_3 concentrations. The simulation's fidelity increases significantly with the inclusion of iodine (Fig. 3.18) but there is little impact from bromine. Whereas modelled IO concentrations at Cape Verde shows agreement with observations (Fig. 3.18), BrO concentrations ($\sim$0.4 pmol mol^{-1}) are significantly lower than reported ($\sim$2 pmol mol^{-1}, Read et al. 2008). This underestimate of surface BrO in the model is a systemic problem (see Chapter II, Section 2.6) and so model estimates of the impact of Br on atmospheric composition described here are probably an underestimate.

Global mean tropospheric concentrations of OH are 12.80, 12.24, 13.02, and 12.47 x10^5 molecules cm^{-3} for the simulations without halogens ("NOHAL"), with just bromine ("BROMINE"), with just iodine ("IODINE"), and with both iodine and bromine chem-

istry ("Br+I") respectively. OH shows a differing response to bromine and iodine chemistry. As discussed in Sect. 3.5.2, inclusion of iodine leads to a small increase in OH concentrations. When solely iodine is considered, OH concentrations increase by 1.8 % compared to when no halogens are included. Bromine chemistry alone leads to a reduction in OH (4.3 %), as reported previously (Parrella et al., 2012), due to enhanced production by HOBr photolysis not compensating for a decrease in the primary OH source (O_3+H_2O+hν) from a reduced O_3 burden. The net impact overall on inclusion of halogens is a global reduction in OH (2.6 %). Again this impact of bromine is roughly comparable to the addition of iodine and bromine chemistry.

In the simulation "Br+I", the global impact of Br and I chemistry are essentially additive with apparently limited impact from the cross reactions. The global impact of iodine appears significantly larger than that of bromine, however, given that the model underestimates the concentrations of Br compounds this should be subject to future study. These interactions between halogens are studied further in Chapter IV, for which the representation of tropospheric chlorine is added and the bromine simulation is updated.

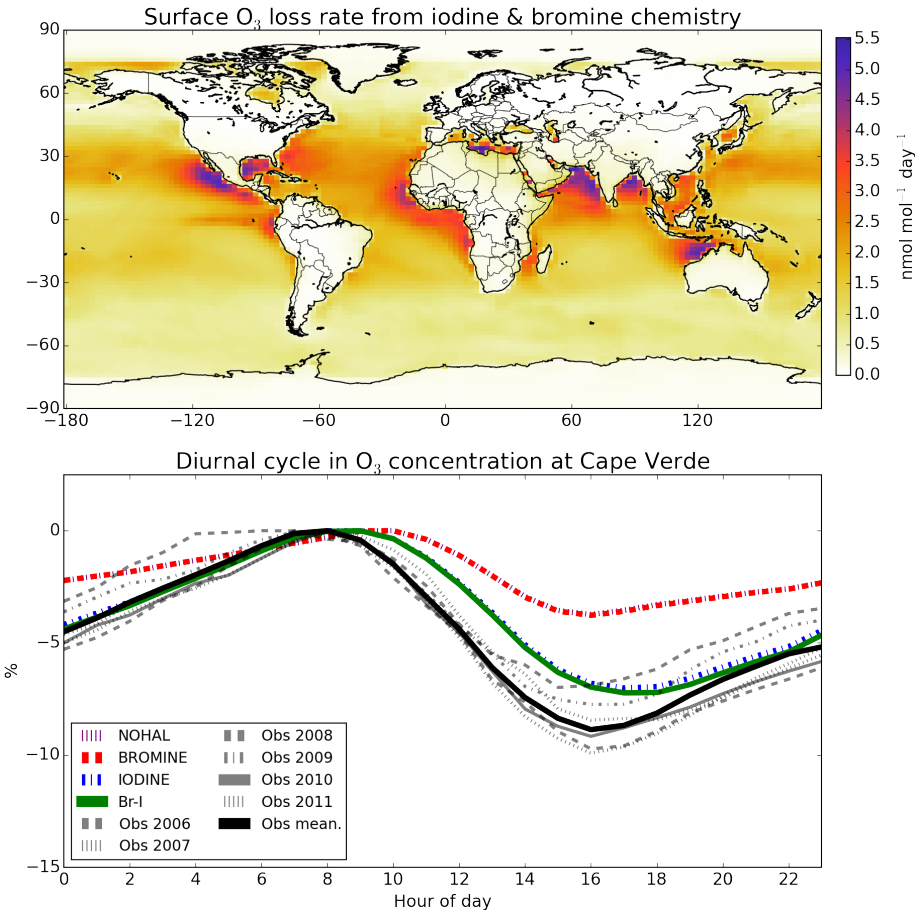

Figure 3.18 – Global annual mean surface O_3 loss (nmol mol^{-1} day^{-1}) in the "Br+I" simulation from both bromine and iodine (top). Comparison between modelled and observed fractional diurnal O_3 cycles at the Cape Verde Observatory for "NOHAL", "BROMINE", "IODINE" and "Br+I" simulations (bottom). Calculation is described in text in Section 3.6. Diurnal changes are averaged over the whole dataset. Lines are black, purple, red, blue and green for mean of observations, "NOHAL", "BROMINE", "IODINE" and "Br+I" respectively. Individual years of observational data are shown in grey.

3.7 Sensitivity studies

As discussed in the introduction (Chapter I), a range of uncertainties exist within tropospheric iodine chemistry. This section describes some sensitivity analysis performed on some of these parameters using the 4^ox5^o version of the "Br+I" simulation. The chosen parameters are: iodine emissions, heterogeneous loss and cycling, photolysis rates and ocean surface iodide concentration.

Values are quoted as a % change from the "Br+I" simulation described in Chapter II, and all differences in key parameters are listed in Table 3.2. Figure 3.19 summarises the fractional impact of these experiments on the globally averaged vertical distribution of I_y, O_3 and vertical profile comparison of observations of IO from the TORERO campaign (Volkamer et al., 2015; Wang et al., 2015).

Table 3.2 – Effects of sensitivity runs on relevant variables. Values are shown as percentage change from the simulation with both iodine and bromine chemistry ("Br+I") in the troposphere as global means unless otherwise stated. MBL = Marine Boundary Layer (900 hPa <p), O_x is defined as in Footnote 2. CH_4 lifetime is calculated globally in the troposphere with respect to loss by reaction with OH.

	Mean IO MBL surface concentration	Chem. O_x loss (LO_x)	Chem. O_x prod. (PO_x)	PO_x -LO_x	O_3 burden	O_3 deposition
NOHAL	-100.00	2.34	-0.75	40.91	15.99	17.75
BROMINE	-100.00	-1.79	-3.90	24.50	9.12	10.42
IODINE	9.63	3.87	2.89	16.16	6.90	6.87
Br+I	0.00	0.00	0.00	0.00	0.00	0.00
Just org. I	−83.45	−1.64	−3.11	17.69	5.53	7.19
I_2O_x loss (γ) ×2	−4.26	−0.15	−0.28	1.61	0.54	0.59
I_2O_x loss (γ)/2	3.93	0.13	0.24	−1.34	−0.44	−0.52
Het. cycle (γ) ×2	2.21	0.04	0.16	−1.61	−0.69	−0.56
Het. cycle (γ)/2	−1.84	−0.06	−0.14	1.07	0.56	0.45
No Het. cycle	−48.03	−1.15	−2.20	12.60	4.09	5.23
Sulphate Uptake	−22.49	−1.25	−2.26	12.06	4.54	4.94
Ocean iodide	−34.28	−0.66	−1.26	7.24	2.06	3.01
I_2O_x X-sections ×2	4.30	0.11	0.22	−1.34	−0.40	−0.47
I_2O_x exp. X-sections	6.73	0.19	0.35	−1.88	−0.60	−0.73
No I_2O_x Photolysis	−39.35	−1.10	−2.12	12.33	5.05	4.86
MBL BrO 2 pmol mol^{-1}	−6.78	−3.59	−2.71	−15.28	−3.73	−6.03

Table 3.3 – Continued.

	OH mean concentration	HO_2 mean concentration	HO_2 :OH	I_y lifetime	IO_x lifetime	I_y burden	CH_4 lifetime
NOHAL	2.49	8.44	5.81	-100.00	105.16	-100.00	-3.73
BROMINE	-1.65	5.72	7.50	-100.00	89.64	-100.00	0.80
IODINE	4.30	2.31	-1.91	-1.31	-1.82	6.96	-4.67
Br+I	0.00	0.00	0.00	0.00	0.00	0.00	0.00
Just org. I	−0.64	3.53	4.19	123.92	16.09	−64.26	0.21
I_2O_x loss (γ) ×2	−0.08	0.27	0.36	−8.38	−0.93	−5.08	0.03
I_2O_x loss (γ)/2	0.05	−0.22	−0.27	8.00	0.55	4.27	−0.01
Het. cycle (γ) ×2	0.09	−0.39	−0.49	4.61	1.13	5.98	0.00
Het. cycle (γ)/2	−0.09	0.32	0.41	−3.89	−0.96	−5.04	0.02
No Het. cycle	−0.47	2.58	3.07	−61.18	5.38	−46.69	0.15
Sulphate Uptake	−0.87	2.70	3.60	−59.60	0.49	−48.49	0.52
Ocean iodide	−0.17	1.22	1.39	16.90	2.77	−23.42	0.01
I_2O_x X-sections ×2	0.05	−0.20	−0.25	5.26	0.61	3.10	−0.01
I_2O_x exp. X-sections	0.08	−0.31	−0.39	8.31	0.84	4.81	−0.01
No I_2O_x Photolysis	−0.90	2.54	3.48	−46.41	−17.68	−34.58	0.32
MBL BrO 2 pmol mol^{-1}	−3.31	−1.44	1.93	−3.72	3.33	−10.07	4.17

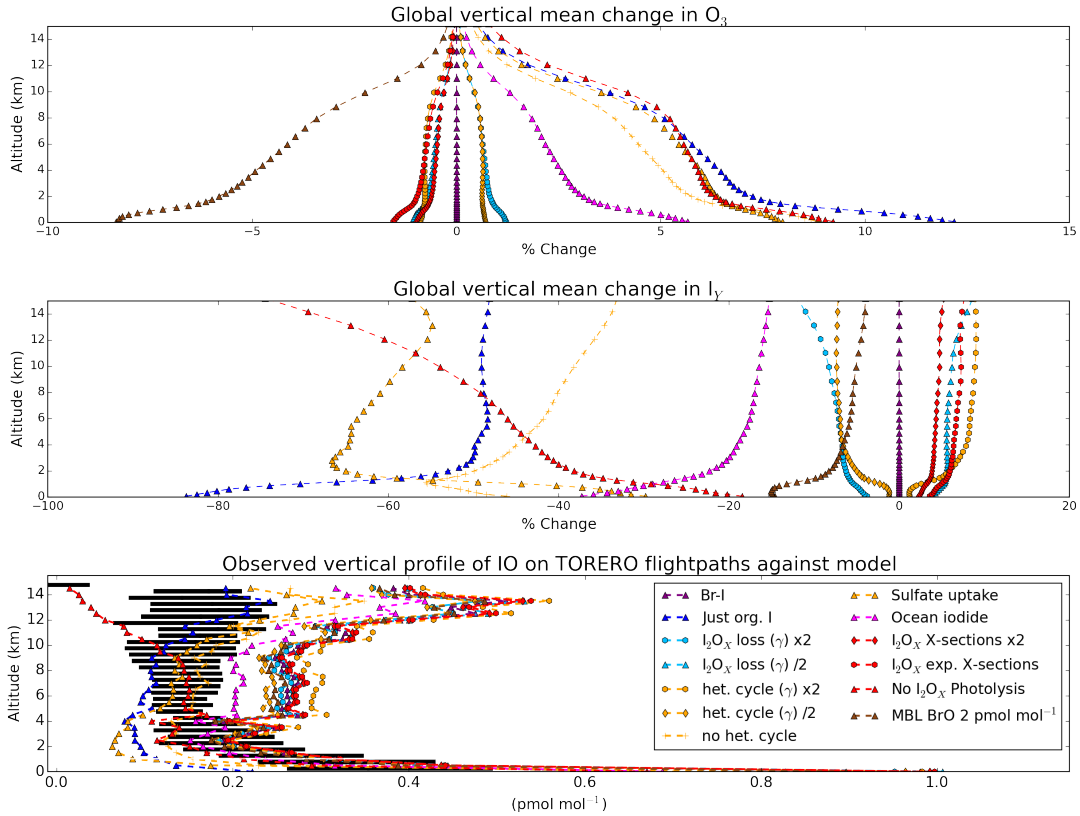

Figure 3.19 – Sensitivity impacts. Upper and middle panels show global mean vertical percentage changes in concentrations of O_3, and I_y, Lower panel gives vertically averaged iodine oxide (IO) mixing ratios (pmol mol^{-1}) calculated along the TORERO (Volkamer et al., 2015; Wang et al., 2015) flight-paths. The legend (bottom) is shared by all plots. The boxplot of IO observations (black) represents the quartiles of the data, with the median shown within the box.

3.7.1 Just organic iodine emissions ("Just I Org")

Until recently, many studies solely considered organic iodine (Jones et al., 2010; Ordóñez et al., 2012) emissions, as the inorganic source was unknown. As discussed in Chapter II (Section 2.2), the "Br+I" simulation uses the Carpenter et al. (2013) inorganic emission parameterisation as well as organic iodine emissions from Ordóñez et al. (2012). Switching off the inorganic iodine emissions (simulation ("Just org. I")) leads to an 85 % reduction in the emission of iodine into the atmosphere. Global I_y burdens decrease (65 %), and mean surface marine boundary layer (900 hPa < p) IO decreases (83 %). The median bias against TORERO IO observations decreases by 68 % to become a negative bias of ∼25 %. The decreased I_y leads to the mean global OH decreasing by 0.64 % and global

tropospheric O_3 increasing by 5.5 % compared to the base "Br+I" simulation.

Inorganic iodine emissions thus have a profound impact on the role of iodine on the composition of the atmosphere. Understanding their magnitude is thus central to our ability to understand the role of iodine in impacting tropospheric composition.

3.7.2 Heterogeneous uptake and cycling

There is limited experimental data for the reaction probability (γ) for iodine species on aerosol. The model (Chapter II Sect. 2.4) follows previous work McFiggans et al. (2000) and assumes a heterogeneous recycling of unity (e.g. HOI $\rightarrow 0.5I_2$) on sea-salt which is not limited by aerosol acidity. However, the acidity of aerosol may limit iodine cycling as not all sea-salt aerosols are acidic (Alexander, 2005) and other aerosols may irreversibly uptake iodine. To explore these uncertainties, four simulations were run: (1) with the values that lead to I_2 release doubled ("het. cycle x2"), (2) with the values halved ("het. cycle/2"), (3) with all uptake reactions leading to a net loss of iodine ("No het. cycle"), and (4) a run where sulfate aerosol leads to a sink for iodine with the reactive uptake coefficients as used for sea-salt ("Sulfate uptake").

Increasing the heterogeneous cycling ("het. cycle x2") converts more HOI (the dominant I_y species) into I_2, thus reducing the rate of HOI deposition. The global I_y burden increases by 6 %, the mean surface marine boundary layer (900 hPa < p) IO concentration increases by 2 % and the median bias with respect to the TORERO IO observations increases by 26 % to 100 % (Fig. 3.19). Decreasing the heterogeneous cycling ("het. cycle/2") has the opposite impact of roughly the same magnitude, global average I_y burden decreases (4.3 %), average surface marine boundary layer IO decreases (1.8 %) and the median bias with respect to the TORERO IO observations decreases (18 %) to 66 %. The impacts of theses changes is small overall; increased iodine cycling leads to a decrease in the tropospheric O_3 burden of 0.69 % and a global mean OH increase of 0.05 %, and decreased iodine cycling leads to the tropospheric O_3 burden increasing by 0.56 % and OH decreasing by 0.09 %.

Making more significant changes by removing entirely the release of I_2 to the gas-phase following uptake of iodine ("no het. cycle") or by considering irreversible iodine loss to sulfate aerosol ("Sulfate uptake") decreases the global I_y burden significantly by 47 and 48 %, respectively. Surface marine boundary layer (900 hPa < p) IO concentration decreases

by 48 % and 22 %, respectively. The median bias with respect to the TORERO IO observations decreases in the case of "no het. cycle" (by 84 %) to 13 % and decreases in "Sulfate uptake" (by 92 %) to 6.7 %. The "Sulfate uptake" scenario shifts the median bias with the TORERO IO observations to be negative, instead of positive (+80% for "Br+I" at 4^ox5^o resolution).

These large decreases in I_y reduces the potency of iodine chemistry. The reductions in the tropospheric O_3 burdens (4.1 and 4.5 % for "no het. cycle" and "Sulfate uptake") are comparable to the simulation where only organic iodine sources are considered (5.5 %, "Just I Org."). Global mean OH decreases slightly by 0.54 and 0.87 % under these two scenarios. These two sensitivity runs represent large perturbations to the iodine system, highlighting the importance and uncertainties in heterogeneous chemistry.

The model shows limited sensitivity to the values of γ used here. They are fast enough not to be rate limiting on a global scale. Switching them off entirely though leads to large changes.

3.7.3 Uncertainties in photolysis parameters

Absorption cross-sections and quantum yields for iodine species are few and their temperature dependencies are not known. Notably, the absorption cross sections for the higher iodine oxides (I_2O_2, I_2O_3, I_2O_4) are highly uncertain (Bloss et al., 2001; Gómez Martín et al., 2005; Spietz et al., 2005) and for this study the INO_3 spectrum is used as a surrogate. This uncertainty was tested in three simulations: (1) absorption cross-sections were doubled ("I_2O_X X-sections x2"), (2) tentative literature assignments of spectra were used for I_2O_3 and I_2O_2 (Bloss et al., 2001; Gómez Martín et al., 2005; Spietz et al., 2005), with I_2O_2 used for I_2O_4 ("I_2O_X exp. X-sections"), (3) and finally no I_2O_X photolysis at all was considered ("No I_2O_X photolysis"). Sensitivity runs "I_2O_X X-sections x2"and "I_2O_X exp. X-sections" increase photolysis rates, resulting in an increase in the I_y lifetime of 5.3 and 8.3 % and the I_y burdens by 3.1 and 4.8 %, respectively. The average surface marine boundary layer (900 hPa < p) IO concentration responds by increasing by 4.3 and 6.7 % for "I_2O_X X-sections 2" and "I_2O_X exp. X-sections" respectively. Both these simulations increase median bias with TORERO IO observations by 4.8 to 84 % and 7.6 to 86 %, respectively. The impacts on O_3 burden are small with a decrease of 0.4 and 0.6

% for "I_2O_X X-sections x2"and "I_2O_X exp. X-sections" respectively. Global mean OH concentrations increase by 0.05 and 0.09 % respectively.

The removal of I_2O_X (X = 2,3,4) photolysis reduces the global tropospheric I_y burden (35 %), reduces surface marine boundary layer (900 hPa < p) IO (40 %), increases tropospheric O_3 burden (5.1 %) and decreases global mean OH (0.9 %) with respect to "Br+I". The median bias with respect to the TORERO IO observations becomes negative and decreases by 81 to 16 %, illustrating a large change in the simulated IO profile by removing the I_2O_X photolysis (Fig. 3.19). This was also noted by Prados-Roman et al. (2015b) with respect to surface observations.

The "No I_2O_X photolysis" simulation is akin to the "base" simulation of Saiz-Lopez et al. (2014). This was presented as a lower bounds for iodine chemistry. Their "JI_xO_y" simulation, is akin to the "Br+I" simulation presented here. Saiz-Lopez et al. (2014) find a decrease in marine tropospheric O_3 column burden of 3.0 and 6.1 % compared to a simulation with no iodine chemistry for their "base" and "JI_xO_y" simulations respectively. Considering the same domain the comparable simulations show values of 4.0 to 8.7 %.

3.7.4 Marine boundary layer BrO concentration

As discussed in Sect. 3.6 and Chapter II (Section 2.6), bromine and iodine chemistry are coupled. GEOS-Chem underestimates BrO (Parrella et al., 2012), with for example, the simulation "Br+I" underestimating the BrO concentrations at Cape Verde (Read et al., 2008) (2 pmol mol^{-1}) by a factor of ∼5.

To test the sensitivity of the model to BrO concentrations, a simulation with BrO concentration fixed at 2 pmol mol^{-1} in the daytime marine boundary layer was run ("MBL BrO 2 pmol mol^{-1}"). Increased BrO leads to increased OIO concentrations (BrO+IO→OIO+Br), which leads to increased higher oxide production which in turn increases I_y loss and decreases the I_y burden (10 %). The median bias in vertical comparisons with TORERO IO observations decreases by 12 to 71 %. Although the overall tropospheric O_3 burden decreases by 3.7 %, the average O_3 change at the surface is larger and shows a decrease of 8 % (Fig. 3.19) which is the largest decrease in O_3 found within these sensitivity simulations.

As there is huge potential for coupling within the halogens (Cl, Br, I) system, it is impor-

tant for all halogens to be well represented within a simulation. The problems with BrO simulation that motivated this sensitivity study are addressed in (Schmidt et al., 2016) and discussed in Chapter IV.

3.7.5 Ocean surface iodide (I^-) concentration

Chance et al. (2014) compiled the available ocean surface iodide (I^-) observations and investigated correlations with various environmental parameters. They found that ocean surface iodide correlated most strongly with the square of sea surface temperature, as used in this work. However MacDonald et al. (2014), using a subset of the Chance et al. (2014) data, found that an Arrhenius parameterisation gave best agreement. Figure 2.2 (Chapter II) shows annual averaged ocean surface iodide generated from both parameterisations. The sea surface temperatures are taken from the annual mean GEOS field used in GEOS-Chem.

The area weighted ocean mean concentrations are 37.6 and 80.8 nM for MacDonald et al. (2014) and Chance et al. (2014), respectively. Both approaches reproduce the latitudinal gradient observed in Fig. 1 of Chance et al. (2014), however large differences are apparent in magnitude. The dataset reported in Chance et al. (2014) has a median value of 77 nM and interquartile range of 28-140 nM, which appears more consistent with the parameterisation published.

Inclusion of the MacDonald et al. (2014) iodide parameterisation ("Ocean Iodide") reduces the inorganic iodine flux by 51 % to 1.9 Tg, which in turn decreases the global tropospheric iodine I_y burden (23 %) and surface IO concentrations (34 %). The median bias in comparison with TORERO vertical profiles decreases by 47 to 42 %. Tropospheric O_3 burden increases by 2.1 % and global mean OH increase by 0.17 % with respect to "Br+I".

The current ocean surface iodide parameterisations offers a new window into global iodine modelling, however further work is required to evaluate their performance on a global scale. Although one scheme appears to give a better comparison with gas-phase observations, it is not clear if this is due to a better representation of global ocean surface iodide or whether this reflects another error somewhere else in the model.

3.7.6 Higher iodine oxide lifetime

Within the model uptake of I_2O_X (X = 2,3,4) to aerosol is considered as an irreversible loss of iodine, with the same reactive probability (γ) as INO_2 (0.02). The sensitivity to this assumption is assessed by running simulations doubling ("I_2O_X (γ) x2") and halving this value ("I_2O_X (γ)/2").

The effect of doubling leads to decreasing global tropospheric I_y burden (5.1 %), decreasing surface marine boundary layer (900 hPa < p) IO (4.6 %), and decreases the median bias in vertical comparisons with TORERO IO (6.9 %) to 75 %. This leads to a slightly increased global tropospheric O_3 burden (0.54 %), and marginally decrease in global mean OH (0.08 %). The effect of halving is essentially symmetrical, with an increased global tropospheric I_y burden (4.3 %), increased surface marine boundary layer (900 hPa < p) IO concentration (4.3 %), and an increased median bias in vertical comparisons with TORERO IO by 4.4 to 84 %. This leads to slightly decreased global tropospheric O_3 burden (0.44 %), and marginally increase in OH (0.05 %).

The end fate of I_2O_X is highly uncertain. For further work to evaluate impacts of this chemistry, more constraints will be required on the reversibility of this chemistry.

3.7.7 Summary of sensitivity simulations

Uncertainties in the atmospheric chemistry of iodine lead to some significant uncertainties on iodine's impact on atmospheric composition. Further laboratory studies on the photolytic properties of higher oxides would reduce uncertainty, as would a more detailed understanding of the rates of heterogeneous cycling on a range of aerosols. The interplay between bromine and iodine chemistry is also potentially significant for the oxidant budgets. Given the inorganic iodine emission's role as the largest source of iodine into the atmosphere, improved constraints on the concentration of oceanic iodide would also reduce uncertainties. This sensitivity study could be extended by further work in which the select parameters could be perturbed by unit sigma values within laboratory uncertainties to give a Monte-Carlo type assessment. It is clear that the understanding of iodine chemistry in the atmosphere is not complete and further laboratory and field observations are necessary to provide a stronger constraint.

3.8 Conclusions

The model ("Br+I") yields an estimated global emission of 3.8 Tg yr^{-1} of iodine, which is consistent with previous work. Iodine emissions are overwhelmingly dominated by the inorganic ocean source, with 76 % of this emission from hypoiodous acid (HOI). The emissions are dominated by the inorganic ocean source (84 %), and the majority (91 %) of deposition is back to the oceans. HOI is also found to be the dominant iodine species in terms of global tropospheric I_y burden (contributing up to 70 %).

Iodine reduces the global tropospheric O_3 burden by ∼9 % in simulation ("Br+I"). Global mean OH concentrations are increased (1.8 %) by the presence of iodine due to the reduction in the O_3-H_2O primary source being compensated for by an increased conversion of HO_2 into OH via the photolysis of HOI. Both changes involve HOI production and destruction cycles. The iodine-driven O_x loss rate (748 Tg O_x yr^{-1}) is by photolysis of HOI (78 %), photolysis of OIO (21 %), and reaction of IO and BrO (1 %).

The understanding of iodine chemistry is hampered by limited laboratory studies of both its gas and aerosol phase chemistry, by limited field measurements of atmospheric iodine compounds and poor understanding of ocean surface iodide and its chemistry. The sensitivity study was performed on a range of parameters and concluded that the simulation's ("Br+I") impacts on O_3 and OH are sensitive to the uncertainty of ocean iodine emissions, the parameterisation of iodine recycling in aerosol, to the photolysis parameters for the higher oxides and to the assumed Br chemistry. Given its role as the largest component of atmospheric iodine, and its central role in both O_3 destruction and HO_2 to IO cycling, a priority should be given to instrumentation to measure HOI.

The new iodine chemistry ("Br+I") combines with previously implemented bromine chemistry ("BROMINE") to yield a total bromine and iodine driven tropospheric O_3 burden decrease of 14.4 % compared to a simulation without iodine and bromine chemistry in the model ("NOHAL").

The following chapter considers the impact of halogen chemistry as a whole (Cl, Br, I) on tropospheric composition by bringing together an updated representation of bromine and chlorine chemistry (Schmidt et al., 2016) with the new iodine chemistry described in this chapter.

Chapter 4

The impact of "coupled" halogen chemistry in the present-day

The content of this chapter is in review as "Global impacts of tropospheric halogens (Cl, Br, I) on oxidants and composition in GEOS-Chem": T. Sherwen, J. A. Schmidt, M. J. Evans, L. J. Carpenter, K. Großmann, S. D. Eastham, D. J. J., B. Dix, T. K. Koenig, R. Sinreich, I. Ortega, R. Volkamer, A. Saiz-Lopez, C. Prados-Roman, A. S. Mahajan and C. Ordóñez, *Atmos. Chem. Phys. Discuss.*, 2016.

Figures 4.10 and 4.9 were prepared by Dr. Johan A. Schmidt from the University of Copenhagen.

4.1 Introduction

Previous studies of halogen chemistry within the GEOS-Chem (www.geos-chem.org) model have focussed on either bromine or chlorine chemistry. Parrella et al. (2012) presented a bromine scheme and its effects on oxidants in the past and present atmosphere. Eastham et al. (2014) presented the Unified tropospheric-stratospheric Chemistry eXtension (UCX), which added a stratospheric bromine and chlorine scheme. This chlorine scheme was then employed in the troposphere with an updated heterogeneous bromine and chlorine scheme by Schmidt et al. (2016). Iodine chemistry was employed in the troposphere in Chapters II/III to consider present day impacts of iodine on oxidants, which used the representation of bromine chemistry from Parrella et al. (2012). However, this field of research is quickly evolving, but up to this point, the chlorine, bromine and iodine simulations within the GEOS-Chem model have been somewhat disparate. This chapter aims to produce a coupled Cl, Br and I scheme which will be able to investigate the full impact of halogen chemistry on the composition of the troposphere.

The simulations in chapter and the thesis from this point onwards uses recent updates to the chlorine (Eastham et al., 2014; Schmidt et al., 2016), bromine (Parrella et al., 2012; Schmidt et al., 2016), and iodine (Chapter II-III and Sherwen et al. 2016a) chemistry in GEOS-Chem with further updates and additions described in Section 4.2. In Section 4.3 the modelled distribution of inorganic halogens is described (Section 4.3.1-4.3.3), and compared with observations (Section 4.3.4). The impact of halogens on oxidants (Section 4.4.1-4.4.2), organic compounds (Section 4.4.3), and other species (Section 4.4.4) is then described.

4.2 Model description

This work uses the GEOS-Chem chemical transport model (www.geos-chem.org, version 10) run at 4^ox5^o spatial resolution. The model is forced by assimilated meteorological and surface fields from NASA's Global Modelling and Assimilation Office (GMAO, GEOS-5). The model chemistry scheme includes O_x, HO_x, NO_x, and VOC chemistry as described in Section 2.1.1. Dynamic and chemical time-step are 30 and 60 minutes, respectively. Stratospheric chemistry is modelled using a linearised mechanism (see Murray et al. 2012b

and Section 2.1.1).

The standard model chemistry is updated to give a representation of chlorine, bromine and iodine chemistry. This version of the model is described as "Cl+Br+I". It is based on the iodine chemistry described in Chapters II Section 2.3, with updates to the bromine and chlorine scheme described by Schmidt et al. (2016) and Eastham et al. (2014). Updated or new reactions not included in Chapters II (Sherwen et al., 2016a), Schmidt et al. (2016), or Eastham et al. (2014) are given in Table 4.1 with a full description of the halogen chemistry scheme used given in Appendix Tables A.1-A.6.

The cross-sections of higher iodine oxides were updated from that of $IONO_2$ used in Chapter II (see Section 2.5) and III. The photolysis of I_2O_3 and I_2O_4 uses the absorption cross-sections reported by Gómez Martín et al. (2005) and Spietz et al. (2005). The photolysis of I_2O_2 uses the cross-section for I_2O_4. A quantum yield of unity was assumed for all I_2O_X species. It is noted that recent work has used an unpublished spectrum for I_2O_4 that is much lower than that I_2O_3 Saiz-Lopez et al. (2014), but this is not expected to have a large effect on conclusions presented here as I_2O_4 is a minor component of I_2O_X (5 % of global tropospheric mass) and only represents a small proportion the I_2O_X loss route to "iodine aerosol" (9 %) .

The parameterisation for oceanic iodide concentration was changed from Chance et al. (2014) used in Chapter II (Section 2.2.3) and III (Sherwen et al., 2016a) to MacDonald et al. (2014). This was motivated by the latter resulting in an improved comparison with observations (see Chapter III Section 3.7.5/Section 7.5 of Sherwen et al. 2016b).

The product of acid catalysed di-halogen release following I^+ (HOI, INO_2, INO_3) uptake was updated from I_2 as in Chapter II (see Section 2.4) and III (Sherwen et al., 2016a) to yield IBr and ICl following McFiggans et al. (2002). Sea-salt acidity is calculated online through titration of sea salt aerosol by uptake of sulfate dioxide (SO_2), nitric acid (HNO_3), and sulfuric acid (H_2SO_4) as described by Alexander (2005). Re-release of IX (X=Cl,Br) is only permitted to proceed if the sea salt is acidic (Alexander, 2005), otherwise uptake results in iodine aerosol production. Thus aerosol cycling of IX in the model is not a net source of I_y (and may be a net sink on non-acid aerosol) but alters the speciation (Sherwen et al., 2016a). The ratio between IBr and ICl was set to be 0.15:0.85 (IBr:ICl), instead of the 0.5:0.5 used previously (Saiz-Lopez et al., 2014; McFiggans et al., 2000).

Table 4.1 – Additional halogen reactions included in this simulation that are not used in previous GEOS-Chem studies (Eastham et al., 2014; Schmidt et al., 2016; Sherwen et al., 2016a). The full reaction scheme is given in the Appendix (Sections A.1-A.6). The rate constant is calculated using a standard Arrhenius expression $Aexp^{(\frac{-Ea}{RT})}$. (•) Reaction from JPL, only considering the major channel (Dale and Poulet. 1996) and product of CH_3O reacts to form CH_2O + HO_2 (CH_3O $+O_2 \rightarrow CH_2O$ + HO_2). (⋆) Only first channel from JPL considered. the 2nd channel forms a criegee (HCl + $C_2H_4O_2$) and therefore cannot be represented by reduced GEOS-Chem chemistry scheme.(◁) Reaction defined by JPL and interpreted as proceeding via hydrogen abstraction, therefore the acetaldehyde product is assumed. ($) K(infinity) rate given in table, K(0) rate = 4.00x10^{-28} with Fc=0.6 as shown in Table A.3). (⊖) Reaction only proceeds on sea-salt aerosol. (*) Reactions which were included in previous work (Sherwen et al. (2016a)), but di-halogen products have been updated split between ICl and IBr (See Section 4.2) and only proceed on acidic sea-salt aerosol following McFiggans et al. (2000). Acidity of aerosol is calculated as described in Alexander (2005). Abbreviations for tracers are expanded in footnote 3.

Rxn ID	Reaction	A	Ea/R	Citation
		cm^{3}molecules^{-1} s^{-1}	K	
M29	IO + ClO → I + OClO	2.59x10^{-12}	280	Atkinson et al. (2007)
M30	IO + ClO → I + Cl + O_2	1.18x10^{-12}	280	Atkinson et al. (2007)
M31	IO + ClO → ICl + O_2	9.40x10^{-13}	280	Atkinson et al. (2007)
M32	Cl + HCOOH → HCl + CO2 + H_2O	2.00x10^{-13}	-	Sander et al. (2011)
M33	Cl + CH_3O_2 → ClO + CH_2O + HO_2(•)	1.60x10^{-10}	-	Sander et al. (2011)
M34	Cl + CH_3OOH → HCl + CH_3O_2	5.70x10^{-11}	-	Sander et al. (2011)
M35	Cl + C_2H_6 → HCl + $C_2H_5O_2$	7.20x10^{-11}	-70	Sander et al. (2011)
M36	Cl + $C_2H_5O_2$ → ClO + HO_2+ ALD2 (⋆)	7.40x10^{-11}	-	Sander et al. (2011)
M37	Cl + EOH → HCl + ALD2 (◁)	9.60x10^{-11}	-	Sander et al. (2011)
M38	Cl + $CH_3C(O)OH$ → HCl + CH_3O_2, + CO2	2.80x10^{-14}	-	Sander et al. (2011)
M39	Cl + C_3H_8 → HCl + A3O2	7.85x10^{-11}	-80	Sander et al. (2011)
M40	Cl + C_3H_8 → HCl + B3O2	6.54x10^{-11}	-	Sander et al. (2011)
M41	Cl + ACET → HCl + ATO2	7.70x10^{-11}	-1000	Sander et al. (2011)
M42	Cl + ISOP → HCl + RIO2	7.70x10^{-11}	500	Sander et al. (2011)
M43	Cl + MOH → HCl + CH_2O + HO_2	5.50x10^{-11}	-	Sander et al. (2011)
M61	Cl + ALK4 → HCl + R4O2	2.05x10^{-10}	-	Atkinson et al. (2006)
M62	Br + PRPE → HCl + PO2	3.60x10^{-12}	-	Atkinson et al. (2006)
M63	Cl + PRPE $\xrightarrow{M}$ HCl + PO2 + M	2.80x10^{-10}($)	-	Atkinson et al. (2006)
H1	$N_2O_5 \xrightarrow{\gamma}$ HNO_3+ $ClNO_2$(⊖)	-	-	(see table caption)
H2	HOI $\xrightarrow{\gamma}$ 0.85ICl + 0.15IBr*	-	-	(see table caption)
H3	$INO_2 \xrightarrow{\gamma}$ 0.85ICl +.015IBr*	-	-	(see table caption)
H4	$INO_3 \xrightarrow{\gamma}$ 0.85ICl + 0.15IBr*	-	-	(see table caption)
P1	ICl $\xrightarrow{h\nu}$ I + Cl	-	-	Sander et al. (2011)
P2	IBr $\xrightarrow{h\nu}$ I + Br	-	-	Sander et al. (2011)
P3	BrCl $\xrightarrow{h\nu}$ Br + Cl	-	-	Sander et al. (2011)

A ratio of 0.5:0.5 gives a large overestimate of BrO with respect to the observations used in Section 4.3.4.2 (Read et al., 2008; Volkamer et al., 2015). This reduction is attributed to the de-bromination of sea-salt which is not considered here, and the potential for the model to over estimate the BrO_x lifetime. This is discussed further in the next section but future laboratory and field studies of these heterogeneous process are needed to help constrain these parameters.

The iodine uptake aerosol has been updated from Chapter II (see Section 2.4). Iodine on aerosol is now represented in the model with separate tracers based on the aerosol on which the irreversible uptake occurs (see Table A.5). Three iodine aerosol tracers are included to represent iodine on accumulation and coarse mode sea-salt and on sulfate aerosol. The physical properties of the iodine aerosol tracers are assumed to be the same as its parent aerosol as previously described for sulfate (Alexander et al., 2012) and sea-salt aerosol (Jaeglé et al., 2011).

Additional chlorine chemistry beyond that in the stratospheric scheme described by Eastham et al. (2014) is included to represent more fully the chlorine chemistry of the troposphere (Atkinson et al., 2006; Sander et al., 2011). The heterogeneous reaction of N_2O_5 on aerosols was updated to yield products of $ClNO_2$ and HNO_3 (Bertram and Thornton, 2009; Roberts et al., 2009) on sea salt, and $2\,HNO_3$ on other aerosol types. Reaction probabilities are unchanged (Evans and Jacob, 2005).

Deposition and photolysis of inter-halogen species (ICI, BrCl, IBr) and the reaction between ClO and IO were also included (Sander et al., 2011).

4.3 Model results

The model was run for two years (2004 and 2005), discarding the first year as a "spin-up" period and using the second year (2005) for analysis. Non-halogen emissions (NO_x, SO_x, VOCs, aerosols, etc.) are identical to those described in Chapter II. A reference simulation without any halogens ("NOHAL") was also performed. Where comparisons with observations are shown, the model is run with a 3 months "spin-up" before the observational dates, unless explicitly stated otherwise. The appropriate month from the 2005 simulation was used as the initialisation for these observational comparisons. The

model was sampled at the nearest timestamp and grid-box. The model only calculates chemistry in the troposphere. To avoid confusion, results above the tropopause (lapse rate of temperature falls below 2 K/km) are not shown.

4.3.1 Emissions

The emissions fluxes of chlorine, bromine, and iodine species are shown in Figure 4.1 with global totals in Table 4.2. The Cl and Br contained within sea-salt is not considered as emitted in this simulation until a chemical process liberates them into the gas-phase (Schmidt et al., 2016). Processes that can liberate sea-salt Cl and Br are the uptake of N_2O_5 and I^+ species on sea-salt. Explicit sea-salt de-bromination chemistry is not included for reasons described in Schmidt et al. (2016).

The organic iodine (CH_3I, CH_2I_2, CH_2ICl, CH_2IBr) emissions are from Ordóñez et al. (2012) as described in Chapter II. Inorganic iodine emissions (HOI, I_2) (Carpenter et al., 2013; MacDonald et al., 2014) are 28 % lower here than reported in Chapter II, due to the use of the MacDonald et al. (2014) parameterisation for ocean surface iodide rather than that of Chance et al. (2014). Heterogeneous iodine aerosol chemistry (Section 4.2 and Appendix Sect. A.0.1) does not lead to a net release of iodine, instead it just recycles from less active forms (INO_2, INO_3, HOI) into more active forms (ICl/IBr).

The organic bromine (CH_3Br, $CHBr_3$, CH_2Br_2) emissions have been reported previously (Parrella et al., 2012; Schmidt et al., 2016) and this simulation is consistent with that work. A further source of 0.031 Tg Br yr^{-1} (3.4 % of total) is included here from CH_2IBr photolysis. The heterogeneous cycling for Br_y (defined in Footnote below[1]) is updated from Schmidt et al. (2016), and described in Section 4.2/Appendix A.0.1. An additional Br_y source not considered by Schmidt et al. (2016) is iodine activated IBr release from sea salt, which amounts to 0.31 Tg Br yr^{-1}. The majority (67 %) of this is tropical (22^oN-22^oS). With all these updates, the tropospheric mean daytime (07:00-19:00) BrO concentration is 1.1 pmol mol^{-1} (0.64 pmol mol^{-1}, 24 hour average), 13 % higher than reported in Schmidt et al. (2016).

[1]Here X_y (X=Cl,Br,I) is the sum of gas-phase inorganic species of a given halogen in units of that halogen

The organic chlorine emission (CH_3Cl, $CHCl_3$, CH_2Cl_2) for this simulation (Table 4.2) has been described previously in Schmidt et al. (2016) and set using fixed surface concentrations. An additional source of 0.046 Tg Cl yr^{-1}(0.94 % of total) is present from CH_2ICl photolysis (Sherwen et al., 2016a). $ClNO_2$ production from the heterogeneous uptake of N_2O_5 provides a source of 0.66 Tg Cl yr^{-1} (14 % of total) with the vast majority (95 %) being in the northern hemisphere, with strongest sources in coastal regions north of 20^oN. For June a global $ClNO_2$ source of 21 Gg Cl $month^{-1}$ is calculated, which is substantially less than the 62 Gg Cl $month^{-1}$ (Pers. com. Sarwar Golam 2016) calculated in a previous study (Sarwar et al., 2014). The difference in NO_x concentrations due to differences in model resolution and differences in sea-salt emissions probably contributes to this. Uptake of HOI, INO_2 and INO_3 to sea-salt aerosol leads to the emission of ICl, giving an additional source of 0.78 Tg Cl yr^{-1} (17.6 % of total) mostly (67 %) in tropical (22^oN-22^oS) locations.

Table 4.2 – Global sources of reactive tropospheric inorganic halogens. Sources with fixed concentration in the model for Cl_y (CH_3Cl, CH_3Cl_2, $CHCl_3$) and Br_y ($CHBr_3$) are shown in terms of chemical release (e.g. +Cl, +OH, $+h\nu$) and are in bold. Inclusion of chlorine and bromine organic species has been reported before in GEOS-Chem (Eastham et al., 2014; Parrella et al., 2012; Schmidt et al., 2016). X_2 (I_2) and HOX (HOI) are the inorganic ocean source from (Carpenter et al., 2013), XNO_2 is the source from the uptake of N_2O_5 on sea-salt ($ClNO_2$).

Sources	I_y (Tg I yr^{-1})	Br_y (Tg Br yr^{-1})	Cl_y (Tg Cl yr^{-1})
CH_3X	0.26	**0.06**	**2.19**
CH_2X_2	0.33	0.09	**0.59**
CHX_3	-	0.41	**0.26**
HOX	2.02	-	-
X_2	0.14	-	-
IX	-	0.31(*)	0.78(*)
XNO_2	-	-	0.66
stratosphere	0.00	0.06	0.43
total source(*)	2.75	0.92	4.90

Most of the emissions of Br and I species in this simulation occur in the tropics. It is notable that the chlorine emissions are more widely distributed. This is as a result of longer lifetimes of chlorine precursor gases which moves their destruction further from their emissions and that the $ClNO_2$ source is primarily in the northern extra tropics.

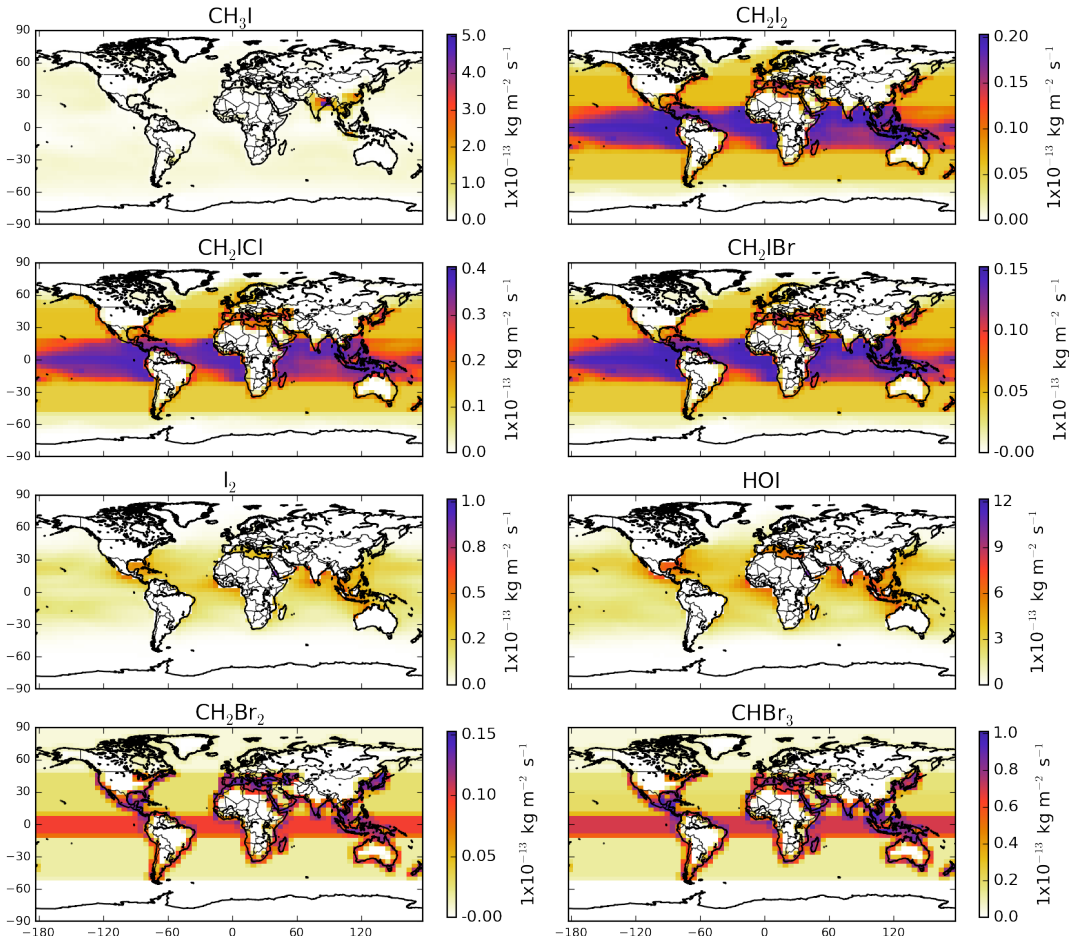

Figure 4.1 – Average annual halogen surface emission of species and column integrated fluxes for species that have fixed surface concentrations in the model (CH_3Cl, CH_3Cl_2, $CHCl_3$, $CHBr_3$) or those with vertically variable sources ($ClNO_2$ from N_2O_5 uptake on sea-salt and IX (X=Cl,Br) production from HOI, lNO_2, and lNO_3 uptake). Values are given in kg X m^{-2} s^{-1} (X=Cl,Br,I).

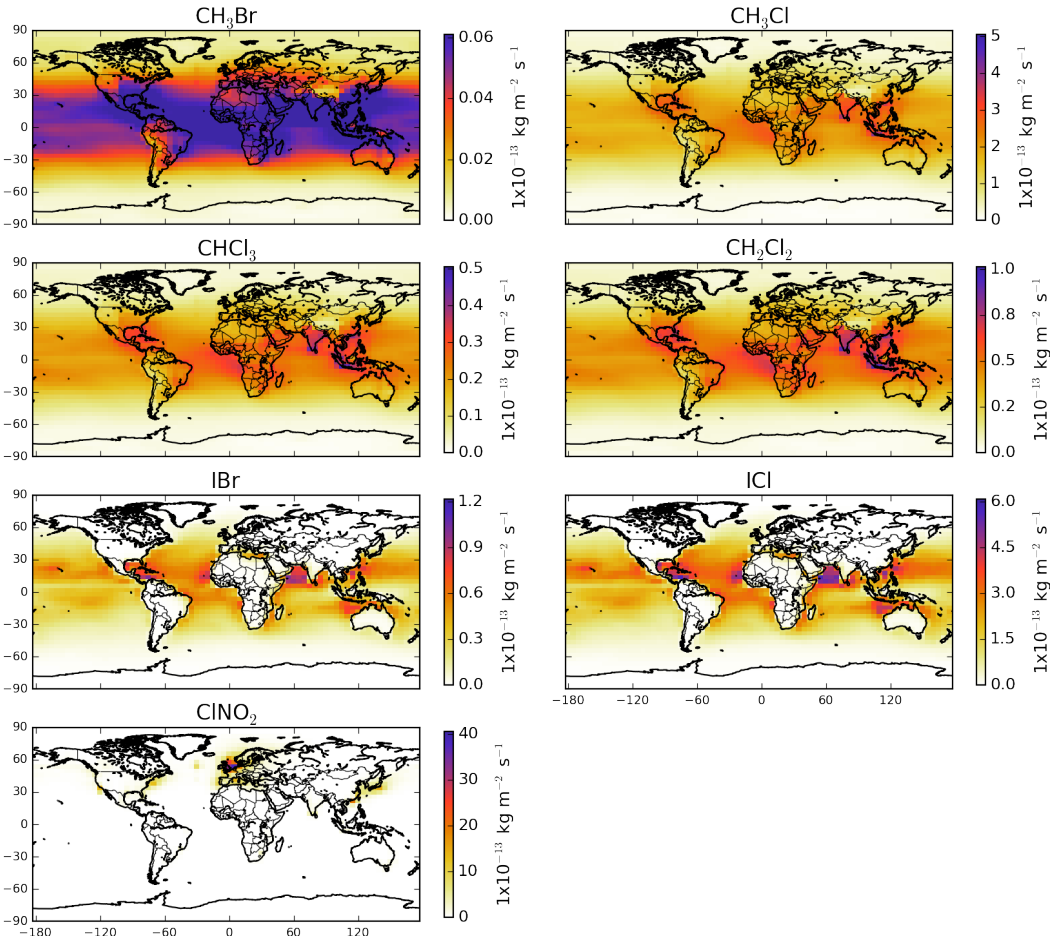

Figure 4.1 – Continued.

4.3.2 Deposition of halogens

Figure 4.2 shows the global annual integrated wet and dry deposition of inorganic X_y (X=Cl, Br,I). Much of the deposition of the halogens occurs over the oceans (69 %, 83 %, and 90 % for Cl_y, Br_y and I_y respectively). It is high over regions of significant tropical precipitation (ITCZ, Maritime continents, Indian Ocean) and much lower at the poles reflecting lower precipitation and emissions.

The major Cl_y depositional sink is HCl (85 %), with HOCl contributing 11 % and $ClNO_3$ 3.2 %. The Br_y sink is split between HBr, HOBr and $BrNO_3$ with fractional contributions of 38, 30 and 24 % respectively. The major I_y sink is HOI deposition which represents 59 % of the depositional flux, with INO_3 and iodine aerosol contributing 22 % and 15 %, respectively.

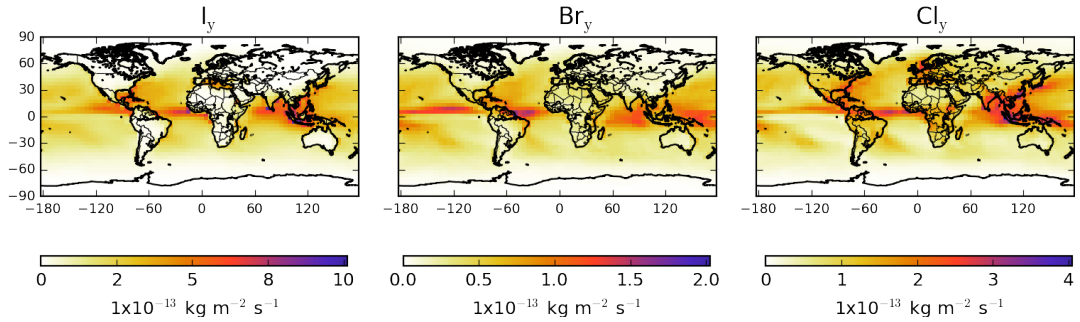

Figure 4.2 – Annual global X_y (X=Cl, Br, I) deposition (defined in Footnote 1). Values are given in terms of mass of halogen deposited (kg X m^{-2} s^{-1}, X=Cl,Br,I).

4.3.3 Halogen species concentrations

Figure 4.3 shows the surface and zonal concentrations of annual mean I_y, Br_y, and Cl_y, with Figure 4.4 showing the same for IO, BrO and Cl, key halogen compounds in the atmosphere. Figure 4.5 shows the global molecule weighted mean vertical profile of the halogen speciation.

Inorganic iodine concentrations are highest in the tropical marine boundary layer consistent with their dominant emissions regions. The highest concentrations are calculated in the coastal tropical regions, where enhanced O_3 concentrations from industrial areas

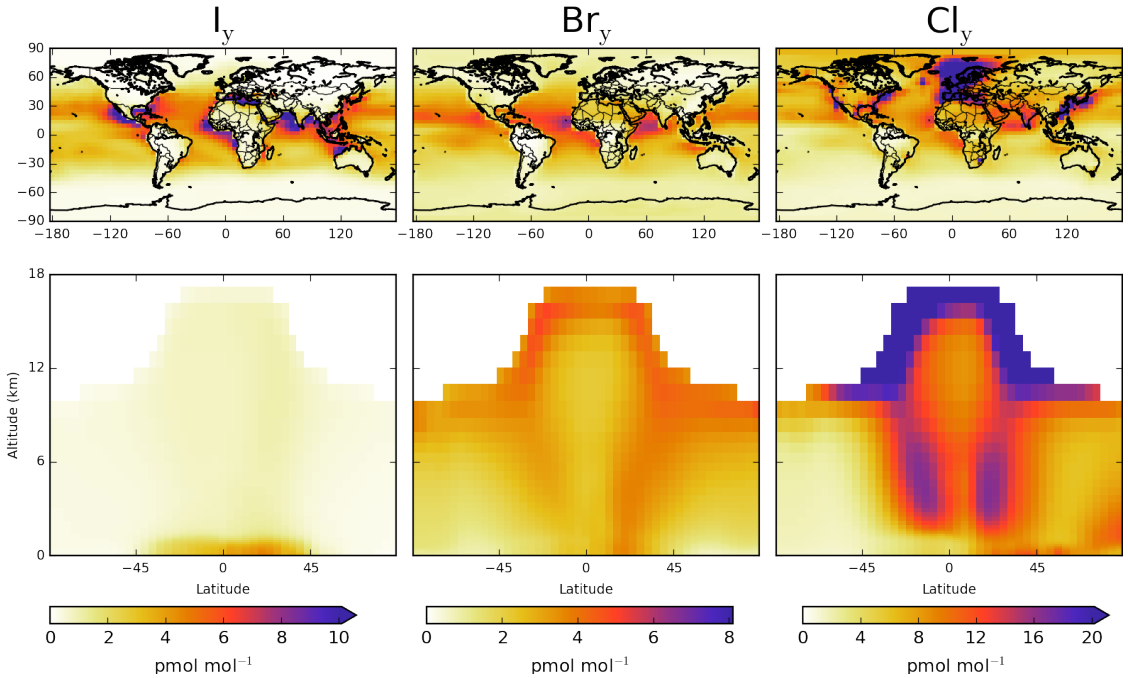

Figure 4.3 – Tropospheric distribution of Cl_y, Br_y, and I_y (defined in Footnote 1) concentrations. Upper plots show surface and lower plots show zonal values. Only boxes that are entirely tropospheric are included in this plot. The Cl_y colourbar is capped at 20 pmol mol^{-1}, with a maximum plotted value of 118 pmol mol^{-1} at the surface over the North Sea. The I_y colourbar is capped at 10 pmol mol^{-1}, with a maximum plotted value of 17 pmol mol^{-1} at the surface over the Red Sea.

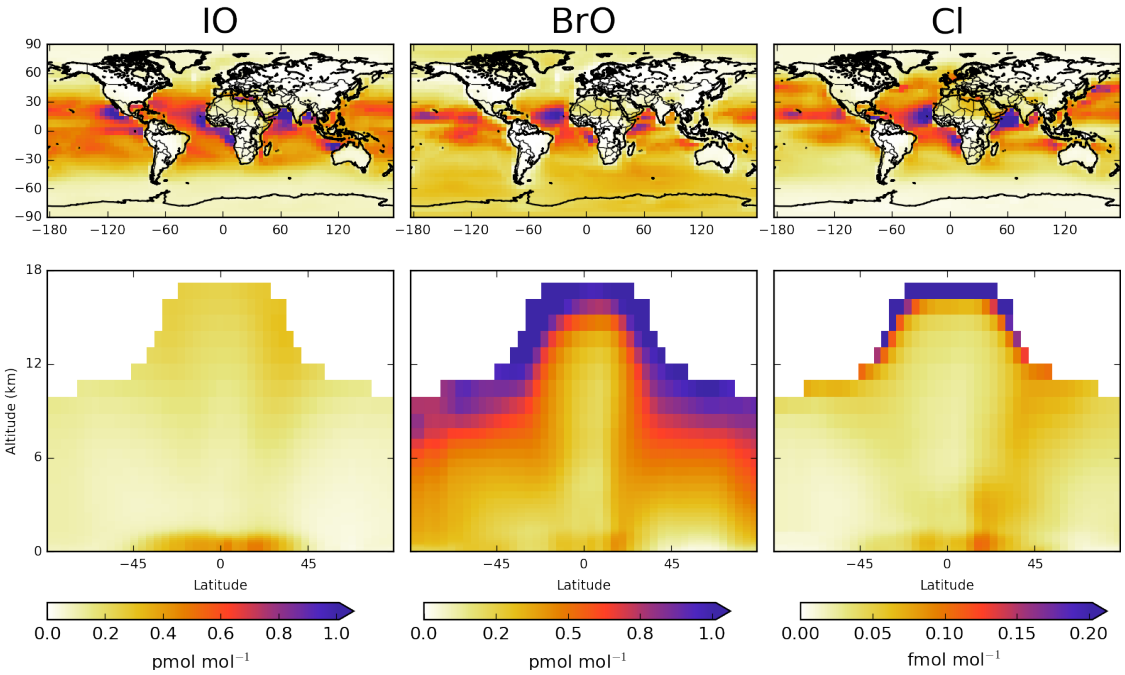

Figure 4.4 – Tropospheric distribution of IO, BrO and Cl concentrations. Upper plots show surface and lower plots show zonal values. Only boxes that are entirely tropospheric are included in this plot.

flow over high oceanic iodide concentrations and lead to increased oceanic inorganic iodine emissions. The organic iodine species also have highest emissions along coastlines. Within the troposphere there is a global mean vertical average of ∼0.5-1 pmol mol^{-1} of I_y consistent with previous model studies (Saiz-Lopez et al., 2014; Sherwen et al., 2016a). The lowest concentrations of I_y are seen just above the marine boundary layer where I_y loss via wet deposition is most favourable due to partitioning towards water soluble HOI. At higher altitudes, lower temperature and high photolysis rates push the I_y speciation to less water soluble compounds (IO, INO_3) and hence the I_y lifetime is longer. IO concentrations (Figure 4.4) follow the concentrations of I_y with high concentrations in the tropical marine boundary layer. The IO concentration increases into the upper troposphere reflecting a partitioning of I_y in this region towards IO (and $IONO_2$) and away from HOI. The global mean tropospheric lifetimes of I_y and IO_x are 2.3 days and 1.3 minutes, respectively.

Total reactive bromine is more equally spread through the atmosphere than iodine. This reflects the longer lifetime of source species with respect to photolysis which gives a more significant source higher in the atmosphere. The highest concentrations are still found in the tropics. Unlike I_y, Br_y increases significantly with altitude, with $BrNO_3$ and HOBr

being the two most dominant species. BrO concentrations (Figure 4.4) follow the concentration of inorganic bromine. In the boundary layer the highest concentrations are found in the tropical marine boundary layer. BrO and IO do not strongly correlate in the tropical marine boundary layer reflecting their differing sources. BrO concentrations increase towards the upper troposphere associated with the increase in total Br_y. The global annual average (molecule weighted) tropospheric BrO mixing ratio in this simulation is 0.64 pmol mol^{-1} (Br_y=4.5 pmol mol^{-1}). When previous implementations (Parrella et al., 2012; Schmidt et al., 2016) are run for the same year and model version as this work (GEOS-Chem v10), the modelled BrO concentrations are found to be 12 % lower than Schmidt et al. (2016), but 17 % higher than Parrella et al. (2012). A tropospheric lifetime of Br_y of 17 days and a BrO_x lifetime of 15 minutes are calculated.

Total inorganic chlorine has a highly non-uniform distribution at the surface reflecting the dominance of the $ClNO_2$ source from N_2O_5 uptake on sea-salt. At the surface $ClNO_2$, HCl, BrCl and HOCl represent around 25 % of the total Cl_y each. The Cl_y peaks in the Northern hemisphere. Away from the surface the $ClNO_2$ concentrations drops off rapidly due to the short lifetime of sea salt. HCl concentrations increase significantly into the middle and upper troposphere and dominate the Cl_y distribution. This suggests that stratospheric chlorine freed from CFCs and organic chlorine strongly contributes to free tropospheric concentrations of Cl_y. However modelled Cl_y is likely a lower limit on the concentrations in the uppermost troposphere (Froidevaux et al., 2008). Cl mixing ratios are very low ($\sim$0.075 fmol mol^{-1} or $\sim$2000 cm^{-3}) in the marine boundary layer. Reactive Cl (i.e. not HCl) drop from the surface to around 10km where it then increases again towards to stratosphere. Cl shows a wider distribution than IO and BrO reflecting the wider distribution of Cl_y. A tropospheric lifetime of Cl_y of 15 days, a ClO_x lifetime of 2 seconds, and a global tropospheric mean inorganic chlorine (Cl_y) concentration of 70 pmol mol^{-1} is calculated in this simulation.

The chemistry of halogens and sea-salt is highly uncertain (Simpson et al., 2015; Saiz-Lopez et al., 2012b; Abbatt et al., 2012). Estimates for sea-salt de-bromination range from 0.51 Tg yr^{-1} (Parrella et al. 2012 implemented in GEOS-Chem v10 and v9-2) to 2.9 Tg yr^{-1} (Fernandez et al., 2014). Some studies have also not included sea-salt de-bromination (von Glasow et al., 2004; Schmidt et al., 2016) as is the case in this work. This work therefore provides a lower estimate of bromine and chlorine sources in the troposphere.

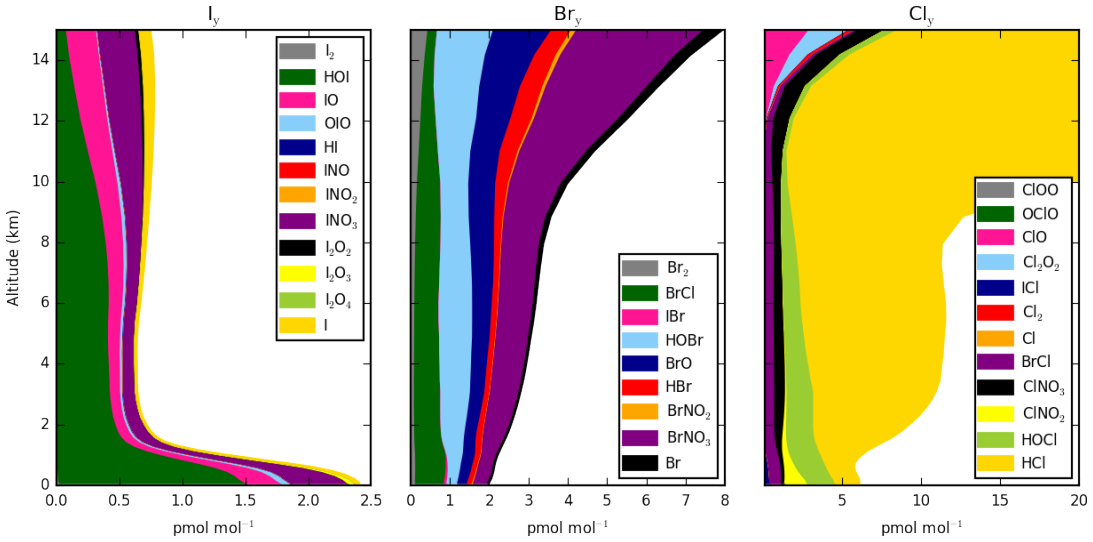

Figure 4.5 – Modelled global average vertical X_y (X=Cl, Br, I) (defined in Footnote 1). Units are pmol mol^{-1} of X (where X=Cl, Br, I). For Cl_y the y-axis is capped at 20 pmol mol^{-1} to show speciation. A Cl_y maximum of 1062 pmol mol^{-1} is found within the altitudes shown due to additional HCl contributions increasing with altitude.

Figure 4.6 shows column integrated BrO and IO, which are the major halogen species for which there are observations (see Section 4.3.4). Tropospheric ClO concentrations within the troposphere are small (see Figure 4.5) and are therefore not shown in Fig 4.6. Tropical maxima are seen for both BrO and IO, with BrO concentrations decreasing towards the equator. For IO a localised maximum is seen in the Arabian Sea. The IO maximum in Antarctica reported from satellite retrievals (Saiz-Lopez et al., 2007a; Schönhardt et al., 2008) is not reproduced, potentially reflecting the lack of polar specific processes in the model.

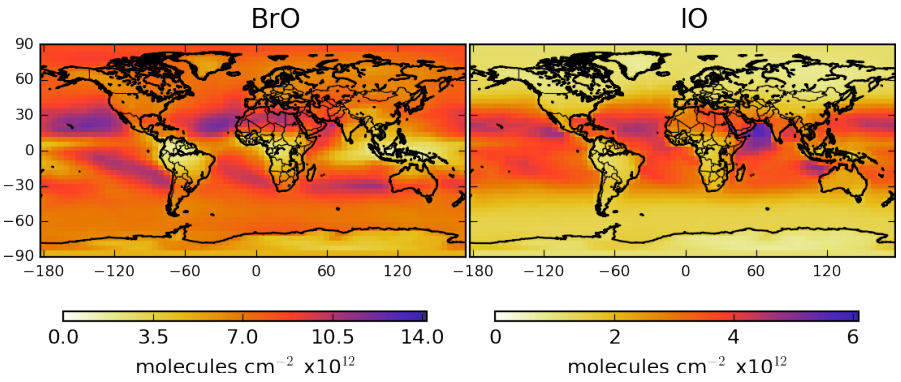

Figure 4.6 – Annual mean integrated model tropospheric column for BrO and IO in molecules cm^{-2}.

4.3.4 Comparison with halogen observations

The observational dataset of tropospheric halogen compounds is sparse. Previous studies have shown comparisons for the organic precursors for chlorine (Eastham et al., 2014; Schmidt et al., 2016), bromine (Parrella et al., 2012; Schmidt et al., 2016), and iodine (Bell et al., 2002; Sherwen et al., 2016a; Ordóñez et al., 2012). The simulation of sea-salt, on which serval halogens sources depend, has previously been evaluated (Alexander, 2005; Jaeglé et al., 2011). The model performance in simulating these halogen compounds has not changed since these previous publications so here the focus is on the available observations of concentrations of IO, BrO, and some inorganic chlorine species ($ClNO_3$, HCl and Cl_2).

4.3.4.1 Iodine monoxide (IO)

A comparison of IO to a suite of recent remote surface observations is shown in Fig 4.7. The model shows an overall negative bias of 21 %. This compares with the 90 % positive bias previously shown in Chapter III. This reduction in bias can be explained by the use of the MacDonald et al. (2014) iodide parameterisation over that of Chance et al. (2014), which has reduced the inorganic emission of iodine, along with the restriction of iodine recycling to acidic aerosol.

Figure 4.8 shows a comparison between modelled IO with altitude against observations in the eastern Pacific (Volkamer et al., 2015; Wang et al., 2015). In general, the model agreement with observations is good. There is an average bias of +40 % in the free troposphere (350 hPa<p<900 hPa), which increases to +58 % in the upper troposphere (350 hPa>p>tropopause). As with the surface measurements, the model bias when comparing to IO observations (Volkamer et al., 2015; Wang et al., 2015) in the free and upper troposphere is decreased from previously reported positive biases in Chapter III of 73 % and 96 %, respectively.

4.3.4.2 Bromine monoxide (BrO)

Comparisons of BrO against seasonal satellite tropospheric BrO observations from GOME-2 (Theys et al., 2011) are shown in Figure 4.9. As shown previously (Parrella et al., 2012;

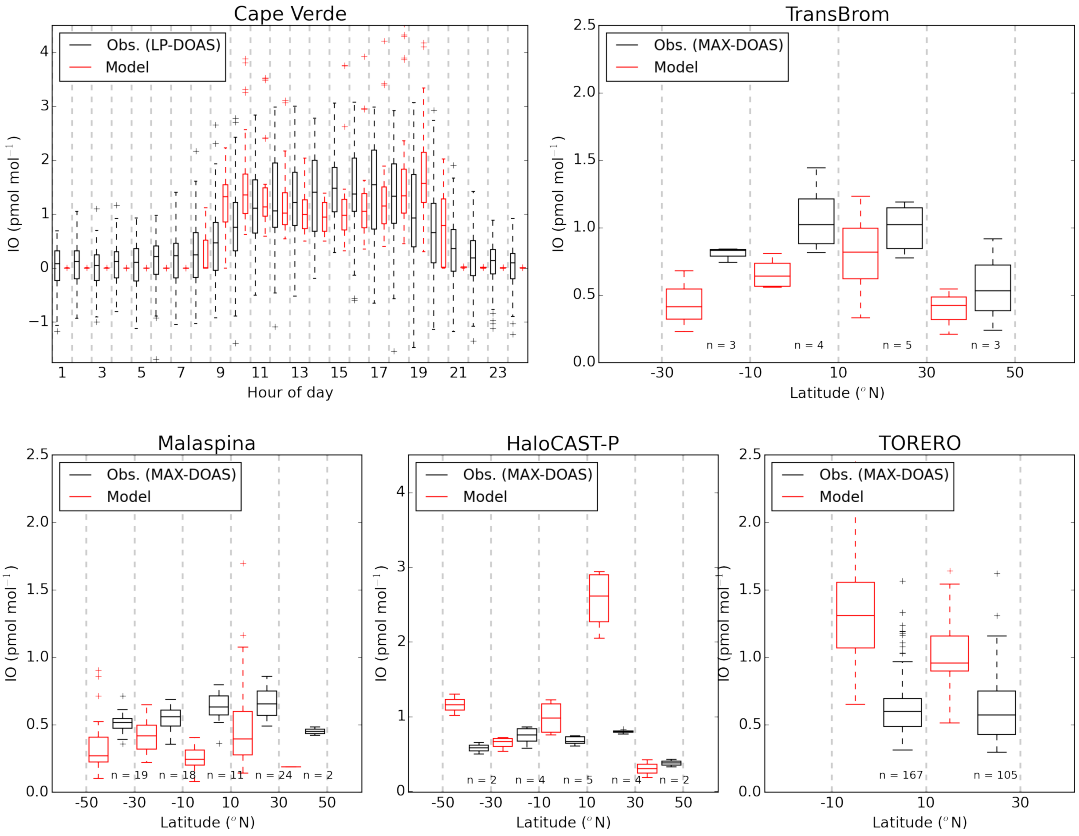

Figure 4.7 – Iodine oxide (IO) surface observations (black) by campaign compared against the simulation with halogen chemistry (“Cl+Br+I”, red). Cape Verde measurements are shown against hour of day and others are shown as a function of latitude. Values are considered in 20^o bins, with observations and modelled values at the same location and time (as described in section 4.2) shown side-by-side around the mid point of each bin. The extent of the bins is highlighted with grey dashed lines. Observations are from Cape Verde (Tropical Atlantic, Mahajan et al. 2010; Read et al. 2008), TransBrom (West Pacific, Großmann et al. 2013), the Malaspina circumnavigation (Prados-Roman et al., 2015b), HaloCAST-P (East Pacific, Mahajan et al. 2012), and TORERO ship (East Pacific, Volkamer et al. 2015). The number of data points within latitudinal bin are shown as “n”. The boxplot extents give the inter-quartile range, with the median shown within the box. The whiskers give the most extreme point within 1.5 times the inter-quartile range.

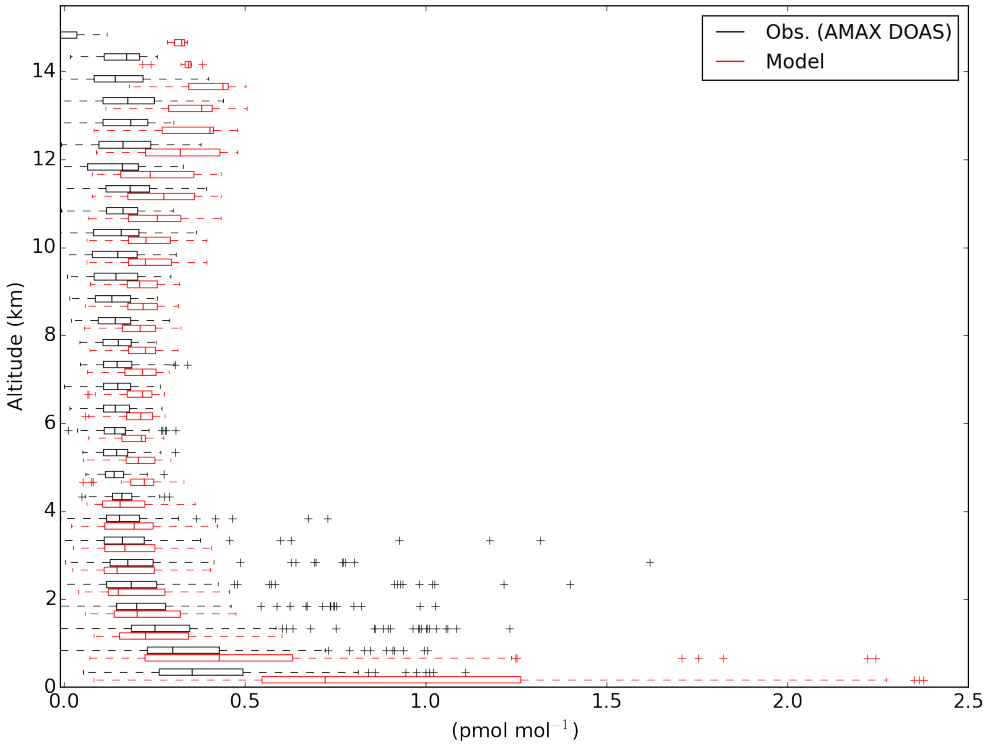

Figure 4.8 – Vertical comparison of the model ("Cl+Br+I") and measured IO during TORERO aircraft campaign (Volkamer et al., 2015; Wang et al., 2015). Model and observations are in red and black respectively. Values are considered in 0.5 km bins, with observations and modelled values at the same location and time (as described in section 4.2) shown side-by-side around the mid point of each bin. Measurements were taken aboard the NSF/NCAR GV research aircraft by the University of Colorado Airborne Multi-Axis DOAS instrument (CU AMAX-DOAS) in the eastern Pacific in January and February 2012 (Volkamer et al., 2015; Wang et al., 2015). The boxplot extents give the inter-quartile range, with the median shown within the box. The whiskers give the most extreme point within 1.5 times the inter-quartile range.

Schmidt et al., 2016) the model has some skill in capturing both the latitudinal and monthly variations in tropospheric BrO columns. However it underestimates the column BrO in the lower southern latitudes (60^oS-90^oS), and to a smaller degree also in lower northern latitudes (60^oN-90^oN) which may reflect the lack of bromine from polar (blown snow, frost flowers etc.) sources and sea-salt de-bromination processes.

Figure 4.10 shows modelled vertical BrO concentrations against observations in the eastern Pacific (Volkamer et al., 2015; Wang et al., 2015). A reasonable agreement is found within the free troposphere (350 hPa<p<900 hPa) in both the tropics and subtropics, with an average negative bias of 15 and 34 %, respectively. A similar comparison is seen in the upper troposphere (350 hPa>p>tropopause) and this shows similar negative biases for the tropics and subtropics, of 20 and 24 %, respectively. The decrease in agreement seen in the TORERO comparison (Fig. 4.10) relative to that previously presented in Schmidt et al. (2016) is due to reduced BrCl and BrO production from slower cloud multiphase chemistry (see Sections A.0.1-A.0.3). The simulation calculates higher BrO concentrations than those observed in the marine boundary layer (Fig. 4.10), however they are lower than those calculated in previous modelling studies (Miyazaki et al., 2016; Long et al., 2014; Pszenny et al., 2004; Keene et al., 2009).

As shown in Fig. 4.11, comparisons between the model and observations of BrO made at Cape Verde (Read et al., 2008; Mahajan et al., 2010) show a negative bias of 50 %. This may be attributable to the locally higher sea-salt loadings at this site (Carpenter et al., 2010), which is situated in the surf zone. This may locally increase the BrO concentrations. The model concentrations of $\sim$1 pmol mol^{-1} are however consistent with other ship borne observations made in the region (Leser et al., 2003).

This model does not include sea-salt de-bromination and yet calculated roughly the correct concentration of BrO. Inclusion of sea-salt de-bromination leads to excessively high BrO concentration in the model (Schmidt et al., 2016). Sea-salt de-bromination however is well observed (Sander et al., 2003; Saiz-Lopez et al., 2012b). The success of the model despite the lack of inclusion of this process suggests model failure in other areas. The BrO_x lifetime may be too long. This is dominated by the reaction between Br and organics to produce HBr. Oceanic sources of VOCs such as acetaldehyde and glyoxyl have been proposed (Millet et al., 2010; Volkamer et al., 2015) and a significant increase in the concentration of these species would lead to lower BrO_x concentrations. Alternatively, a reduction in the

efficiency of cycling of Br_y through aerosol would also have a similar effect. The aerosol phase chemistry is complex and the parameterisations used here may be too simple or fail to capture key processes (e.g. pH, organics). These all require further study in order to help reconcile the rapidly growing body of observation of both gas and aerosol phase bromine in the atmosphere with models.

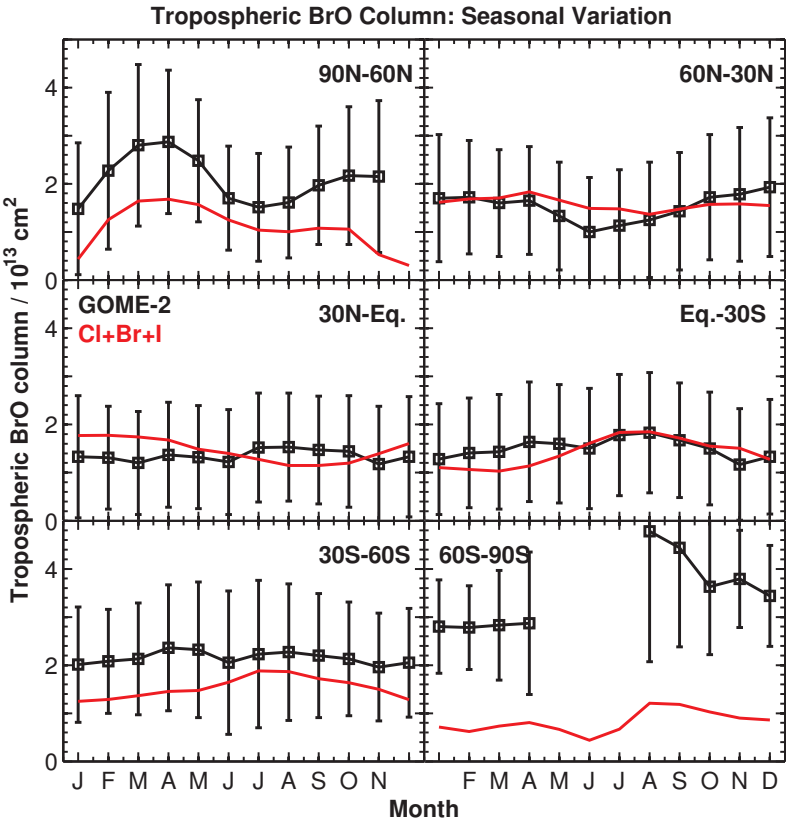

Figure 4.9 – Seasonal variation of zonal mean tropospheric BrO columns in different latitudinal bands. 2007 observations from the GOME-2 satellite instrument (Theys et al., 2011) are compared to GEOS-Chem values at the GOME- 2 local overpass time (9:00-11:00).

4.3.4.3 Nitryl chloride ($ClNO_2$), hydrochloric acid (HCl), hypochlorous acid (HOCl), and molecular chlorine (Cl_2)

Very few constraints on the concentration of tropospheric chlorine species are available. However, a few observations of $ClNO_2$ are available (Table 4.3). It is found that the model does reasonably well in coastal regions, but does not reproduce observations in continental regions or regions with very high NO_x.

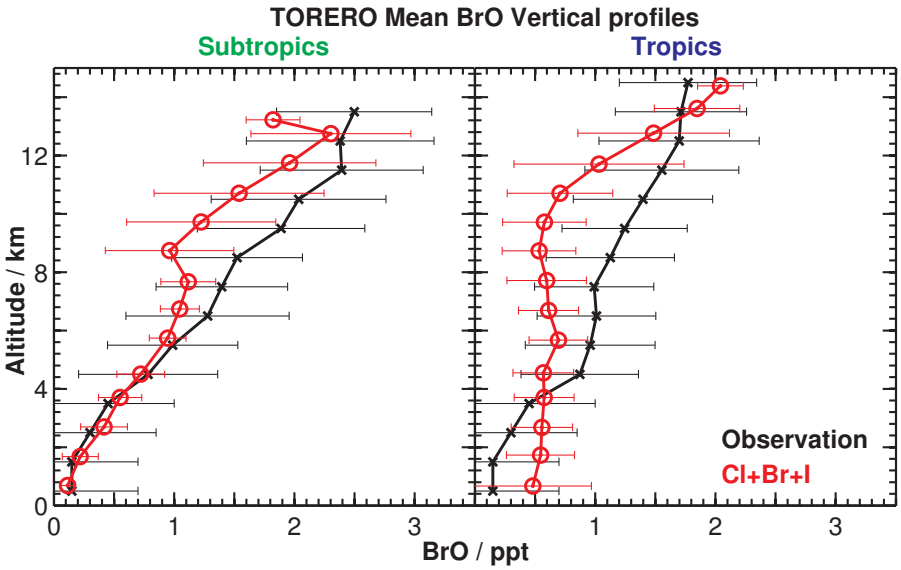

Figure 4.10 – Vertical comparison of the model ("Cl+Br+I") and measured iodine oxide (BrO) during TORERO aircraft campaign (Volkamer et al., 2015; Wang et al., 2015) in the Subtropics (left) and Tropics (right).. Model and observations are in red and black, respectively. Observations and modelled values at the same location and time (as described in section 4.2) are shown side-by-side around the mid point of each bin. Measurements were taken aboard the NSF/NCAR GV research aircraft by the University of Colorado airborne Multi-Axis DOAS instrument (CU AMAX-DOAS) in the eastern Pacific in January and February 2012 (Volkamer et al., 2015; Wang et al., 2015).

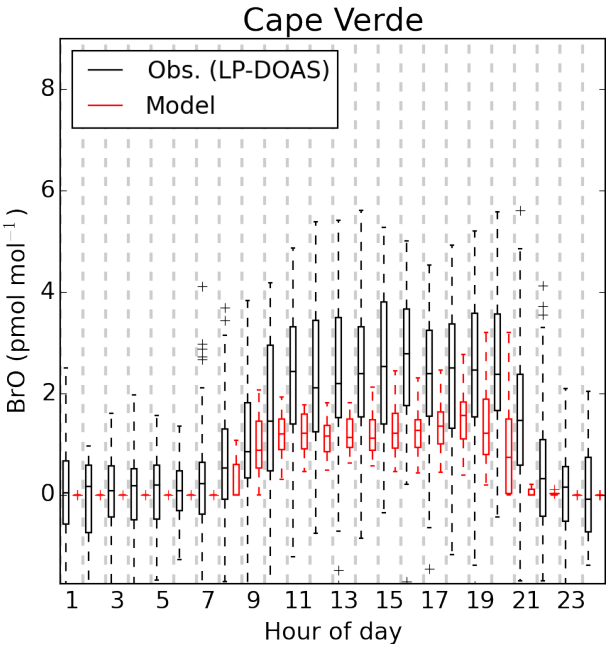

Figure 4.11 – Bromine oxide (BrO) surface observations (black) at Cape Verde (Read et al., 2008; Mahajan et al., 2010) compared against the simulation with halogen chemistry ("Cl+Br+I", red). Values are binned by hour of day.

Lawler et al. (2011) reports measurements of HOCl and Cl_2 at Cape Verde for a week in June 2009. For the first 4 days of the campaign, HOCl concentrations were high and peaked at ∼100 pmol mol^{-1} with Cl_2 concentrations peaking at ∼30 pmol mol^{-1}. For the later days, HOCl concentrations dropped to around 20 pmol mol^{-1} and Cl_2 concentrations to ∼0-10 pmol mol^{-1}. Much lower concentrations of Cl_2 (∼1x10^{-3} pmol mol^{-1}) and HOCl (∼10 pmol mol^{-1}) are calculated. This is similar to findings of Long et al. (2014), who also found better comparisons with the cleaner period of observations. Similar to the comparison with observed $ClNO_2$, this simulation underestimates HOCl and Cl_2.

The model does not include many sources of reactive chlorine. The failure to reproduce continental $ClNO_2$ is likely due to a lack of representation of sources such as salt plains, direct emission from power station and swimming pools, and HCl acid displacement. The inability to reproduce the very high $ClNO_2$ found in cities (Pasadena) and industrialised regions (Texas) may be due to the coarse resolution of the model compared to the spatial inhomogeneity of these observations. The failure to reproduce the Cape Verde observations may be due to the very simple aerosol phase chlorine chemistry included in the model. Overall it is fair to suggest that the model provides a lower limit estimate of the

Table 4.3 – Comparison between modelled and observed $ClNO_2$. Concentrations are shown as the maximum and average of the daily maximum value for the observational and equivalent model time period. Sites marked as (**) are considered continental sites. The model value are taken for the nearest time-step and location within the analysis year (2005).

			Obs.		"Cl+Br+I"		
Location	Lat.	Lon.	Max	Mean	Max	Mean	Reference
Coastal							
Pasedena, CA (2010)	34.2	-118.2	3.46	1.48	0.44	0.20	Mielke et al. (2013)
Southern China (2012)	22.2	114.3	2.00	0.31	0.61	0.18	Tham et al. (2014)
Los Angeles, California (2010)	34.1	-118.2	1.83	0.50	0.44	0.20	Riedel et al. (2012)
Houston, Texas (2006)	30.4	-95.4	1.15	0.80	0.19	0.04	Osthoff et al. (2008)
London, UK (2012)	51.5	-0.2	0.73	0.23	0.51	0.17	Bannan et al. (2015)
Texas (2013)	30.4	-95.4	0.14	0.08	0.19	0.04	Faxon et al. (2015)
Continental							
Hessen, Germany (2011)	50.2	8.5	0.85	0.20	0.16	0.02	Phillips et al. (2012)
Boulder, Colorado (2009)	40.0	-105.3	0.44	0.14	0.00	0.00	Thornton et al. (2010); Riedel et al. (2013)
Calgary, CAN (2010)	51.1	-114.1	0.24	0.22	0.02	0.01	Mielke et al. (2011)

chlorine emissions and therefore burdens within the troposphere. Constraints at the surface concentrations are limited and vertical profiles are not available. Further laboratory work to better define aerosol processes and observations will be necessary to investigate the role of chlorine on tropospheric chemistry.

4.4 Impact of halogens

Now the focus shifts to investigating the impact of the halogen chemistry on the composition of the troposphere. O_3 and OH are investigated first and then attention moves onto other components of the troposphere.

4.4.1 Ozone (O_3)

Figure 4.12 shows changes in column, surface and zonal O_3 both in absolute and fractional terms between simulations with and without halogen emissions ("Cl+Br+I" vs "NOHAL"). Globally the mass-weighted, annual-average mixing ratio is reduced by 7.4 pmol mol^{-1} (14.6%) with the inclusion of halogens ("Cl+Br+I"-"NOHAL")/"NOHAL"*100). A much larger percentage decrease of 25.0 % (7.2 pmol mol^{-1}) is seen over the ocean

surface. Large percentage losses are seen in the oceanic southern hemisphere as reported previously (Long et al., 2014; Schmidt et al., 2016; Sherwen et al., 2016a) reflecting the significant ocean-atmosphere exchange in this regions. The majority (65 %) of the change in O_3 mass due to halogens occurs in the free troposphere (350 hPa<p<900 hPa).

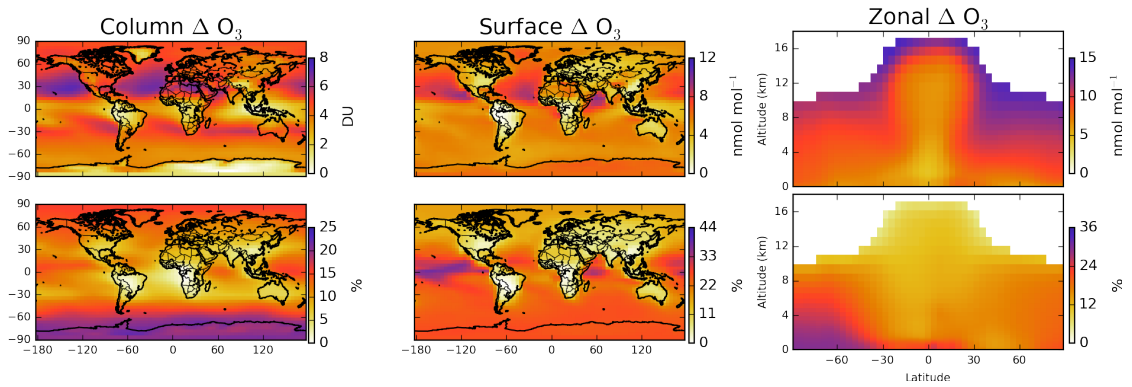

Figure 4.12 – Change in tropospheric O_3 on inclusion of halogen chemistry. Column (left), surface (middle) and zonal (right) change are shown. Upper plots show absolute change and lower plots below give change in % terms (("Cl+Br+I"-"NOHAL")/"NOHAL"*100).

Comparisons of the model and observed surface and sonde O_3 concentrations are given in Figures 4.13 and 4.14. In the tropics the fidelity of the simulation improves with the inclusion of halogens (Schmidt et al., 2016; Sherwen et al., 2016a). Sonde and surface comparisons north of ∼50^{o}N and south of ∼60^{o}S however show that the model now underestimates O_3.

The global odd oxygen budget (O_x, as defined in the footnote below[2]) in the troposphere with ("Cl+Br+I") and without halogens ("NOHAL") is shown in Table 4.4. The O_x loss through chlorine, bromine, and iodine represents 0.46, 5.8 and 12 % of the total O_x loss respectively, thus halogens constitute 18.2 % of the overall O_3 loss. The sum of halogen driven O_x loss is 900 Tg O_x yr^{-1} , which is similar to the magnitude of loss via reaction of O_3 with HO_2 of ∼1100 Tg O_x yr^{-1} (23 % of total). Halogen cross-over reactions (BrO+IO, BrO+ClO, IO+ClO) contribute little to the overall O_3 loss. This number compares with ∼930 Tg O_x yr^{-1} reported in GEOS-Chem in Chapter III for the bromine and iodine only

[2]Here O_x is defined as $O_3 + NO_2 + 2\,NO_3 + PAN + PMN + PPN + HNO_4 + 3\,N_2O_5 + HNO_3 + MPN + XO + HOX + XNO_2 + 2\,XNO_3 + 2\,OIO + 2\,I_2O_2 + 3\,I_2O_3 + 4\,I_2O_4 + 2\,Cl_2O_2 + 2\,OClO$, where X=Cl, Br, I; PAN = peroxyacetyl nitrate; PPN = peroxypropionyl nitrate; MPN = methyl peroxy nitrate; and PMN = peroxymethacryloyl nitrate.

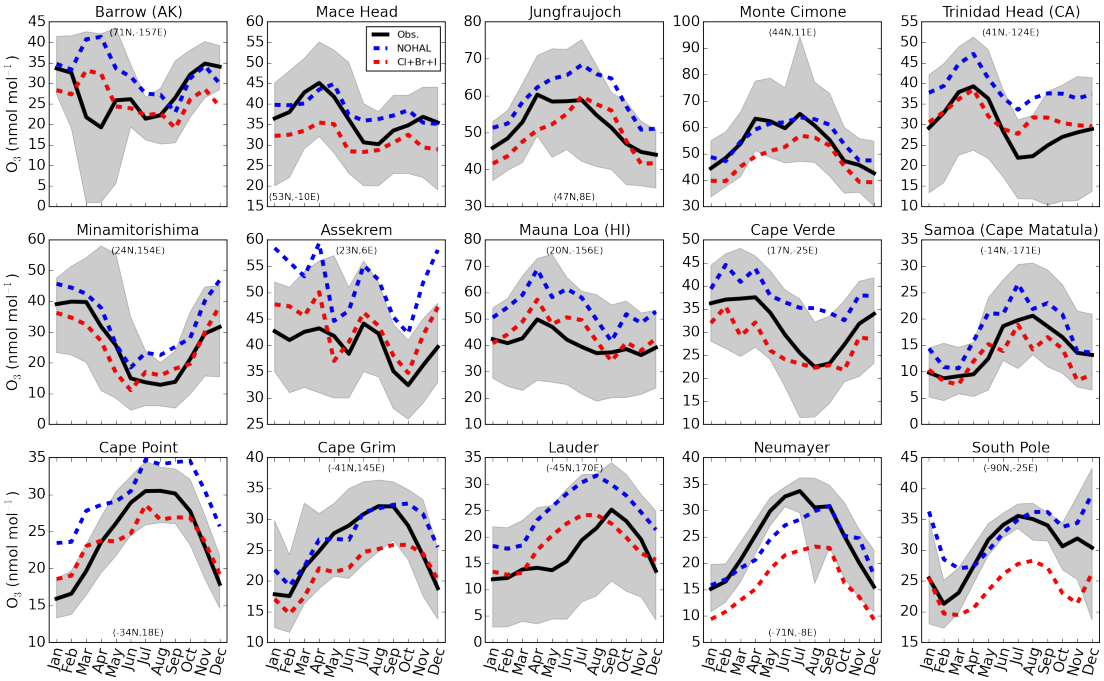

Figure 4.13 – Seasonal cycle of near-surface O_3 at a range of Global Atmospheric Watch (GAW) sites. Observational data shown are 6 year monthly averages (2006-2012). Model data is for 2005. Data is from GAW compiled and processed as described in (Sofen et al., 2016). Blue and red lines represent simulations without halogens ("NOHAL") with halogens ("Cl+Br+I"), respectively. Shaded grey area gives 5^{th} and 95^{th} percentiles of observations.

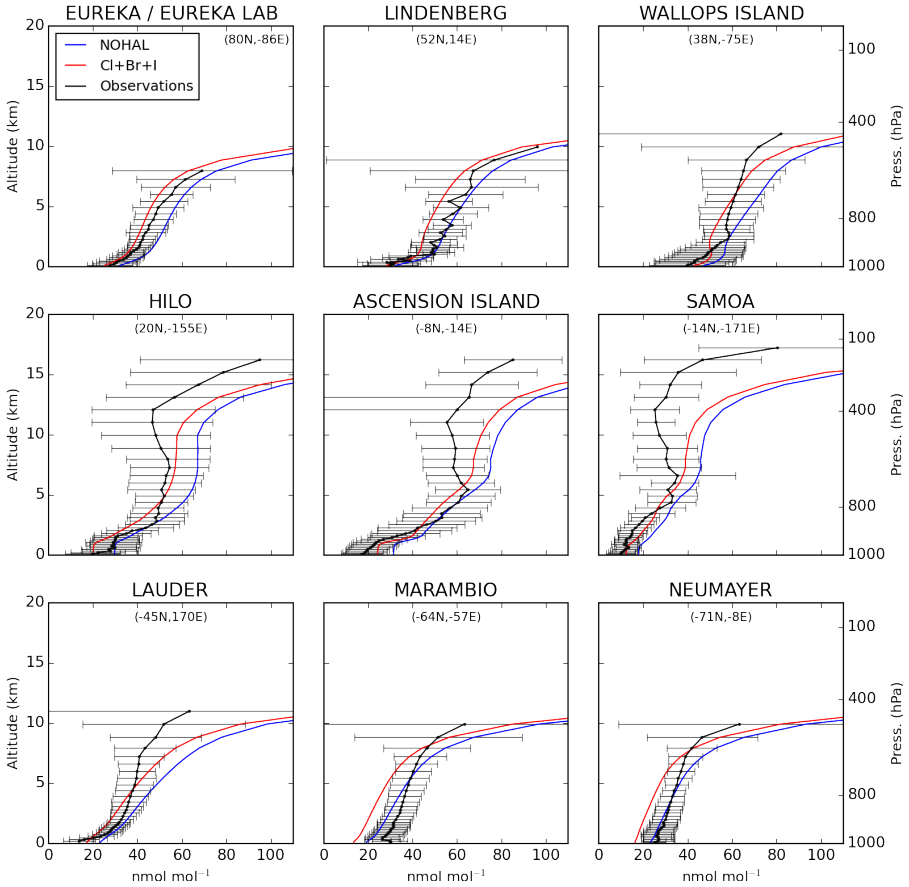

Figure 4.14 – Comparison between annual modelled O_3 profiles and sonde data (2005). Profiles shown are the annual mean of available observations from World Ozone and Ultraviolet Radiation Data Centre (WOUDC, 2014) and model data for 2005 at given locations. Blue and red lines represent simulations without halogens ("NOHAL") with halogens ("Cl+Br+I"), respectively. Observations (in black) show mean concentrations with upper and lower quartiles given by whiskers.

simulation("Br+I"). Saiz-Lopez et al. (2014) found that, between 50^{o}S-50^{o}N and over ocean only, halogens are responsible for the loss of 640 Tg O_x yr^{-1}. Here a comparable value of 670 O_x yr^{-1} is calculated.

The majority of the halogen driven O_3 loss (58.1 %) occurs in the free troposphere (350 hPa<p<900 hPa). Halogens represent 34.9 and 31.0 % of O_x loss in the upper troposphere (350 hPa>p>tropopause) and marine boundary layer (900 hPa<p) respectively as shown in Figure 4.15. The marine boundary layer O_x loss attributable to halogens is equal to the 31 % reported by Prados-Roman et al. (2015a) previously, and it is slightly higher than that reported solely for iodine of 26 % (Sherwen et al., 2016a).

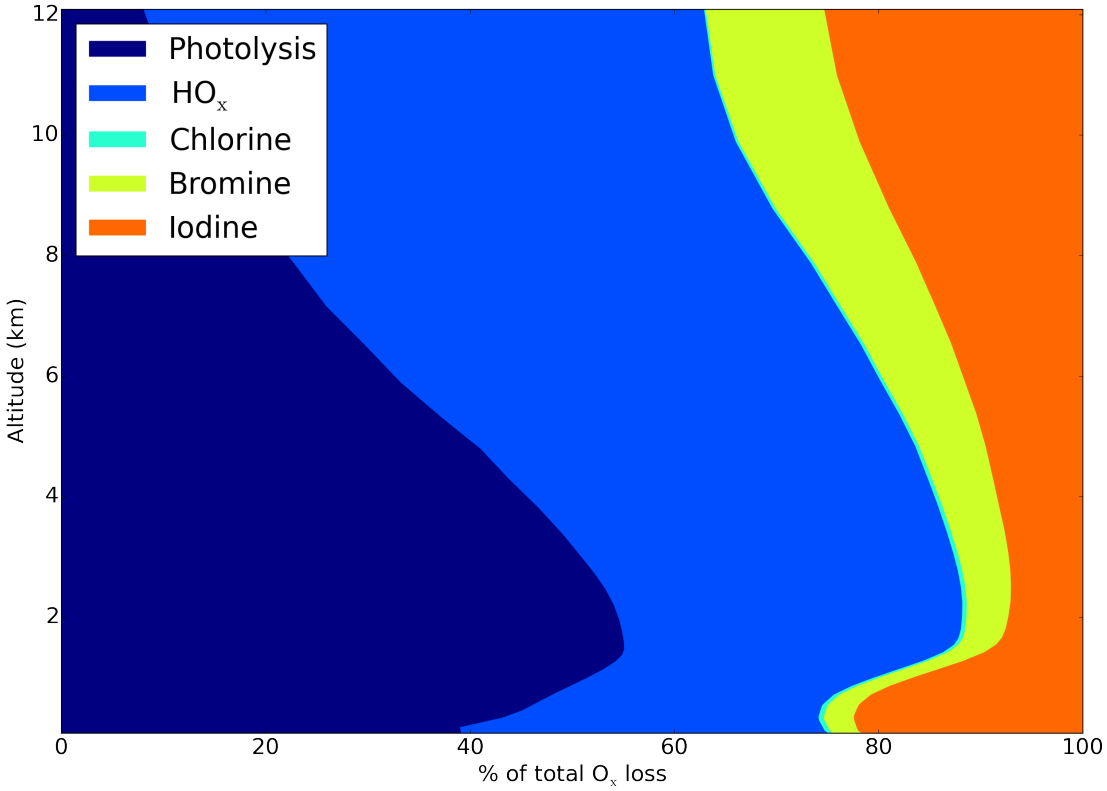

Figure 4.15 – Global annual average tropospheric vertical odd oxygen loss (O_x) through different reaction routes (Photolysis, HO_x, IO_x, BrO_x, and ClO_x).

Although the partitioning between the O_x loss processes is significantly different between the simulations with halogens and without (Table 4.4), the overall annual O_x loss only increases by 2.2 % (4933 vs 4829 Tg yr^{-1}). The O_x production term decreases by 1.0 %. This decrease is due to a reduction in NO_x concentrations due to hydrolysis of XNO_3 (X=Cl, Br, I). The tropospheric NO_x burden decreases by 1.7 % to 168 Gg N (see table

B.1) on inclusion of halogens consistent with previous model studies (Long et al., 2014; von Glasow et al., 2004; Parrella et al., 2012; Schmidt et al., 2016). Globally NO_x loss through $ClNO_3$ and $BrNO_3$ hydrolysis is approximately equal (1:0.86), and overall proceeds at a rate of ∼10 % of the NO_x loss through the NO_2+OH pathway. Iodine nitrite and nitrate (INO_2, INO_3) hydrolysis is much less significant (∼0.25 % of rate of NO_2+OH). Net tropospheric O_x production is the difference between the production and loss terms and the change here is much greater leading to an overall decrease in net production of tropospheric O_3 (PO_x-LO_x) of 26 % (159 Tg yr^{-1}), and a decrease in O_3 lifetime of 14 %.

4.4.2 HO_x (OH+HO_2)

The calculated global molecule weighted average HO_x (OH+HO_2) concentrations are reduced by 8.5 % with the inclusion of halogens, with OH decreasing by 4.5 % from 1.40x10^6 to 1.34x10^6 molecules cm^{-3}. Lower O_3 concentrations decrease the primary OH source ($O_3 \xrightarrow{h\nu} 2OH$) by 15.5 %, and the secondary OH source from HO_2+NO by 2.2 %.

The reduction in the sources of OH is buffered by an additional OH source from the photolysis of HOX (X=Cl, Br, I) which acts to increase the conversion of HO_2 to OH. In Chapter III an increase of 1.8 % in global OH concentrations on inclusion of iodine was shown. However, increased Br_y and reduced I_y concentrations in the simulations described here mean that the increased OH source from HOX photolysis does not compensate fully for the reduced primary source, resulting in an overall 4.5 % reduction in global mean OH. This buffering contributes to a smaller change in OH than reported previously by Schmidt et al. (2016) of 11 %. As reported previously (Long et al., 2014; Schmidt et al., 2016), here it is also found the net effect of halogens on the OH:HO_2 ratio is a small increase (4.4 %).

4.4.3 Organic compounds

The oxidation of volatile organic compounds (VOCs) by halogens is included in this simulation (see Table A.1 for reactions). The global fractional loss due to OH, Cl, Br, NO_3, and photolysis for a range of organics is shown in Figure 4.16.

Globally, Br oxidation is small in this simulation and contributes 2.1 % to the loss of

Table 4.4 – Comparison between global tropospheric O_x budgets of simulations "Cl+Br+I" (with halogen chemistry) and "NOHAL" (without halogen chemistry). Recent average model values from ACCENT (Young et al., 2013) are also shown for comparison. For the X'O+X"O halogen crossover reactions where $X'O \neq X''O$ the O_3 loss is split equally between the two routes. Values are rounded to the nearest integer value.

	"Cl+Br+I"	"NOHAL"	ACCENT
O_3 burden (Tg)	355	416	340 ± 40
O_x chemical sources (Tg yr^{-1})			
NO + HO_2	3526	3607	-
NO + CH_3O_2	1327	1316	-
NO + RO_2	524	508	-
Total chemical O_x sources (PO_x)	5376	5431	5110 ± 606
O_x chemical sinks (Tg yr^{-1})			
O_3 + $H_2O \xrightarrow{h\nu}$ 2OH + O_2	2102	2489	-
O_3 + $HO_2 \rightarrow$ OH + O_2	1136	1432	-
O_3 + OH $\rightarrow$ HO_2 + O_2	611	737	-
HOBr $\xrightarrow{h\nu}$Br + OH	214	-	-
HOBr + HCl $\rightarrow$ BrCl	28	-	-
HOBr + HBr $\rightarrow$ Br_2 + H_2O (aq. aerosol)	13	-	-
BrO + BrO $\rightarrow$ 2Br + O_2	8	-	-
BrO + BrO $\rightarrow$ Br_2 + O_2	3	-	-
BrO + OH $\rightarrow$ Br + HO_2	9	-	-
IO + BrO $\rightarrow$ Br + I + O_2	9	-	-
ClO + BrO $\rightarrow$ Br + ClOO/OClO	2	-	-
Other bromine O_x sinks	0	-	-
Total bromine O_x sinks	284	-	-
HOI $\xrightarrow{h\nu}$I + OH	457	-	-
OIO $\xrightarrow{h\nu}$I + O_2	125	-	-
IO + BrO $\rightarrow$ Br + I + O_2	9	-	-
IO + ClO $\rightarrow$ I + Cl + O_2/ ICl + O_2	0	-	-
Other iodine O_x sinks	2	-	-
Total iodine O_x sinks	593	-	-
HOCl $\xrightarrow{h\nu}$Cl + OH	15	-	-
CH_3O_2 + ClO $\rightarrow$ ClOO	4	-	-
ClO + BrO $\rightarrow$ Br + ClOO/OClO	2	-	-
$ClNO_3$ + HBr $\rightarrow$ BrCl	1	-	-
IO + ClO $\rightarrow$ I + Cl + O_2/ ICl + O_2	0	-	-
Other chlorine O_x sinks	1	-	-
Total chlorine O_x sinks	23	-	-
Other O_x sinks	184	172	-
Total chem. O_x sinks (LO_x)	4933	4829	4668 ± 727
O_3 PO_x-LO_x (Tg yr^{-1})	443	602	618 ± 251
O_3 Dry deposition (Tg yr^{-1})	832	980	1003 ± 200
O_3 Lifetime (days)	22	26	22 ± 2
O_3 STE (PO_x-LO_x-Dry dep.) (Tg yr^{-1})	389	378	552 ± 168

acetaldehyde (CH_3CHO), 0.6 % of the loss of formaldehyde (CH_2O), 0.26 % of the loss of $\geqslant$C4 alkenes, and <0.001 % of the loss of other compounds. Recent work has suggested a significant source of oceanic oxygenated VOCs (Millet et al., 2010; Coburn et al., 2014; Sinreich et al., 2010; Mahajan et al., 2014; Lawson et al., 2015; Volkamer et al., 2015; Myriokefalitakis et al., 2008) which is not included in this simulation. Furthermore although the modelled Br_y is broadly comparable to some previous work (Schmidt et al., 2016; Parrella et al., 2012), it is lower in the marine boundary layer than in other recent work (Long et al., 2014). The combination of these two factors suggest that this model provides a lower bounds of impacts of bromine on VOCs. Significantly higher concentrations of oxygenated-VOCs would decrease the BrO concentrations in the model and might then allow an increased sea-salt source of reactive bromine consistent with observed sea-salt debromination.

The oxidation of VOCs by chlorine is more significant. In this simulation chlorine accounts for 18, 9, and 9 % of the global loss of ethane (C_2H_6), propane (C_3H_8), and acetone ($CH_3C(O)CH_3$)), respectively. Loss of other VOCs is globally small. This increased loss due to Cl is to some extent compensated for by the reduction in the OH concentrations that is calculated here. Thus the overall lifetime of ethane, propane, and acetone changes from 131, 38, 85 days in the simulation without halogens to 120, 37, 82 in the simulation with halogens. Notably the ethane lifetime without halogens is 10% longer than it is with. Given that here the chlorine in the model can be argued to be a lower limit, ethane oxidation by chlorine may in reality be more significant than found here and may provide a significant change in our perspective of the budget of ethane.

Methane is a significant climate gas, as it has the second highest forcing amongst well-mixed greenhouse gases from preindustrial to present day (Myhre et al., 2013). In the simulation without halogens a tropospheric chemical lifetime due to OH of 7.48 years is calculated. With the inclusion of halogen chemistry the OH concentration drops, extending the methane lifetime due to OH to 7.96 years (an increase of 6.5 %). However, in the halogen simulations, chlorine radicals also oxidise methane ($\sim$1 % of the total loss) shortening the lifetime to 7.89 years (0.85 %). As noted previously, the model's chlorine concentrations appear to be underestimated. Allan et al. (2007) estimate a 25 Tg yr^{-1} sink for methane from Cl ($\sim$4 %), significantly higher than the estimate here. Overall the model's CH_4 lifetime still appears to be short compared to the observationally based

estimation of 9.1 ±0.9 from Prather et al. (2012), but halogens decrease this bias.

In these simulations, halogens (essentially chlorine) have a significant but not overwhelming role in the concentrations of hydrocarbons (from ∼1 % of methane loss to ∼18 % of ethane loss). However, as discussed earlier the low biases seen with the very limited observational dataset of chlorine compounds would suggest that the impacts calculated here are probably lower limits.

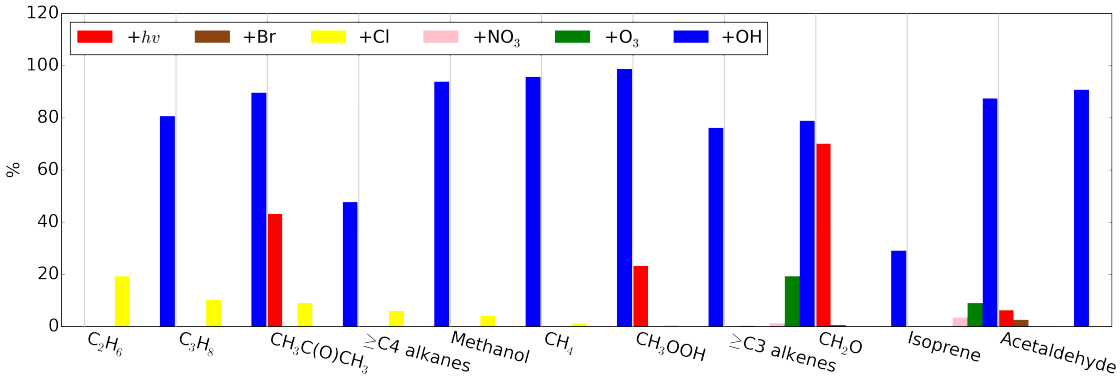

Figure 4.16 – Global loss routes ($+h\nu$, +Br, $+NO_3$, +Cl, +OH) of organic compounds shown as % of total tropospheric losses.

4.4.4 Other species

With the inclusion of halogens in the troposphere there are a large number of changes in the composition of the troposphere. Figure 4.17 illustrates the fractional global change in burden by species (for abbreviation see Footnote[3]).

The spatial and zonal distribution of these changes by species family (HO_x, NO_x, SO_x as defined in Footnote[4]) are shown in Figure 4.18 and for a few VOCs (C_3H_8, C_2H_6, acetone, and ⩾C4 alkanes) in Figure 4.19. A tabulated form of these changes is given within the Appendix (Table B.1)

[3]Abbreviated species names are defined in the GEOS-Chem manual (http://acmg.seas.harvard.edu/geos/doc/man/appendix_6.html) and here: MOH=Methanol, EOH=Ethanol, ALD2=Acetaldehyde, ISOP=Isoprene, ALK4=≥C4 alkanes, CH_3O_2,=Methylperoxy radical, A3O2= primary RO_2 from C_3H_8, B3O2=secondary RO_2 from C_3H_8, ATO2=RO_2 from Acetone, R4O2=RO_2 from ≥C4 alkanes, RIO2=RO_2 from Acetone

[4]Here the definitions the HO_x, NO_x and SO_x families as follows. HO_x: OH + HO_2, NO_x: NO+NO_2, SO_x : SO_2 + SO_4 + SO_4 on sea salt.

As discussed in section 4.4.1 and 4.4.1, a clear decrease in oxidants (O_3, OH, HO_2, H_2O_2) is seen. This drives an increase in the concentrations of some VOCs (2.1 % on a per carbon basis), including CO (2.8 %) and Isoprene (3.4 %). However, as discussed, it also adds an additional Cl sink term which leads to an overall decrease in some species (e.g. C_2H_6, $(CH_3)_2CO$, C_3H_8) particularly in the northern hemisphere oceanic regions. The SO_x burden increases slightly (0.7 %), which can be attributed to decreases in oxidants.

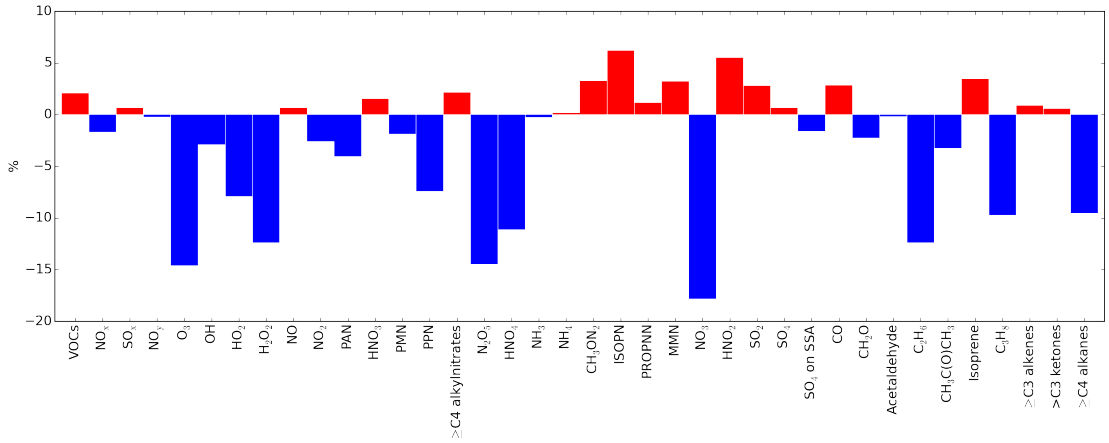

Figure 4.17 – Changes in tropospheric burden of species and families on inclusion of halogens ("Cl+Br+I") compared to no halogens ("NOHAL"). Burdens are considered in elemental terms (e.g Tg S/N/C) and species masses for OH, HO_2, H_2O_2 and O_3. The family denoted by "VOCs" in this plot is defined as the sum of carbon masses of CO, formaldehyde, acetaldehyde, ethane, acetone, isoprene, propane, ≥C4 alkanes, ≥C3 alkenes, and ≥3C ketones. Abbreviations for tracers are expanded in Footnote 3.

4.5 Summary and conclusions

A model of tropospheric composition is presented which has attempted to include the major routes of halogen chemistry impacts. Assessment of the model performance is limited as observations of halogen species are extremely sparse. However, given the available observations it is fair to conclude that the model has some useful skill in predicting the concentration of iodine and bromine species and appears to underestimate the concentrations of chlorine species.

Consistent with previous studies, this model shows significant halogen driven changes in the concentrations of oxidants. The tropospheric O_3 burden and global mean OH decreased by 14.6 %, and 4.5 % respectively, on inclusion of halogens. The methane lifetime increases

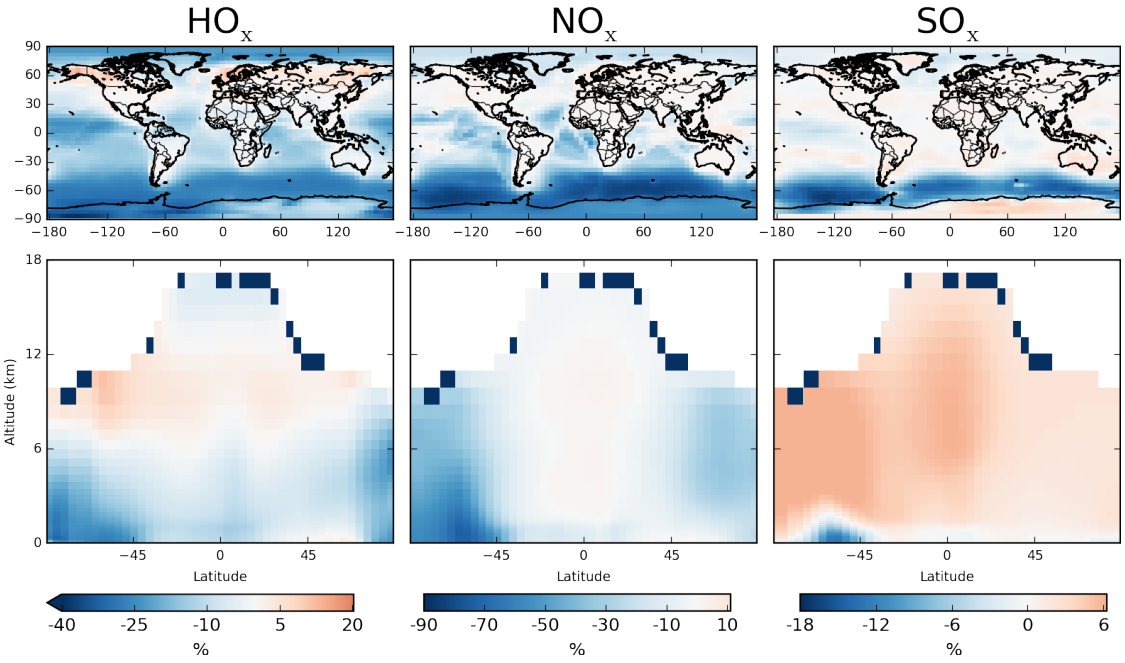

Figure 4.18 – Global annual average surface and zonal change (%) in HO_x, NO_x and SO_x families (as defined in Footnote 4) on inclusion of halogens

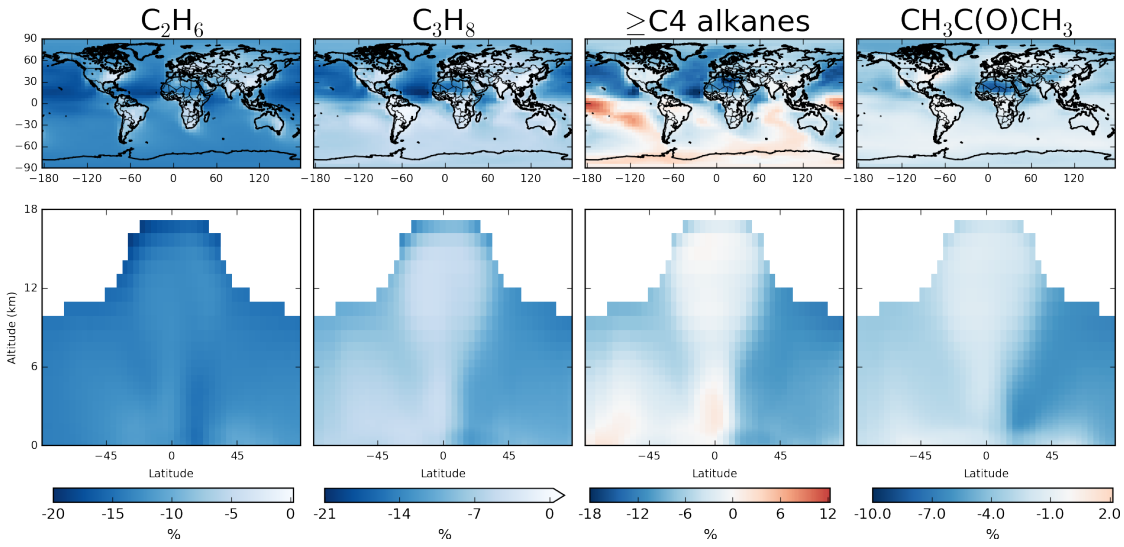

Figure 4.19 – Global annual average surface and zonal change (%) in ethane (C_2H_6), propane (C_3H_8), ≥C4 alkanes, and acetone ($CH_3C(O)CH_3$) on inclusion of halogens. For species where all average changes are negative a continuous colourbar is used (C_3H_8 and C_2H_6) and for species where both negative and positive changes are present a divergent colourbar is used (≥C4 alkanes and $CH_3C(O)CH_3$)

by 6.5 %, improving agreement with observations.

There are a range of changes in the concentrations of other species. Direct reaction with Cl atoms leads to enhanced oxidation of hydrocarbons with ethane showing a significant response. Given the model appears to provide a lower limit for tropospheric atomic Cl concentrations this suggests a major missing oxidation pathway for ethane which is currently not considered. NO_x concentrations are reduced by aerosol hydrolysis of the halogen nitrates which leads to reduced global O_3 production. The simulation of BrO appears to be relatively consistent with those observed, however sea-salt de-bromination is not included. This would suggest that either the heterogeneous cycling of bromine in this model is generally too fast, or that the model does not have sufficiently large BrO_x sinks (potentially oxygenated-VOCs). Both hypotheses warrant further research.

Significant uncertainties however remain in our understanding of halogens in the troposphere. The gas phase chemistry and photolysis parameters of iodine compounds are uncertain, together with the emissions of their organic and inorganic precursors (As discussed further in Chapter III/Sherwen et al. 2016a). For chlorine, bromine and iodine heterogeneous chemistry, little experimental data exists and suitable parameterisations for the complex aerosols found in the atmosphere are unavailable (Abbatt et al., 2012; Saiz-Lopez et al., 2012b; Simpson et al., 2015).

Understanding fully the impact of halogens on tropospheric composition will require significant development of new experimental techniques and more field observations, new laboratory studies and models which are able to exploit these developments.

Chapter 5

Impact of halogen chemistry on tropospheric O_3 radiative forcing

The content of this chapter is in review as an article entitled "Halogen chemistry reduces tropospheric O_3 radiative forcing": T. Sherwen, M. J. Evans, L. J. Carpenter, J. A. Schmidt, and L. J. Mickley, in review. 2016.

5.1 Introduction

Tropospheric ozone (O_3) is a key driver of climate change and a potent air pollutant. Understanding the change between its "natural" pre-industrial (~1750) and present-day concentrations is important in defining its role as a climate gas and as an air pollutant. Global tropospheric O_3 concentrations are thought to have increased substantially in this period, however, the observational record for this change is highly uncertain. Unlike carbon dioxide and methane, O_3 doesn't remain trapped in ice so modern analytical techniques cannot be applied to old air. Past observations suggest much lower concentrations of O_3 than are presently measured, by a factor of 2-3 (Volz and Kley, 1988; Marenco et al., 1994; Pavelin et al., 1999). However, there are only a small number of past observations and significant uncertainties exist in the methods used and their representativeness. Because of concerns over the validity of these observations, our assessment of the change in O_3 concentrations is predominantly based on computer simulations (Hauglustaine et al., 1994; Levy et al., 1997; Myhre et al., 2013; Young et al., 2013). These simulations calculate the concentration of O_3 based on estimates of the emissions of NO_x (NO + NO_2), CH_4, CO, SO_2, NH_3, volatile organic compounds, etc. in the pre-industrial and the present-day (Lamarque et al., 2010), together with an understanding of the chemistry, transport and physics occurring in the atmosphere (Bey et al., 2001; Levy, 1971; Logan, 1985). An assessment of the change in concentrations between the pre-industrial and the present-day and a calculation of the associated radiative forcing was undertaken as part of the ACCMIP project (Lamarque et al., 2013; Stevenson et al., 2013; Young et al., 2013; Voulgarakis et al., 2013). It concluded that pre-industrial O_3 burdens were 98 Tg lower than the present-day and calculated a RF_{TO3}[1] of 0.410 W m^{-2}.

These model calculations are, however, only as good as the emissions used to drive them and their representation of physical and chemical processes. Over the last decades, the emphasis for tropospheric chemistry has been on improving the representation of organic chemistry with particular emphasis on the role of biogenic compounds such as isoprene and monoterpenes (Glasius and Goldstein, 2016). This has contrasted with the stratosphere where the emphasis has been on halogen (predominantly Br and Cl) chemistry

[1] RF_{TO3} = Radiative forcing of tropospheric O_3. Where radiative forcing is defined as the difference in per unit area energy input to the earth at the tropopause.

(Morgenstern et al., 2010).

The tropospheric impact of halogens in polar regions during polar sunrise has been known for some time (Barrie et al., 1988; Jacob et al., 1992), but their significance for the global troposphere has only been evident in the last decade (Read et al., 2008; Saiz-Lopez and von Glasow, 2012; Prados-Roman et al., 2015b; Wang et al., 2015). Reviews of the appropriate processes are given elsewhere (Simpson et al., 2015), but in brief, organic halogen precursor gases are emitted into the atmosphere from predominantly natural sources (CH_3Br, $CHBr_3$, CH_2Br_2, CH_3I, CH_2I_2, CH_2ICl, CH_2IBr) or as a result of both anthropogenic and natural activities (CH_3Cl, $CHCl_3$, CH_2Cl_2, CH_3Br) (Montzka et al., 2011). Heterogeneous chemistry on sea salt can lead to the release of inorganic bromine and chlorine (McFiggans et al., 2000; Braban et al., 2007; Roberts et al., 2009; Bertram and Thornton, 2009), and inorganic iodine compounds can be released from the ocean due to chemistry involving atmospheric O_3 and iodide in the ocean surface (Carpenter et al., 2013; MacDonald et al., 2014). Once emitted into the atmosphere there is rapid photochemical processing of these compounds (Simpson et al., 2015). Catalytic cycles similar to those occurring in the stratosphere can lead to O_3 destruction (von Glasow et al., 2004; Simpson et al., 2015), changes to HO_x and NO_x cycling (Chameides and Davis, 1980; Long et al., 2014) and impacts on the distribution and deposition of mercury (Holmes et al., 2010; Parrella et al., 2012; Schmidt et al., 2016).

This chapter investigates the impact of tropospheric halogen chemistry on the change in O_3 concentrations between the pre-industrial and the present-day using the GEOS-Chem model of tropospheric chemistry and transport (Bey et al., 2001; Mao et al., 2013) which has been extended to provide a description of the chemistry of chlorine, bromine and iodine (Chapter V/Sherwen et al. 2016b). Comparisons between the model and present-day observations of halogen compounds have been shown previously (Eastham et al., 2014; Schmidt et al., 2016; Sherwen et al., 2016a,b). The model provides a good simulation of present-day bromine and iodine compounds but appears (given the limited observational record) to underestimate tropospheric chlorine chemistry (Sherwen et al., 2016b). Simulations are run with pre-industrial and present-day emissions, with halogen and without halogen chemistry (as discussed in Sect. 5.2) and the changes in the tropospheric O_3 concentrations evaualated.

5.2 Model setup

The GEOS-Chem model configuration used here is described in Chapter IV and in recent publications (Eastham et al., 2014; Schmidt et al., 2016; Sherwen et al., 2016a,b). The model is run for two years (2004 and 2005), discarding the first year as a "spin-up" period and using the second year (2005) for analysis. The simulations run with halogen chemistry is described as "Cl+Br+I" whereas the simulation without any halogens is described as "NOHAL". Non-halogen emissions (NO_x, SO_x, VOCs, aerosols, etc.) are identical to those described in Chapter II.

To simulate the pre-industrial troposphere, anthropogenic NO_x, VOC and SO_2 emissions are removed, biomass burning emissions are reduced to 10 % of present-day values and methane concentrations are reduced to 700 pmol mol^{-1} following Wang and Jacob (1998). Organic bromine sources were keep at present-day values, except for CH_3Br. The approach previously taken (Parrella et al., 2012) is followed, by which CH_3Br concentrations are reduced to a fixed concentration of 5 pmol mol^{-1} to match ice core records (Saltzman et al., 2004). Pre-industrial emissions of CH_3Cl, $CHCl_3$, and CH_2Cl_2 are scaled from present-day using the estimated natural contributions to their sources (92.5 %, 75 % and 10 %, respectively; Montzka et al. 2011; Reimann et al. 2014).

The work in this Chapter, as in Chapters II-V, focuses on the troposphererе and chemistry in the stratosphere is not explicitly treated. Instead linearised stratospheric rates (Murray et al., 2012b) are used, which are kept constant from present-day values, except for anthropogenic species (CFCs, Halons etc) which were set to zero. The contributions of Cl_y to tropospheric O_3 loss have been previously shown to be small (Chapter V/Sherwen et al. 2016b), but Br_y has been shown to be significant (Chapter V/Schmidt et al. 2016; Sherwen et al. 2016b). Therefore the concentration of stratospheric Br_y is scaled to pre-industrial concentration (by 0.56; Liang et al. 2010; Montzka et al. 2011), but no changes to Cl_y are considered.

5.3 Results and discussion

5.3.1 Changes from pre-industrial to present-day

Table 5.1 shows the estimated halogen emissions for the pre-industrial and the present-day. Iodine, bromine and chlorine emissions have all increased (50 %, 25 %, 40 %, respectively, on a per Tg of halogen basis) in this period. It is assumed that iodinated halocarbons emissions are unchanged, due to their natural source. The increase in iodine emissions (Fig. 5.4) is due to the increases in the surface ocean inorganic (HOI, I_2) iodine source driven by anthropogenically enhanced surface O_3 (37 % lower at the surface in pre-industrial compared to the present-day, see Fig. 5.9). Bromine emissions increase mainly because of increased anthropogenic emissions of precursor gases but also due to increased iodine driven sea-salt cycling ($HOI \xrightarrow{sea-salt} 0.15IBr + 0.85ICl$, Chapter IV) and an increase in the mixing down of chlorine and bromine species that have built up in the stratosphere from anthropogenic emissions. The largest increase in chlorine emissions is due to increases in heterogeneous uptake of N_2O_5 on sea-salt to liberate $ClNO_2$. This is a very minor source in the pre-industrial (0.5 % of total chlorine sources) but plays a larger role in the present-day (15 %) due to the much higher NO_x abundance. Other increases in chlorine emissions occur because of increased anthropogenic emissions of chlorinated halocarbons and increased iodine driven sea-salt cycling.

These increased emissions lead to increased concentrations of halogens in the present-day compared to the pre-industrial with global burdens of reactive halogens increasing by 19, 42 and 18 % for I, Br and Cl, respectively. This is shown globally within the vertical in Fig. 5.1, and zonal and at the surface in Fig. 5.2.

The burdens of inorganic iodine and chlorine increase by less than the increase in their emissions, whereas the burden of inorganic bromine increases by more. This reflects the changing lifetime of these I_y, Br_y and Cl_y in the pre-industrial and the present-day. The increase in NO_x concentrations in the present-day make the halogen sink from halogen nitrate hydrolysis more efficient (Ammann et al., 2013; Schmidt et al., 2016). This explains the model's shortening of the iodine lifetime and some of the chlorine lifetime shortening. The rest of the chlorine lifetime shortening is due to increased hydrocarbon concentrations which more efficiently convert Cl into HCl which is then rapidly deposited. Inorganic

Table 5.1 – Emission of halogen source gases for the pre-industrial (PI) and present-day (PD). Long lived sources which have fixed concentrations in the model for Cl_y(CH_3Cl, CH_2Cl_2, $CHCl_3$) and Br_y ($CHBr_3$) are shown in terms of chemical release (e.g. reaction with +OH, $+h\nu$, +Cl) and are in in bold. I_2 and HOI are the inorganic ocean source from O_3 reacting with oceanic iodide (Carpenter et al., 2013), IX is from the uptake of iodine gases onto sea salt to release IBr or ICl, $ClNO_2$ is the source from the uptake of N_2O_5 on sea-salt.

	I_y	(Tg I yr^{-1})	Br_y	(Tg Br yr^{-1})	Cl_y	(Tg Cl yr^{-1})
Sources	PI	PD	PI	PD	PI	PD
CH_3X	0.26	0.26	**0.04**	**0.06**	**2.28**	**2.19**
CH_2X_2	0.33	0.33	0.09	0.09	**0.11**	**0.59**
CHX_3	-	-	0.41	0.41	**0.21**	**0.26**
HOI	1.17	2.02	-	-	-	-
I_2	0.08	0.14	-	-	-	-
IX	-	-	0.19	0.31	0.46	0.78
$ClNO_2$	-	-	-	-	0.02	0.66
Stratosphere	0.00	0.00	0.02	0.06	0.44	0.43
Total source	1.84	2.75	0.74	0.92	3.52	4.9

bromine increases more than would be expected due to a change in its source region. The stratospheric flux of inorganic bromine increased by a factor of three between the pre-industrial and the present-day. This flux enters a region of low depositional loss and so the overall lifetime of bromine in the atmosphere effectively increases (by ∼13 %). Simulations with a present-day stratosphere for both the present-day and the pre-industrial shows a decrease in the inorganic bromine lifetime in the same manner as for inorganic iodine and bromine.

The inclusion of the halogen chemistry reduces the concentration of O_3 in both the present-day and the pre-industrial (as shown in DU terms in Fig. 5.9). As shown in Chapter IV, the O_3 simulated in the present-day (Fig. 5.7) appears to be more consistent with observations when including halogen chemistry than without (other than for the Southern Ocean). Figure 5.8 shows a comparison between the limited number of O_3 observations for pre-industrial locations (Marenco et al., 1994; Pavelin et al., 1999; Volz and Kley, 1988) and the model. Globally the surface O_3 concentration is reduced by 9.2 nmol mol^{-1} or 37 % in the pre-industrial with the inclusion of halogens. This reduction is largest over the oceans. Although the model still overestimates the observations (a common problem, see

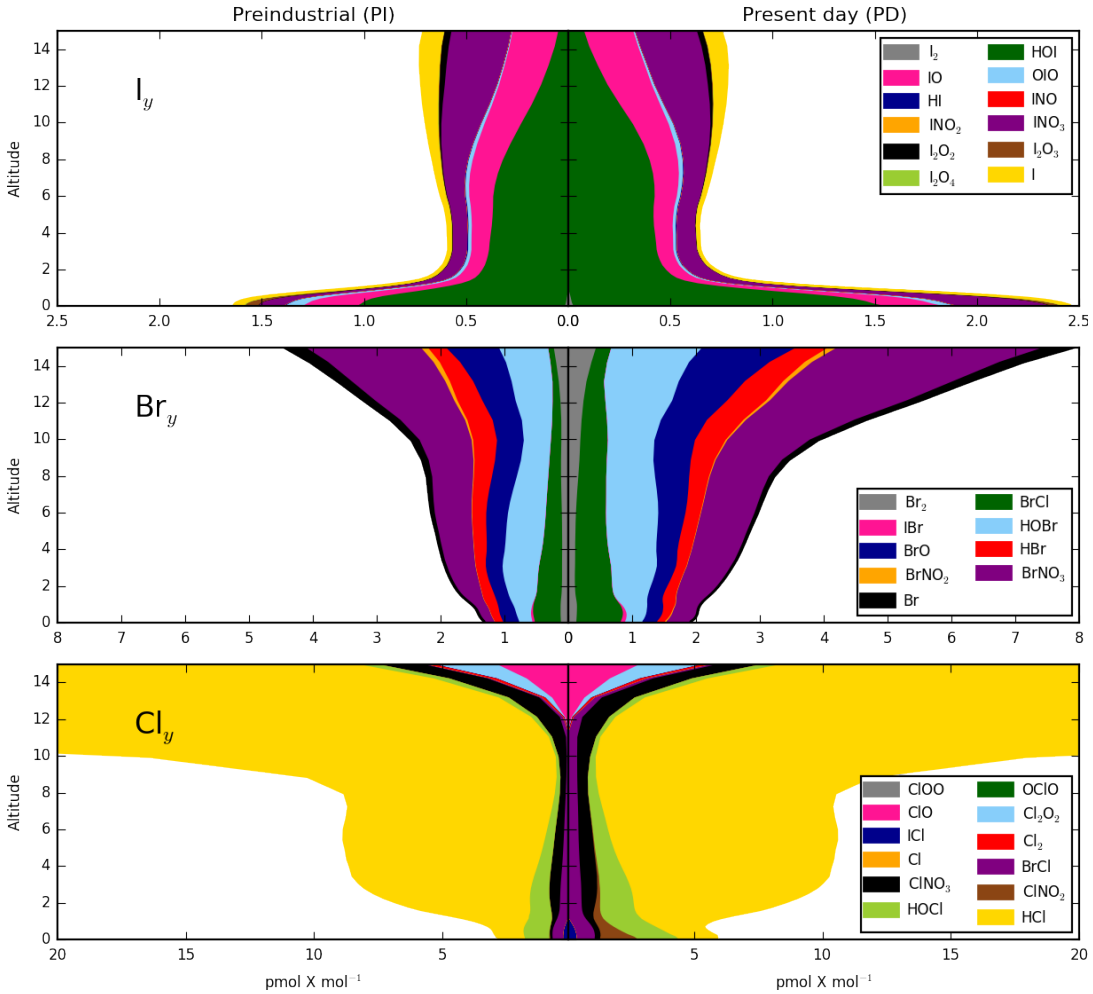

Figure 5.1 – Vertical distribution of inorganic tropospheric halogens. Global mean vertical distribution of iodine, bromine and chlorine inorganic gases (X_y, X=Cl, Br, I) for the pre-industrial (left) and present-day (right) in terms of mixing ratios of halogen. Increased halogen concentrations in the present-day are predominantly evident at the surface for iodine and throughout the column for bromine and chlorine reflecting the different sources of these compounds.

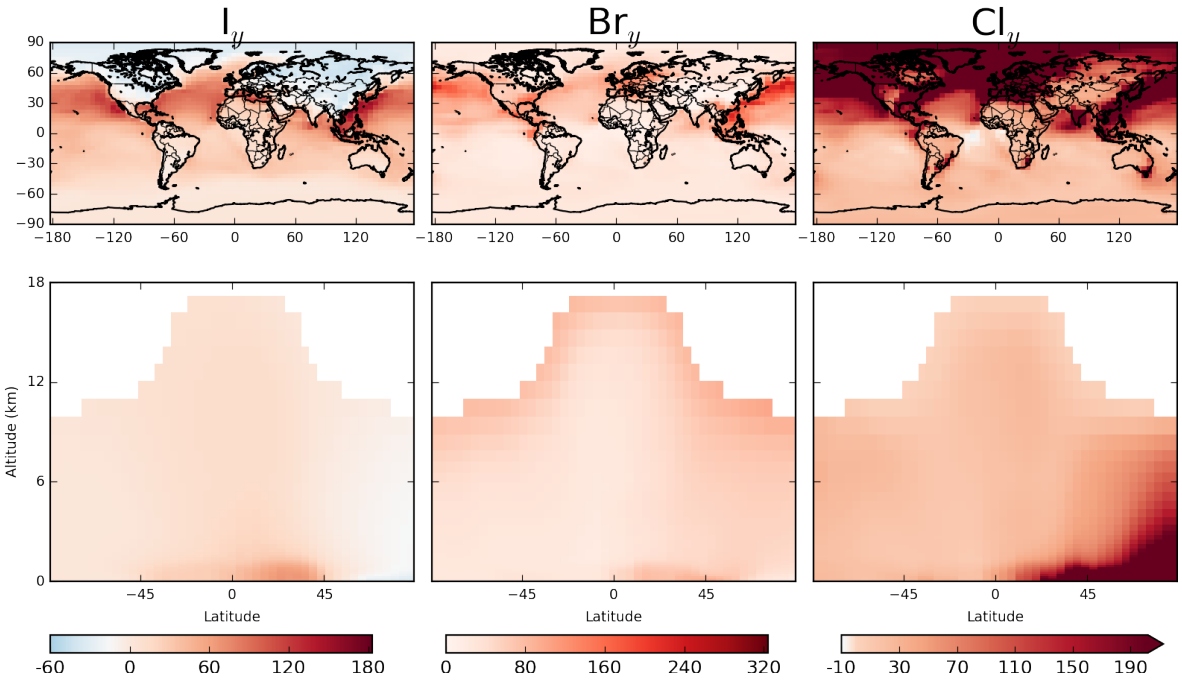

Figure 5.2 – Change from pre-industrial (PI) to present-day (PD) in tropospheric distribution of I_y, Cl_y, Br_y in pmol mol^{-1} ((PD-PI)/PI*100"). Upper plots show surface and lower plots show zonal values.

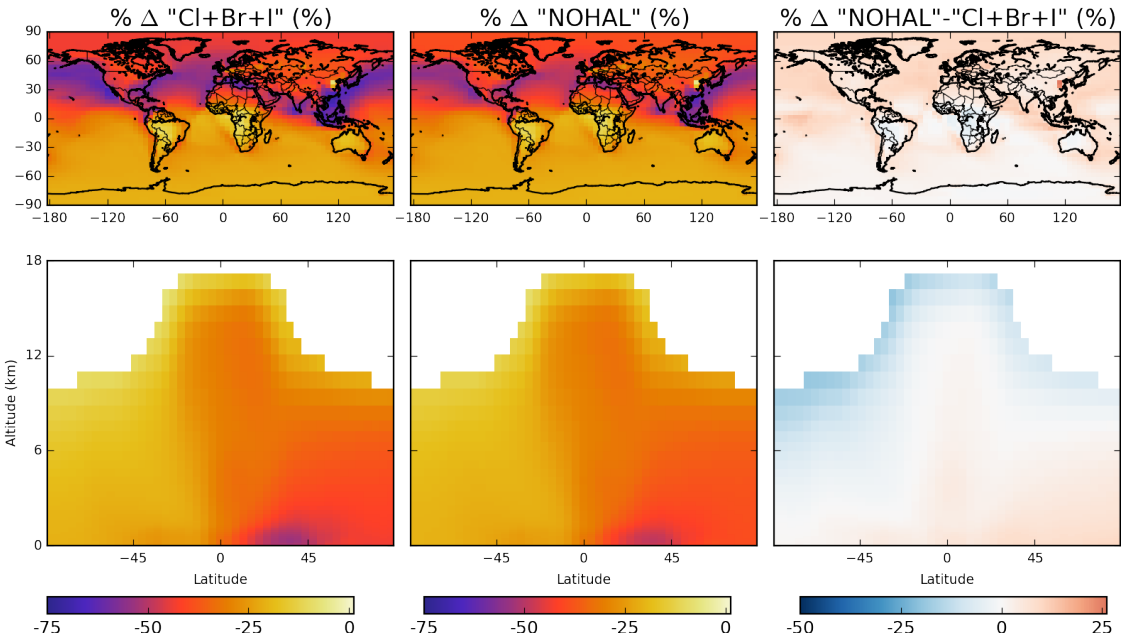

Figure 5.3 – Annually averaged surface (top) and zonal (bottom) O_3 percentage increases between the pre-industrial (PI) and the present-day (PD), with halogen chemistry (left), without halogen chemistry (centre) and the percentage change between these two.

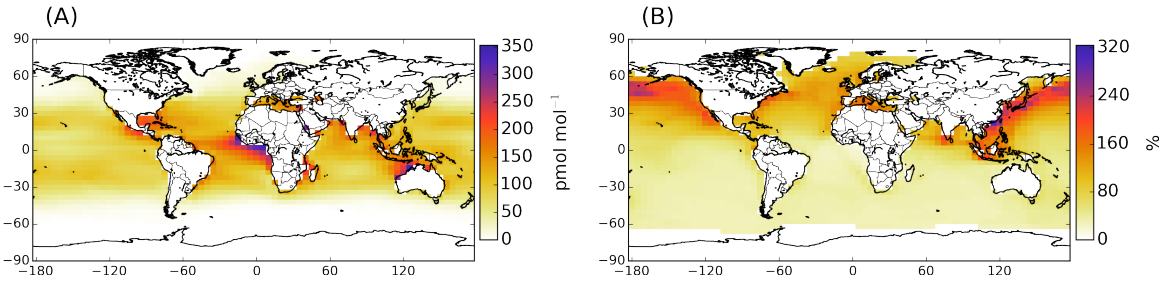

Figure 5.4 – Inorganic emission flux (HOI, I_2) in the pre-industrial (PI) (A) and % change from pre-industrial ((PD-PI)/PI*100) (B).

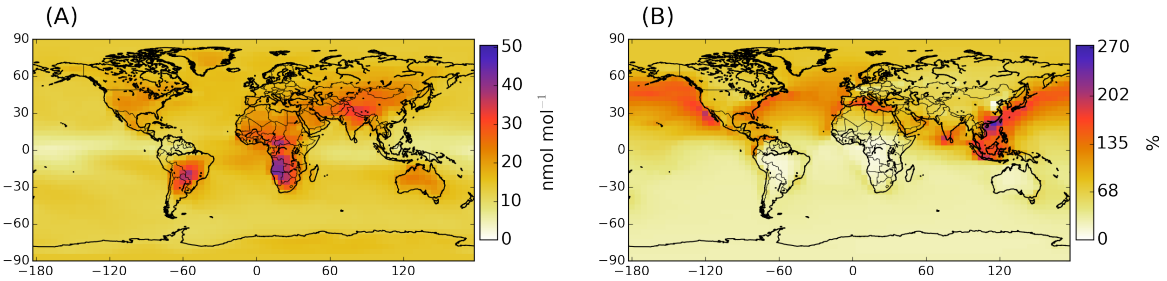

Figure 5.5 – O_3 surface concentration in present-day (PD) (A) and % change in O_3 from pre-industrial (PD-PI)/PI*100).

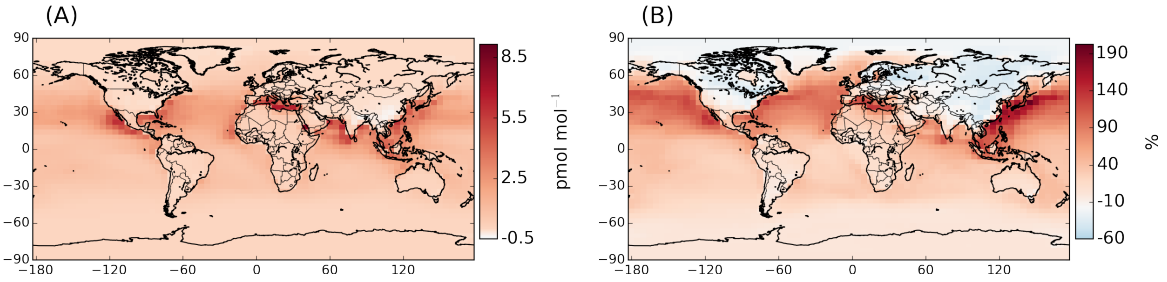

Figure 5.6 – Change in surface I_y concentration from the pre-industrial (PI) to present-day (PD). Shown in actual terms (pmol mol^{-1}, left) and percent change (((PD-PI)/PI*100), right).

Mickley et al. 2001b; Young et al. 2013) the simulation is improved with the inclusion of halogens. However, it is important to reiterate confidence in these observation datasets is low. Globally, halogens reduce the O_3 burden by 61 Tg in the present-day and 43 Tg in the pre-industrial (Table 5.2).

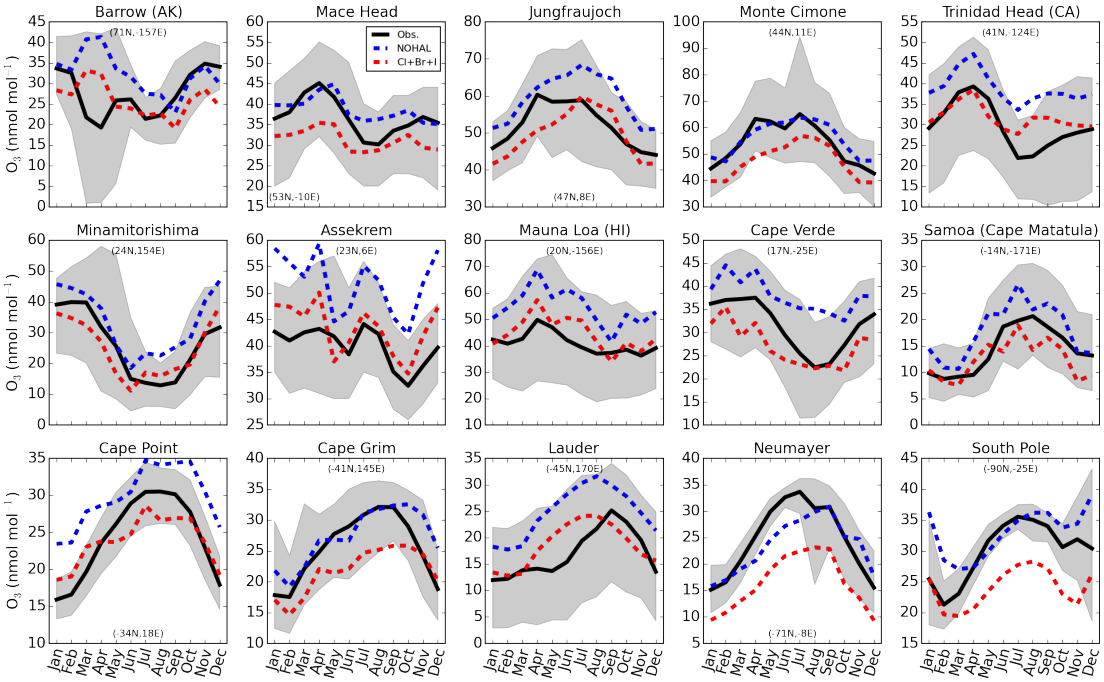

Figure 5.7 – Seasonal cycle of present-day (PD) near-surface O_3 at a range of Global Atmospheric Watch (GAW) sites. Observational data shown are 6 year monthly averages (2006-2012). Model data is for 2005. Data is from GAW compiled and processed as described in (Sofen et al., 2016). Blue and red lines represent simulations without halogens ("NOHAL") with halogens ("Cl+Br+I"), respectively. This figure is reproduced from Chapter IV (Fig. 4.13) for readability.

The O_3 budgets for the four simulations are shown in Table 5.2. In both the present-day and the pre-industrial the halogens are responsible for around 20 % of the O_3 destruction, with iodine dominating in both time periods (66 %: 32 %: 3 % I:Br:Cl for the present-day and 69 %: 28 %: 2 % I:Br:Cl for the pre-industrial). Although chlorine concentrations have increased almost as much as iodine between the pre-industrial and the present, it plays little role in determining O_3 loss (Schmidt et al., 2016; Sherwen et al., 2016a,b) and may slightly increase O_3 pollution (Sarwar et al., 2014). Tropospheric O_3 lifetimes drop from 26 days to 22 days in the present-day with the inclusion of halogens and from 28 days to 25 days in the pre-industrial.

Tropospheric chemistry is a highly coupled system with significant interplays between the

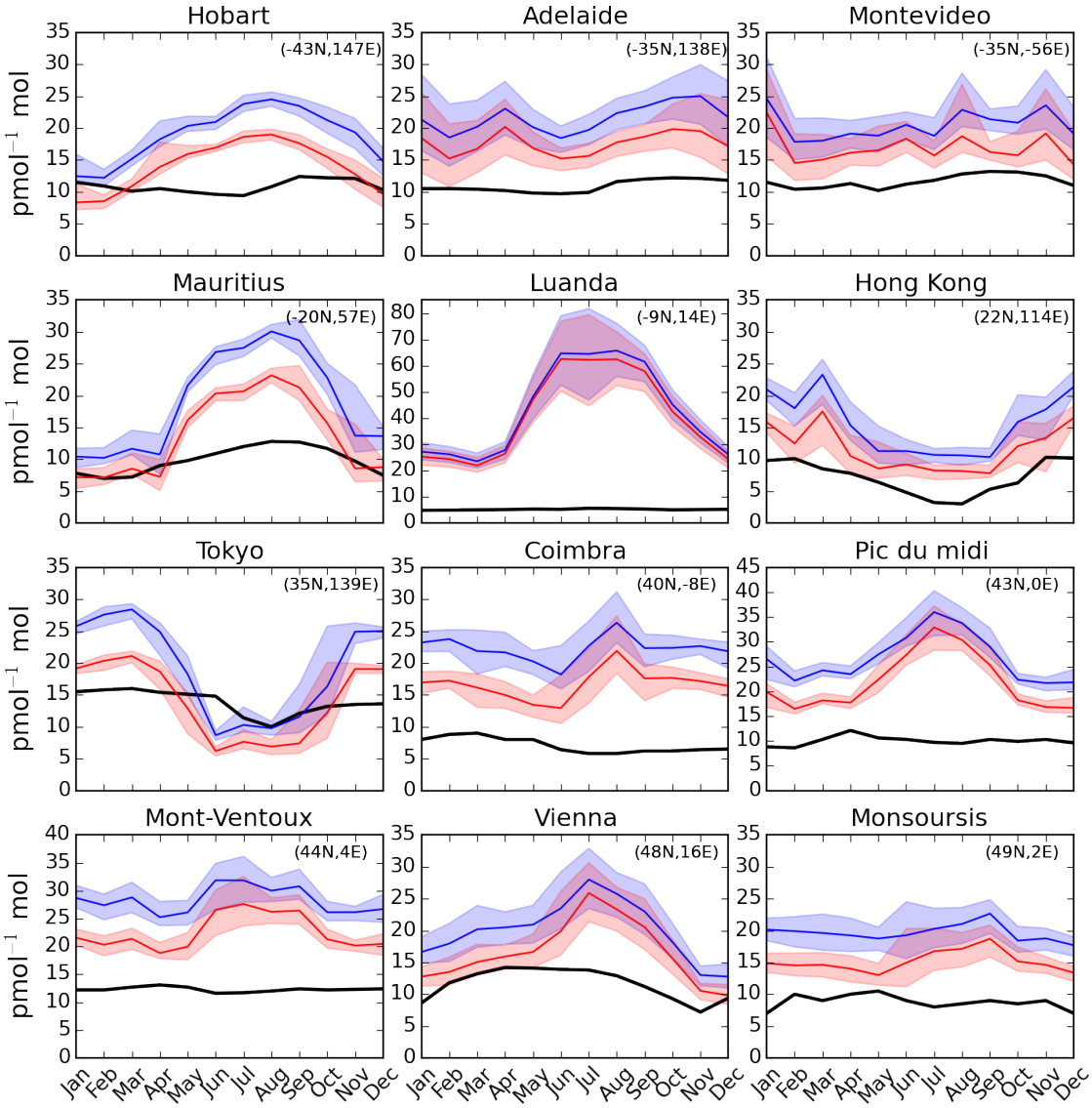

Figure 5.8 – Comparison between observed and modelled pre-industrial (PI) O_3. Observations are shown in black, pre-industrial model simulation with halogens in red and without halogens in blue. The O_3 data is reproduced (Mickley et al., 2001b) from previously reported observations: Mont Ventoux, Hong Kong, Tokyo, Adelaide, Coimbra, Hobart, Luanda, Mauritius, Vienna, and Montevideo (Marenco et al., 1994); Pic du Midi (Pavelin et al., 1999); Montsouris (Volz and Kley, 1988). 1^{st} and 3^{rd} quartiles are given for model data by shaded regions.

NO_x and HO_x systems (Monks et al., 2015). Changes in the individual production and loss terms are relatively small but halogens reduce net O_3 production by 159 Tg yr^{-1} in the present-day yet only 119 Tg yr^{-1} in the pre-industrial. In the pre-industrial simulation with halogens, the troposphere is close to being a net chemical sink for O_3. Thus the impact of halogens chemistry on the overall O_3 burden of the atmosphere is more important for the present-day that it was in the pre-industrial. This is predominantly due to the higher O_3 concentrations in the present-day leading to higher oceanic iodine emissions.

Figure 5.9 shows the change in column O_3 (in Dobson units, DU) between the pre-industrial and the present-day with and without halogens. Consistent with previous work, the largest changes (increases) in column O_3 occur in the northern mid-latitudes notably over eastern North America and Asia (Lamarque et al., 2005). Halogens reduce the column change by an average of 1.6 DU or ∼15 %. The largest halogen-driven reductions (up to 3 DU) are seen over the Northern Pacific and Atlantic oceans. This is where surface O_3 concentration increase the most over the oceans leading to increases in oceanic inorganic iodine emissions which in turn leads to more active O_3 destruction by iodine chemistry.

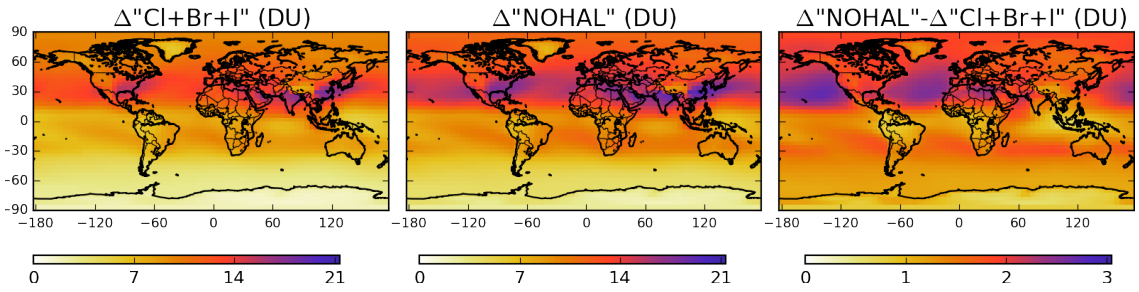

Figure 5.9 – Increases in tropospheric O_3 column between the pre-industrial and present-day with and without halogens. Left and centre panels show the difference in annually averaged column O_3 (DU) between pre-industrial and the present-day with (left="Cl+Br+I") and without halogens (centre='NOHAL"). Right panel shows the difference between the fields.

5.3.2 Implications

The radiative forcing caused by these changes is evaluated here assuming a linear conversion of radiative forcing associated from O_3 column change (0.042 Wm^{-2} DU^{-1}, Myhre et al. 2013). The globally averaged radiative forcing for the simulations without halogens is 0.432 Wm^{-2}, close to the 0.410 Wm^{-2} found from the ACCMIP inter-comparison

(Stevenson et al., 2013). The simulation with halogens however shows a lower radiative forcing of 0.366 Wm^{-2}. Thus, the increases in halogen chemistry associated with human activity is acting to dampen the anthropogenic radiative forcing of O_3. Given that none of the models which participated in the last IPCC assessment incorporated the chemistry of tropospheric halogens, it would appear that there may be an over-estimate of tropospheric O_3 radiative forcing of the order of ∼20 % by the IPCC models. The 0.066 Wm^{-2} halogen-induced reduction in tropospheric O_3 radiative forcing is slightly larger than the 0.05 Wm^{-2} radiative forcing from reduced stratospheric O_3 due to halogen chemistry from mainly anthropogenic sources (e.g. CFCs, halons; Myhre et al. 2013).

Some of this dampening of the increase in tropospheric O_3 due to halogens is associated with the co-emission of industrial pollutants. Human activities release a range of pollutants some of which can produce O_3 (NO_x, VOCs, CO, CH_4) whereas others destroy O_3 (halogenated compounds). Estimates for O_3 radiative forcing which only consider anthropogenic O_3 production gases without considering the co-emitted O_3 destroying gases is likely to overestimate the radiative forcing. A different mechanism for this dampening is the role of the O_3 driven ocean release of iodine. As human generated O_3 has increased so has the release of iodine from the ocean which has acted as a negative feedback (Prados-Roman et al., 2015a). This means that there are three mechanisms for halogens to alter tropospheric O_3 forcing: stratospheric changes in flux, halogen precusor increases in the troposphere, and the iodine flux from the ocean.

A range of sensitivity studies were run to assess the magnitudes of the different mechanisms in play. By removing the O_3-iodine feedback via setting HOI and I_2 fluxes to zero (so only a change in the stratospheric flux and the tropospheric halocarbons) a radiative forcing of 0.411 Wm^{-2} is calculated. Removing the O_3-iodine feedback and the change in the stratospheric flux between pre-industrial and the present-day, leads to a radiative forcing of 0.391 Wm^{-2}. Thus it is possible to attribute ∼40 % of the halogen-driven reduction in O_3 radiative forcing to the ocean-atmosphere O_3-iodine feedback, ∼30 % to the increase in the flux of inorganic halogens from the stratosphere and ∼30 % to the co-emission of halogenated compounds by humans. It is difficult to unambiguously make these attributions as the sources are coupled. Notably the uptake of iodine compounds onto sea-salt causes Br and Cl to be released.

5.4 Conclusions

As discussed in Chapters I, III and IV, there are significant uncertainties in the chemistry of tropospheric halogens. Although the basic gas-phase chemistry is well known there are uncertainties as to the fate of iodine higher oxides and the photolysis of some species (Saiz-Lopez et al., 2012b). The largest uncertainties though likely lie in our understanding of the heterogeneous processing of halogens (Abbatt et al., 2012; Saiz-Lopez et al., 2012b; Sherwen et al., 2016a; Simpson et al., 2015) which affords a coupling between iodine, bromine, chlorine and between the different emission types and sea salt. Relatively small changes to parameters here can make substantial changes to the O_3 radiative forcing. For example, the partitioning between ICl and IBr emissions, which occur after uptake of condensable iodine compounds to sea-salt aerosol (e.g. HOI $\xrightarrow{sea-salt}$ αICl + βIBr), is not well known. Changing the ICl to IBr ratio from 0.85:0.15 (as used here and previously Chaper V/Sherwen et al. 2016b) to 0.75:0.25 changes the halogen induced reduction in O_3 radiative forcing from the 18 % found here to 20 %. Further increasing this to the IBr yield (0.5:0.5), as used in other studies (McFiggans et al., 2000; Saiz-Lopez et al., 2014), increases the reduction in the O_3 radiative forcing yet more (23 %).

Uncertainties in the role of halogens in determining tropospheric O_3 radiative forcing may be reduced by more observations of halogen compounds in the present-day (in the atmosphere and oceans) and by reducing uncertainties in the kinetics of the gas and aerosol phase chemistry. However, it would appear that model estimates of O_3 radiative forcing that do not consider tropospheric halogen chemistry are likely $\sim$20% too large.

Table 5.2 – Global tropospheric O_x budgets of pre-industrial and present-day with and without halogens. Comparative values from the ACCENT multi-model comparison (Young et al., 2013) are also shown for the present-day. For the $X'O+X''O$ halogen crossover reactions where $X' \neq X''$ the O_x loss is split equally between the two routes. Values are rounded to the nearest integer value.

	Pre-industrial	Pre-industrial	present-day	present-day
	With halogens	Without	With halogens	Without
O_3 burden (Tg)	260	303	355	416
O_x chemical sources (Tg yr^{-1})				
$NO + HO_2$	2,256	2,357	3,526	3,607
$NO + CH_3O_2$	662	668	1,327	1,316
$NO + RO_2$	423	375	524	508
Total chemical O_x sources (PO_x)	3,341	3,401	5,376	5,431
O_x chemical sinks (Tg yr^{-1})				
$O_3 + H_2O \xrightarrow{h\nu} 2OH + O_2$	1,421	1,711	2,102	2,489
$O_3 + HO_2 \rightarrow OH + O_2$	641	822	1,136	1,432
$O_3 + OH \rightarrow HO_2 + O_2$	497	601	611	737
$HOBr \xrightarrow{h\nu} Br + OH$	139	-	214	-
$HOBr + HCl \rightarrow BrCl$	13	-	28	-
$HOBr + HBr \rightarrow Br_2 + H_2O$ (aq. aerosol)	7	-	13	-
$BrO + BrO \rightarrow 2Br + O_2$	4	-	8	-
$BrO + BrO \rightarrow Br_2 + O_2$	1	-	3	-
$BrO + OH \rightarrow Br + HO_2$	8	-	9	-
$IO + BrO \rightarrow Br + I + O_2$	7	-	9	-
$ClO + BrO \rightarrow Br + ClOO/OClO$	1	-	2	-
Other bromine O_x sinks	0	-	0	-
Total bromine O_x sinks	180	-	284	-
$HOI \xrightarrow{h\nu} I + OH$	336	-	457	-
$OIO \xrightarrow{h\nu} I + O_2$	99	-	125	-
$IO + BrO \rightarrow Br + I + O_2$	7	-	9	-
$IO + ClO \rightarrow I + Cl + O_2$/ $ICl + O_2$	0	-	0	-
Other iodine O_x sinks	1	-	2	-
Total iodine O_x sinks	443	-	593	-
$HOCl \xrightarrow{h\nu} Cl + OH$	10	-	15	-
$CH_3O_2 + ClO \rightarrow ClOO$	3	-	4	-
$ClO + BrO \rightarrow Br + ClOO/OClO$	1	-	2	-
$ClNO_3 + HBr \rightarrow BrCl$	0	-	1	-
$IO + ClO \rightarrow I + Cl + O_2$/ $ICl + O_2$	0	-	0	-
Other chlorine O_x sinks	1	-	1	-
Total chlorine O_x sinks	15	-	23	-
Other O_x sinks	101	151	184	172
Total chem. O_x sinks (LO_x)	3299	3240	4933	4829
O_3 PO_x-LO_x (Tg yr^{-1})	42	161	443	602
O_3 Dry deposition (Tg yr^{-1})	545	659	832	980
O_3 Lifetime (days)	25	28	22	26
O_3 STE (PO_x-LO_x-Dry dep.) (Tg yr^{-1})	503	498	389	378

Chapter 6

Global modelling of tropospheric iodine aerosol

The content of this chapter is in review as "Global modelling of tropospheric iodine aerosol"' T. Sherwen, M. J. Evans, D. V. Spracklen, L. J. Carpenter, R. Chance, A. R. Baker, J. A. Schmidt, and T. J. Breider, *Geophys. Res. Letts.*, in review. 2016.

6.1 Introduction

Atmospheric aerosols are important for climate as they scatter solar radiation and change cloud properties, with secondary aerosols playing a significant role (Stocker et al., 2000). Anthropogenic activities have changed their global distribution and abundance, but to understand the impact of these aerosols both natural and anthropogenic sources need to be well understood (Carslaw et al., 2013). The oceans cover most of the planet and for the last four decades the most important oceanic secondary source of aerosols has been thought to be the emission of dimethyl sulfide (DMS) and its oxidation to H_2SO_4 (Lovelock et al., 1972; Fitzgerald, 1991). Recent evidence for significant emissions of iodine from the ocean (Carpenter et al., 2013; MacDonald et al., 2014), coupled to previous coastal studies of iodine aerosol production (O'Dowd et al., 2002), suggests the potential for an additional ocean aerosol source from iodine.

The presence of iodine in both the gas and aerosol phase in the marine boundary layer (MBL) has been established over the last few decades (Saiz-Lopez et al., 2012b). Oceanic emissions of methyl iodide was considered the dominant source for many years, but studies have shown that emission of other iodinated hydrocarbons from the open and coastal ocean play an important role (Jones et al., 2010; Saiz-Lopez et al., 2012b). More recently, inorganic iodine compounds (I_2, HOI) produced in the ocean surface layer from the reaction of O_3 with iodide are thought to be the dominant global source of iodine (Carpenter et al., 2013). Observations, box modelling and global model studies (Saiz-Lopez and von Glasow, 2012; Saiz-Lopez et al., 2014) in coastal and remote sites together with Chapters II-IV have shown the ability of iodine to impact the concentration of O_3 and oxidants. Similar studies in coastal and polar sites have shown that gas phase iodine compounds can form low volatile gas phase products which can both condense onto pre-existing aerosol and nucleate to form new particles (O'Dowd et al., 2002; Allan et al., 2015; Roscoe et al., 2015; Sellegri et al., 2016). Open-ocean observations are sparse but suggest iodine aerosol concentrations in the range of 0.1-17 ng (I) m^{-3} (Baker, 2004, 2005; Gilfedder et al., 2010; Lai et al., 2008; Rancher and Kritz, 1980). Aerosol iodine is composed of both inorganic and organic forms (Baker, 2004) with a complex aerosol phase chemistry (Pechtl et al., 2007). It is believed that iodine higher oxides (I_xO_y) formed through the self-reaction of iodine oxides (IO and OIO), and hydroiodic acid (HI) are the gas phase condensables

predominantly responsible for production of the iodine aerosol (Saiz-Lopez et al., 2012b).

Recent advances in the representation of iodine in global chemical transport models (Saiz-Lopez et al., 2012a, 2014) and this thesis allows us, for the first time, to simulate the global distribution of iodine aerosol. A simulation is described here of tropospheric iodine aerosol within the GEOS-Chem chemical transport model, the calculated iodine masses are compared against observations and then the impact of this source of secondary aerosol is evaluated for the present-day and pre-industrial.

6.2 Model setup

This chapter uses GEOS-Chem (www.geos-chem.org) version v10 at 4^ox5^o resolution with a coupled halogen chemistry scheme as described in Chapter IV/Sherwen et al. (2016b). For the work in this chapter we run a simulation in the present-day, and also in the preindustrial as described below and in Chapter V. For the present-day the model is run for two years (2004 and 2005) ignoring the first year as "spin-up" and using the final year for analysis.

As described in Chapter IV, the simulated global iodine emission in the present-day is calculated to be 2.75 Tg (I) yr^{-1} (2.2 Tg (I) yr^{-1} from inorganic species (I_2, HOI) and 0.6 Tg (I) yr^{-1} from organic species) consistent with previous studies (Saiz-Lopez et al., 2014). Although iodine emissions are, on a per area basis, highest in coastal waters, the tropical open-ocean is so large it dominates the total global emission (Fig. 6.1). These emissions rapidly photolyse, leading to a complex gas phase chemistry (Saiz-Lopez et al., 2012b) and ultimately the production of iodine aerosol.

The three iodine aerosol tracers are considered based on the uptake of gas phase iodine species onto coarse and accumulation mode sea-salt aerosol and onto sulfate aerosol. The uptake of iodine species (HI, HOI, INO_2, INO_3, I_2O_2, I_2O_3, I_2O_4) to these aerosols can lead to the iodine being permanently deposited onto that aerosol depending upon species, the aerosol type and its pH (see Appendix Table A.5 and Sect. A.0.1 for details). The physical properties of the iodine aerosol tracers are assumed to be the same as its parent aerosol as previously described (Alexander et al., 2012; Jaeglé et al., 2011). The nucleation of new iodine aerosol particles is not considered. Significant uncertainty exists as to the

molecular state of the iodine in aerosol, with iodide, iodate and organic aerosol all being present (Baker, 2004, 2005). For simplicity, and for comparison with observational data, the modelled iodine aerosol is considered to be iodide (I^-) and all comparisons are therefore in ng (I) m^{-3}.

Oceanic secondary aerosol processes in the model are described in Park et al. (2004) and Alexander (2005). In the GEOS-Chem version used here (v10), DMS emissions are calculated from an ocean water climatology (Kettle et al., 1999) and a transfer velocity (Liss and Merlivat, 1986). This amounts to 16.6 Tg (S) yr^{-1} (21 % of the global sulfur emission of 78.8 Tg (S) yr^{-1} in the model). This is around six times the oceanic iodine emission of 2.75 Tg (I) yr^{-1}. Iodine and DMS emissions are essentially uncorrelated due to their differing sources (see Fig. 6.1). DMS contribution to total aerosol sulfate is estimated through a perturbation experiment. Assuming a linear model response, this allows determination the fraction of the sulfate that is due to DMS within the simulation. Globally, a 10 % increase in DMS emissions leads to a 2.17 % increase in sulfate deposition. From scaling the attributable deposition it is possible to conclude that 22 % of the global burden of sulfate comes from DMS, consistent with previous work (Rap et al., 2013) and a DMS to sulfate conversion efficiency of 19.5 %.

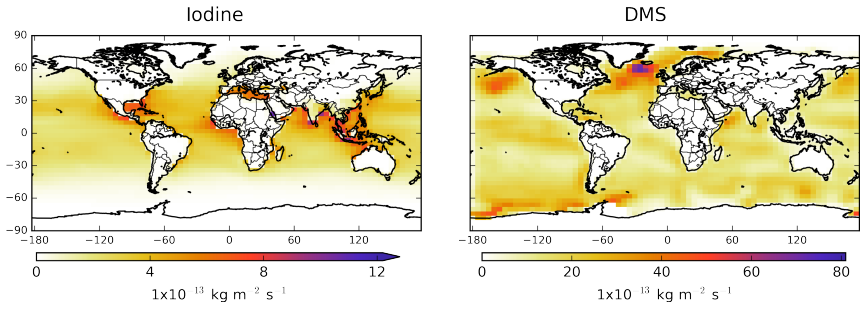

Figure 6.1 – Annual mean surface fluxes for iodine precursors and DMS in kg m^{-2} s^{-1}.

To probe the possible changes of iodine aerosol between pre-industrial and the present-day, the model was also run with pre-industrial emissions as described in Parrella et al. (2012) and in Chapter V. Anthropogenic emissions of O_3 precursors are switched off and natural emissions maintained at their present-day values. Biomass burning emissions are scaled to 10 % of the present-day (Wang and Jacob, 1998). Natural sources of sulfur from DMS and volcanos are unchanged but anthropogenic sourced sulfur emissions are switched off. Emissions of iodinated hydrocarbons are unchanged (they are presumed

entirely natural). Ocean iodide concentrations are unchanged but the O_3 dependence of the emissions parameterisation allows inorganic iodine emissions to change.

6.3 Results

6.3.1 Present-day iodine aerosol

The model's ability to simulate surface and vertical iodine oxide (IO) concentrations has previously been assessed against observations in Chapter IV. The self reactions of IO and OIO lead to the production of higher iodine oxides (O'Dowd et al., 2002; Saiz-Lopez et al., 2012b), which together with uptake of HI (see Section 6.2) and other iodine compounds cause increases in iodine aerosol mass. The surface concentrations of key gas phase iodine species are shown in Figure 6.2, which highlights the tropical nature of the emissions and the strong link of the inorganic iodine source to pollution. Iodine aerosol surface mass concentrations are calculated in the range 0.01 to 90 ng (I) m^{-3} in the monthly means with annual means of 0.01-31 ng (I) m^{-3} (Fig. 6.6, with monthly values given in 6.3).

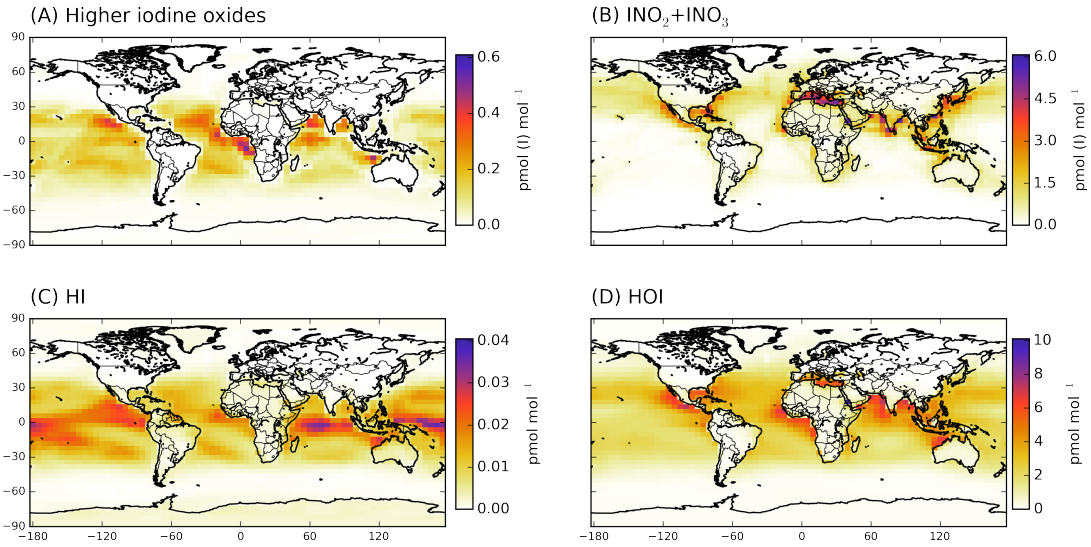

Figure 6.2 – Simulated annual averaged surface concentrations of iodine aerosol precursor species (pmol (I) mol^{-1}). (a) higher iodine oxides (I_2O_X), (b) INO_2 and INO_3 (c) HI (d) HOI

Iodine aerosol is primarily located in the tropics (See monthly spatial plots in Fig. 6.3), where the emission sources are largest (Fig. 6.1), with tropical marine boundary layer concentrations of at least 2.6 ng (I) m^{-3} in the annual mean. Highest concentrations

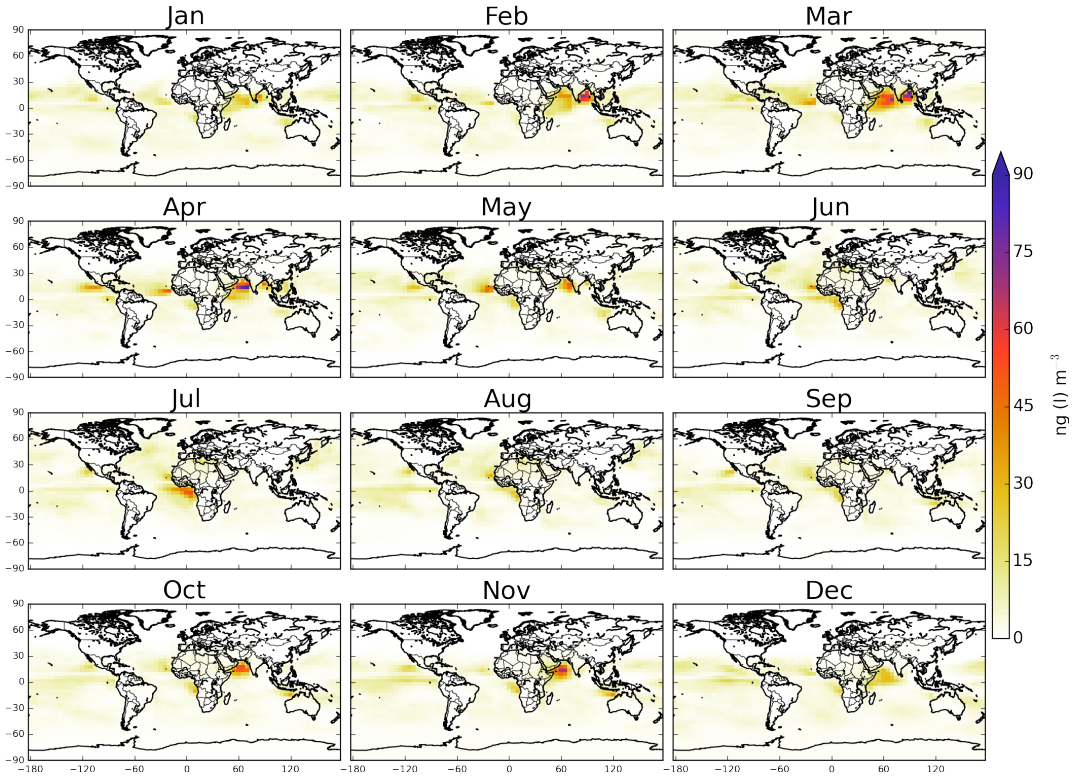

Figure 6.3 – Monthly modelled iodine surface aerosol field in ng (I) m^{-3}

are found within the Arabian Sea, the Bay of Bengal and off the Atlantic coast of central Africa. Concentrations fall off rapidly with altitude (Fig. 6.9). In the northern hemisphere marine boundary layer, the iodine aerosol mass is mostly found on sulfate aerosol (71 %). However, in the southern hemisphere marine boundary layer, where sulfate concentrations are lower, less of the iodine aerosol is found on sulfate (59 %). This is shown spatially in Figures 6.9 and 6.5. The modelled global annual mean iodine aerosol burden is 2.5 Gg (I), with 2.0 Gg (I) in the marine boundary layer, and a globally averaged conversion efficiency of iodine emission into aerosol of 15.3 %.

6.3.2 Observational comparisons

Iodine aerosol observations are sparse, however comparisons to the available observations of open-ocean iodine aerosol are shown in Fig. 6.6 and Table 6.1. The model calculated iodine aerosol mass concentrations are extracted from the model for the month and region of the observation (Fig. 6.6(top)). Due to the scarcity of marine aerosol iodine observations, total soluble iodine data from cruise "M55" (Baker, 2004) is included alongside other

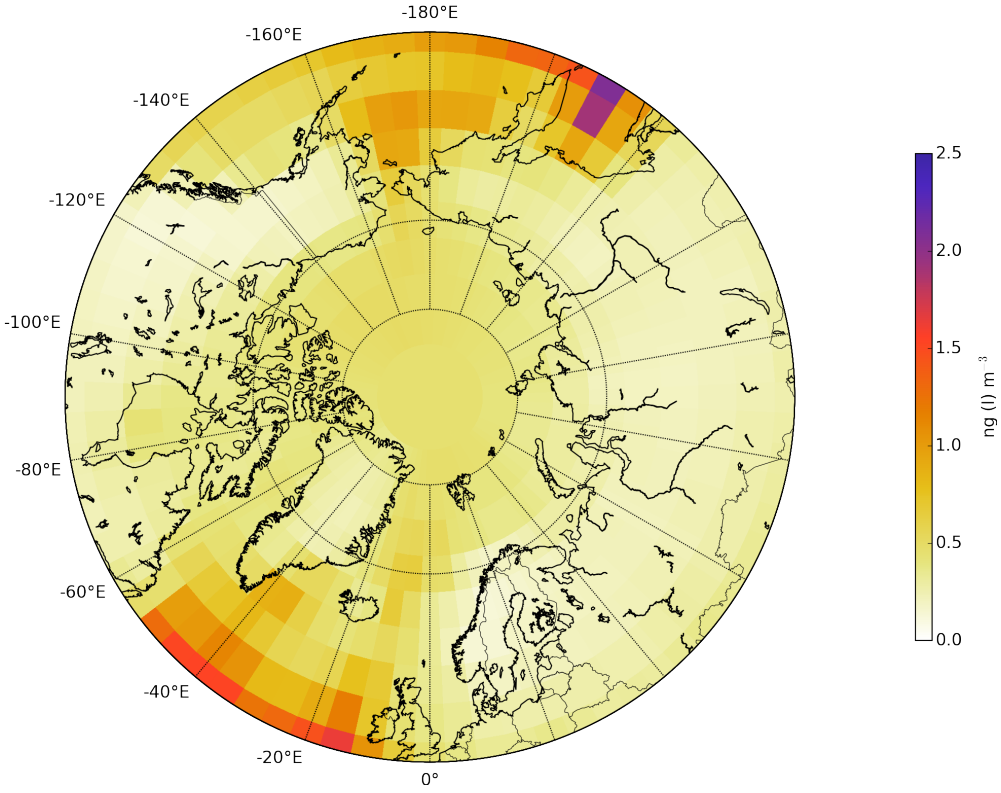

Figure 6.4 – Global annual zonal distribution of iodine aerosol species in ng (I) m^{-3} (left) and their % contribution to total iodine aerosol (right). Iodine aerosol tracers are defined based on the parent species on which uptake occurs. Iodine on coarse mode sea-salt aerosol, accumulation mode sea-salt aerosol, and on sulfate aerosol are referred to as: "I on SS coar.", "I on SS accm." and "I on SO_4", respectively.

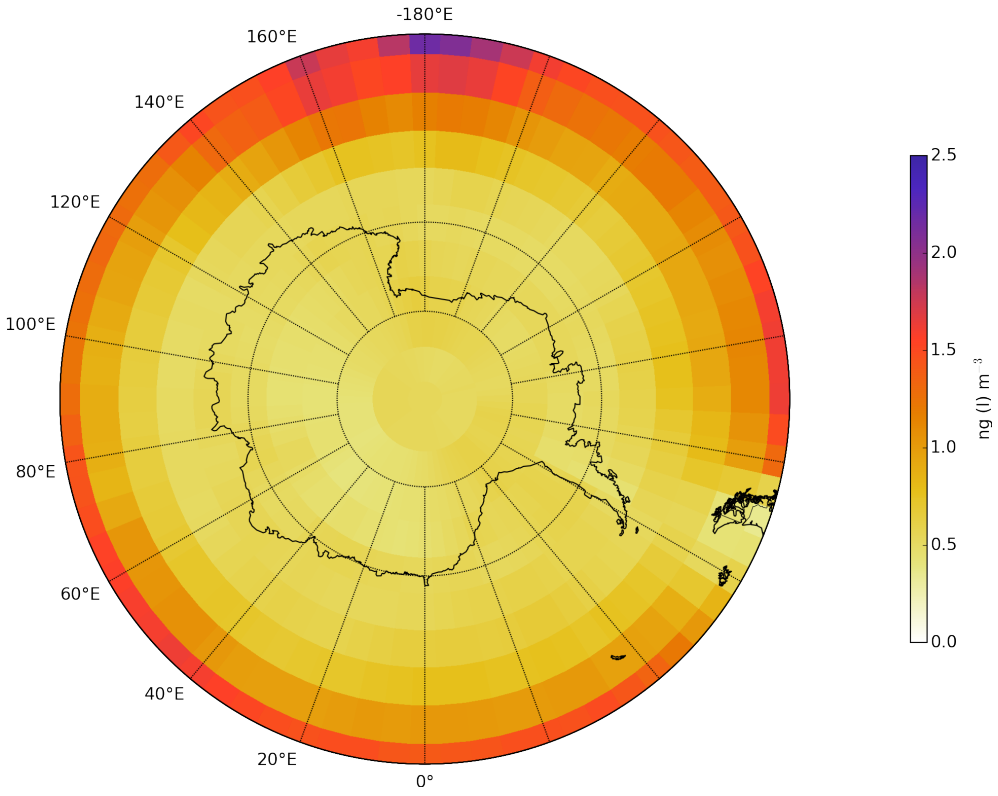

Figure 6.5 – Global annual surface distribution of iodine aerosol species in ng (I) m^{-3} (left) and their % contribution to total iodine aerosol. Iodine on coarse mode sea-salt aerosol, accumulation mode sea-salt aerosol, and on sulfate aerosol are referred to as: "I on SS coar.", "I on SS accm." and "I on SO_4", respectively.

total iodine concentrations in the comparison.

In addition to published datasets, three new datasets ("D325", "D357" and "D361" cruises) are used in this Chapter (see Table 6.1). These were collected from previously reported campaigns using established techniques, but have not been explicitly described in the literature.

Details of the aerosol sampling during cruise D325 ("INSPIRE") are given in Powell et al. (2015) and Gilfedder et al. (2010). Total iodine was determined in these samples using Thermal Extraction and Spectrophotometric Detection (TESI; Gilfedder et al. 2010), and a subset of the data reported here is included in that publication.

For cruise "D357" (Geotraces GA10) the aerosol sampling is described in Chance et al. (2015), and for cruise "D361" (Geotraces GA06) in Powell et al. (2015). The total iodine values reported (see Table 6.1) were determined using instrumental neutron activation analysis (INAA) conducted at the SLOWPOKE nuclear reactor, École Polytechnique, Montreal, Canada.

Although there is a degree of scatter, the model appears broadly consistent with the observations with some indication of a model over-estimate. The observations are not in the regions where the model predicts its highest concentrations ("Arabian Sea") and further observations in these regions would be very useful. It is therefore possible to conclude that given the current observational dataset, and the significant uncertainties in the modelled chemistry and aerosol processes (Chapter III/Sherwen et al. 2016a; Sommariva et al. 2012) the model provides a useful simulation of iodine aerosol.

6.3.3 Comparisons with other secondary aerosol sources

In order to place the calculated iodine aerosol mass into a wider context it is compared here to the calculated sulfate aerosol. For consistency the sulfate aerosol is considered in the same elemental terms as was used for iodine aerosol (ng (S) m^{-3}). Figure 6.7 shows the annual mean surface concentrations of the sulfate (total and from DMS) and their mass (I/S) ratio compared to the iodine aerosol. A zonal comparison is shown in Fig. 6.8. Highest total sulfate aerosol is found over SE Asia, Europe and North America where the anthropogenic source is highest. These concentrations rapidly decay away from the

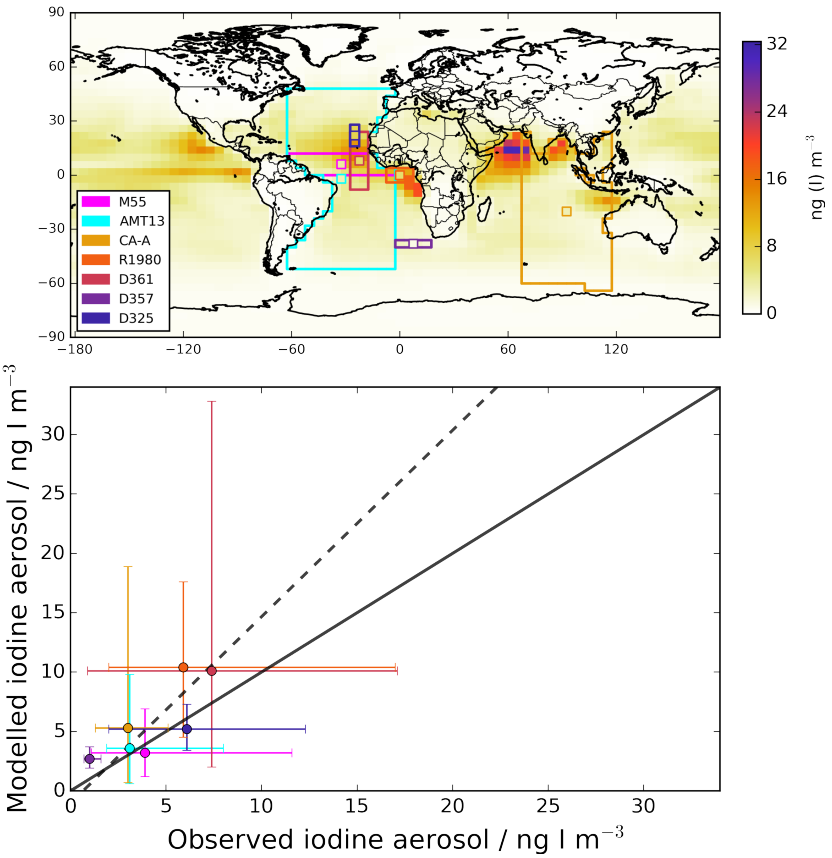

Figure 6.6 – Simulated and observed surface iodine aerosol. Background of the upper plot is the modelled annual mean surface aerosol mass concentrations (ng (I) m^{-3}). Observations (small coloured squares) indicate the average value reported by individual studies (Baker, 2004, 2005; Gilfedder et al., 2010; Lai et al., 2008; Rancher and Kritz, 1980) and datasets "D325", "D357", and "D361" are described in the supplementary material. The small coloured square is located at the centre of the domain (large coloured region). Lower plot shows the observed mean values with the error bar representing the reported maximum and minimum. Each modelled point represents the mean value in the region shown in the top plot with the error bar representing the 5^{th} and 95^{th} percentile of the distribution in that region. The colors of the points are the same as the areas on the map. The continuous black line is the 1:1 line, and the dashed line is the orthogonal linear regression best fit.

Table 6.1 – Comparison between measured and modelled iodine aerosol mass concentrations for open-ocean observations. Observed values are taken from observations presented in paper. Model is sampled over the domains shown in main text Figure 6.6(top) for the month(s) of the observations.

Cruise	Location	Observed aerosol iodine min-**mean**-max ng (I) m^{-3}	Modelled aerosol iodine 5^{th} %-**mean**-95^{th} % ng (I) m^{-3}
M55 (*)	North Atlantic	1.1-**3.9**-11.6	1.2-**3.2**-6.9
AMT13(*)	Atlantic	1.9-**3.1**-8.0	0.6-**3.6**-9.8
CA-A (+)	Western Pacific	1.3-**3.0**-5.1	0.7-**5.3**-18.9
R1980 (+)	Equatorial Atlantic	2.0-**5.9**-17.0	4.5-**10.4**-17.6
D361 (+)	Tropical Atlantic	0.9-**7.4**-17.1	2.0-**10.1**-32.8
D357 (+)	South-East Atlantic	0.7-**1.0**-1.6	1.9-**2.7**-3.7
D325 (+)	Tropical East Atlantic	2.0-**6.1**-12.3	3.4-**5.2**-7.3

sources. Over the ocean, total sulfate concentrations become much smaller (29-452 ng (S) m^{-3} 5^{th} to 95^{th} percentiles of annual mean). Highest DMS sulfate (up to 204 ng (S) m^{-3}) occurs where the DMS emissions are highest over the northern extra-tropical oceans (Fig. 6.1), but generally concentrations are in the range 14-78 ng (S) m^{-3} (5^{th} to 95^{th} percentiles of annual mean).

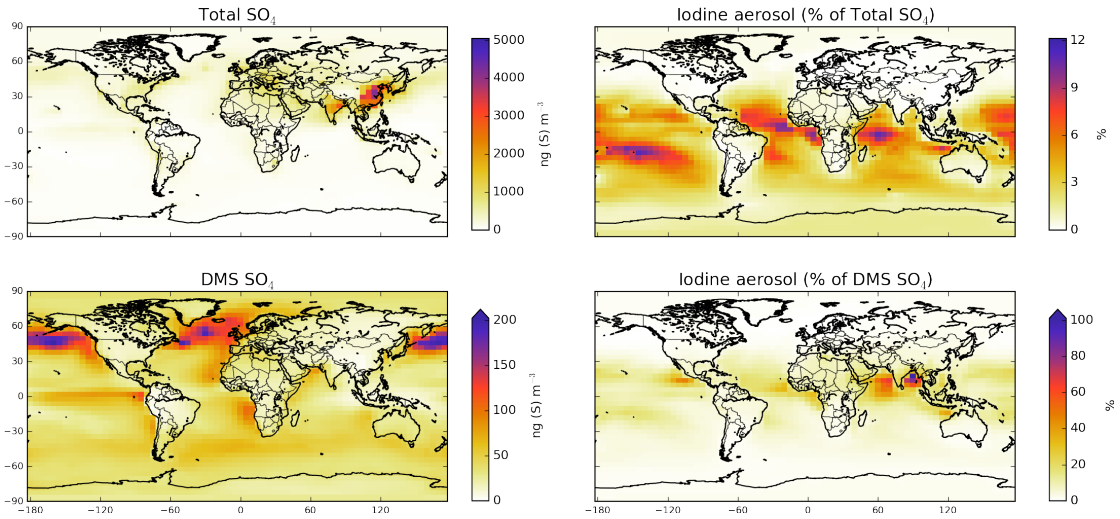

Figure 6.7 – Annual average present-day modelled surface mass concentrations of total (upper left) and DMS (lower left) sourced SO_4^{2-} aerosol in ng S m^{-3} (left). Iodine mass fraction (ng (I) m^{-3}) as % of sulfate species is shown on the (right).

Compared to the total sulfate on an annual basis, iodine aerosol mass is small. Within the

marine boundary layer, the annually averaged iodine aerosol burden is 2.0 Gg (I) which can be compared to 270 Gg (S) for sulfate. Regionally this ratio typically lies between 0.3-5.6 % (5^{th} to 95^{th} percentiles) with a maximum of 11 % (Figure 6.7 and zonally in Fig. 6.8). Regions of the tropical marine boundary layer far from local anthropogenic or volcanic influences and with relatively low DMS emission ratio show the highest significance. This fraction can become as high as 35 % on a monthly basis in these regions. Outside the marine boundary layer (Fig. 6.8) iodine aerosol contributes negligible mass.

Sulfate from DMS is the primary oceanic secondary aerosol source. Compared to the DMS sulfate source, iodine plays a more significant role than it does to the total sulfate aerosol (Figure 6.7 and zonally in Fig. 6.8). Again the iodine aerosol burden of 2.0 Gg (I) in the marine boundary layer can be compared to the 67 Gg (S) due to DMS emissions. Annually this ratio lies in the range of 0.75 to 15 % (5^{th} to 95^{th} percentiles) over the tropical oceans with a maximum of 101 %. On a monthly basis this can increase to in excess of a factor of 4. The iodine to DMS sourced sulfate mass fraction is highest in regions of the tropical marine boundary layer where the iodine emissions are high and DMS emissions low (Indian ocean and the Pacific coast of Mexico). From an ocean-atmosphere perspective iodine thus appears to play a regionally important role in determining the secondary aerosol load of the marine boundary layer.

6.3.4 Pre-industrial concentrations

Understanding the aerosol distribution before human perturbation helps define the direct and indirect effects of aerosol. The simulation of the pre-industrial is described in Section 6.2. Lower O_3 concentrations are found (globally averaged 28 % and 38 % in the marine boundary layer) in the pre-industrial, consistent with previous studies (Lamarque et al., 2010; Parrella et al., 2012). This lower O_3 leads to a reduction in the inorganic ocean iodine source of 42 % to 1.25 Tg (I) yr^{-1}. This is higher than the reduction in marine boundary layer O_3 as the largest reduction in O_3 occurs in the tropics where most of the inorganic iodine emissions occur. Total iodine emissions thus reduces 33 % to 1.84 Tg (I) yr^{-1}. The iodine processing in the atmosphere changes significantly in the pre-industrial, with the lower NO_x concentrations lengthening the I_y lifetime due to reduced $IONO_2$ hydrolysis. Thus, the iodine aerosol burdens only reduces by 23 % from the present-day. Figure 6.9 shows the pre-industrial iodine mass concentrations as a fraction of the pre-industrial total

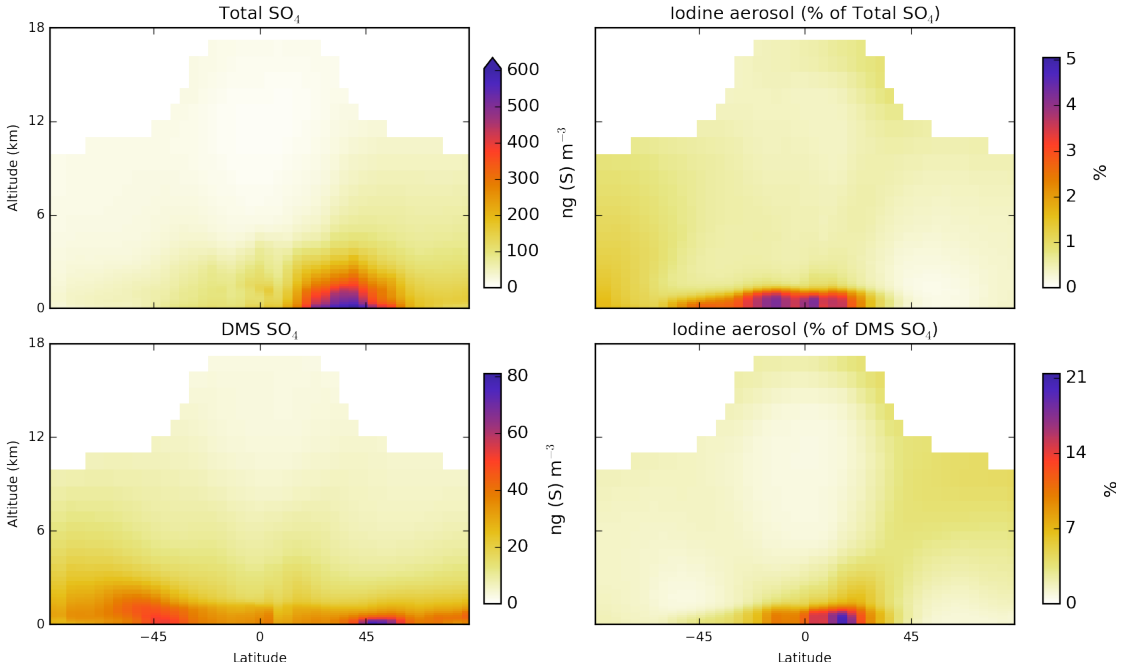

Figure 6.8 – Annual average present-day modelled zonal mass concentrations of total (top) and DMS (bottom) sourced SO_4 aerosol, and iodine mass fraction (ng (I) m^{-3}) as % of aerosol species (right). Species shown are total sulfate aerosol (top) and DMS sourced sulfate aerosol (bottom). Fractional amount of iodine aerosol is shown as % and is calculated as ([iodine aerosol]/[X]*100)

sulfate mass concentration. The reduction in the anthropogenic sulfur emissions, leads to iodine aerosol being a larger fraction of the total sulfate in the pre-industrial. The global iodine burden of 1.6 Gg (I) in the marine boundary layer compares to a total sulfate burden of 181 Gg (S). Spatially, iodine aerosol within the atmosphere above the tropical ocean surface can be up to 21 % (0.2-6.8 %, 5^{th} to 95^{th} percentiles) of the total sulfate mass on an annual basis, with some locations showing iodine aerosol mass being ∼50 % of the sulfate mass in some months. Thus iodine aerosol may have played an important regional role in determining the pre-industrial marine boundary layer aerosol load.

6.4 Implications and conclusions

The size distribution, optical and cloud condensation properties of iodine aerosol are unknown or uncertain, which makes investigating the aerosol radiative impacts difficult. However studies of aerosol optical depth (AOD) have identified model underestimates compared to satellite observations in marine locations such as the Indian Ocean, Oceania

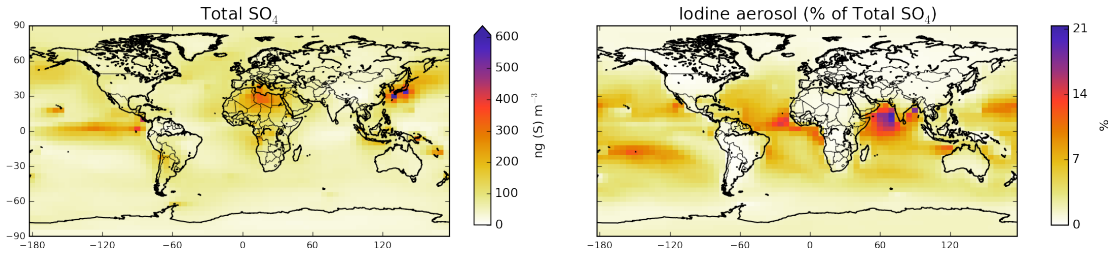

Figure 6.9 – Annual average pre-industrial modelled surface mass concentrations of total sulfate (ng S m^{-3}, left) and the mass of iodine aerosol (ng (I) m^{-3}) as a fraction of this (right).

and the Gulf of Guinea where the highest iodine aerosol mass concentrations are predicted (Lapina et al., 2011). An additional source of aerosol in those regions may help to reconcile observations with models. There is also strong evidence to support the nucleation of new particles from iodine (O'Dowd et al., 2002; Allan et al., 2015; Roscoe et al., 2015; Sellegri et al., 2016). For regions where nucleation due to sulfur compounds is slow, iodine may be an important source of new particles.

There are still significant uncertainties in the magnitude and impacts of the ocean-atmosphere cycling of iodine. However, it would appear from these calculations that iodine aerosol may play an important regional role in determining the aerosol load of the remote tropical ocean both in the present and in the pre-industrial. Further observations in these regions would help us to constrain the magnitude of this role.

Chapter 7

Summary and future perspectives

7.1 Summary of results

This thesis has implemented and assessed a new simulation of tropospheric halogen chemistry within the GEOS-Chem framework. It has investigated the impact of halogens on key components of the gas-phase atmospheric system, on O_3 radiative forcing and on a new source of aerosol. Chapters II-IV presented simulations of the present day gas-phase atmosphere, with Chapters II and III focusing on iodine chemistry and Chapter IV focusing on the wider halogen (Cl, Br, I) system. Chapter V describes the impact of halogens on O_3 radiative forcing and Chapter VI describes simulations of iodine aerosol. The iodine part of "coupled" halogen simulation ("Cl+Br+I") is schematically summarised in Figure 7.1.

Throughout these chapters there has been an emphasis of comparing model predictions to the available observational dataset. The obvious assessment is against the concentration of reactive halogen species in the atmosphere. However, these observations are sparse. The model appears though to do a reasonable job as is discussed in Chapter IV. The comparison with the available iodine aerosol species (Chapter VI, Fig. 6.6) is surprisingly good but further detailed evaluations of pre-existing datasets are required here together with the collection of new datasets.

Larger observational datasets are available for species such as O_3. Arguably the O_3 simulation is not degraded in GEOS-Chem v9-2 on inclusion of halogens ("Br+I"), and GEOS-Chem v10 is improved on inclusion of halogens ("Cl+Br+I"). The daily loss cycle in the remote marine atmosphere is clearly improved on inclusion of halogens (Chapter III, Fig. 3.18). It can be argued that the new implementation of halogens ("Cl+Br+I") in GEOS-Chem therefore as whole improves the simulation of O_3 and reproduction of observed processing.

Chapter V shows the impact of halogens on the change in the composition of the atmosphere between the pre-industrial and the present day. There are various factors at play here, ranging from the increase in ocean inorganic iodine emissions due to increase present day O_3 concentrations, through to the increased flux of inorganic halogens from the stratosphere in the present day, and the increased concentration of halocarbons in the present day. All of which increase the halogen chemistry in the present day over that

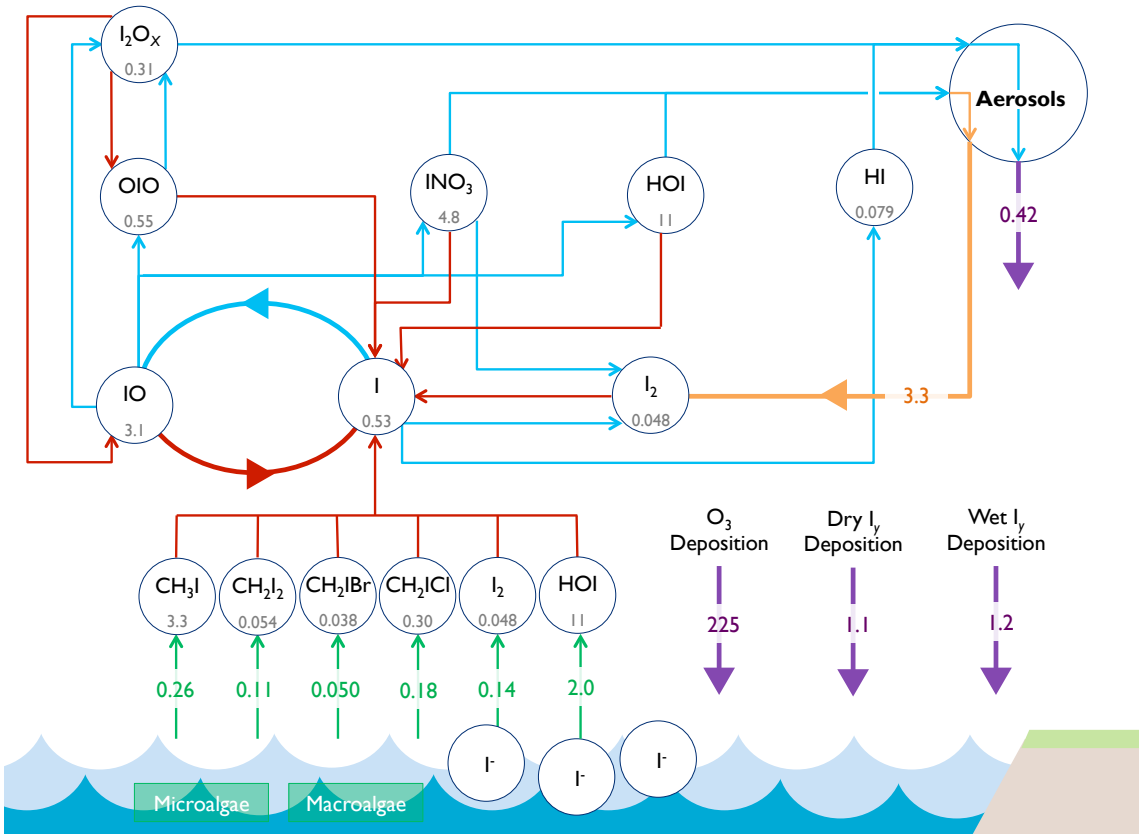

Figure 7.1 – Schematic representation of implemented iodine chemistry in the simulation presented in chapter IV ("Cl+Br+I"). Average global annual mean burdens (Gg I) are shown below key I_y species, with fluxes (Tg (I) yr^{-1}) shown on arrows. Red lines=photolysis, blue=chemical pathways, green lines=emission source, orange lines = heterogeneous pathway, and purple lines=depositional pathway. This equates to a total iodine source and sink of 2.8 Tg (I) yr^{-1}. Oceanic O_3 deposition in Tg is also shown to illustrate the driving force behind the inorganic emissions.

in the preindustrial. This leads to an enhanced halogen driven O_3 loss chemistry in the present day over that in the pre-industrial which in turn reduces the O_3 radiative forcing by ∼20 %.

Chapter VI describes the production of aerosol from iodine chemistry. The simulation compares well with the limited observational dataset. To gain a window into the significance of iodine aerosol, comparisons are made against other secondary aerosol present in the marine boundary layer. Compared to sulfate the modelled masses are small, but iodine aerosol is more significant compared to DMS sourced sulfate (3 % of the MBL burden, up to 101 % regionally). Due to changes in composition in the preindustrial (e.g. anthropogenic sulfur aerosol) and the reduced iodine flux (explored in Chapter V), iodine aerosol's loading and relative contribution to aerosol mass also changes. In the pre-industrial, iodine aerosol makes up 0.88 % of the MBL burden sulfate mass and regionally up to 21 %. It is therefore shown that iodine aerosol may be an important regional mechanism for ocean-atmosphere interaction.

Overall this thesis shows that the prevailing wisdom that tropospheric halogen chemistry is at best of regionally importance is false. Tropospheric halogen chemistry has a profound impact on the composition of the troposphere and needs to be considered in future work.

7.2 Outlook to future work on halogen modelling

Here I describe a few potentially key topics that should be investigated further to better constrain our understanding of halogen chemistry.

7.2.1 Ocean-atmosphere parameterisation

The current parameterisations for inorganic iodine emissions from the ocean and O_3 deposition to the ocean are unconnected. Much of the O_3 deposition to the ocean is due to its reaction with iodine in surface water, with iodine's enhancement of physical deposition estimated to be up to ∼100 % (Chang et al., 2004), and with much of the remainder due to its reaction with dissolved organic material and other ions (e.g. Bromide). Better coupling of O_3 deposition and the iodine emissions would be beneficial. Our work here

estimates that atmospheric iodine leads to ∼600 Tg yr^{-1} loss of O_3 in the troposphere. Roughly 80 % of this number coming from the oceanic emission of inorganic iodine. Here a surface deposition of 832 Tg yr^{-1} is simulated. Oceans contribute around 30 % of the total deposition (Hardacre et al., 2015) and if we assume ∼50 % of this loss comes from iodine, then iodine could represents a significant proportion of the total loss of O_3 in the oceans. Thus overall it can be estimated that ∼700 Tg yr^{-1} of O_3 loss is linked to the concentration of iodide in the ocean. This assessment is obviously rough. A better representation of O_3 sinks and subsequent chemistry in the ocean would obviously help to better define this number. However, it is a significant number and represents a key ocean-atmosphere interaction which up to this point has been studied very little.

Central to this process though is our understanding of the concentration of surface iodide in the ocean. Two parameterisations exist for this, Chance et al. (2014) and MacDonald et al. (2014). The former was used in chapter II and III, and the later has been used elsewhere in the literature, Saiz-Lopez et al. (2014) and in Chapter IV, V and VI as it gives a better comparison with gas-phase iodine observations. However, MacDonald et al. (2014) only uses a subset (Atlantic) of the data from Chance et al. (2014) so it is not possible to say whether its ability to reproduce the limited number of gas-phase iodine oxide observations is due to a better estimate of the flux or due to an error elsewhere in the iodine parameterisation. There is therefore a need to re-visit the parameterisation and consider new methodologies for processing the available datasets of iodide observations into a global dataset.

7.2.2 Impacts on air-quality

Halogens are likely to have an impact on air-quality. Previous studies have shown that the production of $ClNO_2$ from the uptake of N_2O_5 onto sea-salt can enhance O_3 production (Faxon et al., 2015; Simon et al., 2009; Sarwar et al., 2014). This impact can be seen where very high concentrations of Cl_y are simulated over Europe, and off the coasts of Asia and North America (in Chapter IV Figure 4.3). The production of $ClNO_2$ and its photolysis leads to the production of Cl radicals which oxidize VOCs and so enhance the production of the RO_2 radicals necessary for O_3 production. Halogens likely have other impacts. Overall NO_x concentrations are reduced by halogens (see Chapter IV Figures 4.18 and 4.19) which will tend to reduce O_3 concentrations. Impacts on aerosols are minor

in polluted regions. However there is a large impact on background O_3. This is the O_3 entering a region such as Europe or North America and this represents the inflow of O_3 before regional emissions controls take effect. These background O_3 values are used in considering what concentration of O_3 should be considered an air-quality violation. This is significantly reduced by the presence of halogens (around 8ppb for both Mace Head in the Republic of Ireland, and, Trinidad head in California). Thus from a policy perspective there appears to be a potential for halogen chemistry in defining background O_3.

7.2.3 Stratospheric role of iodine

There was a suggestion in the mid 1990s that iodine could significantly contribute to stratospheric O_3 depletion (Solomon et al., 1994). Following this it has generally been thought that iodine would not reach the stratosphere in significant concentrations due to its short lifetime in the troposphere. However more recently observations and modelling have suggested that this is probably not the case (Saiz-Lopez et al., 2015). The GEOS-Chem version model used here solely considers chemistry within the troposphere. However work has been completed that combines tropospheric and stratospheric chemistry schemes (Eastham et al., 2014). It would be relatively easy to add the iodine chemistry to produce a "whole atmosphere" chemistry which could be used to investigate the impact of iodine on the chemistry of the stratosphere.

7.3 Final thoughts

The basis for all of the modelling is our understanding of the fundamental chemical and physical properties. Without a strong constraints on these values the modelling is fundamentally limited. Notable uncertainties lie in the heterogeneous halogen chemistry and these limit the ability to model the complex and coupled aerosol-phase chemistry. It is clear that the interplay between halogen gas- and aerosol- phase chemistry is significant (Sommariva and von Glasow, 2012; Chen et al., 2016; Schmidt et al., 2016). For the science of halogens to move further laboratory work is need to elucidate key parameters to allow for improved process-based modelling and for this modelling to reduce the heterogeneous chemistry to a form that can be used with global chemistry models without huge

computational cost. Of particular note for laboratory focus are uptake coefficients and Henry's law values for iodine species. Without an improved fundamental chemical basis the modelling described here may well be based on a foundation of sand.

Appendix A

Full implemented halogen mechanism

Here is described the full halogen chemistry scheme as presented here and in previous work (Bell et al., 2002; Eastham et al., 2014; Parrella et al., 2012; Schmidt et al., 2016; Sherwen et al., 2016a) and with updates as detailed in section 4.2 and Table 4.1. The complete gas phase photolysis, bimolecular and termolecular reactions are described in Tables A.4,A.1, and A.3, respectively.

The description of Heterogeneous phase chemistry was written by Dr. Johan A. Schmidt.

A.0.1 Heterogeneous reactions

The halogen multiphase chemistry mechanism is based on the iodine mechanism ("Br+I") described in Sherwen et al. (2016a) and the coupled mechanism of Schmidt et al. (2016). The Heterogeneous reactions in the scheme are shown in Table A.5 and with further detail individual detail on certain reactions below.

A.0.2 Aerosols

Here reactions of halogen are considered on sulfate aerosols, sea salt aerosols, and liquid and ice cloud droplets. The implementation of sulfate type aerosols in GEOS-Chem is

Table A.1 – Bimolecular halogen reactions included in scheme. This includes reactions from previous updates to descriptions of halogen chemistry in GEOS-Chem (Parrella et al. (2012); Eastham et al. (2014); Schmidt et al. (2016); Sherwen et al. (2016a)), and those described in Section 4.2. These are given in the Arrhenius form with the rate equal to $A \cdot \exp\left(\frac{-Ea}{RT}\right)$. Unknown values are represented by a dash and these set to zero in the model, reducing the exponent to 1. The bi-molecular reactions with an M above the arrow represent termolecular reactions where the pressure dependence is not known or are uni-molecular decomposition reactions. Abbreviations for tracers are expanded in footnote 3.

Rxn ID	Reaction	A	$-Ea/R$	Citation
		$cm^3 molecules^{-1}\ s^{-1}$	K	
M1	$I + O_3 \rightarrow IO + O_2$	$2.10x10^{-11}$	-830	Atkinson et al. (2007)
M2	$I + HO_2 \rightarrow HI + O_2$	$1.50x10^{-11}$	-1090	Sander et al. (2011)
M3	$I_2 + OH \rightarrow HOI + I$	$2.10x10^{-10}$	–	Atkinson et al. (2007)
M4	$HI + OH \rightarrow I + H_2O$	$1.60x10^{-11}$	440	Atkinson et al. (2007)
M5	$HOI + OH \rightarrow IO + H_2O$	$5.00x10^{-12}$	–	Riffault et al. (2005)
M6	$IO + HO_2 \rightarrow HOI + O_2$	$1.40x10^{-11}$	540	Atkinson et al. (2007)
M7	$IO + NO \rightarrow I + NO_2$	$7.15x10^{-12}$	300	Atkinson et al. (2007)
M8	$HO + CH_3I \rightarrow H_2O + I$	$4.30x10^{-12}$	-1120	Atkinson et al. (2008)
M9	$INO + INO \rightarrow I_2 + 2NO$	$8.40x10^{-11}$	-2620	Atkinson et al. (2007)
M10	$INO_2 + INO_2 \rightarrow I_2 + 2NO_2$	$4.70x10^{-12}$	-1670	Atkinson et al. (2007)
M11	$I_2 + NO_3 \rightarrow I + INO_3$	$1.50x10^{-12}$	–	Atkinson et al. (2007)
M12	$INO_3 + I \rightarrow I_2 + NO_3$	$9.10x10^{-11}$	-146	Kaltsoyannis and Plane (2008)
M13	$I + BrO \rightarrow IO + Br$	$1.20x10^{-11}$	–	Sander et al. (2011)
M14	$IO + Br \rightarrow I + BrO$	$2.70x10^{-11}$	–	Bedjanian et al. (1997)
M15	$IO + BrO \rightarrow Br + I + O_2$	$3.00x10^{-12}$	510	Atkinson et al. (2007)
M16	$IO + BrO \rightarrow Br + OIO$	$1.20x10^{-11}$	510	Atkinson et al. (2007)
M17	$OIO + OIO \rightarrow I_2O_4$	$1.50x10^{-10}$	–	Gómez Martín et al. (2007)
M18	$OIO + NO \rightarrow NO_2 + IO$	$1.10x10^{-12}$	542	Atkinson et al. (2007)
M19	$IO + IO \rightarrow I + OIO$	$2.16x10^{-11}$	180	Atkinson et al. (2007)
M20	$IO + IO \rightarrow I_2O_2$	$3.24x10^{-11}$	180	Atkinson et al. (2007)
M21	$IO + OIO \xrightarrow{M} I_2O_3$	$1.50x10^{-10}$	–	Gómez Martín et al. (2007)
M22	$I_2O_2 \xrightarrow{M} IO + IO$	$1.00x10^{12}$	-9770	Ordóñez et al. (2012)
M23	$I_2O_2 \xrightarrow{M} OIO + I$	$2.50x10^{14}$	-9770	Ordóñez et al. (2012)
M24	$I_2O_4 \xrightarrow{M} 2OIO$	$3.80x10^{-2}$	–	Kaltsoyannis and Plane (2008)
M25	$INO_2 \xrightarrow{M} I + NO_2$	$9.94x10^{17}$	-11859	(McFiggans et al., 2000)
M26	$INO_3 \xrightarrow{M} IO + NO_2$	$2.10x10^{15}$	-13670	Kaltsoyannis and Plane (2008)
M27	$IO + ClO \rightarrow I + OClO$	$2.59x10^{-12}$	280	Atkinson et al. (2007)
M28	$IO + ClO \rightarrow I + Cl + O_2$	$1.18x10^{-12}$	280	Atkinson et al. (2007)

Table A.2 – Continued Table A.1.

Rxn ID	Reaction	A	$-Ea/R$	Citation
		$cm^3 molecules^{-1}\ s^{-1}$	K	
M29	IO + ClO → ICl + O_2	$9.40x10^{-13}$	280	Atkinson et al. (2007)
M30	Cl + HCOOH → HCl + CO2 + H_2O	$2.00x10^{-13}$	-	Sander et al. (2011)
M31	Cl + CH_3O_2→ ClO + CH_2O + HO_2(⋆)	$1.60x10^{-10}$	-	Sander et al. (2011)
M32	Cl + CH_3OOH → HCl + CH_3O_2	$5.70x10^{-11}$	-	Sander et al. (2011)
M33	Cl + C_2H_6→ HCl + $C_2H_5O_2$	$7.20x10^{-11}$	-70	Sander et al. (2011)
M34	Cl + $C_2H_5O_2$=> ClO + HO_2+ ALD2 (⋆)	$7.40x10^{-11}$	-	Sander et al. (2011)
M35	Cl + EOH → HCl + ALD2 (◁)	$9.60x10^{-11}$	-	Sander et al. (2011)
M36	Cl + $CH_3C(O)OH$ → HCl + CH_3O_2, + CO2	$2.80x10^{-14}$	-	Sander et al. (2011)
M37	Cl + C_3H_8→ HCl + A3O2	$7.85x10^{-11}$	-80	Sander et al. (2011)
M38	Cl + C_3H_8 → HCl + B3O2	$6.54x10^{-11}$	-	Sander et al. (2011)
M39	Cl + ACET → HCl + ATO2	$7.70x10^{-11}$	-1000	Sander et al. (2011)
M40	Cl + ISOP → HCl + RIO2	$7.70x10^{-11}$	500	Sander et al. (2011)
M41	Cl + MOH → HCl + CH_2O + HO_2	$5.50x10^{-11}$	-	Sander et al. (2011)
M42	$CHBr_3$ + OH → 3Br + CO	$1.35x10^{-12}$	-600	Sander et al. (2011)
M43	CH_2Br_2 + OH → 2Br + CO	$2.00x10^{-12}$	-840	Sander et al. (2011)
M44	CH_3Br + OH → 3Br + CO	$2.35x10^{-12}$	-1300	Sander et al. (2011)
M45	Br + O_3 → BrO + O_2	$1.60x10^{-11}$	-780	Sander et al. (2011)
M46	Br + CH_2O → HO_2 + CO	$1.70x10^{-11}$	-800	Sander et al. (2011)
M47	Br + HO_2 → HBr + O_2	$4.80x10^{-12}$	-310	Sander et al. (2011)
M48	Br + CH_3CHO → $CH3CO_3$	$1.30x10^{-11}$	-360	Atkinson et al. (2007)
M49	Br + $(CH_3)_2CO$ → $CH3C(O)CH_2OO$	$1.66x10^{-10}$	-7000	King et al. (1970)
M50	Br + C_2H_6 → C2H5OO	$2.36x10^{-10}$	-6411	Seakins et al. (1992)
M51	Br + C_3H_8 → C3H7OO	$8.77x10^{-11}$	-4330	Seakins et al. (1992)
M52	Br + $BrNO_3$ → Br_2 + NO_3	$4.90x10^{-11}$	0	Orlando and Tyndall (1996)
M53	Br + NO_3 → BrO + NO_2	$1.60x10^{-11}$	0	Sander et al. (2011)
M54	HBr + OH → Br + H_2O	$5.50x10^{-12}$	200	Sander et al. (2011)
M55	BrO + NO → Br + NO_2	$8.80x10^{-12}$	260	Sander et al. (2011)
M56	BrO + OH → Br + HO_2	$1.70x10^{-11}$	250	Sander et al. (2011)
M57	BrO + BrO → 2Br + O_2	$2.40x10^{-12}$	40	Sander et al. (2011)
M58	BrO + BrO → Br_2 + O_2	$2.80x10^{-14}$	860	Sander et al. (2011)
M59	BrO + HO_2 → HOBr + O_2	$4.50x10^{-12}$	460	Sander et al. (2011)
M60	Br_2 + OH → HOBr + Br	$2.10x10^{-11}$	240	Sander et al. (2011)
M61	Cl + ALK4 → HCl + R4O2	$2.05x10^{-10}$	-	Atkinson et al. (2006)
M62	Br + PRPE → HBr + PO2	$3.60x10^{-12}$	-	Atkinson et al. (2006)

Table A.3 – Termolecular halogen reactions included in the scheme. This includes reactions from previous updates to halogen chemistry in GEOS-Chem (Eastham et al., 2014; Parrella et al., 2012; Schmidt et al., 2016; Sherwen et al., 2016a), and those detailed in section 4.2. The lower pressure limit rate (k_0) is given by: $A_0 \cdot (\frac{300}{T})^x$. The high pressure limit is given by k_∞. Fc characterises the fall off curve of the reaction as described by Atkinson et al. (2007).

Rxn ID	Reaction	A_0 cm^6,molecules^{-2},s^{-1}	x	k_∞ cm^3molecules^{-1} s^{-1}	Fc	Citation
T1	$I + NO \xrightarrow{M} INO$	1.80x10^{-32}	1	1.70x10^{-11}	0.6	Atkinson et al. (2007)
T2	$I + NO_2 \xrightarrow{M} INO_2$	3.00x10^{-31}	1	6.60x10^{-11}	0.63	Atkinson et al. (2007)
T3	$IO + NO_2 \xrightarrow{M} INO_3$	7.70x10^{-31}	5	1.60x10^{-11}	0.4	Atkinson et al. (2007)
T4	$Br + NO_2 \xrightarrow{M} BrNO_2$	4.20x10^{-31}	2.4	2.70x10^{-11}	0.6	Sander et al. (2011)
T5	$BrO + NO_2 \xrightarrow{M} BrNO_3$	5.20x10^{-31}	3.2	6.90x10^{-12}	0.6	Sander et al. (2011)
T5	$BrO + NO_2 \xrightarrow{M} BrNO_3$	5.20x10^{-31}	3.2	6.90x10^{-12}	0.6	Sander et al. (2011)
T6	$Cl + PRPE \xrightarrow{M} HCl + R4O2$	4.00x10^{-28}	0	2.80x10^{-10}	0.6	Atkinson et al. (2006)
T7	$Cl + O_2 \xrightarrow{M} ClOO$	2.20x10^{-33}	0	1.80x10^{-10}(*)	0.6	Sander et al. (2011)
T8	$Cl_2O_2 \xrightarrow{M} 2ClO$	9.30x10^{-6}	2	1.74x10^{15}(*)	0.6	Sander et al. (2011)
T9	$ClO + ClO \xrightarrow{M} Cl_2O_2$	1.60x10^{-21}	2	3.00x10^{-12}(*)	0.6	Sander et al. (2011)
T10	$ClO + NO_2 \xrightarrow{M} ClNO_3$	1.80x10^{-31}	1.9	1.50x10^{-11}(*)	0.6	Sander et al. (2011)
T11	$ClOO \xrightarrow{M} Cl + O_2$	3.30x10^{-9}	0	2.73x10^{14}(*)	0.6	Sander et al. (2011)

described by Park et al. (2004) and Pye et al. (2009). Sulfate aerosols are assumed to be acidic with pH=0.

The GEOS-Chem sea salt aerosol simulation is as described by Jaeglé et al. (2011). The transport and deposition of sea salt bromide follows that of the parent aerosol. Oxidation of bromide on sea-salt produces volatile forms of bromine that are released to the gas phase. Sea salt aerosol is emitted alkaline, but the alkalinity can be titrated in GEOS-Chem by uptake of HNO_3, SO_2, H_2SO_4 (Alexander, 2005). Sea salt aerosol with no remaining alkalinity is assumed to have pH=5. The assumption is made for no halide oxidation on alkaline sea salt aerosol.

The liquid cloud droplet surface area is modelled using cloud liquid water content from GEOS-FP (Lucchesi, 2013) and assuming effective cloud droplet radii of 10 μ m and 6 μ m for marine and continental clouds, respectively. The ice cloud droplet surface area is modelled in a similar manner assuming effective ice droplet radii of 75 μ m. Here ice cloud chemistry is assumed to be confined to an unfrozen over-layer surrounding the ice crystal following Schmidt et al. (2016). Cloud water pH (typically between 4 and 6) is calculated locally in GEOS-Chem following (Alexander et al., 2012).

Table A.4 – Photolysis reactions of halogens included in scheme. Photolysis is described in Eastham et al. (2014) ($ClNO_2$, $ClNO_3$, and ClOO), Sherwen et al. (2016a) (I_2, HOI, IO, OIO, INO, INO_2, INO_3, I_2O_2, I_2O_3, I_2O_4, CH_3I, CH_2I_2, CH_2ICl, CH_2IBr), and Schmidt et al. (2016) (BrCl, Cl_2, ClO, HOCl, $ClNO_2$, $ClNO_3$, ClOO, Cl_2O_2, CH_3Cl, CH_3Cl_2, and $CHCl_3$.). As stated in Section 4.2, we have used the I_2O_2 cross-section for I_2O_4

ID	Reaction	Cross-section reference
J1	$I_2 \xrightarrow{h\nu} 2I$	Sander et al. (2011)
J2	$HOI \xrightarrow{h\nu} I + OH$	Sander et al. (2011)
J3	$IO\ (+O_2) \xrightarrow{h\nu} I\ (+ O_3)$	Sander et al. (2011)
J4	$OIO \xrightarrow{h\nu} I + O_2$	Sander et al. (2011)
J5	$INO \xrightarrow{h\nu} I + NO$	Sander et al. (2011)
J6	$INO_2 \xrightarrow{h\nu} I + NO_2$	Sander et al. (2011)
J7	$INO_3 \xrightarrow{h\nu} I + NO_3$	Sander et al. (2011)
J8	$I_2O_2 \xrightarrow{h\nu} I + OIO$	Gómez Martín et al. (2005), Spietz et al. (2005)
J9	$CH_3I \xrightarrow{h\nu} I$	Sander et al. (2011)
J10	$CH_2I_2 \xrightarrow{h\nu} 2I$	Sander et al. (2011)
J11	$CH_2ICl \xrightarrow{h\nu} I + Cl$	Sander et al. (2011)
J12	$CH_2IBr \xrightarrow{h\nu} I + Br$	Sander et al. (2011)
J13	$I_2O_4 \xrightarrow{h\nu} 2OIO$	see caption
J14	$I_2O_3 \xrightarrow{h\nu} OIO + IO$	Gómez Martín et al. (2005), Spietz et al. (2005)
J15	$CHBr_3 \xrightarrow{h\nu} 3Br$	Sander et al. (2011)
J16	$Br_2 \xrightarrow{h\nu} 2Br$	Sander et al. (2011)
J17	$BrO\ (+O_2) \xrightarrow{h\nu} Br\ (+O_3)$	Sander et al. (2011)
J18	$HOBr \xrightarrow{h\nu} Br + OH$	Sander et al. (2011)
J19	$BrNO_2 \xrightarrow{h\nu} Br + NO_2$	Sander et al. (2011)
J20	$BrNO_3 \xrightarrow{h\nu} Br + NO_3$	Sander et al. (2011)
J21	$BrNO_3 \xrightarrow{h\nu} BrO + NO_2$	Sander et al. (2011)
J22	$CH_2Br_2 \xrightarrow{h\nu} 2Br$	Sander et al. (2011)
J23	$BrCl \xrightarrow{h\nu} Br + Cl$	Sander et al. (2011)
J24	$Cl_2 \xrightarrow{h\nu} 2Cl$	Sander et al. (2011)
J25	$ClO\ (+O_2) \xrightarrow{h\nu} Cl\ (+O_3)$	Sander et al. (2011)
J26	$OClO\ (+O_2) \xrightarrow{h\nu} ClO\ (+O_3)$	Sander et al. (2011)
J27	$Cl_2O_2 \xrightarrow{h\nu} Cl + ClOO$	Sander et al. (2011)
J28	$ClNO_2 \xrightarrow{h\nu} Cl + NO_2$	Sander et al. (2011)
J29	$ClNO_3 \xrightarrow{h\nu} Cl + NO_3$	Sander et al. (2011)
J30	$ClNO_3 \xrightarrow{h\nu} ClO + NO_2$	Sander et al. (2011)
J31	$HOCl \xrightarrow{h\nu} Cl + OH$	Sander et al. (2011)
J32	$ClOO \xrightarrow{h\nu} Cl$	Sander et al. (2011)
J33	$CH_3Cl \xrightarrow{h\nu} Cl + CH_3O_2$,	Sander et al. (2011)
J34	$CH_3Cl_2 \xrightarrow{h\nu} 2Cl$	Sander et al. (2011)

Table A.5 – Halogen multiphase reactions and reactive uptake coefficients (γ)

ID	Reaction	Reactive uptake coefficient (γ)	Note	Reference
1	$HCl \rightarrow Cl^-(SSA)$	$4.4 \times 10^{-6} \exp(2989\,K/T)$	Sea salt only	Ammann et al. (2013)
2	$HBr \rightarrow Br^-(SSA)$	$1.3 \times 10^{-8} \exp(4290\,K/T)$	Sea salt only	Ammann et al. (2013)
3	$HI \rightarrow I(aerosol)$	0.1		
4	$ClNO_3 \rightarrow HOCl^+HNO_3$	0.024	Hydrolysis	Deiber et al. (2004)
5	$BrNO_3 \rightarrow HOBr^+HNO_3$	0.02	Hydrolysis	Deiber et al. (2004)
6	$INO_3 \rightarrow 0 \cdot 85\,ICl^+0 \cdot 15\,IBr^+HNO_3$	0.01	Sea salt only	
7	$INO_2 \rightarrow 0 \cdot 85\,ICl^+0 \cdot 15\,IBr^+HNO_3$	0.02	Sea salt only	
8	$HOBr^+Cl^-(aq) \rightarrow BrCl$	See text		Ammann et al. (2013)
9	$HOBr^+Br^-(aq) \rightarrow Br_2$	See text		Ammann et al. (2013)
10	$HOI \rightarrow 0 \cdot 85\,ICl^+0 \cdot 15\,IBr$	0.01	Sea salt only	
11	$ClNO_3^+Br^-(aq) \rightarrow BrCl^+HNO_3$	See text		Ammann et al. (2013)
12	$O_3^+Br^-(aq) \rightarrow HOBr$	See text		Ammann et al. (2013)
13	$I_2O_2 \rightarrow I(aerosol)$	0.02		
14	$I_2O_3 \rightarrow I(aerosol)$	0.02		
15	$I_2O_4 \rightarrow I(aerosol)$	0.02		

The reactive uptake coefficients depend on the aerosol halide concentration. For sea salt aerosol, the bromide concentration is calculated directly from the bromide content and the aerosol mass. Sea salt aerosol chloride is assumed to be in excess (see below). For clouds and sulfate aerosol, the bromide and chloride concentration is estimated assuming equilibrium between gas phase HX and aerosol phase X^-.

A.0.3 Reactive uptake coefficients

The following uptake coefficient calculations were implemented in Schmidt et al. (2016) and included in the "Cl+Br+I" simulation. The calculation of cloud ice surface area was updated as described for the implementation simulation here as also described in (Sherwen et al., 2016b). The work presented here is credited to Dr Johan A. Schmidt.

A.0.3.1 HOBr+Cl^-/Br^-

The reactive uptake coefficient is calculated as

$$\gamma = \left(\Gamma^{-1} + \alpha^{-1}\right)^{-1}, \tag{A.0.1}$$

where the mass accommodation coefficient for HOBr is $\alpha = 0.6$ and

$$\Gamma = \frac{4H_{\mathrm{HOBr}}RTk_{\mathrm{HOBr^+X^-}}[\mathrm{X^-}][\mathrm{H^+}]l_r f(r, l_r)}{c}, \tag{A.0.2}$$

with $k_{\mathrm{HOBr^+Cl^-}} = 5.9 \times 10^9\,\mathrm{M^{-2}s^{-1}}$ and $k_{\mathrm{HOBr^+Br^-}} = 1.6 \times 10^{10}\,\mathrm{M^{-2}s^{-1}}$. In the equation above c is the average thermal velocity of HOBr, and $f(l_r, r)$ is a reacto-diffusive correction factor,

$$f(l_r, r) = \coth\left(\frac{r}{l_r}\right) - \frac{l_r}{r}, \tag{A.0.3}$$

with r being the radius of the aerosol. For sea salt aerosol $\mathrm{HOBr^+Cl^-}$ is assumed to be limited by mass accommodation, i.e. $\Gamma \gg \alpha$, due to high concentration of $\mathrm{Cl^-}$ in sea salt aerosol. The reacto-diffusive length scale is

$$l_r = \sqrt{\frac{D_l}{k_{\mathrm{HOBr^+X^-}}[\mathrm{X^-}][\mathrm{H^+}]}}, \tag{A.0.4}$$

where $D_l = 1.4 \times 10^{-5}\,\mathrm{cm^2s^{-1}}$ is the aqueous phase diffusion coefficient for HOBr. The listed parameters are taken from Ammann et al. (2013), and $k_{\mathrm{HOBr^+Br^-}}$ is from Beckwith et al. (1996).

A.0.3.2 $\mathrm{ClNO_3}$+$\mathrm{Br^-}$

The reactive uptake coefficient is calculated as

$$\gamma = \left(\Gamma^{-1} + \alpha^{-1}\right)^{-1}, \tag{A.0.5}$$

where the mass accommodation coefficient for $\mathrm{ClNO_3}$ is $\alpha = 0.108$ and

$$\Gamma = \frac{4WRT\sqrt{[\mathrm{Br^-}]D_l}}{c}, \tag{A.0.6}$$

where c is the average thermal velocity of $\mathrm{ClNO_3}$, $D_l = 5.0 \times 10^{-6}\,\mathrm{cm^2s^{-1}}$ is the aqueous phase diffusion coefficient for $\mathrm{ClNO_3}$, and $W = 10^6\,\sqrt{\mathrm{Ms}}\,\mathrm{bar^{-1}}$.

A.0.3.3 $\mathrm{O_3}$+$\mathrm{Br^-}$

The reactive uptake coefficient is calculated as

$$\gamma = \Gamma_b + \Gamma_s, \tag{A.0.7}$$

where Γ_b is the bulk reaction coefficient,

$$\Gamma_b = \frac{4H_{O_3}RTk_{O_3^+Br^-}[Br^-]l_r f(r,l_r)}{c}, \tag{A.0.8}$$

with $k_{O_3^+Br^-} = 6.8 \times 10^8 \exp(-4450\,\mathrm{K}/T)\,\mathrm{M^{-1}s^{-1}}$. In the equation above c is the average thermal velocity of O_3, and $f(l_r, r)$ is a reacto-diffusive correction factor,

$$f(l_r, r) = \coth\left(\frac{r}{l_r}\right) - \frac{l_r}{r}, \tag{A.0.9}$$

with r being the radius of the aerosol. The reacto-diffusive length scale is

$$l_r = \sqrt{\frac{D_l}{k_{O_3^+Br^-}[Br^-]}}, \tag{A.0.10}$$

where $D_l = 8.9 \times 10^{-6}\,\mathrm{cm^2s^{-1}}$ is the aqueous phase diffusion coefficient for O_3.

The surface reaction coefficient is calculated as,

$$\Gamma_s = \frac{4k_s[Br^-(\mathrm{surf})]K_{\mathrm{LangC}}N_{\max}}{c(1 + K_{\mathrm{LangC}}[O_3(\mathrm{g})])}, \tag{A.0.11}$$

where the surface reaction rate constant is $k_s = 10^{-16}\,\mathrm{cm^2s^{-1}}$, the equilibrium constant for O_3 is $K_{\mathrm{LangC}} = 10^{-13}\,\mathrm{cm^3}$, and the maximum number of available sites is taken as $N_{\max} = 3 \times 10^{14}\,\mathrm{cm^{-2}}$. The surface bromide concentration is estimated as,

$$[Br^-(\mathrm{surf})] = \min(3.41 \times 10^{14}\,\mathrm{cm^{-2}M^{-1}}\,[Br^-], N_{\max}). \tag{A.0.12}$$

Table A.6 – Henry's law coefficients and molar heats of formation of halogen species. Where Henry's law constant equals infinity a very large values is used within the model (1x10^{20} M atm^{-1}). The INO_2 Henry's law constant is assumed equal to that of $BrNO_3$, from Sander (2015), by analogy. For I_2O_X (X=2,3,4) a Henry's law constant of infinity is assumed by analogy with INO_3. (∗) Effective Henry's law of HX is calculated for acid conditions through $K_H^*(T) = K_H(T) * (1 + \frac{K_a}{[H^+]})$.

Species	Henry's Law Constant (H) at 298K M atm^{-1}	Reference	$\frac{\text{d(ln H)}}{\text{d(1/T)}}$ K	Reference
HOBr	6.1x10^3	Frenzel et al. (1998)	6.01x10^3	McGrath and Rowland (1994)
HBr(*)	7.1x10^{13}	Frenzel et al. (1998)	1.02x10^4	Schweitzer et al. (2000)
$BrNO_2$	0.3	Frenzel et al. (1998)	-	-
$BrNO_3$	∞	Sander (2015)	-	-
Br_2	0.76	Dean (1992)	3.72x10^3	Dean (1992)
HOCl	6.5x10^3	Sander (2015)	5.9x10^3	Sander (2015)
HCl(*)	7.1x10^{15}	Sander (2015)	5.9x10^3	Sander (2015)
$ClNO_3$	∞	Sander (2015)	-	-
BrCl	0.97	Sander (2015)	-	-
ICl	1.11x10^2	Sander (2015)	2.11x10^3	Sander et al. (2006)
IBr	2.43x10^1	Sander (2015)	4.92x10^3	Sander et al. (2006)
HOI	1.53x10^4	Sander (2015)	8.37x10^3	Sander et al. (2006)
HI (*)	7.43x10^{13}	Sander (2015)	3.19x10^3	Sander et al. (2006)
INO_3	∞	Vogt et al. (1999)	3.98x10^4	Kaltsoyannis and Plane (2008)
I_2O_2	∞	see caption text	1.89x10^4	Kaltsoyannis and Plane (2008)
I_2	2.63	Sander (2015)	7.51x10^3	Sander et al. (2006)
INO_2	0.3	see caption text	7.24x10^3	Sander et al. (2006)
I_2O_3	∞	see caption text	7.70x10^3	Kaltsoyannis and Plane (2008)
I_2O_4	∞	see caption text	1.34x10^4	Kaltsoyannis and Plane (2008)

Appendix B

Tabulated burden changes on inclusion of halogens

Table B.1 gives the burdens with and without halogens and the fractional change.

Table B.1 – Tropospheric burden of species and families with ("Cl+Br+I") and without halogens ("NOHAL"), and % change. Burdens are considered in elemental terms (e.g Gg S/N/C) and species masses for OH, HO_2, H_2O_2 and O_3 Families are defined in footnote 3

	"NOHAL"	"Cl+Br+I"	% Δ
NO_3	1.23	1.23	-17.8
O_3	415843.25	355123.69	-14.6
N_2O_5	9.38	8.02	-14.5
H_2O_2	3229.09	2828.80	-12.4
C_2H_6	3258.84	2855.31	-12.4
HNO_4	19.84	17.63	-11.1
C_3H_8	609.76	550.68	-9.7
≥C4 alkanes	488.35	441.96	-9.5
HO_2	27.55	25.37	-7.9
PPN	15.82	14.65	-7.4
PAN	202.89	194.70	-4.0
$CH_3C(O)CH_3$	7533.51	7289.92	-3.2
OH	0.28	0.27	-2.9
NO_2	123.53	120.35	-2.6
CH_2O	389.55	380.88	-2.2
PMN	0.68	0.67	-1.8
NO_x	171.01	168.15	-1.7
SO_4 on SSA	1.97	1.94	-1.6
NH_3	126.61	126.28	-0.3

Table B.2 – Continued Table B.1

	"NOHAL"	"Cl+Br+I"	% Δ
NO_y	1374.56	1371.59	-0.2
Acetaldehyde	184.93	184.59	-0.2
NH_4	270.93	271.43	0.2
>C3 ketones	186.99	188.11	0.6
SO_x	398.98	401.59	0.7
SO_4	397.01	399.65	0.7
NO	47.48	47.80	0.7
≥C3 alkenes	97.93	98.79	0.9
PROPNN	7.46	7.55	1.1
HNO_3	463.49	470.69	1.6
VOCs	148193.29	151283.71	2.1
≥C4 alkylnitrates	64.60	65.99	2.2
SO_2	286.11	294.17	2.8
CO	134654.88	138477.76	2.8
MMN	3.15	3.26	3.2
CH_3NO_2	13.80	14.25	3.3
Isoprene	788.55	815.73	3.4
HNO_2	2.76	2.92	5.5
ISOPN	0.65	0.69	6.2

Appendix C

Supplementary Figures and Information

C.1 Monthly iodine emissions of iodine species

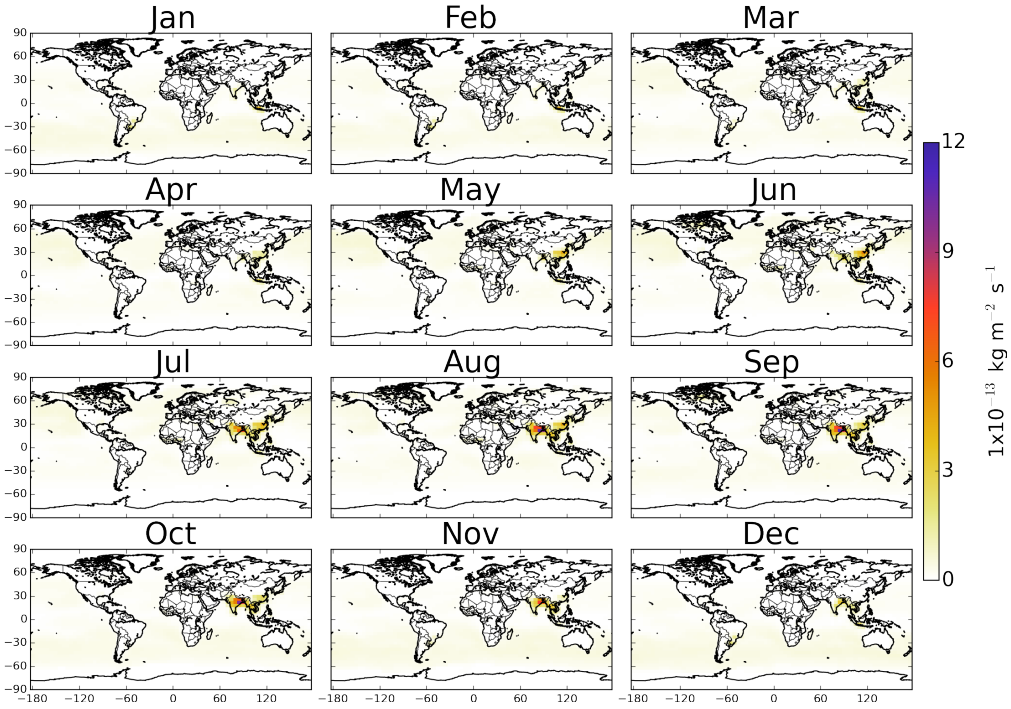

Figure C.1 – Spatial plot of monthly average CH_3I emissions implemented in GEOS-Chem ("Cl+Br+I")

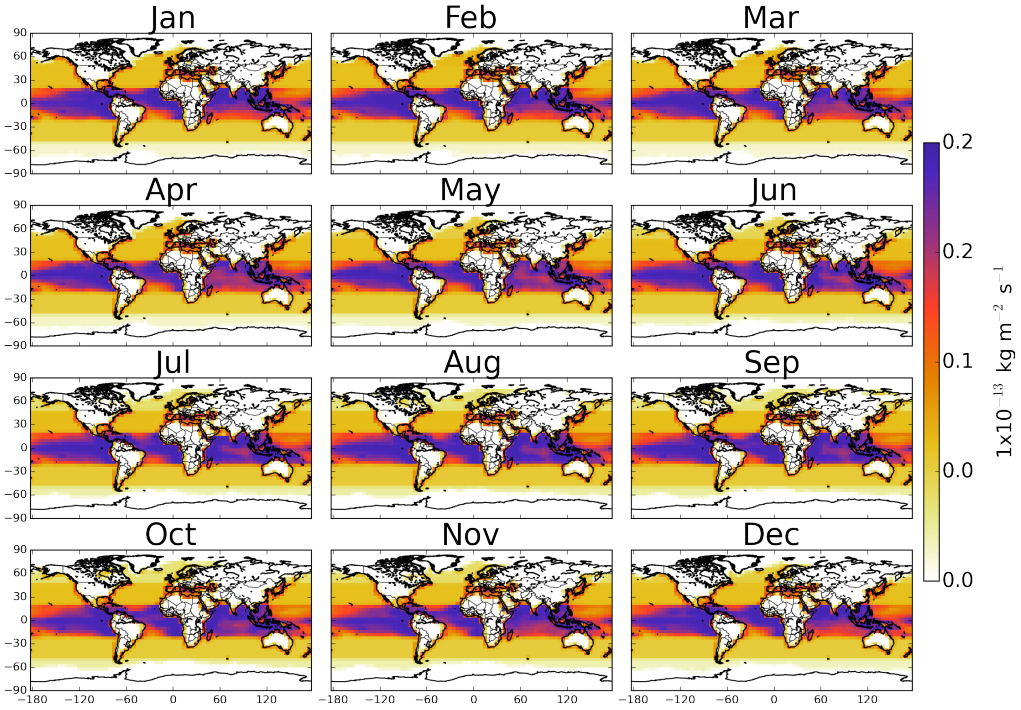

Figure C.2 – Spatial plot of monthly average CH_2I_2 emissions implemented in GEOS-Chem ("Cl+Br+I")

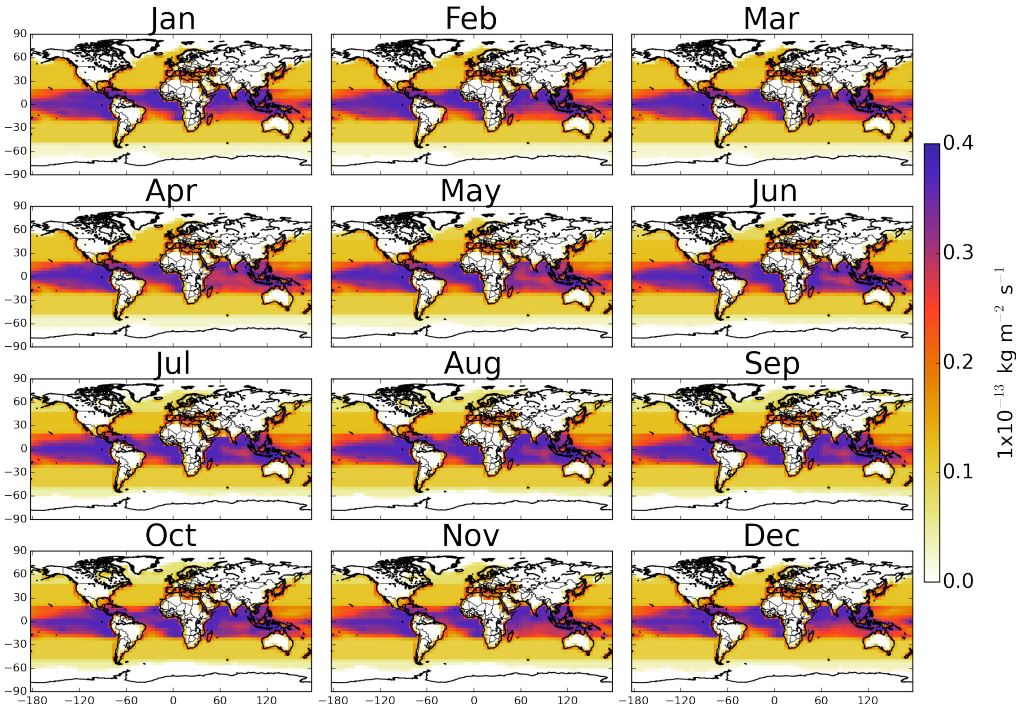

Figure C.3 – Spatial plot of monthly average CH_2ICl emissions implemented in GEOS-Chem ("Cl+Br+I")

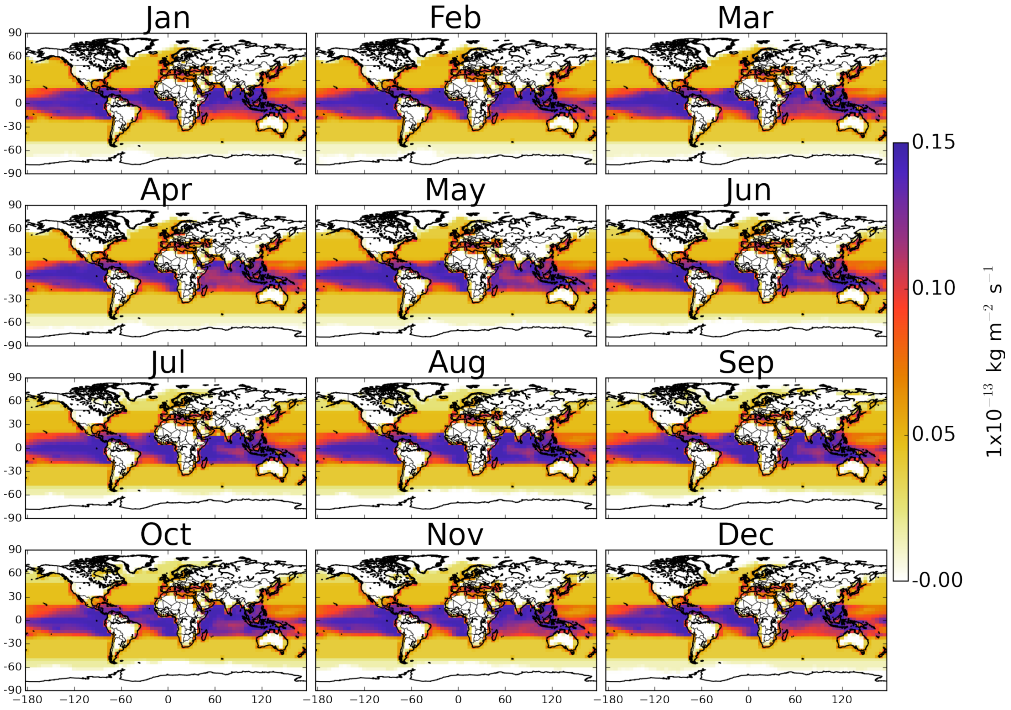

Figure C.4 – Spatial plot of monthly average CH_2IBr emissions implemented in GEOS-Chem ("Cl+Br+I")

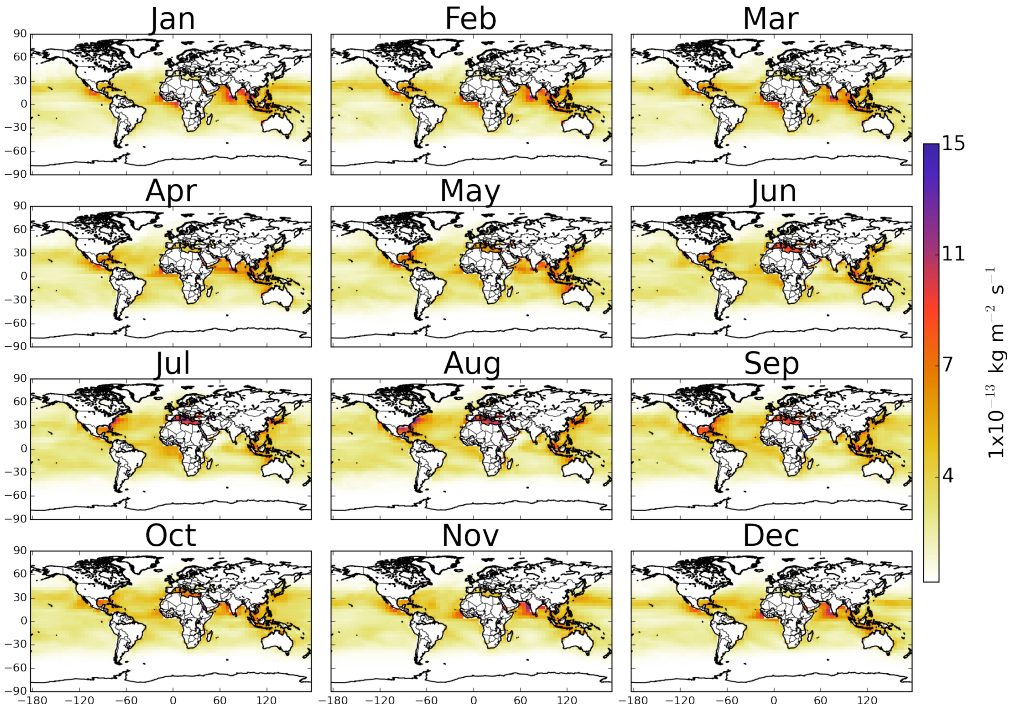

Figure C.5 – Spatial plot of monthly average HOI emissions implemented in GEOS-Chem ("Cl+Br+I")

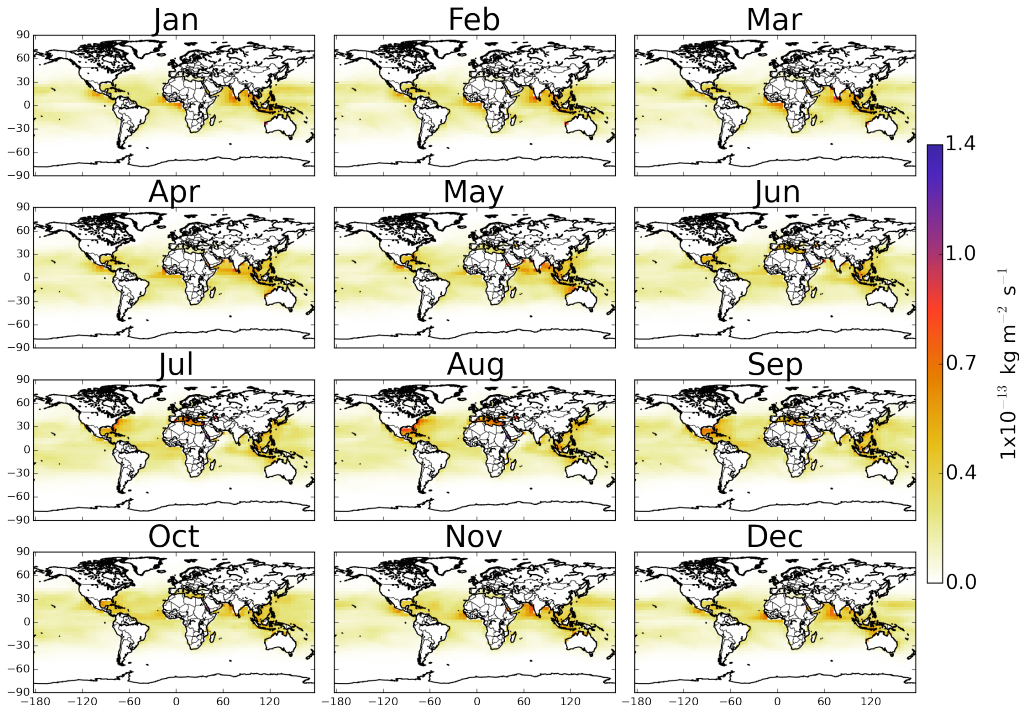

Figure C.6 – Spatial plot of monthly average I_2 emissions implemented in GEOS-Chem ("Cl+Br+I")

C.2 Full and binned iodine cross-sections

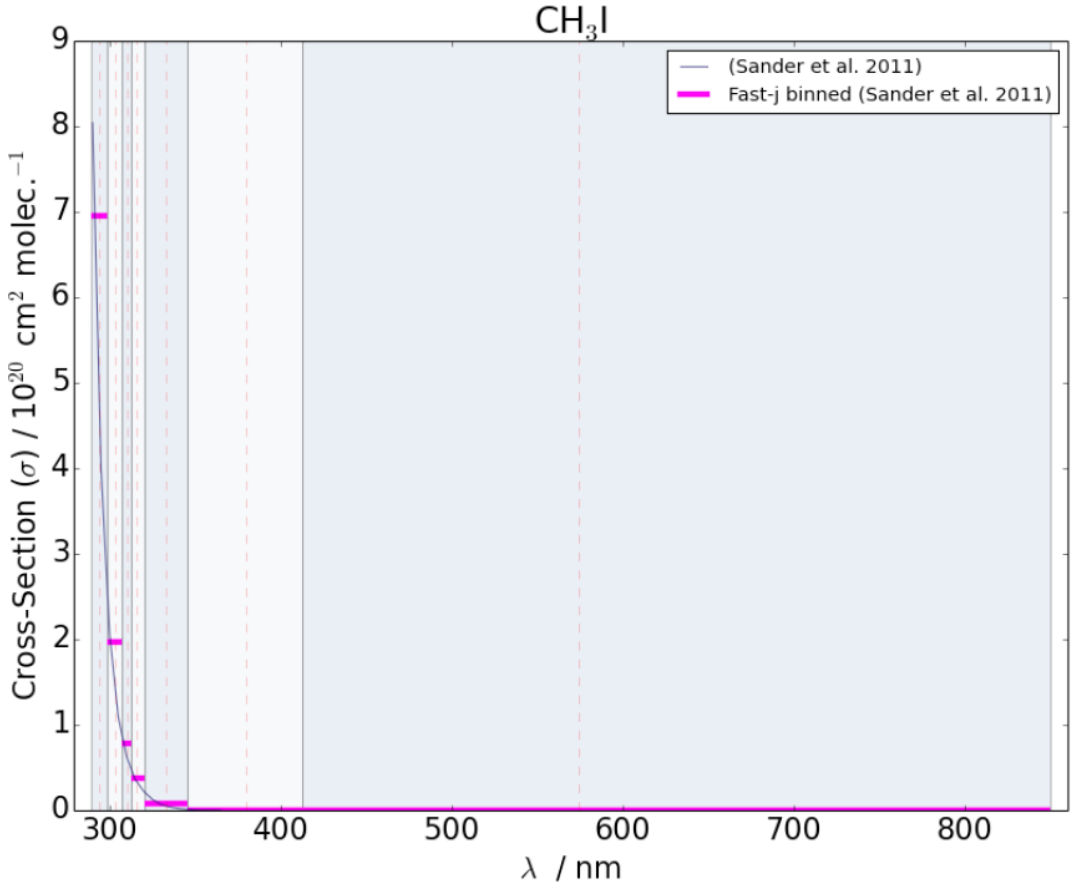

Figure C.7 – Full and FAST-J binned (7 bin) cross-section of CH_3I used in "Cl+Br+I" Simulation.

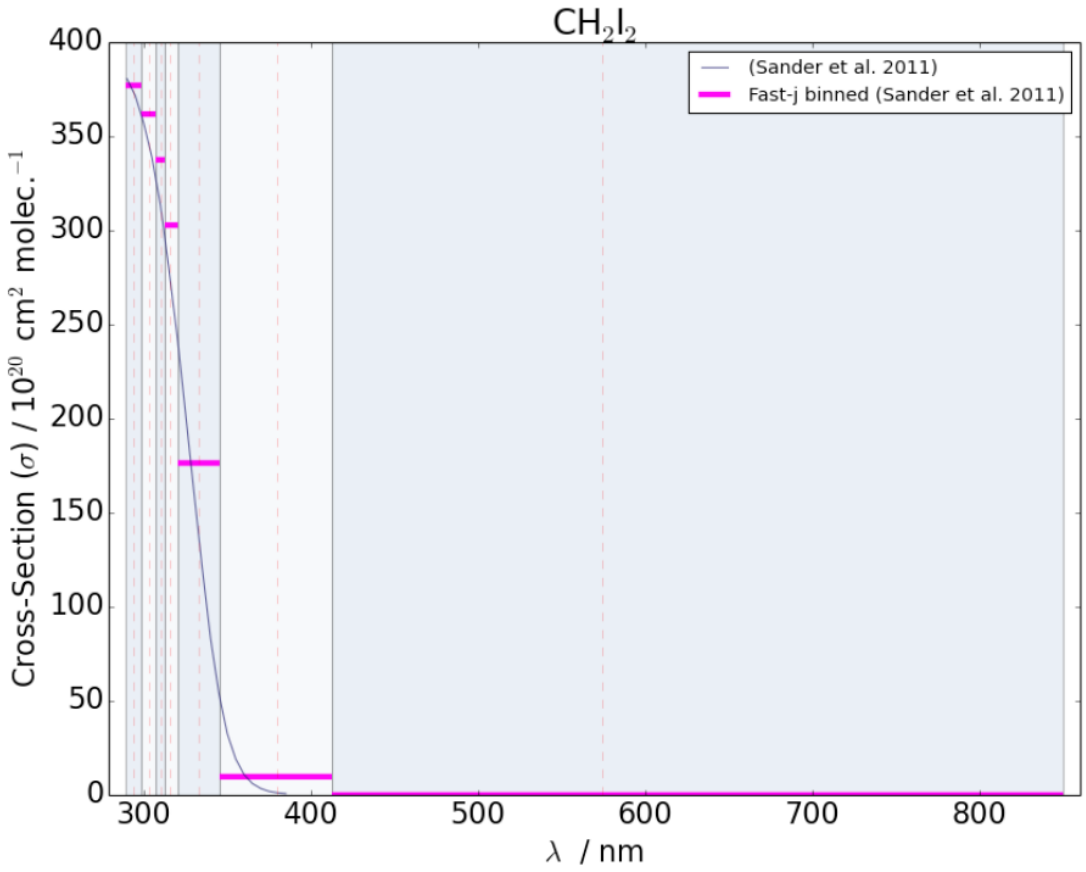

Figure C.8 – Full and FAST-J binned (7 bin) cross-section of CH_2I_2 used in "Cl+Br+I" Simulation.

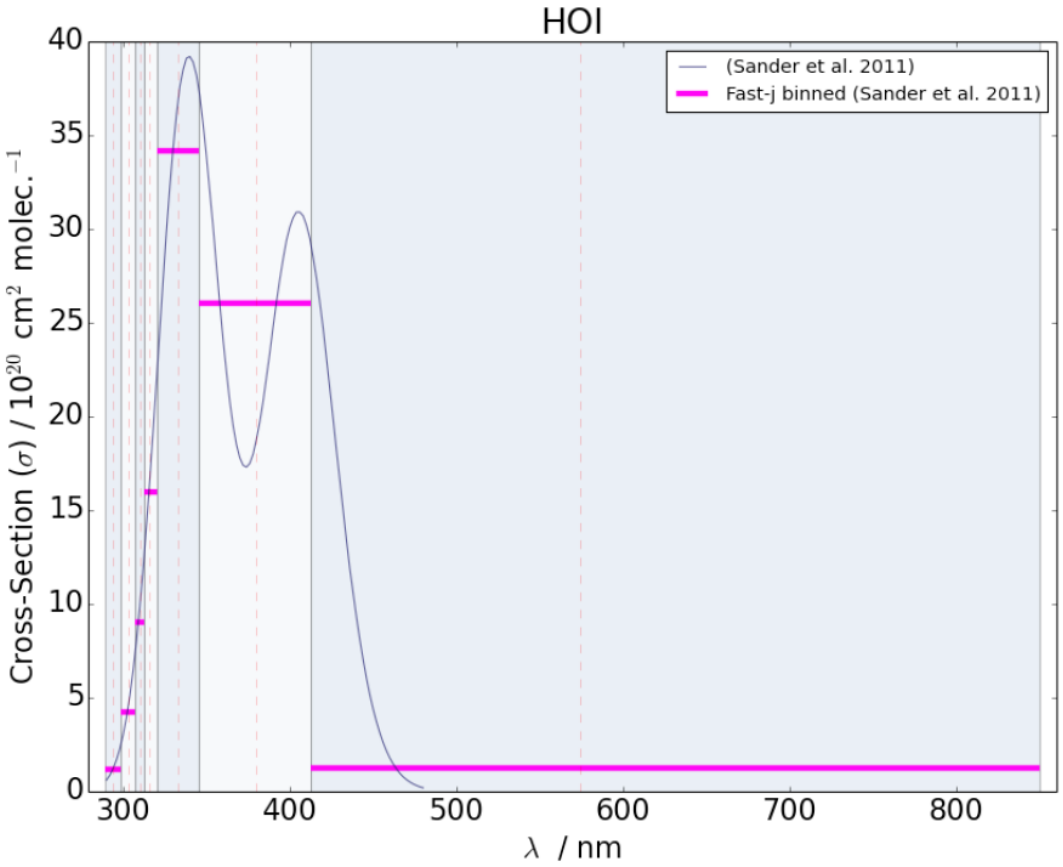

Figure C.9 – Full and FAST-J binned (7 bin) cross-section of HOI used in "Cl+Br+I" Simulation.

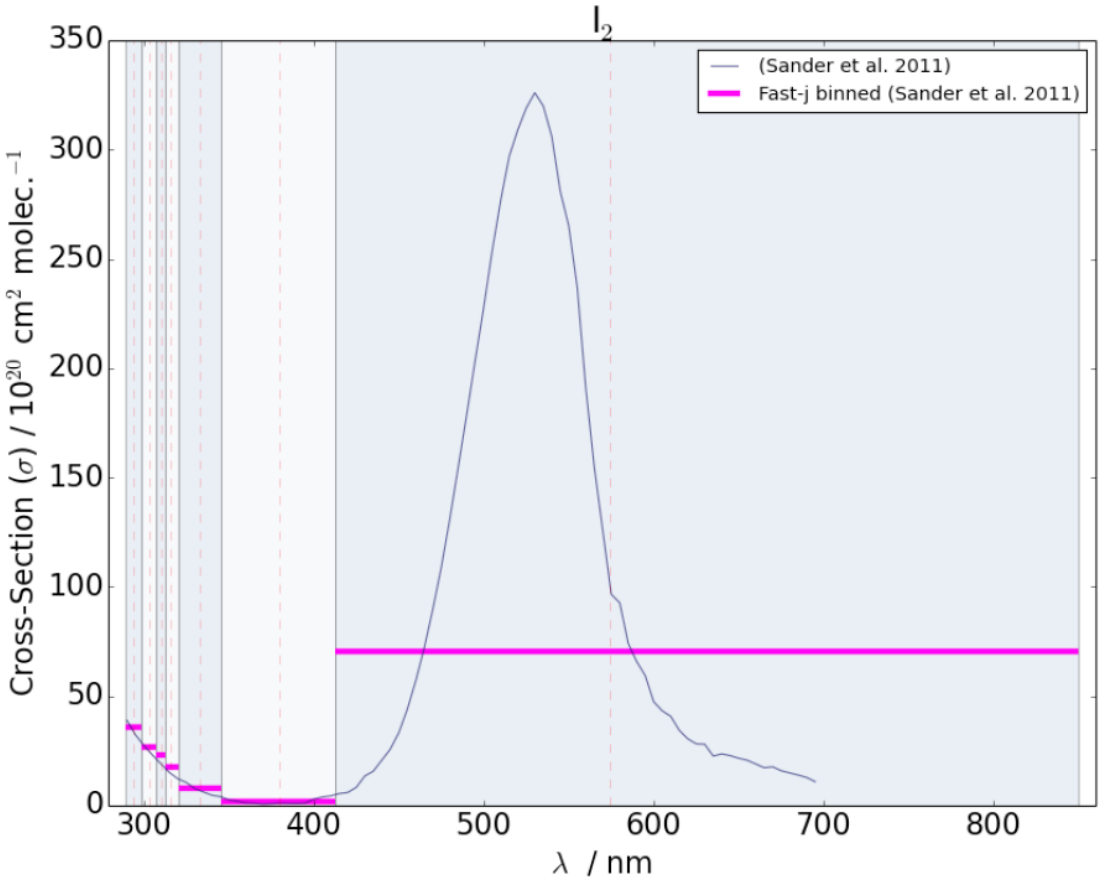

Figure C.10 – Full and FAST-J binned (7 bin) cross-section of I_2 used in "Cl+Br+I" Simulation.

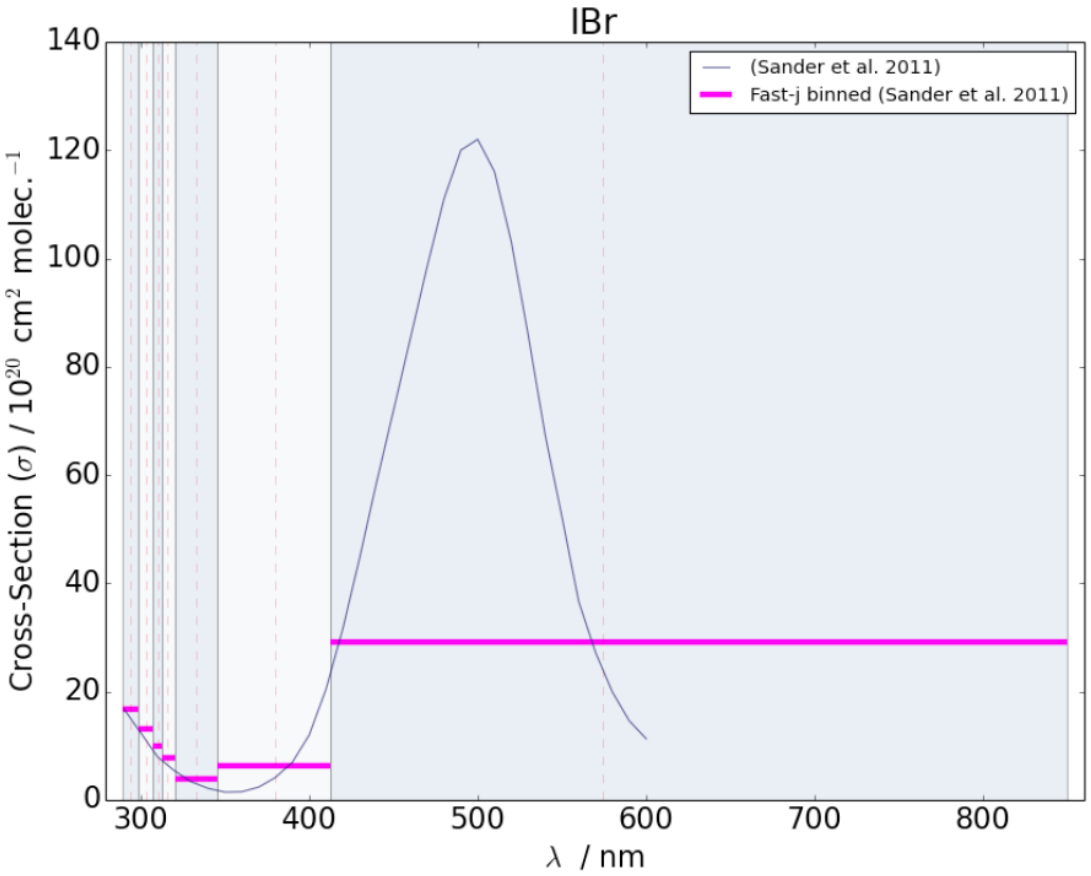

Figure C.11 – Full and FAST-J binned (7 bin) cross-section of IO used in "Cl+Br+I" Simulation.

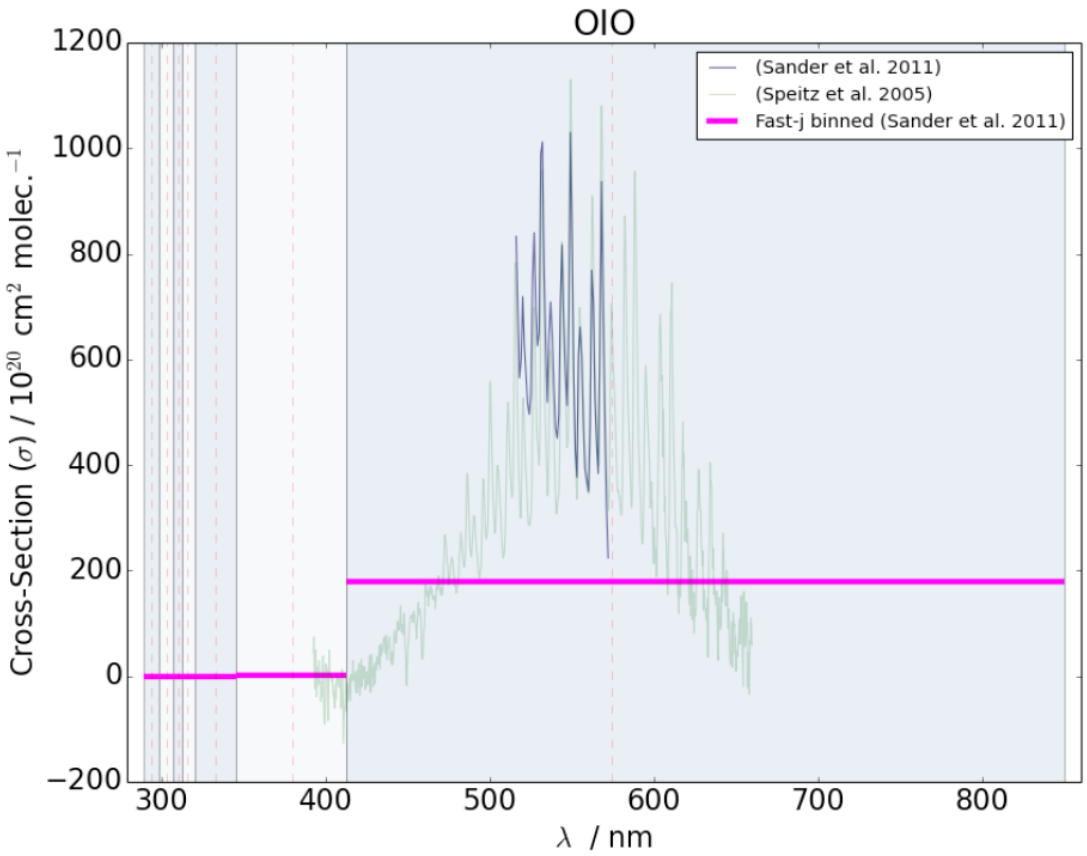

Figure C.12 – Full and FAST-J binned (7 bin) cross-section of OIO used in "Cl+Br+I" Simulation.

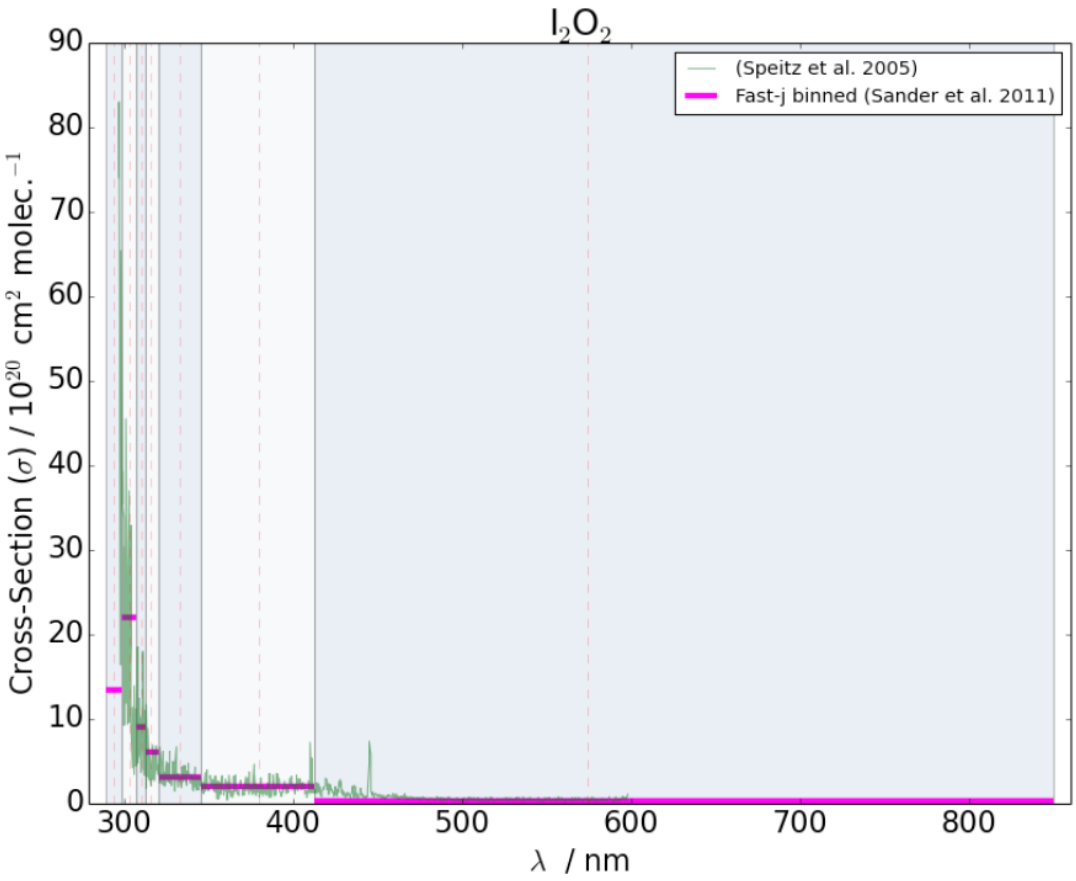

Figure C.13 – Full and FAST-J binned (7 bin) cross-section of I_2O_2 used in "Cl+Br+I" Simulation.

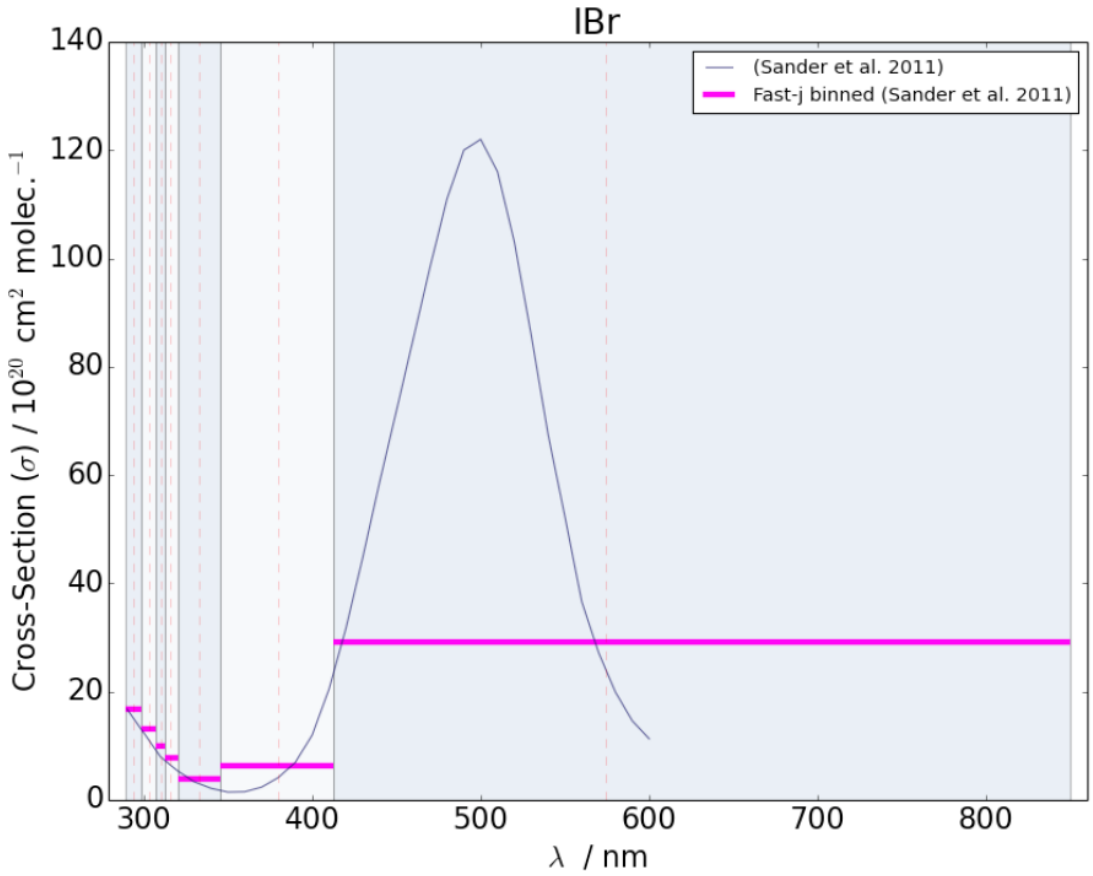

Figure C.14 – Full and FAST-J binned (7 bin) cross-section of IBr used in "Cl+Br+I" Simulation.

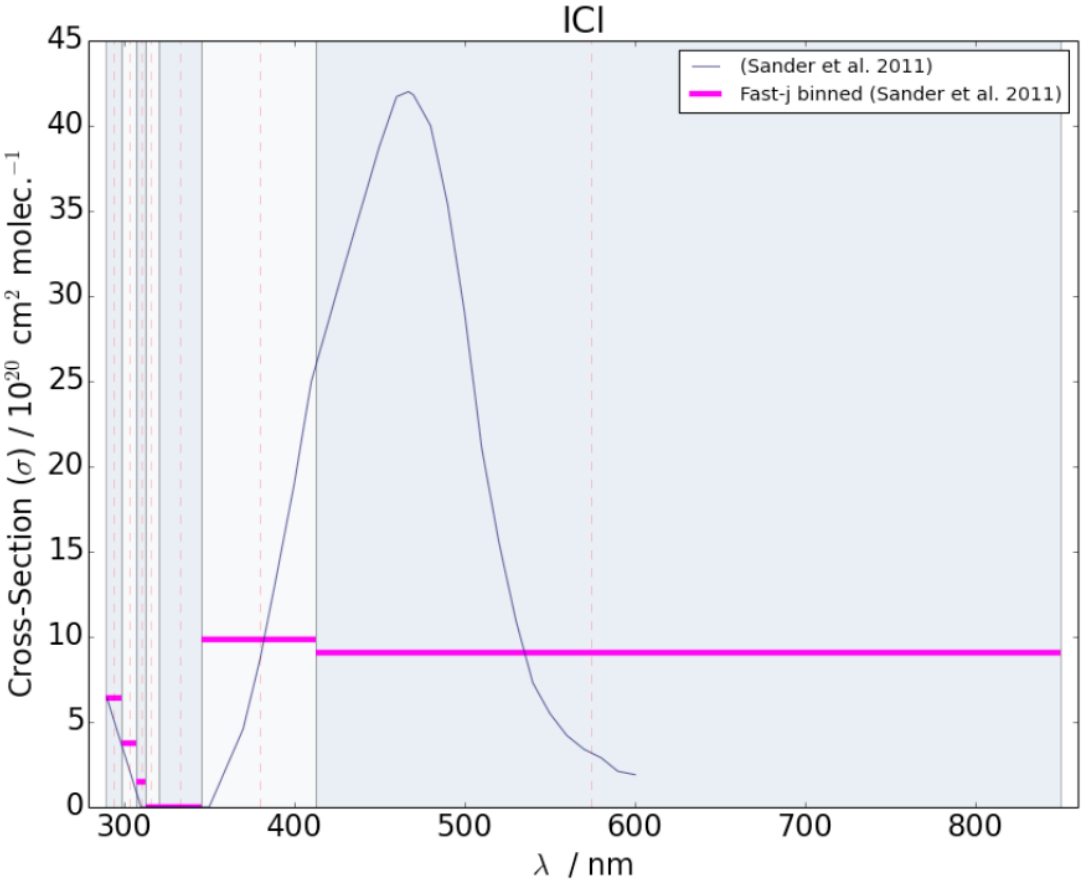

Figure C.15 – Full and FAST-J binned (7 bin) cross-section of ICl used in "Cl+Br+I" Simulation.

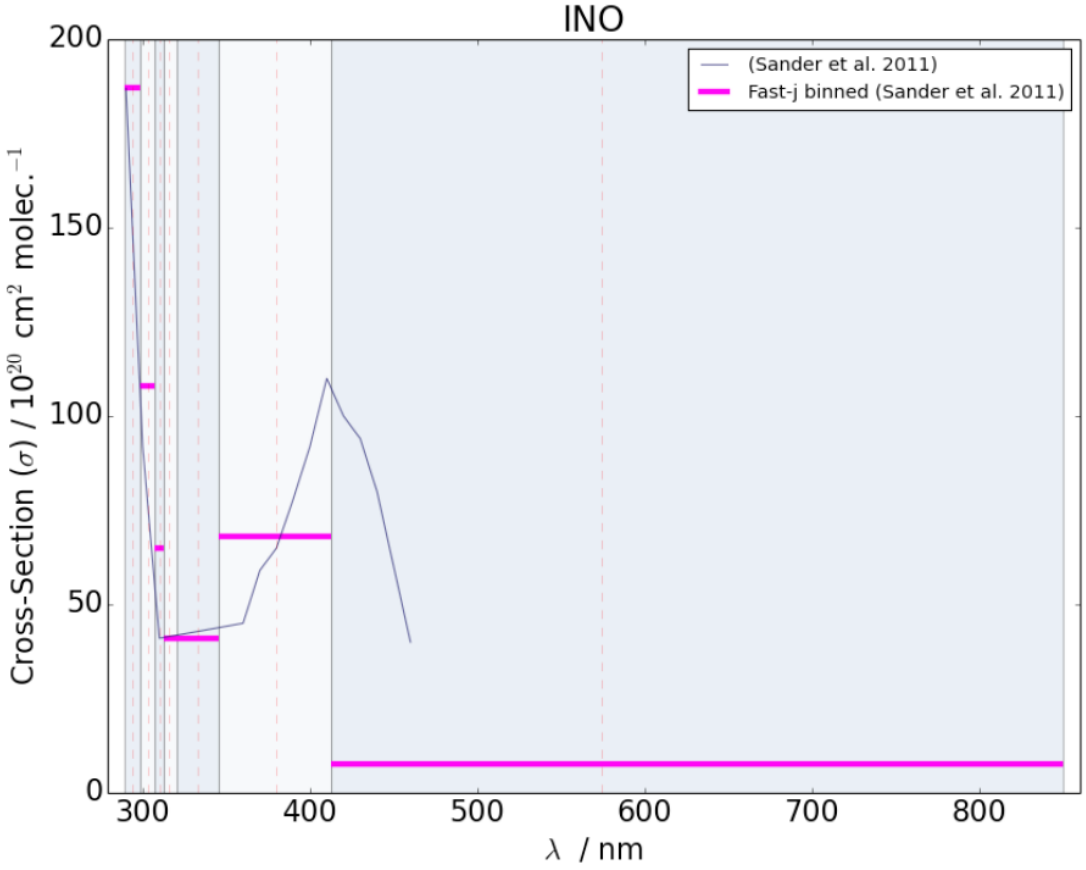

Figure C.16 – Full and FAST-J binned (7 bin) cross-section of INO used in "Cl+Br+I" Simulation.

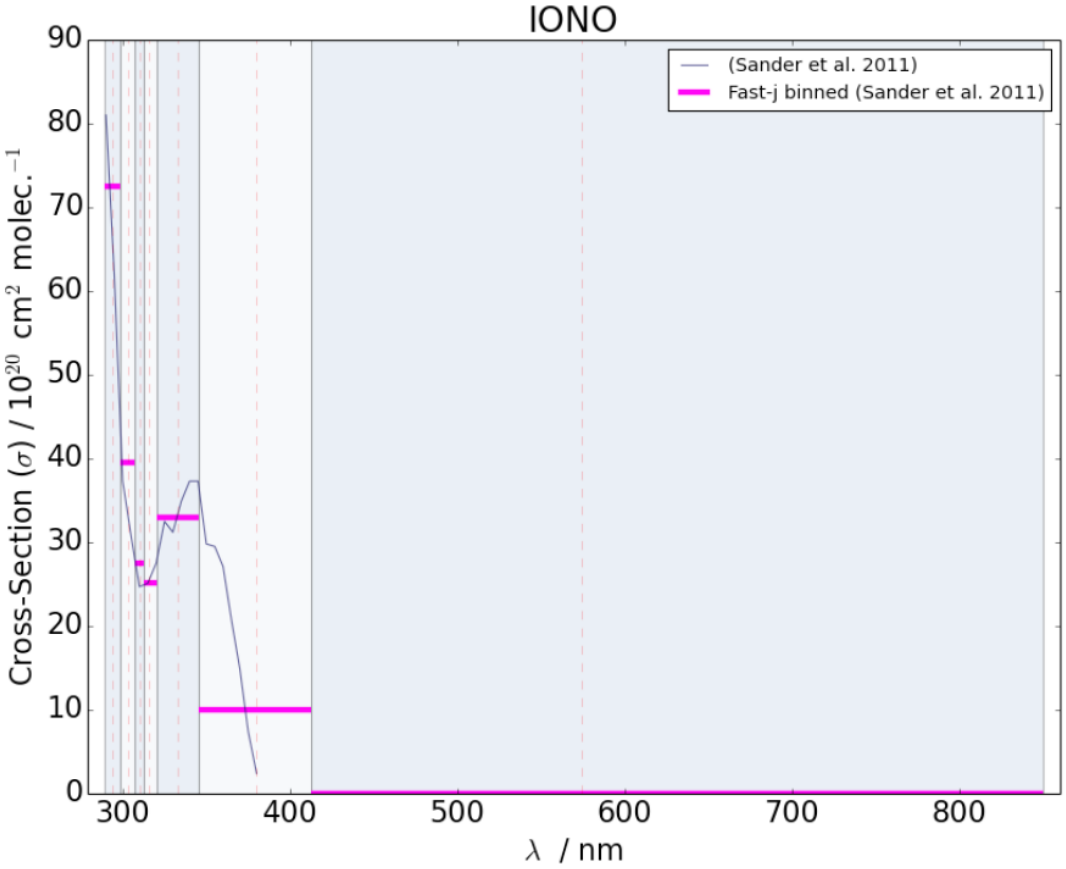

Figure C.17 – Full and FAST-J binned (7 bin) cross-section of INO_2 used in "Cl+Br+I" Simulation.

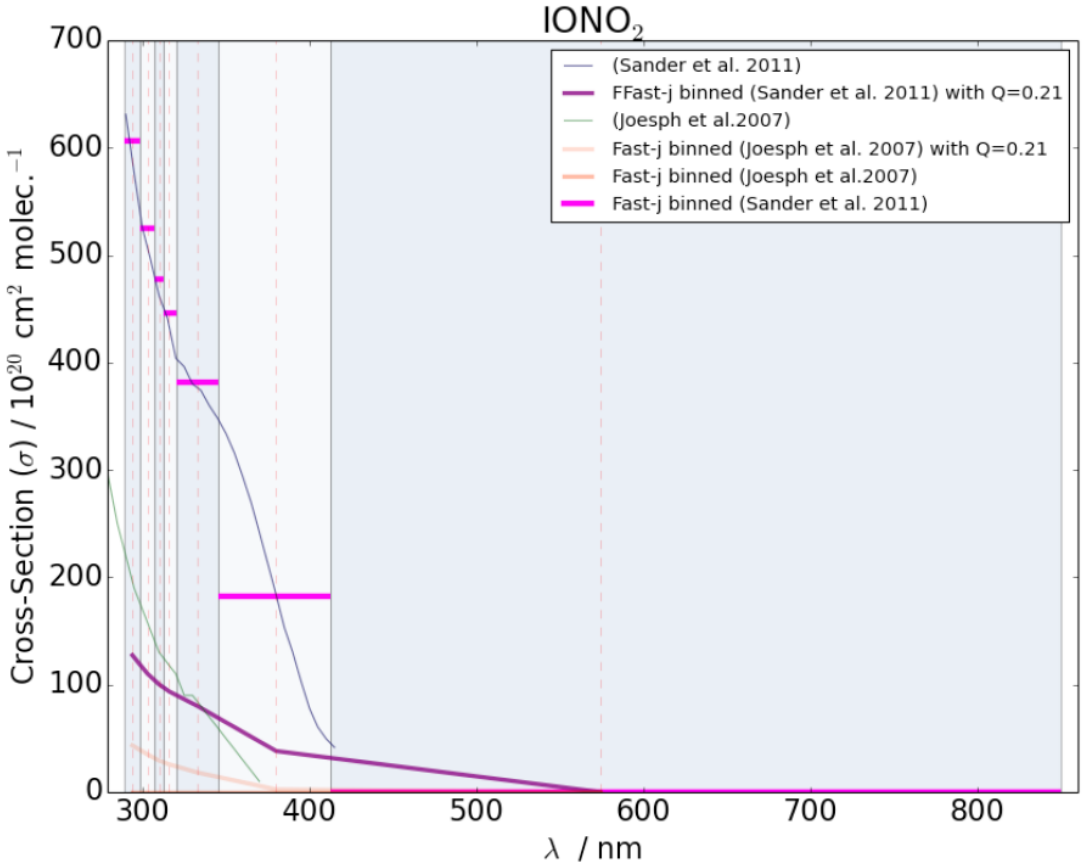

Figure C.18 – Full and FAST-J binned (7 bin) cross-section of INO_3 used in "Cl+Br+I" Simulation.

Abbreviations

AOD	Aerosol Optical Depth
CAST	Combined Airborne Studies in the Tropics
CTM	Chemical Transport Model
CONTRAST	CONvective TRansport of Active Species in the Tropics
DU	Dobson Units
DOM	Desolved Organic Matter
FT	Free Troposphere
GAW	Global Atmospheric Watch
GC-MS	Gas Chromatography Mass Spectrometry
GEOS	Goddard Earth Observation System
GMAO	Global Modelling and Assimilation Office
GMI	Global Modelling Initiative
GOME-2	Global O_3 Monitoring Experiment-2
IUPAC	International Union of Pure and Applied Chemistry
JPL	Jet Propulsion Laborotory
LP-DOAS	Long Path Differential Optical Absorption Spectroscopy
MAXI-DOAS	Multi-Axis Differential Optical Absorption Spectroscopy
MBL	Marine Boundary Layer
NASA	National Aeronautics and Space Administration

SST	Sea Surface Temperature
TORERO	Tropical Ocean tRoposphere Exchange of Reactive halogens and Oxygenated hydrocarbons
VSLH	Very Short-Lived Halocarbons
UT	Upper Troposphere
UV	Ultra Violet
WOUDC	World O_3 and Ultraviolet Radiation Data Centre

References

Abbatt, J. P. D., Lee, A. K. Y., and Thornton, J. A.: Quantifying trace gas uptake to tropospheric aerosol: recent advances and remaining challenges, Chem. Soc. Rev., 41, 6555–6581, doi:10.1039/c2cs35052a, 2012.

Ainsworth, E. A., Yendrek, C. R., Sitch, S., Collins, W. J., and Emberson, L. D.: The Effects of Tropospheric Ozone on Net Primary Productivity and Implications for Climate Change, Annu. Rev. Plant Bio., 63, 637–661, doi:10.1146/annurev-arplant-042110-103829, 2012.

Aldahan, A., Persson, S., Possnert, G., and Hou, X. L.: Distribution of 127 I and 129 I in precipitation at high European latitudes, Geophysical Research Letters, 36, L11 805, doi:10.1029/2009GL037363, URL http://doi.wiley.com/10.1029/2009GL037363, 2009.

Alexander, B.: Sulfate formation in sea-salt aerosols: Constraints from oxygen isotopes, J. Geophys. Res., 110, D10 307, doi:10.1029/2004JD005659, 2005.

Alexander, B., Allman, D. J., Amos, H. M., Fairlie, T. D., Dachs, J., Hegg, D. A., and Sletten, R. S.: Isotopic constraints on the formation pathways of sulfate aerosol in the marine boundary layer of the subtropical northeast Atlantic Ocean, J. Geophys. Res., 117, D06 304, doi:10.1029/2011JD016773, 2012.

Alicke, B., Hebestreit, K., Stutz, J., and Platt, U.: Iodine oxide in the marine boundary layer, Nature, 397, 572–573, doi:http://www.nature.com/nature/journal/v397/n6720/suppinfo/397572b0_S1.html, 1999.

Allan, J. D., Williams, P. I., Najera, J., Whitehead, J. D., Flynn, M. J., Taylor, J. W., Liu, D., Darbyshire, E., Carpenter, L. J., Chance, R., Andrews, S. J., Hackenberg, S. C., and McFiggans, G.: Iodine observed in new particle formation events in the

Arctic atmosphere during ACCACIA, Atmospheric Chemistry and Physics, 15, 5599–5609, doi:10.5194/acp-15-5599-2015, URL http://www.atmos-chem-phys.net/15/5599/2015/, 2015.

Allan, W., Struthers, H., and Lowe, D. C.: Methane carbon isotope effects caused by atomic chlorine in the marine boundary layer: Global model results compared with Southern Hemisphere measurements, J Geophys. Res-Atmos., 112, doi:10.1029/2006JD007369, 2007.

Ammann, M., Cox, R. A., Crowley, J. N., Jenkin, M. E., Mellouki, A., Rossi, M. J., Troe, J., and Wallington, T. J.: Evaluated kinetic and photochemical data for atmospheric chemistry: Volume VI heterogeneous reactions with liquid substrates, Atmos. Chem. Phys., 13, 8045–8228, doi:10.5194/acp-13-8045-2013, 2013.

Amos, H. M., Jacob, D. J., Holmes, C. D., Fisher, J. A., Wang, Q., Yantosca, R. M., Corbitt, E. S., Galarneau, E., Rutter, A. P., Gustin, M. S., Steffen, A., Schauer, J. J., Graydon, J. A., Louis, V. L. S., Talbot, R. W., Edgerton, E. S., Zhang, Y., and Sunderland, E. M.: Gas-particle partitioning of atmospheric Hg(II) and its effect on global mercury deposition, Atmos. Chem. Phys., 12, 591–603, doi:10.5194/acp-12-591-2012, 2012.

Andersson, M., Karumbunathan, V., and Zimmermann, M. B.: Global iodine status in 2011 and trends over the past decade., The Journal of nutrition, 142, 744–50, doi:10.3945/jn.111.149393, URL http://jn.nutrition.org/cgi/content/long/jn.111.149393v1, 2012.

Andrews, S. J., Jones, C. E., and Carpenter, L. J.: Aircraft measurements of very short-lived halocarbons over the tropical Atlantic Ocean, Geophys. Res. Lett., 40, 1005–1010, doi:10.1002/grl.50141, 2013.

Andrews, S. J., Hackenberg, S. C., and Carpenter, L. J.: Technical Note: A fully automated purge and trap GC-MS system for quantification of volatile organic compound (VOC) fluxes between the ocean and atmosphere, Ocean Science, 11, 313–321, doi:10.5194/os-11-313-2015, 2015.

Atkinson, R.: Atmospheric chemistry of {VOCs} and {NOx}, Atmos. Environ., 34, 2063–2101, doi:http://dx.doi.org/10.1016/S1352-2310(99)00460-4, 2000.

Atkinson, R., Baulch, D. L., Cox, R. A., Hampson, R. F., Kerr, J. A., Rossi, M. J., and Troe, J.: Evaluated kinetic and photochemical data for atmospheric chemistry: Supplement VIII, halogen species - IUPAC Subcommittee on Gas Kinetic Data Evaluation for Atmospheric Chemistry, J. Phys. Chem. Ref. Data, 29, 167–266, doi:10.1063/1.556058, 2000.

Atkinson, R., Baulch, D. L., Cox, R. A., Crowley, J. N., Hampson, R. F., Hynes, R. G., Jenkin, M. E., Rossi, M. J., Troe, J., and IUPAC Subcommittee: Evaluated kinetic and photochemical data for atmospheric chemistry: Volume II – gas phase reactions of organic species, Atmos. Chem. Phys., 6, 3625–4055, doi:10.5194/acp-6-3625-2006, 2006.

Atkinson, R., Baulch, D. L., Cox, R. A., Crowley, J. N., Hampson, R. F., Hynes, R. G., Jenkin, M. E., Rossi, M. J., and Troe, J.: Evaluated kinetic and photochemical data for atmospheric chemistry: Volume III - gas phase reactions of inorganic halogens, Atmos. Chem. Phys., 7, 981–1191, 2007.

Atkinson, R., Baulch, D. L., Cox, R. A., Crowley, J. N., Hampson, R. F., Hynes, R. G., Jenkin, M. E., Rossi, M. J., Troe, J., and Wallington, T. J.: Evaluated kinetic and photochemical data for atmospheric chemistry: Volume IV - gas phase reactions of organic halogen species, J. Phys. Chem. Ref. Data, 8, 4141–4496, 2008.

Baker, A. R.: Inorganic iodine speciation in tropical Atlantic aerosol, Geophysical Research Letters, 31, L23S02, doi:10.1029/2004GL020144, URL http://dx.doi.org/10.1029/2004GL020144, 2004.

Baker, A. R.: Marine aerosol iodine chemistry: The importance of soluble organic iodine, Environ. Chem., 2, 295–298, doi:10.1071/en05070, 2005.

Baker, A. R., Tunnicliffe C., and Jickells T. D.: Iodine speciation and deposition fluxes from the marine atmosphere, Journal of Geophysical Research, 106, 28 743–28 749, 2001.

Bannan, T. J., Booth, A. M., Bacak, A., Muller, J. B. A., Leather, K. E., Le Breton, M., Jones, B., Young, D., Coe, H., Allan, J., Visser, S., Slowik, J. G., Furger, M., Prévôt, A. S. H., Lee, J., Dunmore, R. E., Hopkins, J. R., Hamilton, J. F., Lewis, A. C., Whalley, L. K., Sharp, T., Stone, D., Heard, D. E., Fleming, Z. L., Leigh, R., Shallcross, D. E., and Percival, C. J.: The first UK measurements of nitryl chloride

using a chemical ionization mass spectrometer in central London in the summer of 2012, and an investigation of the role of Cl atom oxidation, J Geophys. Res-Atmos., 120, 5638–5657, doi:10.1002/2014JD022629, 2015.

Barrie, L. A., Bottenheim, J. W., Schnell, R. C., Crutzen, P. J., and Rasmussen, R. A.: Ozone destruction and photochemical reactions at polar sunrise in the lower Arctic atmosphere, Nature, 334, 138–141, 1988.

Beckwith, R. C., Wang, T. X., and Margerum, D. W.: Equilibrium and Kinetics of Bromine Hydrolysis, Inorg. Chem., 35, 995–1000, doi:10.1021/ic950909w, 1996.

Bedjanian, Y., Le Bras, G., and Poulet, G.: Kinetic study of the Br + IO, I + BrO and Br + I2 reactions. Heat of formation of the BrO radical, Chem. Phys. lett., 266, 233–238, doi:http://dx.doi.org/10.1016/S0009-2614(97)01530-3, 1997.

Bell, N., Hsu, L., Jacob, D. J., Schultz, M. G., Blake, D. R., Butler, J. H., King, D. B., Lobert, J. M., and Maier-Reimer, E.: Methyl iodide: Atmospheric budget and use as a tracer of marine convection in global models, J. Geophys. Res-Atmos., 107, ACH 8–1–ACH 8–12, doi:10.1029/2001jd001151, 2002.

Bell, R. P.: The Proton in Chemistry. 2nd ed., Cornell University Press, Ithaca, NY, 2nd edn., 1973.

Benkovitz, C. M., Scholtz, M. T., Pacyna, J., Tarrasón, L., Dignon, J., Voldner, E. C., Spiro, P. A., Logan, J. A., and Graedel, T. E.: Global gridded inventories of anthropogenic emissions of sulfur and nitrogen, Journal of Geophysical Research: Atmospheres, 101, 29 239–29 253, doi:10.1029/96JD00126, URL http://doi.wiley.com/10.1029/96JD00126, 1996.

Bertram, T. H. and Thornton, J. A.: Toward a general parameterization of N2O5 reactivity on aqueous particles: the competing effects of particle liquid water, nitrate and chloride, Atmos. Chem. Phys., 9, 8351–8363, doi:10.5194/acp-9-8351-2009, 2009.

Bey, I., Jacob, D. J., Yantosca, R. M., Logan, J. A., Field, B. D., Fiore, A. M., Li, Q., Liu, H. Y., Mickley, L. J., and Schultz, M. G.: Global modeling of tropospheric chemistry with assimilated meteorology: Model description and evaluation, J. Geophys. Res., 106, 23 073–23 095, doi:10.1029/2001JD000807, 2001.

Bian, H. S. and Prather, M. J.: Fast-J2: Accurate simulation of stratospheric photolysis in global chemical models, Journal of Atmospheric Chemistry, 41, 281–296, doi:10.1023/a:1014980619462, 2002.

Bloss, W. J., Rowley, D. M., Cox, R. A., and Jones, R. L.: Kinetics and Products of the IO Self-Reaction, J. Phys. Chem. A, 105, 7840–7854, doi:10.1021/jp0044936, 2001.

Bloss, W. J., Evans, M. J., Lee, J. D., Sommariva, R., Heard, D. E., and Pilling, M. J.: The oxidative capacity of the troposphere: Coupling of field measurements of OH and a global chemistry transport model, Faraday Discuss., 130, 425–436, doi:10.1039/b419090d, 2005a.

Bloss, W. J., Lee, J. D., Johnson, G. P., Sommariva, R., Heard, D. E., Saiz-Lopez, A., Plane, J. M. C., McFiggans, G., Coe, H., Flynn, M., Williams, P., Rickard, A. R., and Fleming, L., Z.: Impact of halogen monoxide chemistry upon boundary layer OH and HO 2 concentrations at a coastal site, Geophys. Res. Lett., 32, L06 814, doi:10.1029/2004GL022084, 2005b.

Bloss, W. J., Camredon, M., Lee, J. D., Heard, D. E., Plane, J. M. C., Saiz-Lopez, A., Bauguitte, S. J. B., Salmon, R. A., and Jones, A. E.: Coupling of HOx, NOx and halogen chemistry in the antarctic boundary layer, Atmos. Chem. Phys., 10, 10 187–10 209, doi:10.5194/acp-10-10187-2010, 2010.

Bond, T. C., Bhardwaj, E., Dong, R., Jogani, R., Jung, S., Roden, C., Streets, D. G., and Trautmann, N. M.: Historical emissions of black and organic carbon aerosol from energy-related combustion, 1850-2000, Global Biogeochemical Cycles, 21, n/a–n/a, doi:10.1029/2006GB002840, URL http://doi.wiley.com/10.1029/2006GB002840, 2007.

Bowley, H. E.: IODINE DYNAMICS IN THE TERRESTRIAL ENVIRONMENT, Ph.D. thesis, University of Nottingham, 2013.

Braban, C. F., Adams, J. W., Rodriguez, D., Cox, R. A., Crowley, J. N., and Schuster, G.: Heterogeneous reactions of HOI, ICl and IBr on sea salt and sea salt proxies, Phys. Chem. Chem. Phys., 9, 3136–3148, doi:10.1039/b700829e, 2007.

Brasseur, G. P. and Jacob, D. J.: Modeling of Atmospheric Chemistry, 2016.

Breider, T. J.: Coupled Halogen-Sulfur-Aerosol Modelling in a 3D Chemical Transport Model, Ph.D. thesis, Univeristy of Leeds, 2010.

Burkholder, J. B., Curtius, J., Ravishankara, A. R., and Lovejoy, E. R.: Laboratory studies of the homogeneous nucleation of iodine oxides, Atmos. Chem. Phys., 4, 19–34, doi:10.5194/acp-4-19-2004, 2004.

Butz, A., Bösch, H., Camy-Peyret, C., Chipperfield, M. P., Dorf, M., Kreycy, S., Kritten, L., Prados-Román, C., Schwärzle, J., and Pfeilsticker, K.: Constraints on inorganic gaseous iodine in the tropical upper troposphere and stratosphere inferred from balloon-borne solar occultation observations, Atmos. Chem. Phys., 9, 7229–7242, doi:10.5194/acp-9-7229-2009, 2009.

Carpenter, L. J.: Iodine in the marine boundary layer, Chem. Rev., 103, 4953–4962, doi:10.1021/cr0206465, 2003.

Carpenter, L. J., Fleming, Z. L., Read, K. A., Lee, J. D., Moller, S. J., Hopkins, J. R., Purvis, R. M., Lewis, A. C., Muller, K., Heinold, B., Herrmann, H., Fomba, K. W., van Pinxteren, D., Muller, C., Tegen, I., Wiedensohler, A., Muller, T., Niedermeier, N., Achterberg, E. P., Patey, M. D., Kozlova, E. A., Heimann, M., Heard, D. E., Plane, J. M. C., Mahajan, A., Oetjen, H., Ingham, T., Stone, D., Whalley, L. K., Evans, M. J., Pilling, M. J., Leigh, R. J., Monks, P. S., Karunaharan, A., Vaughan, S., Arnold, S. R., Tschritter, J., Pohler, D., Friess, U., Holla, R., Mendes, L. M., Lopez, H., Faria, B., Manning, A. J., and Wallace, D. W. R.: Seasonal characteristics of tropical marine boundary layer air measured at the Cape Verde Atmospheric Observatory, J. Atmos. Chem., 67, 87–140, doi:10.1007/s10874-011-9206-1, 2010.

Carpenter, L. J., MacDonald, S. M., Shaw, M. D., Kumar, R., Saunders, R. W., Parthipan, R., Wilson, J., and Plane, J. M. C.: Atmospheric iodine levels influenced by sea surface emissions of inorganic iodine, Nature Geosci., 6, 108–111, doi:10.1038/ngeo1687, 2013.

Carpenter, L. J., Andrews, S. J., Lidster, R. T., Saiz-Lopez, A., Fernandez-Sanchez, M., Bloss, W. J., Ouyang, B., and Jones, R. L.: A nocturnal atmospheric loss of CH2I2 in the remote marine boundary layer, Journal of Atmospheric Chemistry, pp. 1–12, doi:10.1007/s10874-015-9320-6, URL http://dx.doi.org/10.1007/s10874-015-9320-6, 2015.

Carslaw, K. S., Lee, L. A., Reddington, C. L., Pringle, K. J., Rap, A., Forster, P. M., Mann, G. W., Spracklen, D. V., Woodhouse, M. T., Regayre, L. A., and Pierce, J. R.: Large contribution of natural aerosols to uncertainty in indirect forcing, Nature, 503, 67–71, URL http://dx.doi.org/10.1038/nature12674http://10.1038/nature12674, 2013.

Chameides, W. L. and Davis, D. D.: Iodine: Its possible role in tropospheric photochemistry, J Geophys. Res-Oceans, 85, 7383–7398, doi:10.1029/JC085iC12p07383, 1980.

Chance, R., Baker, A. R., Carpenter, L., and Jickells, T. D.: The distribution of iodide at the sea surface, Environ. Sci.: Processes Impacts, 16, 1841–1859, doi: 10.1039/C4EM00139G, 2014.

Chance, R., Jickells, T. D., and Baker, A. R.: Atmospheric trace metal concentrations, solubility and deposition fluxes in remote marine air over the south-east Atlantic, Marine Chemistry, 177, Part, 45–56, doi:http://dx.doi.org/10.1016/j.marchem.2015.06.028, 2015.

Chang, W., Heikes, B. G., and Lee, M.: Ozone deposition to the sea surface: chemical enhancement and wind speed dependence, Atmospheric Environment, 38, 1053–1059, doi:10.1016/j.atmosenv.2003.10.050, 2004.

Chen, Q., Geng, L., Schmidt, J. A., Xie, Z., Kang, H., Dachs, J., Cole-Dai, J., Schauer, A. J., Camp, M. G., and Alexander, B.: Isotopic constraints on the role of hypohalous acids in sulfate aerosol formation in the remote marine boundary layer, Atmospheric Chemistry and Physics Discussions, pp. 1–29, doi:doi:10.5194/acp-2016-395, URL http://www.atmos-chem-phys-discuss.net/acp-2016-395/, 2016.

Chuck, A. L., Turner, S. M., and Liss, P. S.: Oceanic distributions and air-sea fluxes of biogenic halocarbons in the open ocean, J Geophys. Res-Oceans, 110, C10 022, doi: 10.1029/2004jc002741, 2005.

Coburn, S., Ortega, I., Thalman, R., Blomquist, B., Fairall, C. W., and Volkamer, R.: Measurements of diurnal variations and eddy covariance (EC) fluxes of glyoxal in the tropical marine boundary layer: description of the Fast LED-CE-DOAS instrument, Atmospheric Measurement Techniques, 7, 3579–3595, doi:10.5194/amt-7-3579-2014, 2014.

Coburn, S., Dix, B., Edgerton, E., Holmes, C. D., Kinnison, D., Liang, Q., terSchure, A., Wang, S., and Volkamer, R.: Mercury oxidation from bromine chemistry in the free troposphere over the southeasternUS, Atmospheric Chemistry and Physics, 16, 3743–3760, doi:10.5194/acp-16-3743-2016, URL http://www.atmos-chem-phys.net/16/3743/2016/acp-16-3743-2016.html, 2016.

Collins, W., Stevenson, D., Johnson, C., and Derwent, R.: The European regional ozone distribution and its links with the global scale for the years 1992 and 2015, Atmospheric Environment, 34, 255–267, doi:10.1016/S1352-2310(99)00226-5, 2000.

Crowley, J. N., Ammann, M., Cox, R. A., Hynes, R. G., Jenkin, M. E., Mellouki, A., Rossi, M. J., Troe, J., and Wallington, T. J.: Evaluated kinetic and photochemical data for atmospheric chemistry: Volume V heterogeneous reactions on solid substrates, Atmos. Chem. Phys., 10, 9059–9223, doi:10.5194/acp-10-9059-2010, 2010.

Dean, J. A.: Lange's Handbook of Chemistry, McGraw-Hill, Inc., 1992.

Deiber, G., George, C., Le Calvé, S., Schweitzer, F., and Mirabel, P.: Uptake study of ClONO2 and BrONO2 by Halide containing droplets, Atmos. Chem. Phys., 4, 1291–1299, doi:10.5194/acp-4-1291-2004, 2004.

Dix, B., Baidar, S., Bresch, J., Hall, S., Schmidt, K., Wang, S.-Y., and Volkamer, R.: Detection of iodine monoxide in the tropical free troposphere, Proc. Natl. Acad. Sci. U.S.A., 110, 2035–2040, doi:10.1073/pnas.1212386110, 2013.

Duce, R. A. and Hoffman, E. J.: CHEMICAL FRACTIONATION AT AIR-SEA INTERFACE, Annual Review of Earth and Planetary Sciences, 4, 187–228, doi:10.1146/annurev.ea.04.050176.001155, 1976.

Eastham, S. D., Weisenstein, D. K., and Barrett, S. R. H.: Development and evaluation of the unified tropospherichcstratospheric chemistry extension (UCX) for the global chemistry-transport model GEOS-Chem, Atmos. Environ., 89, 52–63, doi:http://dx.doi.org/10.1016/j.atmosenv.2014.02.001, 2014.

Evans, M. J. and Jacob, D. J.: Impact of new laboratory studies of N2O5 hydrolysis on global model budgets of tropospheric nitrogen oxides, ozone, and OH, Geophys. Res. Lett., 32, L09 813, doi:10.1029/2005GL022469, 2005.

Fairlie, D. T., Jacob, D. J., and J.Park, R.: The impact of transpacific transport of mineral dust in the United States, Atmospheric Environment, 41, 1251–1266, doi:10.1016/j.atmosenv.2006.09.048, 2007.

Fairlie, T. D., Jacob, D. J., Dibb, J. E., Alexander, B., Avery, M. A., van Donkelaar, A., and Zhang, L.: Impact of mineral dust on nitrate, sulfate, and ozone in

transpacific Asian pollution plumes, Atmospheric Chemistry and Physics, 10, 3999–4012, doi:10.5194/acp-10-3999-2010, URL http://www.atmos-chem-phys.net/10/3999/2010/acp-10-3999-2010.html, 2010.

Faxon, C. B., Bean, J. K., and Ruiz, L. H.: Inland Concentrations of Cl2 and ClNO2 in Southeast Texas Suggest Chlorine Chemistry Significantly Contributes to Atmospheric Reactivity, Atmosphere, 6, 1487, doi:10.3390/atmos6101487, 2015.

Fernandez, R. P., Salawitch, R. J., Kinnison, D. E., Lamarque, J.-F., and Saiz-Lopez, A.: Bromine partitioning in the tropical tropopause layer: implications for stratospheric injection, Atmospheric Chemistry and Physics, 14, 13 391–13 410, doi:10.5194/acp-14-13391-2014, 2014.

Finlayson-Pitts, B. J. and Pitts, J. N.: Tropospheric Air Pollution: Ozone, Airborne Toxics, Polycyclic Aromatic Hydrocarbons, and Particles, Science, 276, 1045–1051, doi:10.1126/science.276.5315.1045, URL http://science.sciencemag.org/content/276/5315/1045, 1997.

Fiore, A. M., Naik, V., Spracklen, D. V., Steiner, A., Unger, N., Prather, M., Bergmann, D., Cameron-Smith, P. J., Cionni, I., Collins, W. J., Dalsoren, S., Eyring, V., Folberth, G. A., Ginoux, P., Horowitz, L. W., Josse, B., Lamarque, J.-F., MacKenzie, I. A., Nagashima, T., O'Connor, F. M., Righi, M., Rumbold, S. T., Shindell, D. T., Skeie, R. B., Sudo, K., Szopa, S., Takemura, T., and Zeng, G.: Global air quality and climate, Chem. Soc. Rev., 41, 6663–6683, doi:10.1039/C2CS35095E, URL http://dx.doi.org/10.1039/C2CS35095E, 2012.

Fitzgerald, J. W.: Marine aerosols: A review, Atmospheric Environment. Part A. General Topics, 25, 533–545, doi:10.1016/0960-1686(91)90050-H, URL http://www.sciencedirect.com/science/article/pii/096016869190050H, 1991.

Fowler, D., Amann, M., Anderson, R., Ashmore, M., Cox, P., Depledge, M., Derwent, D., Grennfelt, P., Hewitt, N., Hov, O., Jenkin, M., Kelly, F., Liss, P., Pilling, M., Pyle, J., Slingo, J., and Stevenson, D.: Ground-level ozone in the 21st century: future trends, impacts and policy implications, Tech. rep., The Royal Society, 2008.

Frenzel, A., Scheer, V., Sikorski, R., George, C., Behnke, W., and Zetzsch, C.: Heterogeneous Interconversion Reactions of BrNO2, ClNO2, Br2, and Cl2, J. Phys. Chem. A, 102, 1329–1337, doi:10.1021/jp973044b, 1998.

Froidevaux, L., Jiang, Y. B., Lambert, A., Livesey, N. J., Read, W. G., Waters, J. W., Fuller, R. A., Marcy, T. P., Popp, P. J., Gao, R. S., Fahey, D. W., Jucks, K. W., Stachnik, R. A., Toon, G. C., Christensen, L. E., Webster, C. R., Bernath, P. F., Boone, C. D., Walker, K. A., Pumphrey, H. C., Harwood, R. S., Manney, G. L., Schwartz, M. J., Daffer, W. H., Drouin, B. J., Cofield, R. E., Cuddy, D. T., Jarnot, R. F., Knosp, B. W., Perun, V. S., Snyder, W. V., Stek, P. C., Thurstans, R. P., and Wagner, P. A.: Validation of Aura Microwave Limb Sounder HCl measurements, Journal of Geophysical Research: Atmospheres, 113, doi:10.1029/2007JD009025, 2008.

Fuge, R.: Iodine Deficiency: An Ancient Problem in a Modern World, AMBIO: A Journal of the Human Environment, 36, 70–72, doi:10.1579/0044-7447(2007)36[70:IDAAPI]2.0.CO;2, URL http://dx.doi.org/10.1579/0044-7447(2007)36[70:IDAAPI]2.0.COhttp://2, 2007.

Fuge, R. and Johnson, C. C.: The geochemistry of iodine — a review, Environmental Geochemistry and Health, 8, 31–54, doi:10.1007/BF02311063, URL http://dx.doi.org/10.1007/BF02311063, 1986.

Ganzeveld, L., Helmig, D., Fairall, C. W., Hare, J., and Pozzer, A.: Atmosphere-ocean ozone exchange: A global modeling study of biogeochemical, atmospheric, and waterside turbulence dependencies, Global Biogeochem. Cycles, 23, GB4021, doi:10.1029/2008GB003301, 2009.

Garland, J. A. and Curtis, H.: Emission of Iodine From the Sea Surface in the Presence of Ozone, J. Geophys. Res., 86, 3183–3186, doi:10.1029/JC086iC04p03183, URL http://dx.doi.org/10.1029/JC086iC04p03183, 1981.

GAW: Global Atmosphere Watch (GAW) Ozone Monitoring Community, World Meteorological Organization-Global Atmosphere Watch Program (WMO-GAW) [Data]., URL http://gaw.empa.ch/gawsis/, 2014.

Gilfedder, B. S., Chance, R., Dettmann, U., Lai, S. C., and Baker, A. R.: Determination of total and non-water soluble iodine in atmospheric aerosols by thermal extraction and spectrometric detection (TESI), Analytical and Bioanalytical Chemistry, 398, 519–526, doi:10.1007/s00216-010-3923-1, URL http://dx.doi.org/10.1007/s00216-010-3923-1, 2010.

Glasius, M. and Goldstein, A. H.: Recent Discoveries and Future Challenges in Atmospheric Organic Chemistry, Environmental Science & Technology, 50, 2754–2764, doi: 10.1021/acs.est.5b05105, 2016.

Gómez Martín, J. C., Spietz, P., and Burrows, J. P.: Spectroscopic studies of the I2/O3 photochemistry: Part 1: Determination of the absolute absorption cross sections of iodine oxides of atmospheric relevance, J Photoch. Photobio. A, 176, 15–38, doi:http: //dx.doi.org/10.1016/j.jphotochem.2005.09.024, 2005.

Gómez Martín, J. C., Spietz, P., and Burrows, J. P.: Kinetic and Mechanistic Studies of the I2/O3 Photochemistry, J. Phys. Chem. A, 111, 306–320, doi:10.1021/jp061186c, 2007.

Gómez Martín, J. C., Ashworth, S. H., Mahajan, A. S., and Plane, J. M. C.: Photochemistry of OIO: Laboratory study and atmospheric implications, Geophys. Res. Lett., 36, L09 802, doi:10.1029/2009GL037642, 2009.

Gómez Martín, J. C., Galvez, O., Baeza-Romero, M. T., Ingham, T., Plane, J. M. C., and Blitz, M. A.: On the mechanism of iodine oxide particle formation, Phys. Chem. Chem. Phys., 15, 15 612–15 622, doi:10.1039/C3CP51217G, 2013a.

Gómez Martín, J. C., Mahajan, A. S., Hay, T. D., Prados-Roman, C., Ordonez, C., MacDonald, S. M., Plane, J. M. C., Sorribas, M., Gil, M., Mora, J. F. P., Reyes, M. V. A., Oram, D. E., Leedham, E., and Saiz-Lopez, A.: Iodine chemistry in the eastern Pacific marine boundary layer, J. Geophys. Res-Atmos., 118, 887–904, doi: 10.1002/jgrd.50132, 2013b.

Großmann, K., Frieß, U., Peters, E., Wittrock, F., Lampel, J., Yilmaz, S., Tschritter, J., Sommariva, R., von Glasow, R., Quack, B., Krüger, K., Pfeilsticker, K., and Platt, U.: Iodine monoxide in the Western Pacific marine boundary layer, Atmos. Chem. Phys., 13, 3363–3378, doi:10.5194/acp-13-3363-2013, 2013.

Guenther, A. B., Jiang, X., Heald, C. L., Sakulyanontvittaya, T., Duhl, T., Emmons, L. K., and Wang, X.: The Model of Emissions of Gases and Aerosols from Nature version 2.1 (MEGAN2.1): an extended and updated framework for modeling biogenic emissions, Geoscientific Model Development, 5, 1471–1492, doi:10.5194/gmd-5-1471-2012, URL http://www.geosci-model-dev.net/5/1471/2012/, 2012.

Hardacre, C., Wild, O., and Emberson, L.: An evaluation of ozone dry deposition in global scale chemistry climate models, Atmospheric Chemistry and Physics, 15, 6419–6436, doi:10.5194/acp-15-6419-2015, URL http://www.atmos-chem-phys.net/15/6419/2015/, 2015.

Hauglustaine, D. A., Granier, C., Brasseur, G. P., and Mégie, G.: The importance of atmospheric chemistry in the calculation of radiative forcing on the climate system, J Geophys. Res-Atmos., 99, 1173–1186, doi:10.1029/93JD02987, 1994.

Hayase, S., Yabushita, A., Kawasaki, M., Enami, S., Hoffmann, M. R., and Colussi, A. J.: Heterogeneous Reaction of Gaseous Ozone with Aqueous Iodide in the Presence of Aqueous Organic Species, J Phys. Chem. A, 114, 6016–6021, doi:10.1021/jp101985f, URL http://dx.doi.org/10.1021/jp101985f, 2010.

Holmes, C. D., Jacob, D. J., Mason, R. P., and Jaffe, D. A.: Sources and deposition of reactive gaseous mercury in the marine atmosphere, Atmospheric Environment, 43, 2278–2285, doi:10.1016/j.atmosenv.2009.01.051, 2009.

Holmes, C. D., Jacob, D. J., Corbitt, E. S., Mao, J., Yang, X., Talbot, R., and Slemr, F.: Global atmospheric model for mercury including oxidation by bromine atoms, Atmos. Chem. Phys., 10, 12 037–12 057, doi:10.5194/acp-10-12037-2010, 2010.

Hudman, R. C., Moore, N. E., Mebust, A. K., Martin, R. V., Russell, A. R., Valin, L. C., and Cohen, R. C.: Steps towards a mechanistic model of global soil nitric oxide emissions: implementation and space based-constraints, Atmospheric Chemistry and Physics, 12, 7779–7795, doi:10.5194/acp-12-7779-2012, URL http://www.atmos-chem-phys.net/12/7779/2012/, 2012.

J Risher, L. K.: IODINE AND INORGANIC IODIDES:HUMAN HEALTH ASPECTS, Tech. rep., World Health Organisation, 2009.

Jacob, D. J.: Heterogeneous chemistry and tropospheric ozone, Atmos. Environ., 34, 2131–2159, doi:http://dx.doi.org/10.1016/S1352-2310(99)00462-8, 2000.

Jacob, D. J., Wofsy, S. C., Bakwin, P. S., Fan, S.-M., Harriss, R. C., Talbot, R. W., Bradshaw, J. D., Sandholm, S. T., Singh, H. B., Browell, E. V., Gregory, G. L., Sachse, G. W., Shipham, M. C., Blake, D. R., and Fitzjarrald, D. R.: Summertime photochem-

istry of the troposphere at high northern latitudes, Journal of Geophysical Research: Atmospheres, 97, 16 421–16 431, doi:10.1029/91JD01968, 1992.

Jacobson, M. Z. and Turco, R. P.: SMVGEAR: A sparse-matrix, vectorized gear code for atmospheric models, Atmospheric Environment, 28, 273–284, doi:http://dx.doi.org/10.1016/1352-2310(94)90102-3, 1994.

Jaeglé, L., Quinn, P. K., Bates, T. S., Alexander, B., and Lin, J. T.: Global distribution of sea salt aerosols: new constraints from in situ and remote sensing observations, Atmos. Chem. Phys., 11, 3137–3157, doi:10.5194/acp-11-3137-2011, 2011.

Janssens-Maenhout, G., Petrescu, A. M., Muntean, M., and Blujdea, V.: Verifying Greenhouse Gas Emissions: Methods to Support International Climate Agreements, Greenhouse Gas Measurement and Management, 1, 132–133, doi:10.1080/20430779.2011.579358, 2011.

Johnson, C. C.: Database of the iodine content of soils populated with data from published literature - Commissioned Report CR/03/004N, Tech. rep., British Geological Survey, 2003a.

Johnson, C. C.: The geochemistry of iodine and its application to environmental strategies for reducing the risks from iodine deficiency disorders (IDD), Tech. rep., British Geological Survey, 2003b.

Johnson, C. C., Fordyce, F. M., and Stewart, A. G.: Environmental Controls In Iodine Deficiency Disorders - Commissioned Report CR/03/058N., Tech. rep., British Geological Survey, 2003.

Jones, C. E., Hornsby, K. E., Sommariva, R., Dunk, R. M., Von Glasow, R., McFiggans, G., and Carpenter, L. J.: Quantifying the contribution of marine organic gases to atmospheric iodine, Geophys. Res. Lett., 37, L18 804, doi:10.1029/2010gl043990, 2010.

Kaltsoyannis, N. and Plane, J. M. C.: Quantum chemical calculations on a selection of iodine-containing species (IO, OIO, INO3, (IO)2, I2O3, I2O4 and I2O5) of importance in the atmosphere, Phys. Chem. Chem. Phys., 10, 1723–1733, 2008.

Keene, W. C., Long, M. S., Pszenny, A. A. P., Sander, R., Maben, J. R., Wall, A. J., O'Halloran, T. L., Kerkweg, A., Fischer, E. V., and Schrems, O.: Latitudinal variation in the multiphase chemical processing of inorganic halogens and related species over

the eastern North and South Atlantic Oceans, Atmospheric Chemistry and Physics, 9, 7361–7385, doi:10.5194/acp-9-7361-2009, 2009.

Keller, C. A., Long, M. S., Yantosca, R. M., Da Silva, A. M., Pawson, S., and Jacob, D. J.: HEMCO v1.0: a versatile, ESMF-compliant component for calculating emissions in atmospheric models, Geoscientific Model Development, 7, 1409–1417, doi:10.5194/gmd-7-1409-2014, 2014.

Kettle, A. J., Andreae, M. O., Amouroux, D., Andreae, T. W., Bates, T. S., Berresheim, H., Bingemer, H., Boniforti, R., Curran, M. A. J., DiTullio, G. R., Helas, G., Jones, G. B., Keller, M. D., Kiene, R. P., Leck, C., Levasseur, M., Malin, G., Maspero, M., Matrai, P., McTaggart, A. R., Mihalopoulos, N., Nguyen, B. C., Novo, A., Putaud, J. P., Rapsomanikis, S., Roberts, G., Schebeske, G., Sharma, S., Simó, R., Staubes, R., Turner, S., and Uher, G.: A global database of sea surface dimethylsulfide (DMS) measurements and a procedure to predict sea surface DMS as a function of latitude, longitude, and month, Global Biogeochemical Cycles, 13, 399–444, doi:10.1029/1999GB900004, URL http://dx.doi.org/10.1029/1999GB900004, 1999.

Kim, K.-H., Shon, Z.-H., Nguyen, H. T., and Jeon, E.-C.: A review of major chlorofluorocarbons and their halocarbon alternatives in the air, Atmos. Environ., 45, 1369–1382, doi:http://dx.doi.org/10.1016/j.atmosenv.2010.12.029, 2011.

King, K. D., Golden, D. M., and Benson, S. W.: Kinetics of the gas-phase thermal bromination of acetone. Heat of formation and stabilization energy of the acetonyl radical, J. Am. Chem. Soc, 92, 5541–5546, doi:10.1021/ja00722a001, 1970.

Knipping, E. M. and Dabdub, D.: Impact of Chlorine Emissions from Sea-Salt Aerosol on Coastal Urban Ozone, Environmental Science & Technology, 37, 275–284, doi:10.1021/es025793z, URL http://dx.doi.org/10.1021/es025793z, 2003.

Koch, D., Bauer, S. E., Genio, A. D., Faluvegi, G., McConnell, J. R., Menon, S., Miller, R. L., Rind, D., Ruedy, R., Schmidt, G. A., and Shindell, D.: Coupled Aerosol-ChemistryClimate Twentieth-Century Transient Model Investigation: Trends in Short-Lived Species and Climate Responses, Journal of Climate, 24, 2693–2714, doi:10.1175/2011JCLI3582.1, URL http://dx.doi.org/10.1175/2011JCLI3582.1, 2011.

Kocher, D.: A dynamic model of the global iodine cycle and estimation of dose to the world population from releases of iodine-129 to the environment, Environment Inter-

national, 5, 15–31, doi:10.1016/0160-4120(81)90110-0, URL http://linkinghub.elsevier.com/retrieve/pii/0160412081901100, 1981.

Krupp, G. and Aumann, D. C.: Iodine-129 in rainfall over Germany, Journal of Environmental Radioactivity, 46, 287–299, doi:10.1016/s0265-931x(98)00148-9, 1999.

Lai, S. C., Hoffmann, T., and Xie, Z. Q.: Iodine speciation in marine aerosols along a 30,000 km round-trip cruise path from Shanghai, China to Prydz Bay, Antarctica, Geophysical Research Letters, 35, L21 803, doi:10.1029/2008GL035492, URL http://dx.doi.org/10.1029/2008GL035492, 2008.

Lamarque, J. F., Hess, P., Emmons, L., Buja, L., Washington, W., and Granier, C.: Tropospheric ozone evolution between 1890 and 1990, J Geophys. Res-Atmos., 110, D08 304, doi:10.1029/2004JD005537, 2005.

Lamarque, J.-F., Bond, T. C., Eyring, V., Granier, C., Heil, A., Klimont, Z., Lee, D., Liousse, C., Mieville, A., Owen, B., Schultz, M. G., Shindell, D., Smith, S. J., Stehfest, E., Van Aardenne, J., Cooper, O. R., Kainuma, M., Mahowald, N., McConnell, J. R., Naik, V., Riahi, K., and van Vuuren, D. P.: Historical (18502000) gridded anthropogenic and biomass burning emissions of reactive gases and aerosols: methodology and application, Atmos. Chem. Phys., 10, 7017–7039, doi:10.5194/acp-10-7017-2010, 2010.

Lamarque, J.-F., Shindell, D. T., Josse, B., Young, P. J., Cionni, I., Eyring, V., Bergmann, D., Cameron-Smith, P., Collins, W. J., Doherty, R., Dalsoren, S., Faluvegi, G., Folberth, G., Ghan, S. J., Horowitz, L. W., Lee, Y. H., MacKenzie, I. A., Nagashima, T., Naik, V., Plummer, D., Righi, M., Rumbold, S. T., Schulz, M., Skeie, R. B., Stevenson, D. S., Strode, S., Sudo, K., Szopa, S., Voulgarakis, A., and Zeng, G.: The Atmospheric Chemistry and Climate Model Intercomparison Project (ACCMIP): overview and description of models, simulations and climate diagnostics, Geoscientific Model Development, 6, 179–206, doi:10.5194/gmd-6-179-2013, 2013.

Landis, J. D., Hamm, N. T., Renshaw, C. E., Dade, W. B., Magilligan, F. J., and Gartner, J. D.: Surficial redistribution of fallout iodine in a small temperate catchment., Proceedings of the National Academy of Sciences of the United States of America, 109, 4064–9, doi:10.1073/pnas.1118665109, URL http://www.pnas.org/cgi/content/long/109/11/4064, 2012.

Lapina, K., Heald, C. L., Spracklen, D. V., Arnold, S. R., Allan, J. D., Coe, H., McFiggans, G., Zorn, S. R., Drewnick, F., Bates, T. S., Hawkins, L. N., Russell, L. M., Smirnov, A., O'Dowd, C. D., and Hind, A. J.: Investigating organic aerosol loading in the remote marine environment, Atmospheric Chemistry and Physics, 11, 8847–8860, doi:10.5194/acp-11-8847-2011, 2011.

Law, K. S. and Sturges, W. T.: Scientific Assessment of Ozone Depletion, 2006 Chapter 2: Halogenated Very Short-Lived Substances, Tech. rep., 2006.

Lawler, M. J., Sander, R., Carpenter, L. J., Lee, J. D., von Glasow, R., Sommariva, R., and Saltzman, E. S.: HOCl and Cl2 observations in marine air, Atmos. Chem. Phys., 11, 7617–7628, doi:10.5194/acp-11-7617-2011, 2011.

Lawler, M. J., Mahajan, A. S., Saiz-Lopez, A., and Saltzman, E. S.: Observations of I2 at a remote marine site, Atmos. Chem. Phys. Discuss., 13, 25 911–25 937, doi:10.5194/acpd-13-25911-2013, 2013.

Lawler, M. J., Mahajan, A. S., Saiz-Lopez, A., and Saltzman, E. S.: Observations of I_{2} at a remote marine site, Atmos. Chem. Phys., 14, 2669–2678, doi:10.5194/acp-14-2669-2014, 2014.

Lawson, S. J., Selleck, P. W., Galbally, I. E., Keywood, M. D., Harvey, M. J., Lerot, C., Helmig, D., and Ristovski, Z.: Seasonal in situ observations of glyoxal and methylglyoxal over the temperate oceans of the Southern Hemisphere, Atmospheric Chemistry and Physics, 15, 223–240, doi:10.5194/acp-15-223-2015, 2015.

Leser, H., Hönninger, G., and Platt, U.: MAX-DOAS measurements of BrO and NO2 in the marine boundary layer, Geophys. Res. Lett., 30, 1537, doi:10.1029/2002GL015811, URL http://dx.doi.org/10.1029/2002GL015811, 2003.

Levy, H.: Normal Atmosphere: Large Radical and Formaldehyde Concentrations Predicted, Science, 173, 141–143, URL http://science.sciencemag.org/content/173/3992/141.abstract, 1971.

Levy, H., Kasibhatla, P. S., Moxim, W. J., Klonecki, A. A., Hirsch, A. I., Oltmans, S. J., and Chameides, W. L.: The global impact of human activity on tropospheric ozone, Geophysical Research Letters, 24, 791–794, doi:10.1029/97GL00599, 1997.

Liang, Q., Stolarski, R. S., Kawa, S. R., Nielsen, J. E., Douglass, A. R., Rodriguez, J. M., Blake, D. R., Atlas, E. L., and Ott, L. E.: Finding the missing stratospheric Bry: a global modeling study of CHBr3 and CH2Br2, Atmos. Chem. Phys., 10, 2269–2286, doi:10.5194/acp-10-2269-2010, 2010.

Liss, P. and Merlivat, L.: Air-Sea Gas Exchange Rates: Introduction and Synthesis, in: The Role of Air-Sea Exchange in Geochemical Cycling SE - 5, edited by Buat-Ménard, P., vol. 185 of *NATO ASI Series*, pp. 113–127, Springer Netherlands, doi: 10.1007/978-94-009-4738-2_5, URL http://dx.doi.org/10.1007/978-94-009-4738-2{_}5, 1986.

Liu, H., Jacob, D. J., Bey, I., and Yantosca, R. M.: Constraints from 210Pb and 7Be on wet deposition and transport in a global three-dimensional chemical tracer model driven by assimilated meteorological fields, Journal of Geophysical Research: Atmospheres, 106, 12 109–12 128, doi:10.1029/2000JD900839, 2001.

Logan, J. A.: Nitrogen oxides in the troposphere: Global and regional budgets, Journal of Geophysical Research: Oceans, 88, 10 785–10 807, doi:10.1029/JC088iC15p10785, URL http://dx.doi.org/10.1029/JC088iC15p10785, 1983.

Logan, J. A.: Tropospheric ozone: Seasonal behavior, trends, and anthropogenic influence, Journal of Geophysical Research: Atmospheres, 90, 10 463–10 482, doi:10.1029/JD090iD06p10463, URL http://doi.wiley.com/10.1029/JD090iD06p10463, 1985.

Long, M. S., Keene, W. C., Easter, R. C., Sander, R., Liu, X., Kerkweg, A., and Erickson, D.: Sensitivity of tropospheric chemical composition to halogen-radical chemistry using a fully coupled size-resolved multiphase chemistryglobal climate system: halogen distributions, aerosol composition, and sensitivity of climate-relevant gases, Atmos. Chem. Phys., 14, 3397–3425, doi:10.5194/acp-14-3397-2014, 2014.

Lovelock, J. E., MAGGS, R. J., and RASMUSSEN, R. A.: Atmospheric Dimethyl Sulphide and the Natural Sulphur Cycle, Nature, 237, 452–453, URL http://dx.doi.org/10.1038/237452a0, 1972.

Lucchesi, R.: No TitleFile Specification for GEOS-5 FP. GMAO Office Note No. 4 (Version 1.0), Tech. rep., 2013.

MacDonald, S. M., Gómez Martín, J. C., Chance, R., Warriner, S., Saiz-Lopez, A., Carpenter, L. J., and Plane, J. M. C.: A laboratory characterisation of inorganic iodine emissions from the sea surface: dependence on oceanic variables and parameterisation for global modelling, Atmos. Chem. Phys., 14, 5841–5852, doi:10.5194/acp-14-5841-2014, 2014.

Mahajan, A. S., Oetjen, H., Saiz-Lopez, A., Lee, J. D., McFiggans, G. B., and Plane, J. M. C.: Reactive iodine species in a semi-polluted environment, Geophys. Res. Lett., 36, L16 803, doi:10.1029/2009GL038018, 2009.

Mahajan, A. S., Plane, J. M. C., Oetjen, H., Mendes, L., Saunders, R. W., Saiz-Lopez, A., Jones, C. E., Carpenter, L. J., and McFiggans, G. B.: Measurement and modelling of tropospheric reactive halogen species over the tropical Atlantic Ocean, Atmos. Chem. Phys., 10, 4611–4624, doi:10.5194/acp-10-4611-2010, 2010.

Mahajan, A. S., Gómez Martín, J. C., Hay, T. D., Royer, S.-J., Yvon-Lewis, S., Liu, Y., Hu, L., Prados-Roman, C., Ordóñez, C., Plane, J. M. C., and Saiz-Lopez, A.: Latitudinal distribution of reactive iodine in the Eastern Pacific and its link to open ocean sources, Atmos. Chem. Phys., 12, 11 609–11 617, doi:10.5194/acp-12-11609-2012, 2012.

Mahajan, A. S., Prados-Roman, C., Hay, T. D., Lampel, J., Pöhler, D., Groβmann, K., Tschritter, J., Frieß, U., Platt, U., Johnston, P., Kreher, K., Wittrock, F., Burrows, J. P., Plane, J. M. C., and Saiz-Lopez, A.: Glyoxal observations in the global marine boundary layer, Journal of Geophysical Research: Atmospheres, 119, 6160–6169, doi: 10.1002/2013JD021388, 2014.

Mao, J., Jacob, D. J., Evans, M. J., Olson, J. R., Ren, X., Brune, W. H., Clair, J. M. S., Crounse, J. D., Spencer, K. M., Beaver, M. R., Wennberg, P. O., Cubison, M. J., Jimenez, J. L., Fried, A., Weibring, P., Walega, J. G., Hall, S. R., Weinheimer, A. J., Cohen, R. C., Chen, G., Crawford, J. H., McNaughton, C., Clarke, A. D., Jaeglé, L., Fisher, J. A., Yantosca, R. M., Le Sager, P., and Carouge, C.: Chemistry of hydrogen oxide radicals (HOx) in the Arctic troposphere in spring, Atmos. Chem. Phys., 10, 5823–5838, doi:10.5194/acp-10-5823-2010, 2010.

Mao, J., Paulot, F., Jacob, D. J., Cohen, R. C., Crounse, J. D., Wennberg, P. O., Keller, C. A., Hudman, R. C., Barkley, M. P., and Horowitz, L. W.: Ozone and organic nitrates

over the eastern United States: Sensitivity to isoprene chemistry, J Geophys. Res-Atmos., 118, 11,256–11,268, doi:10.1002/jgrd.50817, 2013.

Marenco, A., Gouget, H., Nédélec, P., Pagés, J.-P., and Karcher, F.: Evidence of a long-term increase in tropospheric ozone from Pic du Midi data series: Consequences: Positive radiative forcing, Journal of Geophysical Research: Atmospheres, 99, 16 617–16 632, doi:10.1029/94JD00021, 1994.

Martino, M., Mills, G. P., Woeltjen, J., and Liss, P. S.: A new source of volatile organoiodine compounds in surface seawater, Geophys. Res. Lett., 36, L01 609, doi:10.1029/2008GL036334, 2009.

McFiggans, G., Plane, J. M. C., Allan, B. J., Carpenter, L. J., Coe, H., and O'Dowd, C.: A modeling study of iodine chemistry in the marine boundary layer, J Geophys. Res-Atmos., 105, 14 371–14 385, doi:10.1029/1999JD901187, 2000.

McFiggans, G., Cox, R. A., Mossinger, J. C., Allan, B. J., and Plane, J. M. C.: Active chlorine release from marine aerosols: Roles for reactive iodine and nitrogen species, J Geophys. Res-Atmos., 107, doi:10.1029/2001jd000383, 2002.

McFiggans, G., Coe, H., Burgess, R., Allan, J., Cubison, M., Alfarra, M. R., Saunders, R., Saiz-Lopez, A., Plane, J. M. C., Wevill, D., Carpenter, L., Rickard, A. R., and Monks, P. S.: Direct evidence for coastal iodine particles from Laminaria macroalgae linkage to emissions of molecular iodine, Atmospheric Chemistry and Physics, 4, 701–713, doi:10.5194/acp-4-701-2004, URL http://www.atmos-chem-phys.net/4/701/2004/acp-4-701-2004.html?FrameEngine=false, 2004.

McFiggans, G., Bale, C. S. E., Ball, S. M., Beames, J. M., Bloss, W. J., Carpenter, L. J., Dorsey, J., Dunk, R., Flynn, M. J., Furneaux, K. L., Gallagher, M. W., Heard, D. E., Hollingsworth, A. M., Hornsby, K., Ingham, T., Jones, C. E., Jones, R. L., Kramer, L. J., Langridge, J. M., Leblanc, C., LeCrane, J.-P., Lee, J. D., Leigh, R. J., Longley, I., Mahajan, A. S., Monks, P. S., Oetjen, H., Orr-Ewing, A. J., Plane, J. M. C., Potin, P., Shillings, A. J. L., Thomas, F., von Glasow, R., Wada, R., Whalley, L. K., and Whitehead, J. D.: Iodine-mediated coastal particle formation: an overview of the Reactive Halogens in the Marine Boundary Layer (RHaMBLe) Roscoff coastal study, Atmos. Chem. Phys., 10, 2975–2999, doi:10.5194/acp-10-2975-2010, 2010.

McGrath, M. P. and Rowland, F. S.: Ideal Gas Thermodynamic Properties of HOBr, J Phys Chem-US, 98, 4773–4775, doi:10.1021/j100069a001, 1994.

McKenna, D. S.: A new Chemical Lagrangian Model of the Stratosphere (CLaMS) 2. Formulation of chemistry scheme and initialization, J Geophys. Res-Atmos., 107, 4256, doi:10.1029/2000JD000113, URL http://doi.wiley.com/10.1029/2000JD000113, 2002a.

McKenna, D. S.: A new Chemical Lagrangian Model of the Stratosphere (CLaMS) 2. Formulation of chemistry scheme and initialization, Journal of Geophysical Research, 107, 4256, doi:10.1029/2000JD000113, 2002b.

McLinden, C. A., Olsen, S. C., Hannegan, B., Wild, O., Prather, M. J., and Sundet, J.: Stratospheric ozone in 3-D models: A simple chemistry and the cross-tropopause flux, J. Geophys. Res., 105, 14 653, doi:10.1029/2000JD900124, 2000.

Mickley, L. J., Jacob, D. J., and Rind, D.: Uncertainty in preindustrial abundance of tropospheric ozone: Implications for radiative forcing calculations, JOURNAL OF GEOPHYSICAL RESEARCH-ATMOSPHERES, 106, 3389–3399, doi:10.1029/2000JD900594, 2001a.

Mickley, L. J., Jacob, D. J., and Rind, D.: Uncertainty in preindustrial abundance of tropospheric ozone: Implications for radiative forcing calculations, Journal of Geophysical Research: Atmospheres, 106, 3389–3399, doi:10.1029/2000JD900594, URL http://dx.doi.org/10.1029/2000JD900594, 2001b.

Mielke, L. H., Furgeson, A., and Osthoff, H. D.: Observation of ClNO2 in a Mid-Continental Urban Environment, Environ. Sci. Technol., 45, 8889–8896, doi:10.1021/es201955u, 2011.

Mielke, L. H., Stutz, J., Tsai, C., Hurlock, S. C., Roberts, J. M., Veres, P. R., Froyd, K. D., Hayes, P. L., Cubison, M. J., Jimenez, J. L., Washenfelder, R. A., Young, C. J., Gilman, J. B., de Gouw, J. A., Flynn, J. H., Grossberg, N., Lefer, B. L., Liu, J., Weber, R. J., and Osthoff, H. D.: Heterogeneous formation of nitryl chloride and its role as a nocturnal NOx reservoir species during CalNex-LA 2010, J Geophys. Res-Atmos., 118, 10,610–638,652, doi:10.1002/jgrd.50783, 2013.

Millet, D. B., Guenther, A., Siegel, D. A., Nelson, N. B., Singh, H. B., de Gouw, J. A., Warneke, C., Williams, J., Eerdekens, G., Sinha, V., Karl, T., Flocke, F., Apel, E.,

Riemer, D. D., Palmer, P. I., and Barkley, M.: Global atmospheric budget of acetaldehyde: 3-D model analysis and constraints from in-situ and satellite observations, Atmospheric Chemistry and Physics, 10, 3405–3425, doi:10.5194/acp-10-3405-2010, 2010.

Miyake, Y. and Tsunogai, S.: Evaporation of iodine from the ocean, Journal of Geophysical Research, 68, 3989–3993, doi:10.1029/JZ068i013p03989, 1963.

Miyazaki, Y., Coburn, S., Ono, K., Ho, D. T., Pierce, R. B., Kawamura, K., and Volkamer, R.: Contribution of dissolved organic matter to submicron water-soluble organic aerosols in the marine boundary layer over the eastern equatorial Pacific, Atmospheric Chemistry and Physics Discussions, 2016, 1–24, doi:10.5194/acp-2016-164, 2016.

Monks, P. S., Archibald, A. T., Colette, A., Cooper, O., Coyle, M., Derwent, R., Fowler, D., Granier, C., Law, K. S., Mills, G. E., Stevenson, D. S., Tarasova, O., Thouret, V., von Schneidemesser, E., Sommariva, R., Wild, O., and Williams, M. L.: Tropospheric ozone and its precursors from the urban to the global scale from air quality to short-lived climate forcer, Atmos. Chem. Phys., 15, 8889–8973, doi:10.5194/acp-15-8889-2015, 2015.

Montzka, S. A., Reimann, S., Engel, A., Krueger, K., O'Doherty, S., Sturges, W. T., Blake, D., Dorf, M., Fraser, P., Froidevaux, L., Jucks, K., Kreher, K., Kurylo, M. J., Mellouki, A., Miller, J., Nielsen, O.-J., Orkin, V. L., Prinn, R. G., Rhew, R., Santee, M. L., and Verdonik, D.: Ozone-Depleting Substances (ODSs) and Related Chemicals. Chapter 1 in Scientific Assess-ment of Ozone Depletion: 2010, Global Ozone Research and Monitoring ProjectReport No. 52, 516 pp., World Meteorological Organization, Geneva, Switzerland,, Tech. rep., World Health Organisation, Geneva, Switzerland, 2011.

Morgenstern, O., Giorgetta, M. A., Shibata, K., Eyring, V., Waugh, D. W., Shepherd, T. G., Akiyoshi, H., Austin, J., Baumgaertner, A. J. G., Bekki, S., Braesicke, P., Brühl, C., Chipperfield, M. P., Cugnet, D., Dameris, M., Dhomse, S., Frith, S. M., Garny, H., Gettelman, A., Hardiman, S. C., Hegglin, M. I., Jöckel, P., Kinnison, D. E., Lamarque, J.-F., Mancini, E., Manzini, E., Marchand, M., Michou, M., Nakamura, T., Nielsen, J. E., Olivié, D., Pitari, G., Plummer, D. A., Rozanov, E., Scinocca, J. F., Smale, D., Teyssèdre, H., Toohey, M., Tian, W., and Yamashita, Y.: Review of the formulation

of present-generation stratospheric chemistry-climate models and associated external forcings, doi:10.1029/2009JD013728, 2010.

Murray, B. J., Haddrell, A. E., Peppe, S., Davies, J. F., Reid, J. P., O'Sullivan, D., Price, H. C., Kumar, R., Saunders, R. W., Plane, J. M. C., Umo, N. S., and Wilson, T. W.: Glass formation and unusual hygroscopic growth of iodic acid solution droplets with relevance for iodine mediated particle formation in the marine boundary layer, Atmos. Chem. Phys., 12, 8575–8587, doi:10.5194/acp-12-8575-2012, 2012a.

Murray, L. T., Jacob, D. J., Logan, J. A., Hudman, R. C., and Koshak, W. J.: Optimized regional and interannual variability of lightning in a global chemical transport model constrained by LIS/OTD satellite data, J Geophys. Res-Atmos., 117, D20 307, doi: 10.1029/2012JD017934, 2012b.

Myhre, G., Shindell, D., Bréon, F.-M., Collins, W., Fuglestvedt, J., Huang, J., Koch, D., Lamarque, J.-F., Lee, D., Mendoza, B., Nakajima, T., Robock, A., Stephens, G., Takemura, T., and H. Zhang, .: Anthropogenic and Natural Radiative Forcing. In: Climate Change 2013: The Physical Science Basis. Contribution of Working Group I to the Fifth Assessment Report of the Intergovernmental Panel on Climate Change, Tech. rep., 2013.

Myriokefalitakis, S., Vrekoussis, M., Tsigaridis, K., Wittrock, F., Richter, A., Brühl, C., Volkamer, R., Burrows, J. P., and Kanakidou, M.: The influence of natural and anthropogenic secondary sources on the glyoxal global distribution, Atmospheric Chemistry and Physics, 8, 4965–4981, doi:10.5194/acp-8-4965-2008, 2008.

O'Dowd, C. D., Jimenez, J. L., Bahreini, R., Flagan, R. C., Seinfeld, J. H., Hameri, K., Pirjola, L., Kulmala, M., Jennings, S. G., and Hoffmann, T.: Marine aerosol formation from biogenic iodine emissions, Nature, 417, 632–636, URL http://dx.doi.org/10.1038/nature00775, 2002.

Olivier, J. G., Bloos, J. P. J., Berdowski, J. J., Visschedijk, A. J., and Bouwman, A. F.: A 1990 global emission inventory of anthropogenic sources of carbon monoxide on 11 developed in the framework of EDGAR/GEIA, Chemosphere - Global Change Science, 1, 1–17, doi:10.1016/S1465-9972(99)00019-7, 1999.

Olson, D. M., Dinerstein, E., Wikramanayake, E. D., Burgess, N. D., Powell, G. V. N., Underwood, E. C., D'amico, J. A., Itoua, I., Strand, H. E., Morrison, J. C., Loucks, C. J.,

Allnutt, T. F., Ricketts, T. H., Kura, Y., Lamoreux, J. F., Wettengel, W. W., Hedao, P., and Kassem, K. R.: Terrestrial Ecoregions of the World: A New Map of Life on Earth, BioScience, 51, 933, doi:10.1641/0006-3568(2001)051[0933:TEOTWA]2.0.CO;2, URL http://bioscience.oxfordjournals.org/content/51/11/933.full, 2001.

Ordóñez, C., Lamarque, J. F., Tilmes, S., Kinnison, D. E., Atlas, E. L., Blake, D. R., Santos, G. S., Brasseur, G., and Saiz-Lopez, A.: Bromine and iodine chemistry in a global chemistry-climate model: description and evaluation of very short-lived oceanic sources, Atmos. Chem. Phys., 12, 1423–1447, doi:10.5194/acp-12-1423-2012, 2012.

Orlando, J. J. and Tyndall, G. S.: Rate Coefficients for the Thermal Decomposition of BrONO2 and the Heat of Formation of BrONO2, J Phys Chem-US, 100, 19 398–19 405, doi:10.1021/jp9620274, 1996.

Osthoff, H. D., Roberts, J. M., Ravishankara, A. R., Williams, E. J., Lerner, B. M., Sommariva, R., Bates, T. S., Coffman, D., Quinn, P. K., Dibb, J. E., Stark, H., Burkholder, J. B., Talukdar, R. K., Meagher, J., Fehsenfeld, F. C., and Brown, S. S.: High levels of nitryl chloride in the polluted subtropical marine boundary layer, Nature Geosci, 1, 324–328, doi:http://www.nature.com/ngeo/journal/v1/n5/suppinfo/ngeo177_S1.html, 2008.

Park, R. J., Jacob, D. J., Field, B. D., Yantosca, R. M., and Chin, M.: Natural and transboundary pollution influences on sulfate-nitrate-ammonium aerosols in the United States: Implications for policy, J Geophys. Res-Atmos., 109, n/a—-n/a, doi:10.1029/2003JD004473, 2004.

Parrella, J. P., Jacob, D. J., Liang, Q., Zhang, Y., Mickley, L. J., Miller, B., Evans, M. J., Yang, X., Pyle, J. A., Theys, N., and Van Roozendael, M.: Tropospheric bromine chemistry: implications for present and pre-industrial ozone and mercury, Atmos. Chem. Phys., 12, 6723–6740, doi:10.5194/acp-12-6723-2012, 2012.

Pavelin, E. G., Johnson, C. E., Rughooputh, S., and Toumi, R.: Evaluation of pre-industrial surface ozone measurements made using Schönbein's method, Atmospheric Environment, 33, 919–929, doi:http://dx.doi.org/10.1016/S1352-2310(98)00257-X, 1999.

Pechtl, S., Schmitz, G., and von Glasow, R.: Modelling iodide-iodate speciation in atmo-

spheric aerosol: Contributions of inorganic and organic iodine chemistry, Atmos. Chem. Phys., 7, 1381–1393, 2007.

Phillips, G. J., Tang, M. J., Thieser, J., Brickwedde, B., Schuster, G., Bohn, B., Lelieveld, J., and Crowley, J. N.: Significant concentrations of nitryl chloride observed in rural continental Europe associated with the influence of sea salt chloride and anthropogenic emissions, Geophys. Res. Lett., 39, doi:10.1029/2012GL051912, 2012.

Powell, C. F., Baker, A. R., Jickells, T. D., Bange, H. W., Chance, R. J., and Yodle, C.: Estimation of the Atmospheric Flux of Nutrients and Trace Metals to the Eastern Tropical North Atlantic Ocean, J. Atmos. Sci., 72, 4029–4045, doi:10.1175/JAS-D-15-0011.1, URL http://dx.doi.org/10.1175/JAS-D-15-0011.1, 2015.

Prados-Roman, C., Cuevas, C. A., Hay, T., Fernandez, R. P., Mahajan, A. S., Royer, S.-J., Galí, M., Simó, R., Dachs, J., Großmann, K., Kinnison, D. E., Lamarque, J.-F., and Saiz-Lopez, A.: Iodine oxide in the global marine boundary layer, Atmos. Chem. Phys. Discuss., 14, 22 217–22 243, doi:10.5194/acpd-14-22217-2014, 2014.

Prados-Roman, C., Cuevas, C. A., Fernandez, R. P., Kinnison, D. E., Lamarque, J.-F., and Saiz-Lopez, A.: A negative feedback between anthropogenic ozone pollution and enhanced ocean emissions of iodine, Atmos. Chem. Phys., 15, 2215–2224, doi:10.5194/acp-15-2215-2015, 2015a.

Prados-Roman, C., Cuevas, C. A., Hay, T., Fernandez, R. P., Mahajan, A. S., Royer, S.-J., Galí, M., Simó, R., Dachs, J., Großmann, K., Kinnison, D. E., Lamarque, J.-F., and Saiz-Lopez, A.: Iodine oxide in the global marine boundary layer, Atmos. Chem. Phys., 15, 583–593, doi:10.5194/acp-15-583-2015, 2015b.

Prather, M. J., Holmes, C. D., and Hsu, J.: Reactive greenhouse gas scenarios: Systematic exploration of uncertainties and the role of atmospheric chemistry, Geophys. Res. Lett., 39, n/a—-n/a, doi:10.1029/2012GL051440, 2012.

Pszenny, A. A. P., Moldanová, J., Keene, W. C., Sander, R., Maben, J. R., Martinez, M., Crutzen, P. J., Perner, D., and Prinn, R. G.: Halogen cycling and aerosol pH in the Hawaiian marine boundary layer, Atmospheric Chemistry and Physics, 4, 147–168, doi:10.5194/acp-4-147-2004, 2004.

Puentedura, O., Gil, M., Saiz-Lopez, A., Hay, T., Navarro-Comas, M., Gomez-Pelaez, A., Cuevas, E., Iglesias, J., and Gomez, L.: Iodine monoxide in the north subtropical free troposphere, Atmos. Chem. Phys., 12, 4909–4921, doi:10.5194/acp-12-4909-2012, 2012.

Pye, H. O. T. and Seinfeld, J. H.: A global perspective on aerosol from low-volatility organic compounds, Atmospheric Chemistry and Physics, 10, 4377–4401, doi:10.5194/acp-10-4377-2010, URL http://www.atmos-chem-phys.net/10/4377/2010/, 2010.

Pye, H. O. T., Liao, H., Wu, S., Mickley, L. J., Jacob, D. J., Henze, D. K., and Seinfeld, J. H.: Effect of changes in climate and emissions on future sulfate-nitrate-ammonium aerosol levels in the United States, J. Geophys. Res., 114, D01 205, doi:10.1029/2008JD010701, 2009.

Quinn, P. K. and Bates, T. S.: The case against climate regulation via oceanic phytoplankton sulphur emissions, Nature, 480, 51–56, URL http://dx.doi.org/10.1038/nature10580, 2011.

Rancher, J. and Kritz, M. A.: Diurnal fluctuations of Br and I in the tropical marine atmosphere, Journal of Geophysical Research: Oceans, 85, 5581–5587, doi:10.1029/JC085iC10p05581, URL http://dx.doi.org/10.1029/JC085iC10p05581, 1980.

Rap, A., Scott, C. E., Spracklen, D. V., Bellouin, N., Forster, P. M., Carslaw, K. S., Schmidt, A., and Mann, G.: Natural aerosol direct and indirect radiative effects, Geophys. Res. Lett., 40, 3297–3301, doi:10.1002/grl.50441, 2013.

Read, K. A., Mahajan, A. S., Carpenter, L. J., Evans, M. J., Faria, B. V. E., Heard, D. E., Hopkins, J. R., Lee, J. D., Moller, S. J., Lewis, A. C., Mendes, L., McQuaid, J. B., Oetjen, H., Saiz-Lopez, A., Pilling, M. J., and Plane, J. M. C.: Extensive halogen-mediated ozone destruction over the tropical Atlantic Ocean, Nature, 453, 1232–1235, doi:10.1038/nature07035, 2008.

Reeser, D. I. and Donaldson, D. J.: Influence of water surface properties on the heterogeneous reaction between O-3(g) and I((aq))over bar, Atmos. Environ., 45, 6116–6120, doi:10.1016/j.atmosenv.2011.08.042, 2011.

Reimann, S., Carpenter, L. J., Lead), A., Burkholder, J., Clerbaux, C., B.D., Hall, Hossaini, R., Laube, J., Yvon-Lewis, and S.A.: Ozone-Depleting Substances (ODSs) and Other Gases of Interest to the Montreal Protocol Chapter 1 in Scientific Assessment of

Ozone Depletion: 2014, Global Ozone Research and Monitoring Project Report No. 55, Tech. rep., World Meteorological Organization, Geneva, Switzerland, 2014.

Reithmeier, H., Lazarev, V., Rühm, W., and Nolte, E.: Anthropogenic 129I in the atmosphere: Overview over major sources, transport processes and deposition pattern, Science of The Total Environment, 408, 5052–5064, doi:10.1016/j.scitotenv.2010.07.015, 2010.

Riedel, T. P., Bertram, T. H., Crisp, T. A., Williams, E. J., Lerner, B. M., Vlasenko, A., Li, S.-M., Gilman, J., de Gouw, J., Bon, D. M., Wagner, N. L., Brown, S. S., and Thornton, J. A.: Nitryl Chloride and Molecular Chlorine in the Coastal Marine Boundary Layer, Environ. Sci. Technol., 46, 10 463–10 470, doi:10.1021/es204632r, 2012.

Riedel, T. P., Wagner, N. L., Dubé, W. P., Middlebrook, A. M., Young, C. J., Öztürk, F., Bahreini, R., VandenBoer, T. C., Wolfe, D. E., Williams, E. J., Roberts, J. M., Brown, S. S., and Thornton, J. A.: Chlorine activation within urban or power plant plumes: Vertically resolved ClNO2 and Cl2 measurements from a tall tower in a polluted continental setting, J Geophys. Res-Atmos., 118, 8702–8715, doi:10.1002/jgrd.50637, URL http://dx.doi.org/10.1002/jgrd.50637, 2013.

Riffault, V., Bedjanian, Y., and Poulet, G.: Kinetic and mechanistic study of the reactions of OH with IBr and HOI, J Photoch. Photobio. A, 176, 155–161, doi:http://dx.doi.org/10.1016/j.jphotochem.2005.09.002, 2005.

Roberts, J. M., Osthoff, H. D., Brown, S. S., Ravishankara, A. R., Coffman, D., Quinn, P., and Bates, T.: Laboratory studies of products of N2O5 uptake on Cl containing substrates, Geophys. Res. Lett., 36, doi:10.1029/2009GL040448, 2009.

Roeckner, E., Bäuml, G., Bonaventura, L., Brokopf, R., M.Kornblueh, Giorgetta, M., Hagemann, S., Kirchner, I., L.Schlese, Manzini, E., Rhodin, A., Schulzweida, U., and Tompkins, A.: The atmospheric general circulation model ECHAM5 - Part I, Tech. rep., Max-Planck-Institut für Meteorologie, Hamburg, Germany, 2003.

Roscoe, H. K., Jones, A. E., Brough, N., Weller, R., Saiz-Lopez, A., Mahajan, A. S., Schoenhardt, A., Burrows, J. P., and Fleming, Z. L.: Particles and iodine compounds in coastal Antarctica, J Geophys. Res-Atmos., 120, 7144–7156, doi:10.1002/2015JD023301, URL http://doi.wiley.com/10.1002/2015JD023301, 2015.

Saiz-Lopez, A. and von Glasow, R.: Reactive halogen chemistry in the troposphere, Chem. Soc. Rev., 41, 6448–6472, doi:10.1039/c2cs35208g, 2012.

Saiz-Lopez, A., Chance, K., Liu, X., Kurosu, T. P., and Sander, S. P.: First observations of iodine oxide from space, Geophys. Res. Lett., 34, L12 812, doi:10.1029/2007gl030111, 2007a.

Saiz-Lopez, A., Mahajan, A. S., Salmon, R. A., Bauguitte, S. J. B., Jones, A. E., Roscoe, H. K., and Plane, J. M. C.: Boundary layer halogens in coastal Antarctica, Science, 317, 348–351, doi:10.1126/science.1141408, 2007b.

Saiz-Lopez, A., Plane, J. M. C., Mahajan, A. S., Anderson, P. S., Bauguitte, S. J. B., Jones, A. E., Roscoe, H. K., Salmon, R. A., Bloss, W. J., Lee, J. D., and Heard, D. E.: On the vertical distribution of boundary layer halogens over coastal Antarctica: implications for O3, HOx, NOx and the Hg lifetime, Atmos. Chem. Phys., 8, 887–900, doi:10.5194/acp-8-887-2008, 2008.

Saiz-Lopez, A., Lamarque, J. F., Kinnison, D. E., Tilmes, S., Ordonez, C., Orlando, J. J., Conley, A. J., Plane, J. M. C., Mahajan, A. S., Santos, G. S., Atlas, E. L., Blake, D. R., Sander, S. P., Schauffler, S., Thompson, A. M., and Brasseur, G.: Estimating the climate significance of halogen-driven ozone loss in the tropical marine troposphere, Atmos. Chem. Phys., 12, 3939–3949, doi:10.5194/acp-12-3939-2012, 2012a.

Saiz-Lopez, A., Plane, J. M. C., Baker, A. R., Carpenter, L. J., von Glasow, R., Martin, J. C. G., McFiggans, G., and Saunders, R. W.: Atmospheric Chemistry of Iodine, Chem. Rev., 112, 1773–1804, doi:10.1021/cr200029u, 2012b.

Saiz-Lopez, A., Fernandez, R. P., Ordóñez, C., Kinnison, D. E., Gómez Martín, J. C., Lamarque, J.-F., and Tilmes, S.: Iodine chemistry in the troposphere and its effect on ozone, Atmos. Chem. Phys.., 14, 19 985–20 044, doi:10.5194/acpd-14-19985-2014, 2014.

Saiz-Lopez, A., Baidar, S., Cuevas, C. A., Koenig, T. K., Fernandez, R. P., Dix, B., Kinnison, D. E., Lamarque, J.-F., Rodriguez-Lloveras, X., Campos, T. L., and Volkamer, R.: Injection of iodine to the stratosphere, Geophysical Research Letters, 42, 6852–6859, doi:10.1002/2015GL064796, URL http://doi.wiley.com/10.1002/2015GL064796, 2015.

Sakamoto, Y., Yabushita, A., Kawasaki, M., and Enami, S.: Direct emission of I2 molecule

and IO radical from the heterogeneous reactions of gaseous ozone with aqueous potassium iodide solution, J Phys Chem A, 113, 7707–7713, doi:10.1021/jp903486u, 2009.

Saltzman, E. S., Aydin, M., De Bruyn, W. J., King, D. B., and Yvon-Lewis, S. A.: Methyl bromide in preindustrial air: Measurements from an Antarctic ice core, Journal of Geophysical Research: Atmospheres, 109, n/a—-n/a, doi:10.1029/2003JD004157, 2004.

Sander, R.: Compilation of Henry's Law Constants for Inorganic and Organic Species of Potential Importance in Environmental Chemistry, 1999.

Sander, R.: Compilation of Henry's law constants (version 4.0) for water as solvent, Atmos. Chem. Phys., 15, 4399–4981, doi:10.5194/acp-15-4399-2015, 2015.

Sander, R., Vogt, R., Harrris, G. W., and Crutzen, P. J.: Modelling the chemistry of ozone, halogen compounds, and hydrocarbons in the arctic troposphere during spring, Tellus B, 49, 522–532, doi:10.1034/j.1600-0889.49.issue5.8.x, URL http://dx.doi.org/10.1034/j.1600-0889.49.issue5.8.x, 1997.

Sander, R., Keene, W. C., Pszenny, A. A. P., Arimoto, R., Ayers, G. P., Baboukas, E., Cainey, J. M., Crutzen, P. J., Duce, R. A., Hönninger, G., Huebert, B. J., Maenhaut, W., Mihalopoulos, N., Turekian, V. C., and Van Dingenen, R.: Inorganic bromine in the marine boundary layer: a critical review, Atmos. Chem. Phys., 3, 1301–1336, doi:10.5194/acp-3-1301-2003, 2003.

Sander, S. P., Golden, D. M., Kurylo, M. J., Moortgat, G. K., Wine, P. H., Ravishankara, A. R., Kolb, C. E., Molina, M. J., Finlayson-Pitts, B. J., Huie, R. E., and Orkin, V. L.: Chemical kinetics and photochemical data for use in Atmospheric Studies Evaluation Number 15, 2006.

Sander, S. P., Friedl, R. R., Abbatt, J. P. D., Barker, J. R., Burkholder, J. B., Golden, D. M., Kolb, C. E., Kurylo, M. J., Moortgat, G. K., Wine, P. H., Huie, R. E., and Orkin, V. L.: Chemical kinetics and photochemical data for use in atmospheric studies, Evaluation Number 17, Tech. rep., NASA Jet Propulsion Laboratory, 2011.

Sarwar, G., Simon, H., Xing, J., and Mathur, R.: Importance of tropospheric ClNO2 chemistry across the Northern Hemisphere, Geophys. Res. Lett., 41, 4050–4058, doi:10.1002/2014GL059962, 2014.

Sarwar, G., Gantt, B., Schwede, D., Foley, K., Mathur, R., and Saiz-Lopez, A.: Impact of Enhanced Ozone Deposition and Halogen Chemistry on Tropospheric Ozone over the Northern Hemisphere., Environmental science & technology, 49, 9203–11, doi:10.1021/acs.est.5b01657, URL http://pubs.acs.org/doi/abs/10.1021/acs.est.5b01657{\#}.V34Z63z{_}EFM.mendeley, 2015.

Sarwar, G., Kang, D., Foley, K., Schwede, D., Gantt, B., and Mathur, R.: Technical note: Examining ozone deposition over seawater, doi:10.1016/j.atmosenv.2016.06.072, 2016.

Schmidt, J. A., Jacob, D. J., Horowitz, H. M., Hu, L., Sherwen, T., Evans, M. J., Liang, Q., Suleiman, R. M., Oram, D. E., Breton, M. L., Percival, C. J., Wang, S., Dix, B., and Volkamer, R.: Modeling the observed tropospheric BrO background: Importance of multiphase chemistry and implications for ozone, OH, and mercury, J Geophys. Res-Atmos., 2016.

Schönhardt, A., Richter, A., Wittrock, F., Kirk, H., Oetjen, H., Roscoe, H. K., and Burrows, J. P.: Observations of iodine monoxide columns from satellite, Atmos. Chem. Phys., 8, 637–653, doi:10.5194/acp-8-637-2008, 2008.

Schultz, M. G., Heil, A., Hoelzemann, J. J., Spessa, A., Thonicke, K., Goldammer, J. G., Held, A. C., Pereira, J. M. C., and van het Bolscher, M.: Global wildland fire emissions from 1960 to 2000, Global Biogeochemical Cycles, 22, n/a–n/a, doi:10.1029/2007GB003031, URL http://doi.wiley.com/10.1029/2007GB003031, 2008.

Schweitzer, F., Mirabel, P., and George, C.: Uptake of Hydrogen Halides by Water Droplets, J Phys Chem A, 104, 72–76, doi:10.1021/jp992621o, URL http://dx.doi.org/10.1021/jp992621o, 2000.

Seakins, P. W., Pilling, M. J., Niiranen, J. T., Gutman, D., and Krasnoperov, L. N.: Kinetics and thermochemistry of R + HBr <=> RH + Br reactions : determinations of the heat of formation of C2H5, i-C3H7, sec-C4H9, and t-C4H9, J. Phys. Chem., 96, 9847–9855, 1992.

Sellegri, K., Pey, J., Rose, C., Culot, A., DeWitt, H. L., Mas, S., Schwier, A. N., Temime-Roussel, B., Charriere, B., Saiz-Lopez, A., Mahajan, A. S., Parin, D., Kukui, A., Sempere, R., D'Anna, B., and Marchand, N.: Evidence of atmospheric nanoparticle formation from emissions of marine microorganisms, Geophysical Research Letters, pp. n/a—-n/a, doi:10.1002/2016GL069389, 2016.

Selminen, R.: Foregs Geochemical Atlas, URL http://weppi.gtk.fi/publ/foregsatlas/, 2013.

Shacklette, H. and Boerngen, J.: Element concentrations in soils and other surficial materials of the conterminous United States, Tech. rep., Environmenat Protection Agency, 1984.

Shaw, M. D. and Carpenter, L. J.: Modification of Ozone Deposition and I2 Emissions at the AirAqueous Interface by Dissolved Organic Carbon of Marine Origin, Environ. Sci. Technol., 47 (19), 10 947–10 954, doi:10.1021/es4011459, 2013.

Sherwen, T., Evans, M. J., Carpenter, L. J., Andrews, S. J., Lidster, R. T., Dix, B., Koenig, T. K., Sinreich, R., Ortega, I., Volkamer, R., Saiz-Lopez, A., Prados-Roman, C., Mahajan, A. S., and Ordóñez, C.: Iodine's impact on tropospheric oxidants: a global model study in GEOS-Chem, Atmos. Chem. Phys., 16, 1161–1186, doi:10.5194/acp-16-1161-2016, 2016a.

Sherwen, T., Schmidt, J. A., Evans, M. J., Carpenter, L. J., Großmann4, K., Eastham, S. D., J., D. J., Dix, B., Koenig, T. K., Sinreich, R., Ortega, I., Volkamer, R., Saiz-Lopez, A., Prados-Roman, C., Mahajan, A. S., and C. Ordóñez: Global impacts of tropospheric halogens (Cl, Br, I) on oxidants and composition in GEOS-Chem, Atmos. Chem. Phys. Discuss., 2016b.

Shetaya, W., Young, S., Watts, M., Ander, E., and Bailey, E.: Iodine dynamics in soils, Geochimica et Cosmochimica Acta, 77, 457–473, doi:10.1016/j.gca.2011.10.034, 2012.

Shetaya, W. H. A. H.: IODINE DYNAMICS IN SOIL, Ph.D. thesis, University of Nottingham, 2011.

Simon, H., Kimura, Y., McGaughey, G., Allen, D. T., Brown, S. S., Osthoff, H. D., Roberts, J. M., Byun, D., and Lee, D.: Modeling the impact of ClNO 2 on ozone formation in the Houston area, Journal of Geophysical Research, 114, D00F03, doi:10.1029/2008JD010732, URL http://doi.wiley.com/10.1029/2008JD010732, 2009.

Simpson, W. R., Brown, S. S., Saiz-Lopez, A., Thornton, J. A., and von Glasow, R.: Tropospheric Halogen Chemistry: Sources, Cycling, and Impacts, Chemical Reviews, 115, 4035–4062, doi:10.1021/cr5006638, 2015.

Sinreich, R., Coburn, S., Dix, B., and Volkamer, R.: Ship-based detection of glyoxal over the remote tropical Pacific Ocean, Atmospheric Chemistry and Physics, 10, 11 359–11 371, doi:10.5194/acp-10-11359-2010, 2010.

Sofen, E. D., Bowdalo, D., Evans, M. J., Apadula, F., Bonasoni, P., Cupeiro, M., Ellul, R., Galbally, I. E., Girgzdiene, R., Luppo, S., Mimouni, M., Nahas, A. C., Saliba, M., and Tørseth, K.: Gridded global surface ozone metrics for atmospheric chemistry model evaluation, Earth Syst Sci Data, 8, 41–59, doi:10.5194/essd-8-41-2016, 2016.

Solomon, S., Garcia, R. R., and Ravishankara, A. R.: On the role of iodine in ozone depletion, J Geophys. Res-Atmos., 99, 20 491–20 499, doi:10.1029/94JD02028, 1994.

Sommariva, R. and von Glasow, R.: Multiphase halogen chemistry in the tropical Atlantic Ocean, Environ. Sci. Technol., 46, 10 429–10 437, doi:10.1021/es300209f, 2012.

Sommariva, R., Bloss, W. J., and von Glasow, R.: Uncertainties in gas-phase atmospheric iodine chemistry, Atmos. Environ., 57, 219–232, doi:10.1016/j.atmosenv.2012.04.032, 2012.

Spietz, P., Gómez Martín, J. C., and Burrows, J. P.: Spectroscopic studies of the I2/O3 photochemistry: Part 2. Improved spectra of iodine oxides and analysis of the IO absorption spectrum, J Photoch. Photobio. A, 176, 50–67, doi:http://dx.doi.org/10.1016/j.jphotochem.2005.08.023, 2005.

Stettler, M., Eastham, S., and Barrett, S.: Air quality and public health impacts of UK airports. Part I: Emissions, Atmospheric Environment, 45, 5415–5424, doi:10.1016/j.atmosenv.2011.07.012, 2011.

Stevenson, D. S., Young, P. J., Naik, V., Lamarque, J.-F., Shindell, D. T., Voulgarakis, A., Skeie, R. B., Dalsoren, S. B., Myhre, G., Berntsen, T. K., Folberth, G. A., Rumbold, S. T., Collins, W. J., MacKenzie, I. A., Doherty, R. M., Zeng, G., van Noije, T. P. C., Strunk, A., Bergmann, D., Cameron-Smith, P., Plummer, D. A., Strode, S. A., Horowitz, L., Lee, Y. H., Szopa, S., Sudo, K., Nagashima, T., Josse, B., Cionni, I., Righi, M., Eyring, V., Conley, A., Bowman, K. W., Wild, O., and Archibald, A.: Tropospheric ozone changes, radiative forcing and attribution to emissions in the Atmospheric Chemistry and Climate Model Intercomparison Project (ACCMIP), Atmospheric Chemistry and Physics, 13, 3063–3085, doi:10.5194/acp-13-3063-2013, 2013.

Stocker, T., Qin, D., Plattner, G.-K., Tignor, M., Allen, S., Boschung, J., Nauels, A., Xia, Y., Bex, V., and (eds.), P. M.: IPCC, 2013: Climate Change 2013: The Physical Science Basis. Contribution of Working Group I to the Fifth Assessment Report of the Intergovernmental Panel on Climate Change, Tech. rep., Cambridge University Press, Cambridge, United Kingdom and New York, NY, USA, doi:10.1017/CBO9781107415324., 2000.

Stuart, A. L. and Jacobson, M. Z.: A timescale investigation of volatile chemical retention during hydrometeor freezing: Nonrime freezing and dry growth riming without spreading, J. Geophys. Res., 108, 4178, doi:10.1029/2001JD001408, 2003.

Stutz, J., Pikelnaya, O., Hurlock, S. C., Trick, S., Pechtl, S., and von Glasow, R.: Daytime OIO in the Gulf of Maine, Geophys. Res. Lett., 34, L22 816, doi:10.1029/2007GL031332, URL http://dx.doi.org/10.1029/2007GL031332, 2007.

Tham, Y. J., Yan, C., Xue, L., Zha, Q., Wang, X., and Wang, T.: Presence of high nitryl chloride in Asian coastal environment and its impact on atmospheric photochemistry, Chin. Sci. Bull, 59, 356–359, doi:10.1007/s11434-013-0063-y, 2014.

Theys, N., Van Roozendael, M., Hendrick, F., Yang, X., De Smedt, I., Richter, A., Begoin, M., Errera, Q., Johnston, P. V., Kreher, K., and De Mazière, M.: Global observations of tropospheric BrO columns using GOME-2 satellite data, Atmos. Chem. Phys., 11, 1791–1811, doi:10.5194/acp-11-1791-2011, 2011.

Thornton, J. A., Kercher, J. P., Riedel, T. P., Wagner, N. L., Cozic, J., Holloway, J. S., Dubé, W. P., Wolfe, G. M., Quinn, P. K., Middlebrook, A. M., Alexander, B., and Brown, S. S.: A large atomic chlorine source inferred from mid-continental reactive nitrogen chemistry, Nature, 464, 271–274, 2010.

Truesdale, V. W.: On the feasibility of some photochemical reactions of iodide in seawater, Marine Chemistry, 104, 266–281, doi:10.1016/j.marchem.2006.12.003, 2007.

van der Werf, G. R., Randerson, J. T., Giglio, L., Collatz, G. J., Mu, M., Kasibhatla, P. S., Morton, D. C., DeFries, R. S., Jin, Y., and van Leeuwen, T. T.: Global fire emissions and the contribution of deforestation, savanna, forest, agricultural, and peat fires (19972009), Atmospheric Chemistry and Physics, 10, 11 707–11 735, doi:10.5194/acp-10-11707-2010, URL http://www.atmos-chem-phys.net/10/11707/2010/, 2010.

Vestreng, V., Ntziachristos, L., Semb, A., Reis, S., Isaksen, I. S. A., and Tarrasón, L.: Evolution of NO_x emissions in Europe with focus on road transport control measures, Atmospheric Chemistry and Physics, 9, 1503–1520, doi:10.5194/acp-9-1503-2009, URL http://www.atmos-chem-phys.net/9/1503/2009/, 2009.

Vinken, G. C. M., Boersma, K. F., Jacob, D. J., and Meijer, E. W.: Accounting for non-linear chemistry of ship plumes in the GEOS-Chem global chemistry transport model, Atmospheric Chemistry and Physics, 11, 11 707–11 722, doi:10.5194/acp-11-11707-2011, URL http://www.atmos-chem-phys.net/11/11707/2011/, 2011.

Vogt, R., Sander, R., Von Glasow, R., and Crutzen, P. J.: Iodine chemistry and its role in halogen activation and ozone loss in the marine boundary layer: A model study, J Atmos. Chem., 32, 375–395, doi:10.1023/a:1006179901037, 1999.

Volkamer, R., Baidar, S., Campos, T., Coburn, S., DiGangi, J., Dix, B., Eloranta, E., Koenig, T., Moley, B., Ortega, I., Pierce, B., Reeves, M., Sinreich, R., Wang, S.-Y., Zondlo, M., and Romashkin, P.: Aircraft measurements of BrO, IO, glyoxal, NO2, H2O, O2-O2 and aerosol extinction profiles in the tropics: Comparison with aircraft-/ship-based in situ and lidar measurements, Atmos. Meas. Tech., 8, 623–687, doi:10.5194/amt-8-2121-2015, 2015.

Volz, A. and Kley, D.: Evaluation of the Montsouris series of ozone measurements made in the nineteenth century, Nature, 332, 240–242, URL http://dx.doi.org/10.1038/332240a0, 1988.

von Glasow, R., Sander, R., Bott, A., and Crutzen, P. J.: Modeling halogen chemistry in the marine boundary layer 2. Interactions with sulfur and the cloud-covered MBL, J Geophys. Res-Atmos., 107, 4323, doi:10.1029/2001JD000943, 2002.

von Glasow, R., von Kuhlmann, R., Lawrence, M. G., Platt, U., and Crutzen, P. J.: Impact of reactive bromine chemistry in the troposphere, Atmos. Chem. Phys., 4, 2481–2497, doi:10.5194/acp-4-2481-2004, 2004.

Voulgarakis, A., Naik, V., Lamarque, J.-F., Shindell, D. T., Young, P. J., Prather, M. J., Wild, O., Field, R. D., Bergmann, D., Cameron-Smith, P., Cionni, I., Collins, W. J., Dalsøren, S. B., Doherty, R. M., Eyring, V., Faluvegi, G., Folberth, G. A., Horowitz, L. W., Josse, B., MacKenzie, I. A., Nagashima, T., Plummer, D. A., Righi, M., Rumbold, S. T., Stevenson, D. S., Strode, S. A., Sudo, K., Szopa, S., and Zeng, G.: Analysis

of present day and future OH and methane lifetime in the ACCMIP simulations, Atmos. Chem. Phys., 13, 2563–2587, doi:10.5194/acp-13-2563-2013, 2013.

Wang, Q., Jacob, D. J., Fisher, J. A., Mao, J., Leibensperger, E. M., Carouge, C. C., Le Sager, P., Kondo, Y., Jimenez, J. L., Cubison, M. J., and Doherty, S. J.: Sources of carbonaceous aerosols and deposited black carbon in the Arctic in winter-spring: implications for radiative forcing, Atmospheric Chemistry and Physics, 11, 12 453–12 473, doi:10.5194/acp-11-12453-2011, URL http://www.atmos-chem-phys.net/11/12453/2011/, 2011.

Wang, S.-Y., Schmidtd, J., Baidar, S., Coburn, S., Dix, B., Koenig, T., Apel, E., Bowdalo, D., Campos, T., Eloranta, E., Evans, M., DiGangii, J., Zondlo, M., Gao, R.-S., Haggerty, J., Hall, S., Hornbrook, R., Jacob, D., Morley, B., Pierce, B., Reeves, M., Romashkin, P., ter Schure, A., and Volkamer, R.: Active and widespread halogen chemistry in the tropical and subtropical free troposphere, Proc. Natl. Acad. Sci. U.S.A., 112, 9281–9286, doi:10.1073/pnas.1505142112, 2015.

Wang, Y. and Jacob, D. J.: Anthropogenic forcing on tropospheric ozone and OH since preindustrial times, J Geophys. Res-Atmos., 103, 31 123–31 135, doi:10.1029/1998JD100004, 1998.

Wayne, R. P.: Chemistry of Atmospheres, OUP, Oxford, 2000.

Wesely, M. and Hicks, B.: A review of the current status of knowledge on dry deposition, Atmospheric Environment, 34, 2261–2282, doi:10.1016/S1352-2310(99)00467-7, 2000.

Wesely, M. L.: Parameterization of surface resistances to gaseous dry deposition in regional-scale numerical models, Atmos. Environ., 23, 1293–1304, doi:http://dx.doi.org/10.1016/0004-6981(89)90153-4, 1989.

Whitehead, D.: The distribution and transformations of iodine in the environment, Environment International, 10, 321–339, doi:10.1016/0160-4120(84)90139-9, 1984.

WHO: IODINE AND INORGANIC IODIDES: HUMAN HEALTH ASPECTS, Tech. rep., WHO, 2009.

Wild, O., Zhu, X., and Prather, M. J.: Fast-j: Accurate simulation of in- and below-cloud photolysis in tropospheric chemical models, Journal of Atmospheric Chemistry, 37, 245–282, doi:10.1023/a:1006415919030, 2000.

World Health Organistion: 7 million premature deaths annually linked to air pollution, 2014.

WOUDC: WOUDC Ozone Monitoring Community, World Meteorological Organization-Global Atmosphere Watch Program (WMO-GAW)/World Ozone and Ultraviolet Radiation Data Centre (WOUDC) [Data]., doi:10.14287/10000001, URL http://www.woudc.org, 2014.

Xiao, Y., Logan, J. A., Jacob, D. J., Hudman, R. C., Yantosca, R., and Blake, D. R.: Global budget of ethane and regional constraints on U.S. sources, Journal of Geophysical Research, 113, D21 306, doi:10.1029/2007JD009415, URL http://doi.wiley.com/10.1029/2007JD009415, 2008.

Yang, X., Pyle, J. A., and Cox, R. A.: Sea salt aerosol production and bromine release: Role of snow on sea ice, Geophysical Research Letters, 35, L16 815, doi:10.1029/2008GL034536, URL http://doi.wiley.com/10.1029/2008GL034536, 2008.

Yevich, R. and Logan, J. A.: An assessment of biofuel use and burning of agricultural waste in the developing world, Global Biogeochemical Cycles, 17, n/a–n/a, doi:10.1029/2002GB001952, URL http://doi.wiley.com/10.1029/2002GB001952, 2003.

Young, P. J., Archibald, A. T., Bowman, K. W., Lamarque, J. F., Naik, V., Stevenson, D. S., Tilmes, S., Voulgarakis, A., Wild, O., Bergmann, D., Cameron-Smith, P., Cionni, I., Collins, W. J., Dalsøren, S. B., Doherty, R. M., Eyring, V., Faluvegi, G., Horowitz, L. W., Josse, B., Lee, Y. H., MacKenzie, I. A., Nagashima, T., Plummer, D. A., Righi, M., Rumbold, S. T., Skeie, R. B., Shindell, D. T., Strode, S. A., Sudo, K., Szopa, S., and Zeng, G.: Pre-industrial to end 21st century projections of tropospheric ozone from the Atmospheric Chemistry and Climate Model Intercomparison Project (ACCMIP), Atmos. Chem. Phys., 13, 2063–2090, doi:10.5194/acp-13-2063-2013, 2013.

Ziska, F., Quack, B., Abrahamsson, K., Archer, S. D., Atlas, E., Bell, T., Butler, J. H., Carpenter, L. J., Jones, C. E., Harris, N. R. P., Hepach, H., Heumann, K. G., Hughes, C., Kuss, J., Krüger, K., Liss, P., Moore, R. M., Orlikowska, A., Raimund, S., Reeves, C. E., Reifenhäuser, W., Robinson, A. D., Schall, C., Tanhua, T., Tegtmeier, S., Turner, S., Wang, L., Wallace, D., Williams, J., Yamamoto, H., Yvon-Lewis, S., and Yokouchi, Y.: Global sea-to-air flux climatology for bromoform, dibromomethane and methyl iodide, Atmos. Chem. Phys., 13, 8915–8934, doi:10.5194/acp-13-8915-2013, 2013.